Intermediates in Organometallic Photochemistry

by Anthony Haynes, B.Sc.

Thesis submitted to the University of Nottingham for the degree of Doctor of Philosophy, October 1989.

BRITISH LIBRARY

IMAGING SERVICES NORTH

Boston Spa, Wetherby
West Yorkshire, LS23 7BQ
www.bl.uk

PAGE NUMBERING AS ORIGINAL

For Mum, Dad

and Carole

ACKNOWLEDGEMENTS

I would like to thank my supervisors, Professor Jim Turner and Dr. Martyn Poliakoff, for their boundless encouragement and advice throughout the past three years.

I am also grateful to Professor Jack Norton of Colorado State University and Dr. Neil Boag and Marjorie Green of the University of Salford, for helpful discussions regarding this research.

My gratitude is extended to Dr. Mike Healy, Jim Gamble and the workshop staff in the Chemistry Department for their technical assistance. Special thanks to John Whalley, for rescuing an ageing displex!

Some of this research would not have been possible without the help of my colleagues. Thanks must go to Andy Dixon, Steve Firth, Steve Howdle, Mike George and Mark Haward in this respect. I would also like to thank Mike Hodges, Sarah Jackson, Paul Glyn and Charlie Gordon for making B19/21 a happy place to work. Thanks to Steve Howdle for escorting me to the Baseball Ground and to Arthur Cox for taking Derby County F.C. back to Division One!

I would like to acknowledge the SERC for financial support.

Finally, a big "thank-you" to Carole and my family, for their love and support over the past three years.

ABSTRACT

CHAPTER 1: A background to the techniques of matrix isolation, liquid xenon solution and flash photolysis with fast IR detection is presented. The application of infrared spectroscopy in structural studies of metal carbonyl compounds is also discussed.

CHAPTER 2: Photolysis of $((\eta^5\text{-}C_5R_5)Pt(CO))_2$ (R = H, Me) in frozen gas matrices results in production of $(\eta^5\text{-}C_5R_5)_2Pt_2(\mu\text{-}CO)$. ^{13}CO enrichment and polarised photochemistry show that the photoproduct contains a single symmetrically bridging CO group. Photolysis of $(CpNi(\mu\text{-}CO))_2$ in frozen gas matrices results in formation of $Cp_2Ni_2(CO)$ with a terminal CO ligand. The stability these dinuclear photoproducts in room temperature solution has been investigated using fast TRIR spectroscopy. Photolysis in CO matrices leads to M-M bond cleavage and reaction with CO to give $Pt(CO)_4$ or $Ni(CO)_4$ as the final product.

CHAPTER 3: Photolysis of $Os_2(CO)_9$ or $Os_2(CO)_8$-$(\mu\text{-}\eta^1,\eta^1\text{-}C_2H_4)$ in frozen gas matrices leads to formation of $Os_2(CO)_8$, which has only terminal CO groups. The thermal and photochemical reactivity of $Os_2(CO)_8$ towards CO, N_2 and C_2H_4 is investigated. Photolysis using plane polarised light provides confirmation of the C_{2v} structure of $Os_2(CO)_9$, and gives evidence favouring a D_{2h} structure for $Os_2(CO)_8$.

Prolonged UV photolysis of $Os_2(CO)_9$ in CO matrices leads to cleavage of the Os-Os bond and production of $Os(CO)_5$.

CHAPTER 4: The mechanism of the photochemical deoligomerisation of $FpSiMe_2SiMe_3$ is investigated using a variety of techniques. The reaction is shown to proceed via two photochemical steps. Primary CO-loss is followed by intramolecular trapping to give a silyl(silylene) intermediate. The second step involves expulsion of an $SiMe_2$ fragment and coordination of a ligand, L, to give $CpFe(CO)(L)SiMe_3$ (L = CO, PPh_3, C_2H_4 or N_2).

CHAPTER 5: A study of the photochemistry of Fp-disilyl complexes containing β-silyl hydrogens implies β-H transfer from Si to Fe as the dominant process following photodissociation of CO. The product, a metalladisilacyclopropane or η^2-disilene complex, is implicated as an intermediate in the photochemical formation of FpH in this system.

CHAPTER 6: The experimental techniques and spectrometers used in this research are described, along with a discussion of the theory and advantages of FTIR spectroscopy.

ABBREVIATIONS

Cp = η^5-C_5H_5

Cp* = η^5-C_5Me_5

Cp' = η^5-C_5H_4Me

Cy = cyclohexyl

Fp = (η^5-C_5H_5)$Fe(CO)_2$

Fp* = (η^5-C_5Me_5)$Fe(CO)_2$

Fp' = (η^5-C_5H_4Me)$Fe(CO)_2$

HOMO = Highest Occupied Molecular Orbital

IR = Infrared

LUMO = Lowest Unoccupied Molecular Orbital

NMR = Nuclear Magnetic Resonance

PVC = Polyvinylchloride

TRIR = Time-Resolved Infrared

UV = Ultraviolet

Vis = Visible

Throughout the text, the symbols "v", "n" and "u" are used instead of the Greek letters "ν", "η" and "μ".

e.g. v(CO) = ν(CO)

n^5 = η^5

u-CO = μ-CO

CONTENTS

CHAPTER 1: INTRODUCTION

1.1 PREFACE 1

1.2 MATRIX ISOLATION 3

1.3 ORGANOMETALLIC PHOTOCHEMISTRY IN LIQUID NOBLE GASES 6

1.4 FLASH PHOTOLYSIS; TIME-RESOLVED IR SPECTROSCOPY 7

1.5 INFRARED SPECTROSCOPY OF METAL CARBONYLS 8

1.6 THE C-O FACTORED FORCE FIELD 11

SECTION ONE: THE PHOTOCHEMISTRY OF SOME DINUCLEAR GROUP TRANSITION METAL CARBONYL COMPLEXES. 8

INTRODUCTION 13

THE EIGHTEEN ELECTRON RULE 15

BONDING MODES IN METAL CARBONYLS 15

CYCLOPENTADIENYL COMPLEXES 18

THE PHOTOCHEMISTRY OF DINUCLEAR METAL CARBONYLS 19

POLARISED PHOTOCHEMISTRY OF DINUCLEAR METAL CARBONYLS 20

CHAPTER 2: THE PHOTOCHEMISTRY OF THE CYCLOPENTADIENYL CARBONYL DIMERS OF PLATINUM AND NICKEL

2.1 INTRODUCTION 24

2.2 THE MATRIX PHOTOCHEMISTRY OF $(CpPt(CO))_2$ 32

Photolysis of $(CpPt(CO))_2$ in Argon Matrices 32

Photolysis of $(CpPt(CO))_2$ in N_2 Matrices 35

Photolysis of $(CpPt(CO))_2$ in CO Matrices 37

2.3 THE MATRIX PHOTOCHEMISTRY OF $(Cp^*Pt(CO))_2$ 40

Photolysis of $(Cp^*Pt(CO))_2$ in Argon Matrices 40

Photolysis of $(Cp^*Pt(CO))_2$ in N_2 Matrices 42

Photolysis of $(Cp^*Pt(CO))_2$ in CO Matrices 43

2.4 ^{13}CO ISOTOPIC ENRICHMENT STUDIES ON $(Cp^*Pt(CO))_2$ 47

2.5 STRUCTURAL CHARACTERISATION OF $Cp^*_2Pt_2(u\text{-}CO)$ 53

Polarised Photochemistry of $(Cp^*Pt(CO))_2$ 55

The Electronic Ground State of $(\eta^5\text{-}C_5R_5)_2Pt_2(\mu\text{-}CO)$ 58

2.6 FLASH PHOTOLYSIS OF $((\eta^5\text{-}C_5R_5)Pt(CO))_2$ 61

2.7 THE MATRIX PHOTOCHEMISTRY OF $(CpNi(\mu\text{-}CO))_2$ 64

Photolysis of $(CpNi(\mu\text{-}CO))_2$ in Argon Matrices 65

Photolysis of $(CpNi(\mu\text{-}CO))_2$ in N_2 Matrices 67

Photolysis of $(CpNi(\mu\text{-}CO))_2$ in CO Matrices 71

2.8 STRUCTURAL CHARACTERISATION OF $Cp_2Ni_2(CO)$ 79

Polarised Photochemistry of $(CpNi(\mu\text{-}CO))_2$ 80

2.9 FLASH PHOTOLYSIS OF $(CpNi(\mu\text{-}CO))_2$ 82

2.10 DISCUSSION 83

2.11 CONCLUSIONS 85

CHAPTER 3: THE PHOTOCHEMISTRY OF DINUCLEAR OSMIUM CARBONYL COMPLEXES

3.1 INTRODUCTION 87

3.2 THE MATRIX PHOTOCHEMISTRY OF DINUCLEAR OSMIUM CARBONYL COMPLEXES 94

Photolysis of $Os_2(CO)_9$ in Argon Matrices 94

Photolysis of $Os_2(CO)_8(\mu\text{-}C_2H_4)$ in Argon Matrices 100

Photolysis of $Os_2(CO)_9$ in N_2 Matrices 106

Photolysis of $Os_2(CO)_9$ in CO Matrices 111

Photolysis of $Os_2(CO)_9$ in Methane Matrices 114

3.3 STRUCTURAL CHARACTERISATION OF $Os_2(CO)_8$ 115

Polarised Photochemistry of $Os_2(CO)_9$ 116

The Dichroic IR Spectrum of $Os_2(CO)_9$ After Plane Polarised Photolysis 118

The Dichroic IR Spectrum of $Os_2(CO)_8$ Generated by Plane Polarised Photolysis 120

3.4 ROOM TEMPERATURE SOLUTION AND GAS PHASE IDENTIFICATION OF $Os_2(CO)_8$ 124

Flash Photolysis of $Os_2(CO)_8(\mu\text{-}C_2H_4)$ in Room Temperature Solution 124

$Os_2(CO)_8$ in the Gas Phase 127

3.5 CONCLUSIONS 128

SUMMARY: THE STRUCTURE OF UNSATURATED DINUCLEAR PHOTOPRODUCTS 131

SECTION TWO: THE PHOTOCHEMISTRY OF CYCLOPENTADIENYL IRON DICARBONYL SILYL COMPLEXES

INTRODUCTION 138

CHAPTER 4: THE PHOTOINDUCED DEOLIGOMERISATION OF DISILYL IRON COMPLEXES

4.1 INTRODUCTION 142

4.2 THE MATRIX PHOTOCHEMISTRY OF $FpSiMe_2SiMe_3$ 150

Photolysis of $FpSiMe_2SiMe_3$ in N_2 Matrices 150

Photolysis of $FpSiMe_2SiMe_3$ in Argon Matrices 153

Photolysis of $FpSiMe_2SiMe_3$ in CO Matrices 153

4.3 THE MATRIX PHOTOCHEMISTRY OF $FpSiMe_3$ 154

Photolysis of $FpSiMe_3$ in Argon Matrices 154

Photolysis of $FpSiMe_3$ in N_2 Matrices 154

Discussion 157

4.4 FLASH PHOTOLYSIS OF Fp-SILYL COMPLEXES 160

Flash Photolysis of $FpSiMe_2SiMe_3$ 160

Flash Photolysis of $FpSiMe_3$ 164

Flash Photolysis of $FpSiMe_2SiMe_3$ or $FpSiMe_3$ in the Presence of PPh_3 167

Discussion 170

4.5 THE ROOM TEMPERATURE SOLUTION PHOTOCHEMISTRY OF Fp-SILYL COMPLEXES 171

Photolysis of $FpSiMe_3$ or $FpSiMe_2SiMe_3$ with no Added Ligands 171

Photolysis of $FpSiMe_3$ or $FpSiMe_2SiMe_3$ in the Presence of added CO 174

Photolysis of $FpSiMe_3$ or $FpSiMe_2SiMe_3$ in the Presence of PPh_3 176

Photolysis of $FpSiMe_3$ or $FpSiMe_2SiMe_3$ in the Presence of Ethylene 178

Photolysis of $FpSiMe_3$ in the Presence of N_2 181

4.6 THE PHOTOCHEMISTRY OF Fp-SILYL COMPLEXES IN LOW TEMPERATURE LIQUID XENON SOLUTION 183

Photolysis of $FpSiMe_3$ in Liquid Xenon 184

Photolysis of $FpSiMe_2SiMe_3$ in Liquid Xenon 186

4.7 DISCUSSION 190

The Primary Photochemistry of $FpSiMe_2SiMe_3$ 191

The Oxidative Addition of Covalent Bonds 195

The Reactivity of Si-Si Bonds Towards Unsaturated Transition Metal Complexes 199

The Fate of the $SiMe_2$ Fragment 204

4.8 CONCLUSIONS 208

CHAPTER 5: THE PHOTOCHEMISTRY OF DISILYL IRON COMPLEXES CONTAINING β-SILYL HYDROGENS

5.1 INTRODUCTION 209

5.2 THE PHOTOCHEMISTRY OF $FpSiMe_2SiMe_2H$ 213

Photolysis of $FpSiMe_2SiMe_2H$ in N_2 Matrices 213

Flash Photolysis of $FpSiMe_2SiMe_2H$ 215

Photolysis of $FpSiMe_2SiMe_2H$ in Liquid Xenon 217

Discussion 218

5.3 THE PHOTOCHEMISTRY OF $FpSiH_2SiH_3$ 222

Flash Photolysis of $FpSiH_2SiH_3$ 222

5.4 CONCLUSIONS 226

THE PHOTOCHEMISTRY OF CYCLOPENTADIENYL IRON DICARBONYL SILYL COMPLEXES:

SUMMARY 227

CHAPTER 6: EXPERIMENTAL TECHNIQUES

6.1	THE MATRIX ISOLATION APPARATUS	229
	Matrix Deposition	231
	The Matrix Cryostat for MCD Spectroscopy	237
6.2	LIQUID NOBLE GAS TECHNIQUES	238
6.3	FLASH PHOTOLYSIS/FAST TRIR SPECTROSCOPY	238
6.4	ROOM TEMPERATURE SOLUTION PHOTOCHEMISTRY	239
6.5	INFRARED SPECTROSCOPY	240
	Dispersive Spectrometer	240
	Fourier Transform Spectrometers	241
	Theory of FTIR Spectroscopy	243
	Advantages of FTIR Spectroscopy	246
6.6	UV/VIS SPECTROSCOPY	249
6.7	PHOTOLYSIS SOURCES	250
6.8	POLARISED PHOTOCHEMISTRY	251
6.9	CHEMICALS	254

REFERENCES 255

CHAPTER 1

INTRODUCTION

1.1 PREFACE

Chemical intermediates are highly reactive molecules which have a fleeting existence during chemical reactions. When a new reaction is reported in the chemical literature, the mechanism by which it occurs is frequently the subject of considerable debate. Many proposed mechanisms contain one or more intermediate species, via which the process is thought to occur. If the evolution of a chemical reaction is to be properly understood, the intermediates involved must be identified and characterised.

Organometallic Chemistry continues to grow at an exponential rate. The long term aims of many projects in this field are directed towards catalysis or the activation of small molecules. Many thermal reactions of organometallic compounds are considered to proceed via unstable intermediate species. Observation of such molecules during a thermal process can sometimes be achieved using the stopped flow method. However, it is often possible to generate the same reactive intermediates involved in thermal reactions using photochemical methods (Wrighton 1979). Absorption of a

photon of light of the necessary energy can cause bond dissociation and production of highly unstable fragments which react in various ways, depending upon the conditions. It is these reactive molecules which are the subject of the research described in this thesis.

Intermediates are discrete molecules, with measurable physical and chemical properties. Low temperature methods are commonly employed to reduce the rate at which unstable species decay, thus allowing observation. An alternative approach is to monitor an intermediate in "real time" under ambient conditions, using fast detection.

All the compounds studied in this work contain carbonyl ligands coordinated to a transition metal atom. Both mononuclear and dinuclear systems have been studied, some containing ligands other than CO. The background of each molecule under research is given in the appropriate section.

The Introduction to this Thesis describes the general approaches used in the identification of intermediates in organometallic photochemistry. The reasons why infrared spectroscopy is such a useful tool for the study of transition metal carbonyl complexes are also explained.

1.2 MATRIX ISOLATION

Matrix isolation is well established as an important technique for the study of highly reactive molecules. The lifetimes of such species can be extended almost indefinitely, by trapping them in a large excess of an inert solid at low temperature. Provided that the solid matrix is sufficiently rigid, the isolated species will be unable to diffuse, and is thus prevented from reacting with other species in the matrix. The recent Voyager II mission has revealed an interesting example of matrix isolation on a planetary scale! Parts of the surface of Tritan, a moon of Neptune, have a bright pink colouration. This is explained by the presence organic molecules, generated by high energy cosmic irradiation of methane, trapped in solid nitrogen on the cold surface.

Under experimental conditions, the matrix material employed is a commonly a frozen inert gas such as argon or xenon, but more reactive frozen gases, such as N_2, CO and CH_4, are also frequently used as the host lattice. Solid noble gases are transparent over the entire infrared spectrum. IR bands of trapped species are generally very narrow, which is essential for structural determination using isotopic enrichment. However, frozen noble gases evaporate at low temperature (40 K for argon), so it is impossible to monitor thermal reactions by warming the matrix to room

temperature. This problem can be avoided by using frozen hydrocarbon glasses (Hepp 1984) or cast polymer films (Hooker 1986) as the matrix host. However, both glasses and films possess IR absorptions which mask regions of the spectrum, and IR bands of isolated molecules are generally broader than in frozen gases. Reaction of unstable molecules with the host material can also lead to problems.

Matrix isolation has proved extremely useful in the study of organometallic photochemistry (Hitam 1984, Almond 1989). First, a stable molecule is isolated in a large excess of an inert solid at low temperature. Unstable fragments are generated by irradiation of the matrix. Highly reactive photoproducts, which would decay rapidly at room temperature, can be trapped under these conditions and studied at leisure. A variety of spectroscopic techniques are available with which to study matrix isolated species. The most important of these are Infrared and UV/Visible spectroscopy, but Raman, Electron Spin Resonance (ESR), Magnetic Circular Dichroism (MCD) Fluorescence and Mossbauer spectroscopy have also been successfully applied to organometallic systems.

The determination of molecular structures of reactive intermediates using matrix isolation is a useful exercise, both in the development of bonding theories such as the isolobal analogy, and in the

understanding of the mechanisms by which chemical reactions occur.

However, the special environment of a low temperature matrix places limitations on the information that can be gathered using this method. The restricted temperature range means that very little kinetic data is available. Also, the rigid crystal lattice of the solid matrix can cut off particular photochemical routes. For example, it is known that photolysis of $Mn_2(CO)_{10}$ in solution can lead to CO loss or Mn-Mn cleavage (Church 1984). However in low temperature matrices, only $Mn_2(CO)_9$ can be generated, with no evidence for $Mn(CO)_5$ (Hepp 1983). It is thought that the bulky radicals are forced to recombine rapidly within the matrix cage.

The "cage effect" can, however, be a useful ally. Since bulky molecules are prevented from reorientation, the use of plane polarised light for photolysis and spectroscopy can give valuable information relating to the direction of UV and IR transition moments of matrix isolated species. This knowledge helps in structural characterisation of both reactants and products (Dunkin 1984, Fletcher 1985, 1986).

1.3 ORGANOMETALLIC PHOTOCHEMISTRY IN LIQUID NOBLE GASES

Liquid noble gases provide an excellent medium in which to study the photochemistry of organometallic systems (Upmacis 1986, Jackson 1988). The lifetime of an unstable molecule with a significant barrier to reaction can be extended by the use of a low temperature noble gas as a solvent. Variable temperature experiments can provide kinetic data, giving rate constants, and activation energies. Truly unsaturated complexes with vacant coordination sites are too unstable to be observed in liquid xenon. However this medium is ideal for the study of coordinatively saturated molecules which happen to be unstable at room temperature. The characterisation of dihydrogen complexes (e.g. $Cr(CO)_5)(H_2)$) has provided a particularly interesting avenue of research (Upmacis 1986, Jackson 1988).

Liquid noble gases do not absorb light in the IR region. This allows a long pathlength solution cell to be used, allowing the detection of very weak IR absorption bands of dissolved species. The quality of FTIR spectra obtained from liquid xenon solutions is of a very high standard. For example, the ν(HH) band of coordinated H_2 in $Cr(CO)_5)(H_2)$ can be detected. Using a high pressure cell, high concentrations of dissolved gases can be added to the liquid xenon (e.g. N_2, H_2 and

C_2H_4) allowing production of large yields of complexes containing these species as ligands.

1.4 FLASH PHOTOLYSIS; TIME-RESOLVED IR SPECTROSCOPY

Matrix isolation and liquid xenon solutions are low temperature techniques, which rely on the stabilisation of reactive molecules for conventional spectroscopic analysis. By contrast, flash photolysis is generally a room temperature method. In a flash photolysis experiment, the solution is irradiated with a short pulse of light to generate transient species, the spectra of which are detected using a rapid detection system. This enables the decay kinetics of photoproducts to be studied, giving an insight into reaction mechanisms.

Conventional flash photolysis involves detection in the UV/visible region. The electronic absorptions of photoproducts formed in room temperature solution can thus be compared with those observed in low temperature matrices. However, the UV/visible bands of organometallic species are generally broad and featureless and give little structural information. A more recent innovation involves flash photolysis coupled with fast detection of transients in the IR region (Dixon 1986, Poliakoff 1986). This allows direct comparison of the IR spectra of photoproducts in

room temperature solution and low temperature matrices. This method is particularly useful in the characterisation of metal carbonyl intermediates, since the intense ν(CO) bands of such species are rich in structural information.

1.5 INFRARED SPECTROSCOPY OF METAL CARBONYLS

Infrared spectroscopy is the most widely used technique for determining the structure of transition metal carbonyl fragments. The vibrational modes of an M-C-O system, and the region of the IR spectrum in which each absorbs are given below.

Vibrational mode	**Frequency (cm^{-1})**
Terminal C-O stretch	2150 - 1850
Bridging C-O stretch	1850 - 1700
M-C-O bend	700 - 500
M-C stretch	500 - 300
C-M-C bend	250 - 50

(These frequencies apply to neutral molecules).

The table above indicates that the C-O stretching frequencies are well removed from those of other fundamental vibrations. This means that to a first approximation, coupling between ν(CO) vibrations and other vibrational modes can be ignored. This makes the

ν(CO) region of the IR spectrum extremely useful when assigning structures for metal carbonyl fragments. In addition, ν(CO) modes commonly give rise to sharp, intense absorptions, even though free molecular CO absorbs IR light only weakly. This difference arises from the nature of the bonding in transition metal carbonyls. When the C-O bond in such a system stretches, a corresponding decrease in the energy of the CO π^* orbital occurs, bringing it closer in energy to the metal d-orbitals. Subsequent electron drift from the metal into the CO π^* orbital leads to a relatively large dipole moment change and therefore, intense ν(CO) bands in the IR spectrum. This phenomenon is known as orbital following.

The ν(CO) region of the IR spectrum provides three principal pieces of information, namely the frequency, number and relative intensity of bands. Each of these properties can help in structural determination.

Frequency: The frequency of ν(CO) absorptions reflects the electron density on the metal atom. High electron density, (e.g. in anionic complexes) leads to increased back bonding from the metal d orbitals to the CO π^* orbital, thus weakening the C-O bond and lowering the C-O stretching frequency.

Bridging CO ligands absorb at lower frequency than terminal CO ligands (see Table above). Essentially

this is because a bridging CO group experiences back donation of electrons from more than one metal atom.

Number of Bands: The number of ν(CO) bands in the IR spectrum of a metal carbonyl fragment can be used to infer its symmetry. Typically, various structures are possible for a particular complex. Group theory is used to predict the number of IR active ν(CO) vibrational modes for each structure on symmetry grounds. Comparison of the observed spectrum with these predictions can allow assignment to a particular point group. However, ambiguities due to weak or coincident bands may prevent definitive assignment. Isotopic substitution, together with force constant calculations can often help in the determination of molecular symmetry. A detailed account of this procedure, along with other points relating to the IR spectra of metal carbonyls, can be found in the work by Braterman (1975).

Relative Intensities: The relative intensities of the ν(CO) bands of a metal carbonyl fragment can be used to calculate the bond angles between carbonyl groups. This procedure is particularly useful when crystal structure determination is impossible (e.g. for an unstable matrix isolated molecule). The determination of bond angles from intensity patterns has been discussed by Burdett (1976).

1.6 THE C-O FACTORED FORCE FIELD

Since the C-O stretching vibrations are, to a first approximation, uncoupled to any other vibrations of the molecule, a very simple force field may be set up to describe them. For any polyatomic molecule, determination of the force field depends on solving the secular equation:

$$\left|G\,F - \lambda E\right| = 0$$

The F matrix is made up of force constants, while the G matrix consists of mass weighted internal coordinates, determined by molecular geometry and the inverse masses of the constituent atoms. The terms in λE then give the fundamental vibrational frequencies of the molecule (Braterman 1975).

The treatment of C-O stretching vibrations as uncoupled harmonic oscillators allows simplification of the equation for metal carbonyls. The G matrix contains no off-diagonal terms, since no pair of CO groups have a common atom. The diagonal terms are simply the reduced masses of the CO groups. The F matrix contains C-O stretching force constants as diagonal terms with CO,CO interaction force constants in the off-diagonal positions. The observed ν(CO) frequencies can, therefore, in principle be used to calculate the force field and hence the structure of

the molecule. The problem can only be solved in practice if the number force constants does not exceed the number of observed frequencies. Isotopic labelling can be used to increase the number of frequencies. The C-O factored force field, combined with ^{13}CO isotopic enrichment, has been used to determine the structures of many transition metal carbonyl fragments.

During this research, infrared spectroscopy has been combined with matrix isolation, liquid noble gas solvents and flash photolysis, in order to investigate the intermediates involved in the photochemical reactions of organometallic compounds. Each experimental approach has its own characteristic strengths and weaknesses. When these methods are combined, it is possible to gather far more information about a particular system than is available from the application of a single technique.

This Thesis is divided into two sections. Section One is devoted to the photochemistry of dinuclear transition metal carbonyl compounds. In Section Two, the photochemical reactions of several iron silyl complexes is investigated.

Section One

The Photochemistry of some Dinuclear Group 8 Transition Metal Carbonyl Complexes

SECTION ONE

THE PHOTOCHEMISTRY OF SOME DINUCLEAR GROUP 8 TRANSITION METAL CARBONYL COMPLEXES.

INTRODUCTION

A wide variety of compounds containing metal-metal bonds is formed by elements in the d-block of the Periodic Table. The field of transition metal cluster chemistry is the subject of considerable interest, with research being aimed both at the synthesis of new cluster compounds, and the study of their chemical activity.

Polymetallic systems can be considered to model the environment on the surface of a bulk metal. Thus, ligands bonded to a metal cluster can be compared with molecules adsorbed onto a metal surface. It is hoped that a knowledge of the interactions of metal clusters with small molecules will lead to a greater understanding of the processes involved in catalytic systems, and may lead to the development of improved catalysts.

The simplest examples of polymetallic systems are those where only two metal atoms are involved. A multitude of dinuclear transition metal complexes is known to exist, many with the metal atoms in low

positive, zero or negative oxidation states. Such complexes often contain ligands such as carbon monoxide, isonitriles and phosphines, which can stabilise low oxidation states by accepting electron density from the metal atoms into vacant ligand π orbitals. This prevents the build up of electronic charge on the metal, caused by donation from ligand σ orbitals.

The presence of CO as a ligand in these complexes is frequently encountered. Those transition metals known to form coordinatively saturated homodinuclear complexes, $M_2(CO)_n$, are listed below.

n	12	11	10	9	8	7	6
	V*	-	Mn	Fe	Co	Ni*	Cu*
	-	-	Tc	Ru	Rh*	-	Ag*
	-	-	Re	Os	Ir*	-	-

* Unstable at room temperature. Evidence for these complexes has been obtained, principally, by deposition of CO matrices containing high metal atom concentrations (Hanlan 1974, Huber 1975, Kundig 1975, Ford 1976, McIntosh 1976).

The list of saturated binary dinuclear metal carbonyls can be extended by the inclusion of heteronuclear systems, such as $MnRe(CO)_{10}$.

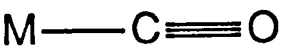
THE EIGHTEEN ELECTRON RULE

All the dinuclear complexes shown in the table above possess a single metal-metal bond, and obey the 18 electron rule for transition metal complexes. This requires that for each metal atom, the sum of the electrons donated by ligands, plus the valence electron count of the metal atom, is equal to the number of electrons in the valence shell of the succeeding noble gas atom, i.e. eighteen. A metal-metal bond is considered to add one electron to the count of each metal atom in this system. The rule is widely applicable to stable transition metal complexes, but exceptions do exist (e.g. $V(CO)_6$, a 17 electron species).

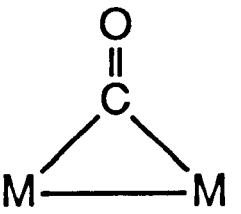
BONDING MODES IN METAL CARBONYLS

There are several ways in which CO ligands can be bonded to polymetallic systems:

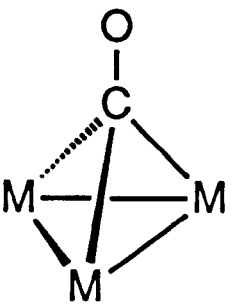
1) Bonded to one metal atom as a terminal CO group, as in a mononuclear complex:



2) Bonded to two metal atoms as a doubly bridging μ^2-CO group:

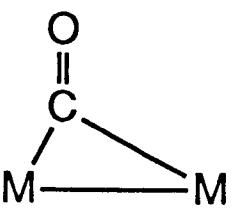


3) Bonded to three metal atoms as a triply bridging μ^3-CO group:



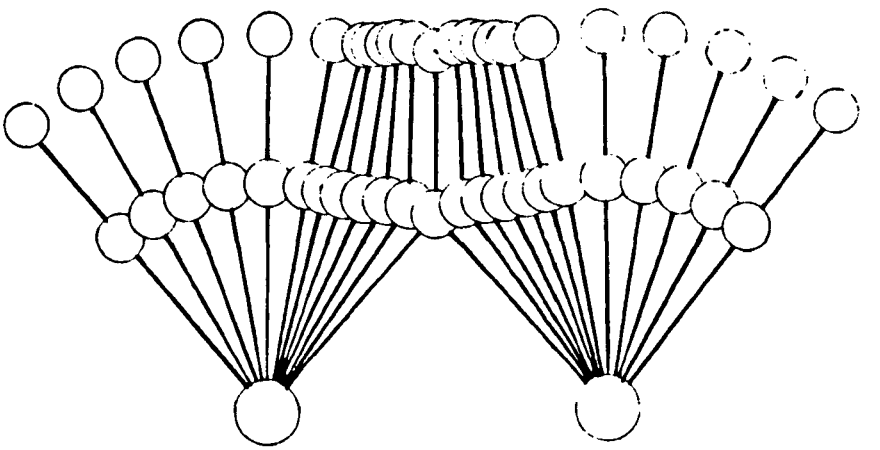
In addition, there are several structural variations on the μ^2-CO ligand. The CO ligand shown in (2) above bridges the two metal atoms in a symmetrical fashion. However, some compounds contain asymmetrical bridging CO ligands:

a) The bent semibridging CO group:



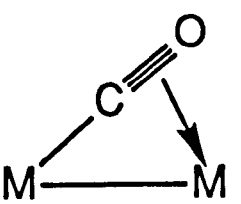
In this structure, the two M-C bonds differ in

length, but the C-O orientation remains approximately perpendicular to the M-M bond. A detailed analysis by Crabtree (1986) showed that the bent semibridging CO group forms part of a smooth reaction trajectory in terminal-bridge-terminal carbonyl exchange between two metal atoms, as illustrated below.



(Adapted from Crabtree 1986)

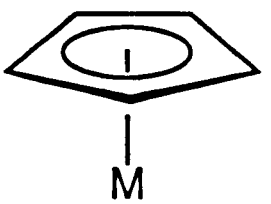
b) The linear semibridging μ-η^1,η^2-CO group.



A carbonyl group in this bonding mode can be considered to be a four electron donor. It is $\eta^1(\sigma)$-bonded to one metal atom and $\eta^2(\pi)$-bonded to the other (c.f η^2-olefin coordination). This structural type contains several sub-categories depending on the two metals involved (Crabtree 1986).

CYCLOPENTADIENYL COMPLEXES.

The variety of dinuclear metal carbonyls is greatly enhanced when one considers compounds containing ligands other than CO. One ligand of particular interest is the η^5-C_5H_5 (Cp) ring, first encountered in the sandwich molecule, ferrocene. In complexes, the Cp ring is coordinated to the metal atom through delocalised π-bonds such that each carbon atom is equidistant from the metal atom.



Since the preparation of ferrocene, a large number of transition metal cyclopentadienyl complexes have been produced, including a series of metal carbonyl dimers containing this ligand. Perhaps the most widely known is the iron dimer, $(CpFe(CO)_2)_2$. The properties of cyclopentadienyl compounds can be adjusted by introducing substituents on the Cp ring. For instance, the η^5-C_5Me_5 (Cp^*) ring can often be used to increase solubility for a given system.

THE PHOTOCHEMISTRY OF DINUCLEAR METAL CARBONYLS

A rich photochemistry exists for dinuclear transition metal carbonyl compounds. Previous studies have shown that two primary photochemical processes are generally observable, both for binary carbonyls and cyclopentadienyl systems:

1) M-M cleavage, leading to formation of highly reactive 17 electron metal centred radicals.

$$L_n(CO)_xM\text{-}M(CO)_xL_n \longrightarrow 2\ L_n(CO)_xM^{\cdot}$$

These mononuclear radicals can recombine or participate in further reactions. For example, in chlorinated solvents, chlorine abstraction to give $L_n(CO)_xMCl$ can occur.

2) CO loss, resulting in formation of a coordinatively unsaturated dinuclear photoproduct

$$(L_nM(CO)_x)_2 \longrightarrow L_{2n}M_2(CO)_{2x-1} + CO$$

The unsaturated species can recombine with CO or react with other potential ligands such as phosphines or isonitriles.

In inert low temperature matrices, CO-loss is generally the only observable process. However

mononuclear products can sometimes be trapped by reaction with a more reactive matrix host such as CO.

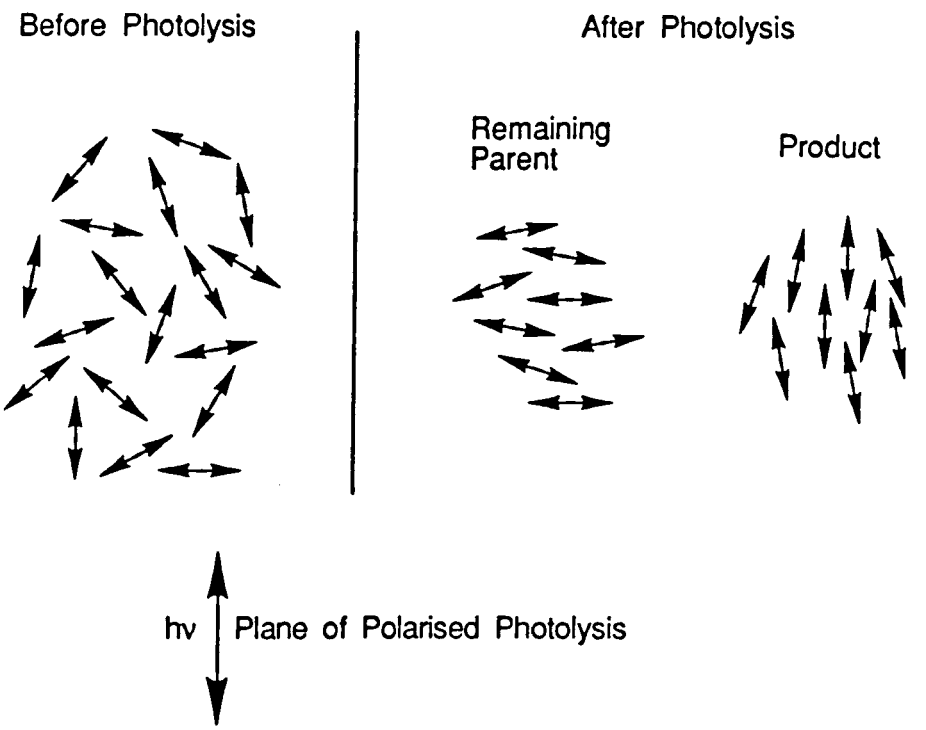
POLARISED PHOTOCHEMISTRY OF DINUCLEAR METAL CARBONYLS.

Matrix isolation has proved an excellent method for the generation and characterisation of unstable photoproducts from dinuclear metal carbonyls. A refinement of this technique which provides greater structural information is the use of polarised light, for both photolysis and spectroscopy. Polarisation studies of this type have been used for several unstable metal carbonyls in low temperature matrices, including $Cr(CO)_5$ (Perutz 1974, Burdett 1975, 1978), $Fe(CO)_4$ (Davies 1977), $Mn_2(CO)_9$ (Dunkin 1984) and $Re_2(CO)9$ (Firth 1987) $Fe_2(CO)_8$ (Fletcher 1985, 1986).

Polarised photochemistry relies on the low thermal energy possessed by matrix isolated species. This means that the thermal rotation of large molecules within the matrix cage is prevented. Under normal circumstances, a matrix isolated sample will show random orientation, but irradiation using plane polarised light can lead to the production of partially oriented samples of both parent and photoproduct. This is because only those molecules with the correct orientation are able to absorb a photon of light and so undergo a photochemical reaction. The probability of

absorption of light by a molecule is proportional to $\cos^2\theta$, where θ is the angle made between the plane of polarisation of the incident light and the direction of the photoactive transition moment. Thus, no light is absorbed by molecules for which $\theta = 90^\circ$.

The effect of plane polarised photolysis is illustrated schematically below.



The arrows represent the directions of the photoactive transition moments of individual molecules in a low temperature matrix. Before irradiation, these exhibit random orientation. Preferential absorption by molecules of particular orientation then leads to partially aligned samples of parent and photoproduct.

The presence of such alignment can be detected by recording spectra with polarised light. For a particular sample, two spectra are recorded, through a polariser oriented either parallel or perpendicular to the plane of photolysis. If there is a difference in absorption intensities between these two spectra, then the sample is said to exhibit LINEAR DICHROISM, which indicates a preferred orientation of molecules. (A randomly oriented sample will not show any linear dichroism).

There are several other terms which describe the phenomena observed in polarised photochemistry:

a) Linear dichroism in the absorption bands of the parent compound is known as DICHROIC PHOTODEPLETION.

b) Linear dichroism in the absorption bands of a photoproduct is known as DICHROIC PHOTOPRODUCTION. If the photoproduct is rigidly held in the matrix, with a transition moment in the same direction as the starting material, then the product will display dichroism which is in the opposite sense to that of the remaining parent molecules.

c) Excitation by a photon of light can lead to reorientation of the molecule, which is then held rigid in the matrix. This will lead to an accumulation of molecules in a position that is

blind to the photolysing source. This is known as DICHROIC REORIENTATION and the resulting spectra display linear dichroism. The dichroism can be reversed by rotating the plane of photolysis by 90°.

Observation of linear dichroism caused by any of these phenomena can give information about the orientation of the transition moment for individual absorptions, relative to the geometry of the molecule. Thus, the ability to assign spectral features is greatly enhanced.

In Section One of this Thesis, the photochemistry of several dinuclear complexes is considered in detail. Chapter 2 deals with the cyclopentadienyl carbonyl dimers of platinum and nickel, $(CpM(CO))_2$. Chapter 3 covers the quite recently synthesised $Os_2(CO)_9$ and a related complex with a bridging ethylene ligand, $(\mu\text{-}\eta^1,\eta^1\text{-}C_2H_4)Os_2(CO)_8$.

In both of these studies, matrix isolation has proved to be an essential tool in establishing the primary photochemical processes. In each case polarised photochemistry has been applied in the structural characterisation of photoproducts.

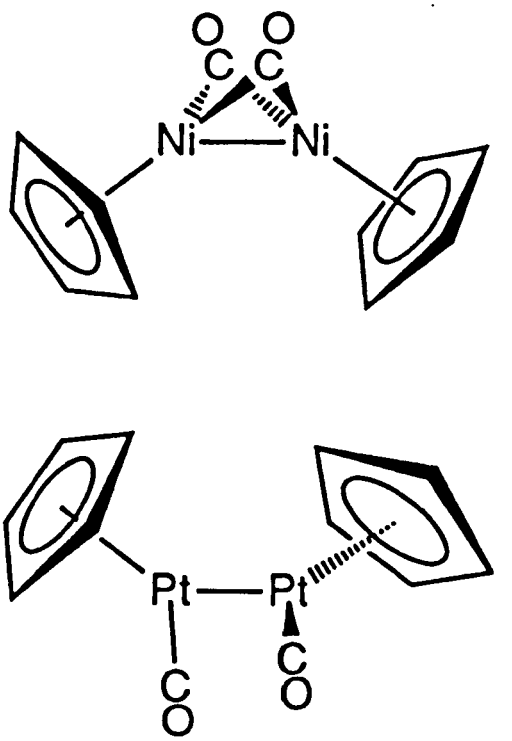
CHAPTER 2

THE PHOTOCHEMISTRY OF THE CYCLOPENTADIENYL CARBONYL DIMERS OF PLATINUM AND NICKEL

2.1 INTRODUCTION

The photochemistry of dinuclear transition metal cyclopentadienyl carbonyl complexes has recently been the subject of extensive investigation (Meyer 1985, Hooker 1986). The dimers $((\eta^5\text{-}C_5R_5)M(CO)_n)_2$ (R = H, Me; n = 3, M = Cr, Mo, W; n = 2, M = Fe, Ru), have received particular attention, both in solution and in low temperature matrices. However, the photochemistry of the closely related compounds of nickel and platinum, $((\eta^5\text{-}C_5R_5)M(CO))_2$, has been relatively neglected.

The cyclopentadienyl complexes, $(CpM(CO))_2$ (M = Ni, Pt), were originally prepared by Fischer (1958, 1963). The bonding mode of the carbonyl groups in these dinuclear complexes differs according to the particular metal involved, as illustrated below.



When M = Ni, the two carbonyl groups bridge the Ni-Ni bond symmetrically. The solution IR spectrum exhibits two bridging ν(CO) bands, indicative of a non linear dicarbonyl system with a C_{2v} structure (Mcardle 1971). This was confirmed by an X-ray diffraction study which showed that in the solid state, $(CpNi(CO))_2$ consists of two independent molecules with differently bent $Ni_2(\mu\text{-}CO)_2$ cores (Byers 1980). The IR spectrum of $(Cp'Ni(\mu\text{-}CO))_2$ ($Cp' = \eta^5\text{-}C_5H_4Me$) shows that it has a similar C_{2v} structure in solution, but in this case the X-ray structure reveals a planar $Ni_2(\mu\text{-}CO)_2$ unit in the crystalline state. The analogous palladium complex, $(Cp^*Pd(\mu\text{-}CO))_2$, is temperature sensitive, but is believed to have a planar $Pd_2(\mu\text{-}CO)_2$ unit in solution, on the basis of a single bridging ν(CO) band in its IR spectrum (Boag 1988a).

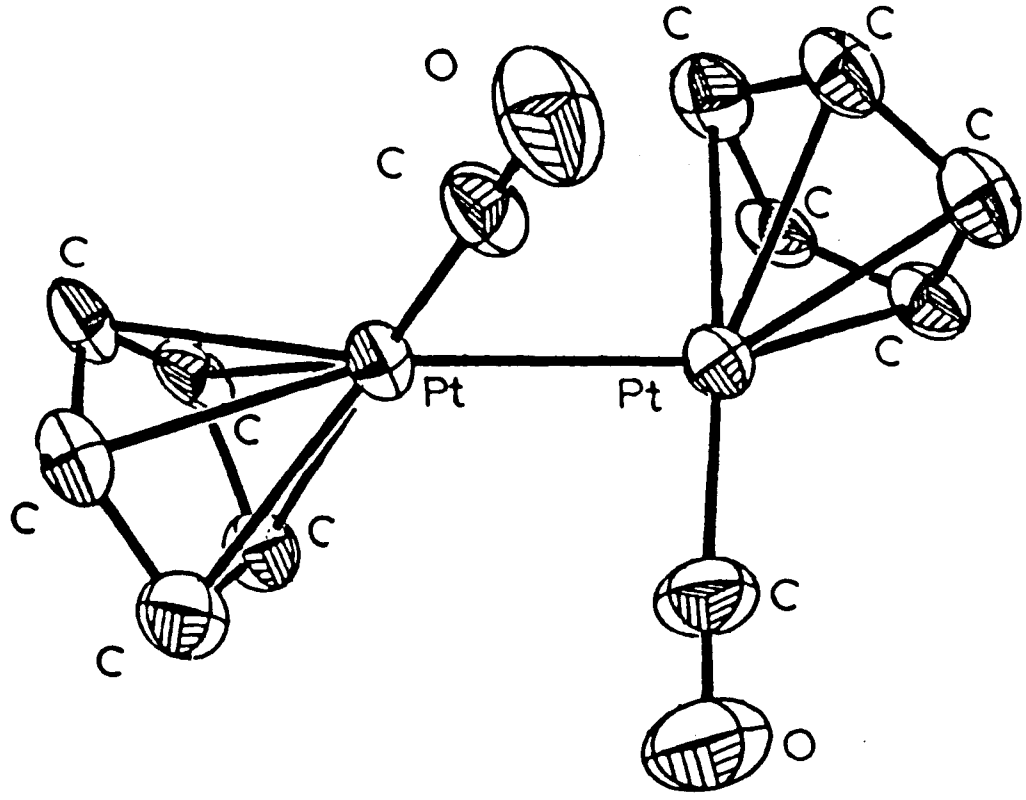


Figure 2.1: A perspective drawing of $(Cp^*Pt(CO))_2$. Methyl groups of the Cp^* rings are omitted for clarity. All atoms are represented by 50% probability ellipsoids (adapted from Boag 1988b).

By contrast, $(CpPt(CO))_2$, and the more recently synthesised complex, $(Cp^*Pt(CO))_2$, each have two terminal CO groups. This is attributable to the longer metal-metal bond for third row transition metal complexes, which makes CO-bridging less favourable. The X-ray structure has been determined for the Cp^* complex and is reproduced in Figure 2.1. The relative orientation of the two terminal Pt-CO bonds in this complex is reminiscent of the two O-H bonds in H_2O_2 with an angle between the two C-O vectors of approximately 105°. The two CO groups are somewhat bent over the Pt-Pt bond (average Pt-Pt-C angle 79.7°), which is relatively long compared with other platinum dimers. This may be due to the steric requirements of the bulky Cp^* ligands. The ^{13}C and ^{195}Pt NMR spectra of both of the platinum dimers show broad features consistent with intramolecular CO site exchange, presumably via the bridged intermediates, $((\eta^5\text{-}C_5R_5)Pt(\mu\text{-}CO))_2$ (R = H, Me) (Boag 1983, 1988b).

The photochemistry of cyclopentadienyl transition metal carbonyl dimers has been shown to be dominated by the CO-loss and metal-metal bond cleavage. For example, flash photolysis of the iron dimer, $(CpFe(CO)_2)_2$, in room temperature hydrocarbon solvents, initiates the reactions shown in Equations 2.1 and 2.2 (Moore 1984, Dixon 1986b, 1987, 1989).

$$(CpFe(CO)_2)_2 \xrightarrow{h\nu} Cp_2Fe_2(\mu\text{-}CO)_3 + CO \qquad 2.1$$

$$(CpFe(CO)_2)_2 \xrightarrow{h\nu} 2\ CpFe(CO)_2 \qquad 2.2$$

The unsaturated dinuclear product arising from CO-loss, $Cp_2Fe_2(\mu\text{-}CO)_3$, reacts with CO, or with added ligands to give species $Cp_2Fe_2(CO)_3L$ (L = phosphine, acetonitrile). The mononuclear metal centred radicals, $CpFe(CO)_2$, are more short-lived and recombine rapidly in solution. In chlorinated solvents such as CCl_4, chlorine abstraction can occur, to give $CpFe(CO)_2Cl$ (Giannotti 1976, Abrahamson 1979). In inert low temperature matrices, only the CO-loss product is observed, presumably due to rapid in-cage recombination of the bulky mononuclear radicals (Hooker 1983, 1986, Hepp 1984). However, in a more reactive CO matrix, evidence for the mononuclear species, $CpFe(CO)_3$, was obtained (Firth 1987b)

The unsaturated dinuclear products which are produced by dissociation of CO from these cyclopentadienyl complexes are often relatively stable, and some can be isolated at room temperature. Crystal structures have been obtained for several of these species, including $Cp^*_2Fe_2(\mu\text{-}CO)_3$ (Blaha 1985). The occurrence and properties of unsaturated dimetal cyclopentadienyl carbonyl complexes, containing formal

M-M multiple bonds, is the subject of a considerable body of research which has recently been reviewed by Winter (1989).

Reports of the photochemical activity of the cyclopentadienyl carbonyl dimers of nickel and platinum, however, are scarce. These complexes have electronic absorption spectra which are comparable with related dinuclear systems. The spectra of $(CpPt(CO))_2$ and $(Cp^*Pt(CO))_2$, shown in Figure 2.2 are very similar, with a shift to longer wavelength for each absorption on moving from the Cp to the Cp^* species. Analogy with related cyclopentadienyl metal carbonyl dimers (Meyer 1985, Stiegman 1984), allows assignment of two lowest energy absorptions as $d\pi \rightarrow \sigma^*$ and $\sigma \rightarrow \sigma^*$ transitions, as indicated in Figure 2.2. Both of these transitions lead to population of the Pt-Pt antibonding σ^* MO, which could cause homolysis of the Pt-Pt bond. In addition, the $d\pi \rightarrow \sigma^*$ transition leads to depopulation of the metal $d\pi$ orbital. This decreases the potential for Pt to CO back donation, possibly causing dissociation of CO. It has been suggested that the the higher energy absorptions involve $M \rightarrow (CO)\pi^*$ charge transfer. The π^* orbitals are M-C antibonding, so excitation of these charge transfer transitions might also lead to M-CO bond cleavage.

Irradiation of a solution containing both of the platinum dimers, $(CpPt(CO))_2$ and $(Cp^*Pt(CO))_2$ is known

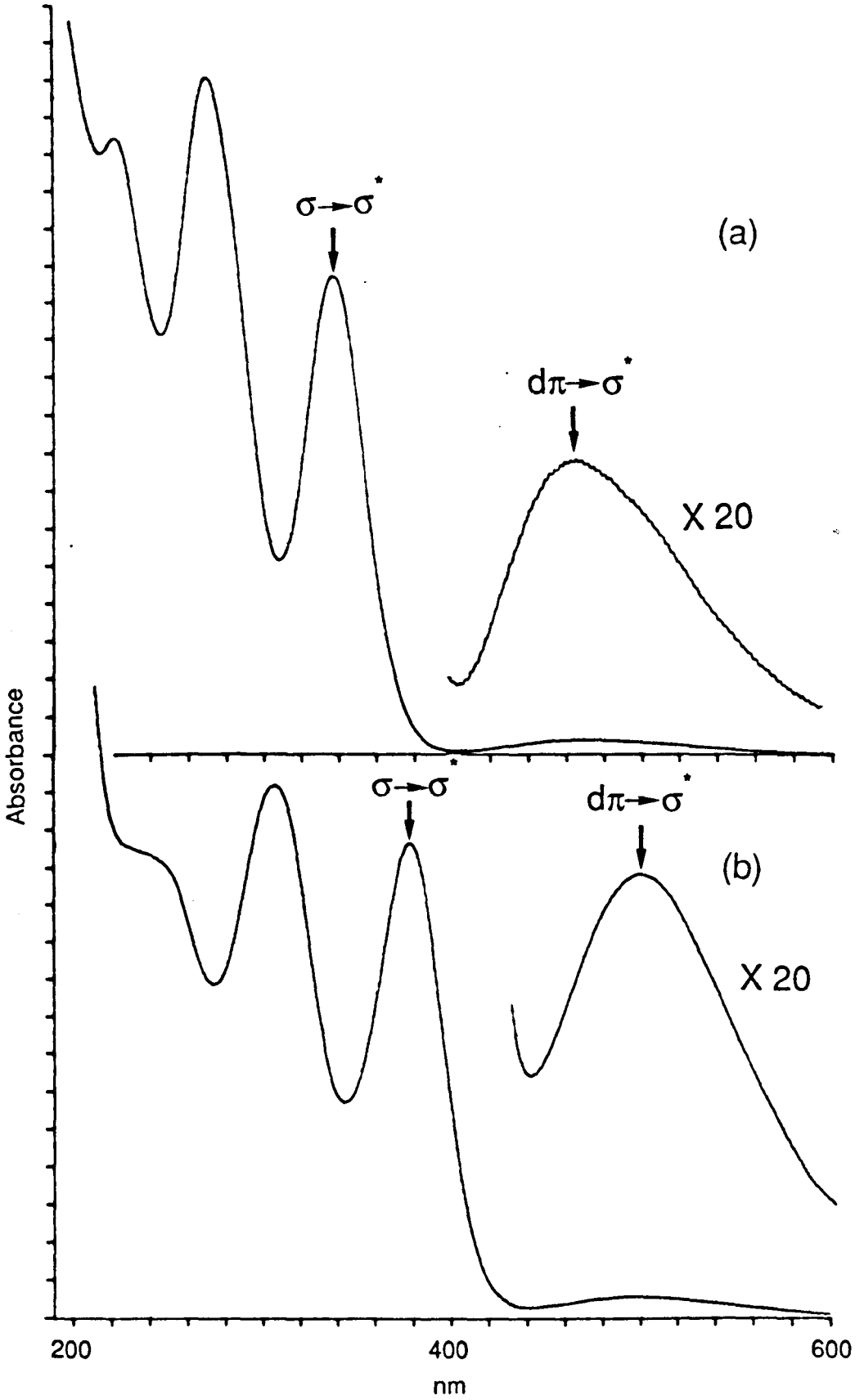


Figure 2.2: Electronic absorption spectra of (a) $(CpPt(CO))_2$ and (b) $(Cp^*Pt(CO))_2$ in cyclohexane at room temperature. The bands assigned as $\sigma \rightarrow \sigma^*$ and $d\pi \rightarrow \sigma^*$ transitions are arrowed. The weak visible absorptions are shown on an expanded absorbance scale.

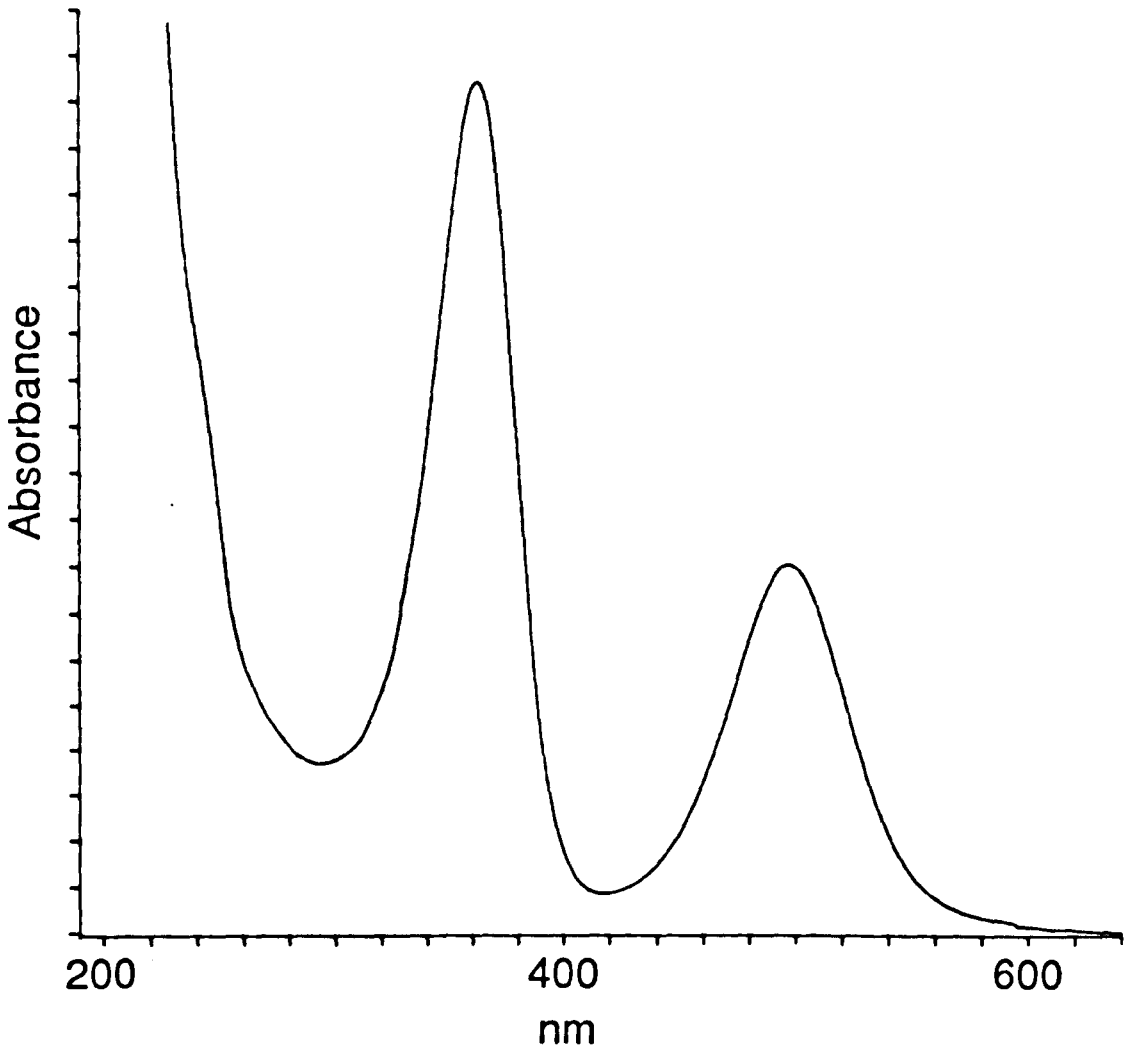
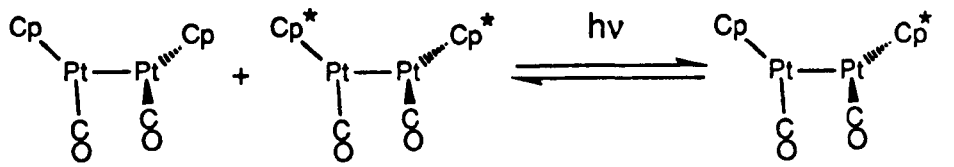


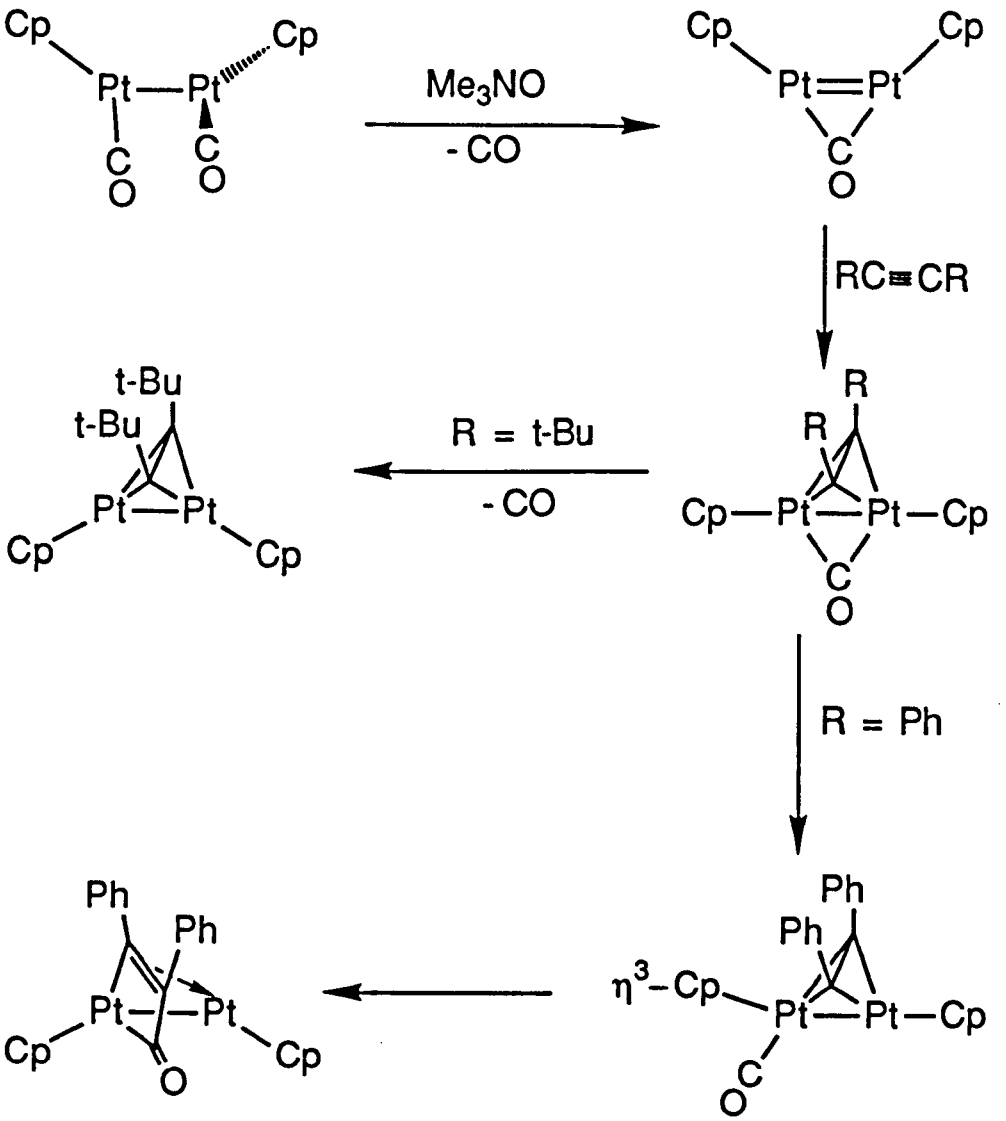
Figure 2.2(c): Electronic absorption spectrum of $(CpNi(\mu\text{-}CO))_2$ in n-heptane solution at room temperature.

to result in the formation of an equilibrium mixture of the starting materials, together with the mixed dimer, $Cp(CO)PtPt(CO)Cp^*$ as shown in Equation 2.3 (Boag 1988b). This reaction is thought to proceed via Pt-Pt bond homolysis, generating the mononuclear radicals, $CpPt(CO)$ and $Cp^*Pt(CO)$, which combine to give the observed product mixture.



2.3

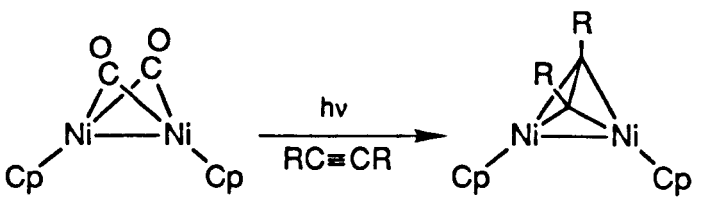
The thermal reaction of $(CpPt(CO))_2$ with alkynes in the presence of trimethylamine oxide is also of relevance to the current study. The mechanism proposed for these reactions is shown in Scheme 2.1 (Boag 1983). The first step involves loss of a CO group from $(CpPt(CO))_2$ to give an unsaturated dinuclear species, $Cp_2Pt_2(\mu\text{-}CO)$. (Me_3NO is known to remove CO ligands from metal carbonyl compounds as CO_2. This step can be regarded as analogous to photochemical CO-loss). The unsaturated product subsequently reacts with a molecule of alkyne, to give a structure containing a bridging CO and a transverse bridging alkyne ligand. With ditert-butylacetylene, the second CO ligand is lost in the final step. With diphenylacetylene, a different



Scheme 2.1: Reaction of $(CpPt(CO))_2$ with alkynes in the presence of Me_3NO (adapted from Boag 1983).

product is obtained, in which the carbonyl group is retained. The CO group is coupled with the alkyne ligand to give a bridging C(Ph)C(Ph)C(O) group.

The electronic absorption spectra of $(CpNi(\mu\text{-}CO))_2$ has absorptions at 362 and 497 nm (Figure 2.2(c)), and might also be expected to exhibit CO loss and M-M bond cleavage as primary photochemical processes. Irradiation of $(CpNi(\mu\text{-}CO))_2$ in the presence of alkynes yields dinuclear species without CO groups (Equation 2.4) (Forbes 1982). These products are isostructural with the platinum species formed by reaction of $(CpPt(CO))_2$ with ditert-butylacetylene, in the presence of Me_3NO (see Scheme 2.1).



2.4

Low temperature studies of the photochemistry of nickel dimers have also been reported. Irradiation of $(CpNi(\mu\text{-}CO))_2$, in a CO matrix leads to generation of small amounts of the mononuclear products, CpNi(CO) and $CpNi(CO)_2$ (Crichton 1977). Photolysis of $(Cp'Ni(\mu\text{-}CO))_2$ in a PVC film at 77 K results in loss of a CO ligand, and production of the unsaturated dinuclear species $Cp'_2Ni_2(\mu\text{-}CO)$.

In this Chapter the results of an investigation into the photochemistry of $(CpPt(CO))_2$, $(Cp^*Pt(CO))_2$ and $(CpNi(\mu\text{-}CO))_2$ are described. Experiments have been carried out both in low temperature matrices, and in solution at room temperature (using fast TRIR spectroscopy). Techniques such as ^{13}CO isotopic enrichment and polarised photochemistry have yielded detailed information about the structure of the photoproducts formed on irradiation of these dimers.

A preliminary account of the studies on the platinum dimers was included as an Appendix to the Ph.D Thesis of Dr. Stephen Firth, whose advice in the early stages of this project is deeply appreciated.

2.2 THE MATRIX PHOTOCHEMISTRY OF $(CpPt(CO))_2$

Photolysis of $(CpPt(CO))_2$ in Argon Matrices

The IR spectrum of $(CpPt(CO))_2$ dissolved in n-heptane at room temperature, shown in Figure 2.3(a), exhibits two bands in the terminal ν(CO) region and none in the bridging ν(CO) region. These absorptions are assigned to the symmetric (high frequency) and antisymmetric (low frequency) C-O stretching modes of the two terminal CO groups of $(CpPt(CO))_2$, assuming a positive interaction force constant between the two CO groups. The IR spectrum of $(CpPt(CO))_2$, isolated in an argon matrix at 20 K, Figure 2.4(a) is identical to the solution spectrum, apart from small shifts in frequency and a slight matrix splitting of one band. In the matrix spectrum, there is an additional weak band at higher frequency due to traces of molecular CO in the matrix, probably originating from slight decomposition of $(CpPt(CO))_2$ under vacuum.

UV irradiation (230-345 nm) of the matrix leads to a decrease in intensity of IR bands of $(CpPt(CO))_2$ and the growth of two new absorptions (coloured black in Figure 2.4(b)). One of these new absorptions occurs near 1815 cm^{-1}, in the region of the IR spectrum where bridging carbonyl groups normally absorb. The other new band, at 2139 cm^{-1}, is much less intense, and is due to an increase in the amount of uncoordinated CO

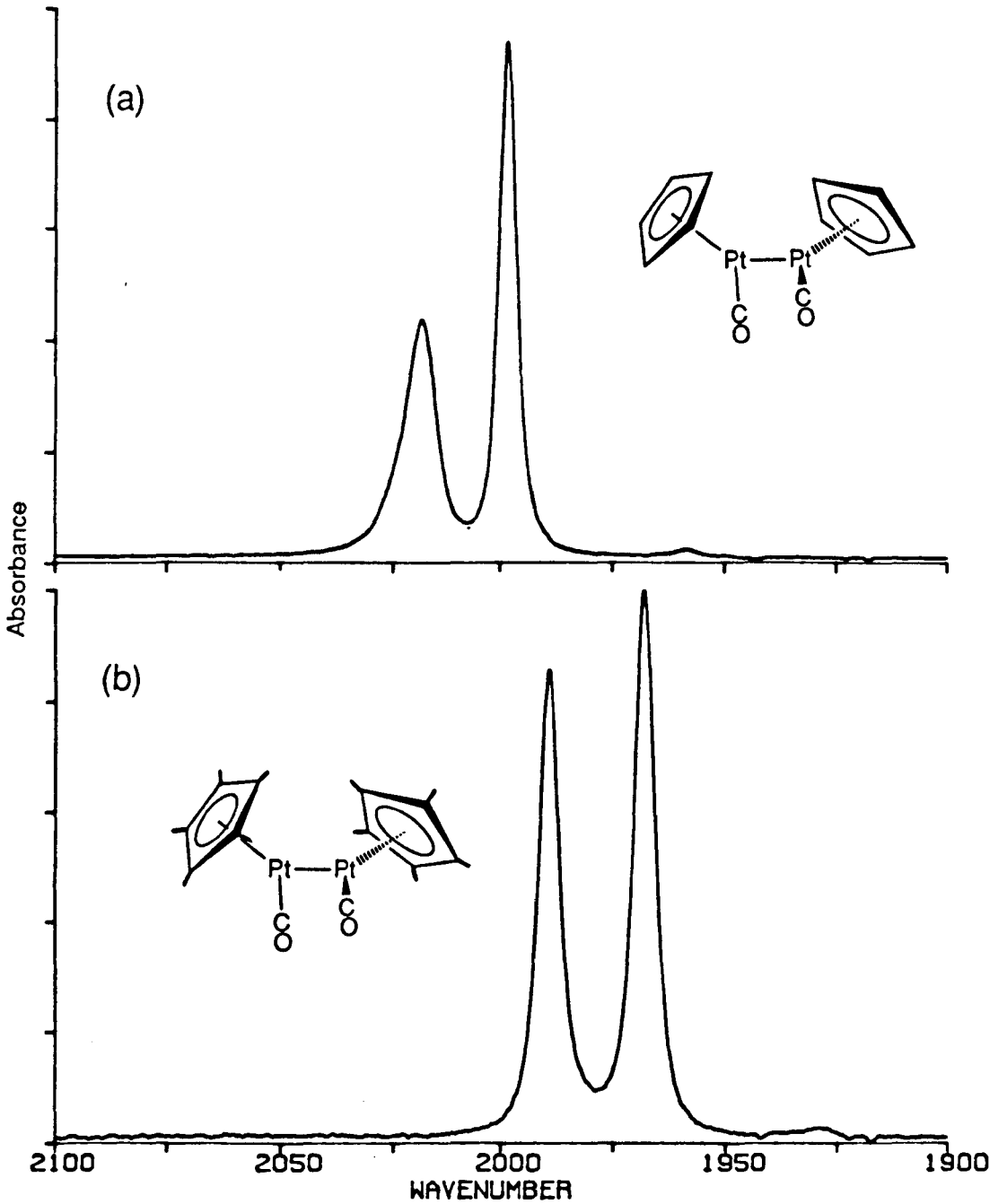


Figure 2.3: IR spectra of (a) $(CpPt(CO))_2$ and (b) $(Cp^*Pt(CO))_2$ in n-heptane solution at room temperature.

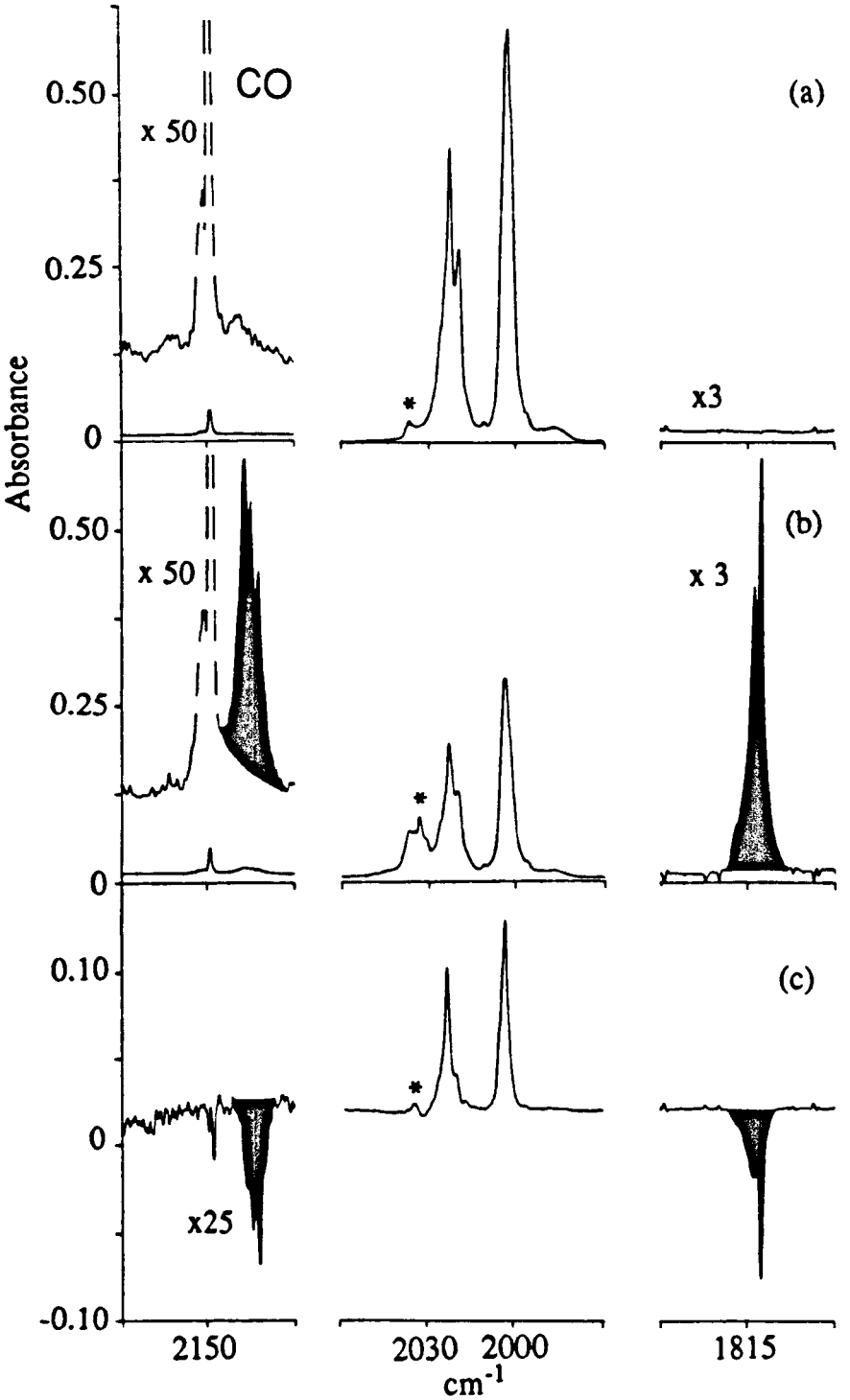


Figure 2.4: (a) IR spectrum of $(CpPt(CO))_2$ isolated in an argon matrix at 20K. The band shown with broken lines is due to matrix isolated CO; the band marked with an asterisk is due to an oligomeric species (this absorption was found to be more intense in experiments where the concentration of $(CpPt(CO))_2$ was high). (b) After 90 mins filtered UV irradiation (230 - 345 nm); bands coloured black are due to CO and $Cp_2Pt_2(\mu\text{-}CO)$. (c) IR difference spectrum showing the effects of 90 mins photolysis with visible light (>400 nm). Note the absorbance scale expansion factors.

present in the matrix.

The changes in the matrix IR spectrum suggest that UV photolysis causes photoejection of CO and production of a photoproduct in which the remaining CO ligand occupies a position bridging the two platinum atoms, as shown in Equation 2.5.

$$(CpPt(CO))_2 \xrightarrow[Ar\ /\ 20\ K]{UV} Cp_2Pt_2(\mu\text{-}CO) + CO \qquad 2.5$$

The IR absorptions of $(CpPt(CO))_2$ and $Cp_2Pt_2(\mu\text{-}CO)$ in both low temperature matrices and room temperature solution are given in Table 2.1.

Crystals and hydrocarbon solutions of the parent complex are purple, due to a weak electronic absorption at 465 nm (see Figure 2.2(a) and Table 2.2), but matrices containing $(CpPt(CO))_2$ appear colourless due to the low intensity of this absorption. However, during UV photolysis the matrix develops a striking pink colour, easily visible to the naked eye after only a few minutes irradiation. A photograph of such a coloured matrix containing is shown in Plate 2.1.

The electronic absorption spectrum of the matrix after UV photolysis shown in Figure 2.5 reveals an intense visible absorption with peaks at 470 and 520 nm

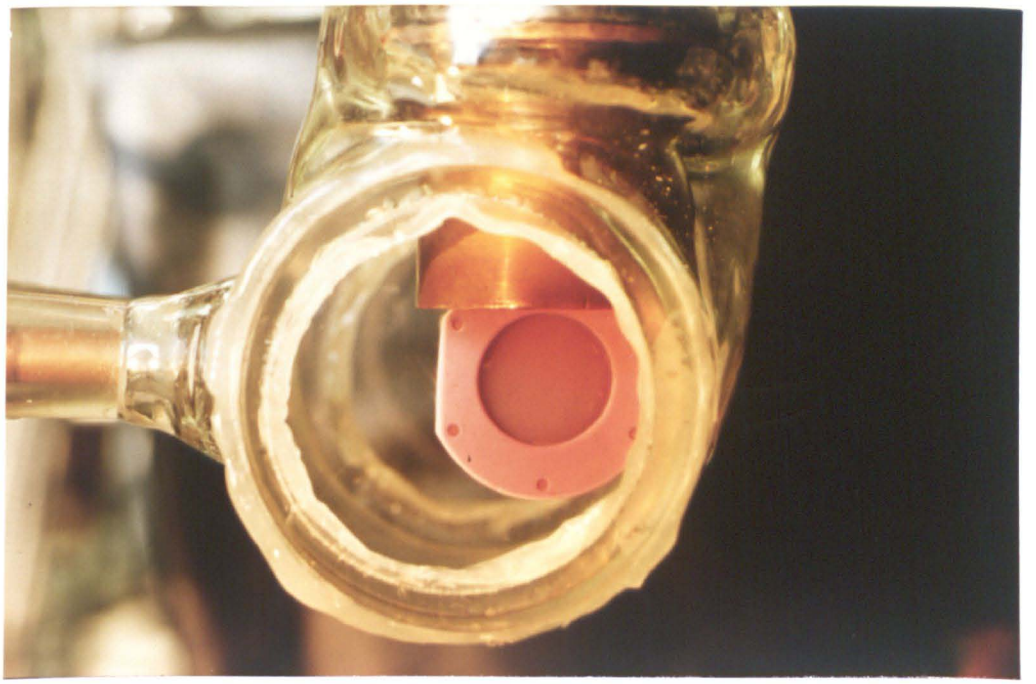


Plate 2.1: A photograph showing the intense colour of $Cp_2Pt_2(\mu\text{-}CO)$, generated by UV photolysis of matrix isolated $(CpPt(CO))_2$.

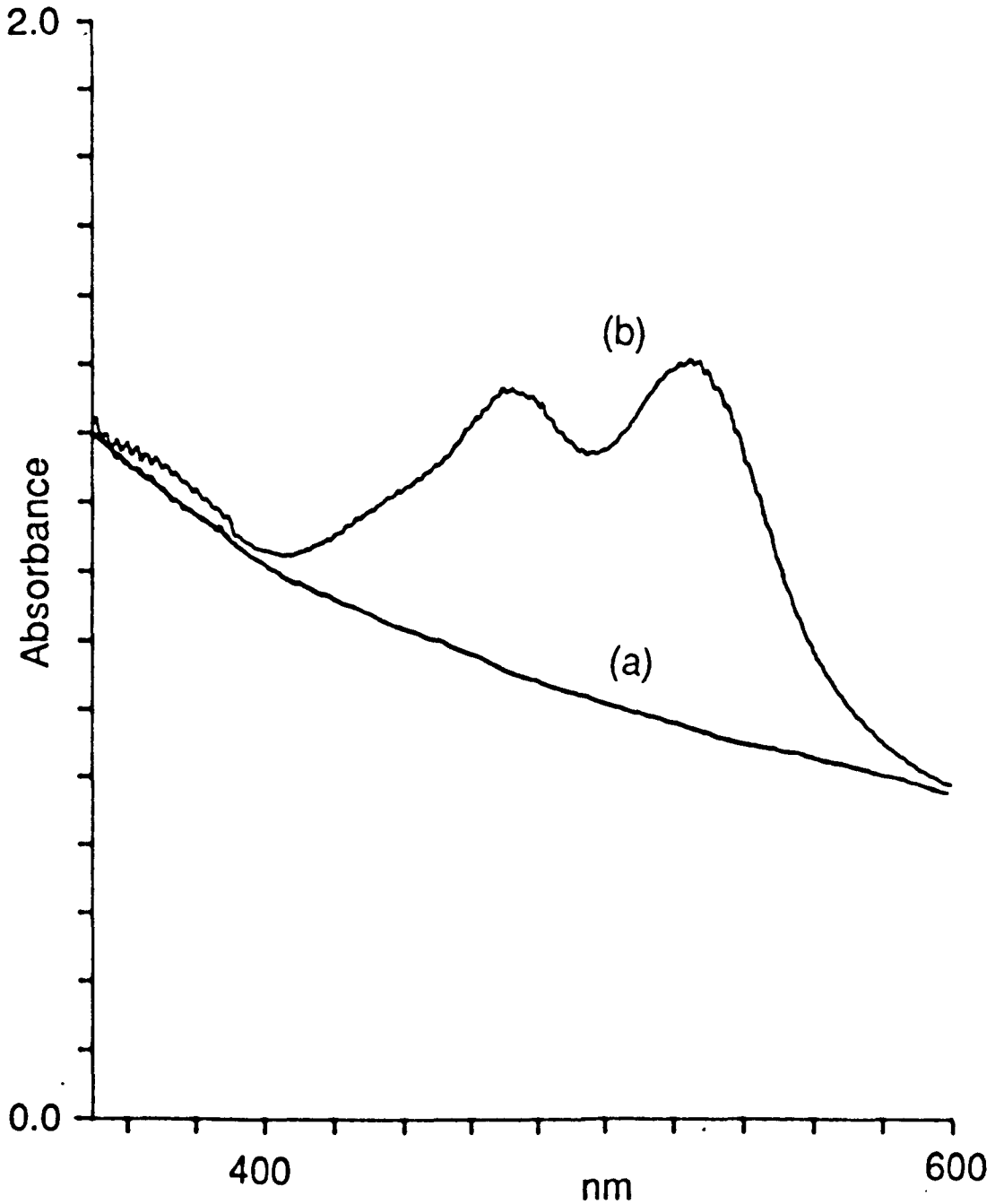


Figure 2.5: Visible spectra (a) before and (b) after 90 mins UV photolysis (230-345 nm) of $(CpPt(CO))_2$ in an argon matrix at 20 K. Note the growth of absorptions due to $Cp_2Pt_2(\mu\text{-}CO)$.

not present before photolysis. These bands grow in intensity at a rate which exactly parallels the growth of the IR band due the bridging CO group of $Cp_2Pt_2(\mu\text{-}CO)$. Thus it is reasonable to assume that the pink colour of the matrix is associated with the same photoproduct.

In several previous studies on the photochemistry of dinuclear transition metal carbonyls, the coordinatively unsaturated dinuclear photoproducts produced by photodissociation of CO have been shown to exhibit electronic absorptions in the visible region. For example, $Cp_2Rh_2(\mu\text{-}CO)_2$, produces strongly purple coloured matrices due to an intense visible absorption at 545 nm (McCamley 1988). Similarly, the unsaturated iron dimer, $Cp_2Fe_2(\mu\text{-}CO)_3$ has an electronic absorption band at 510 nm (Hooker 1983, Hepp 1984). Selective irradiation into this visible absorption was found to cause recombination of the unsaturated species with CO.

Figure 2.4(c) shows an IR difference spectrum illustrating the effect of visible (> 400 nm) irradiation of the matrix containing $Cp_2Pt_2(\mu\text{-}CO)$ (i.e. the spectrum after visible irradiation minus the spectrum before). The two negative peaks, indicate a decrease in the amounts of both $Cp_2Pt_2(\mu\text{-}CO)$ and molecular CO, whilst the positive peaks show regeneration of parent. The visible absorption bands

of $Cp_2Pt_2(\mu\text{-}CO)$ (470 and 520 nm) also decrease in intensity in a similar manner. Clearly, excitation with visible light can promote the recombination of $Cp_2Pt_2(\mu\text{-}CO)$ with CO, Equation 2.6.

$$Cp_2Pt_2(\mu\text{-}CO) + CO \xrightarrow[Ar\ /\ 20\ K]{> 400\ nm} (CpPt(CO))_2 \qquad 2.6$$

Photolysis of $(CpPt(CO))_2$ in N_2 Matrices

Identical photochemistry was observed for $(CpPt(CO))_2$ in an N_2 matrix at 20 K. The IR spectra shown in Figures 2.6(a) and 2.6(b) indicate that UV photolysis causes dissociation of CO from $(CpPt(CO))_2$ to give a photoproduct with a single bridging $\nu(CO)$ absorption, near 1800 cm^{-1}. (The high frequency symmetric $\nu(CO)$ band of the parent complex is split into several components these spectra, presumably due to site effects in the N_2 matrix). A bright pink matrix is again produced upon UV photolysis. Visible absorptions responsible for this colour are observed to grow at 474 and 525 nm as illustrated in Figure 2.7. These results are consistent with photodissociation of CO, giving $Cp_2Pt_2(\mu\text{-}CO)$.

Subsequent visible photolysis of the matrix causes the reverse photochemical reaction to occur. The IR

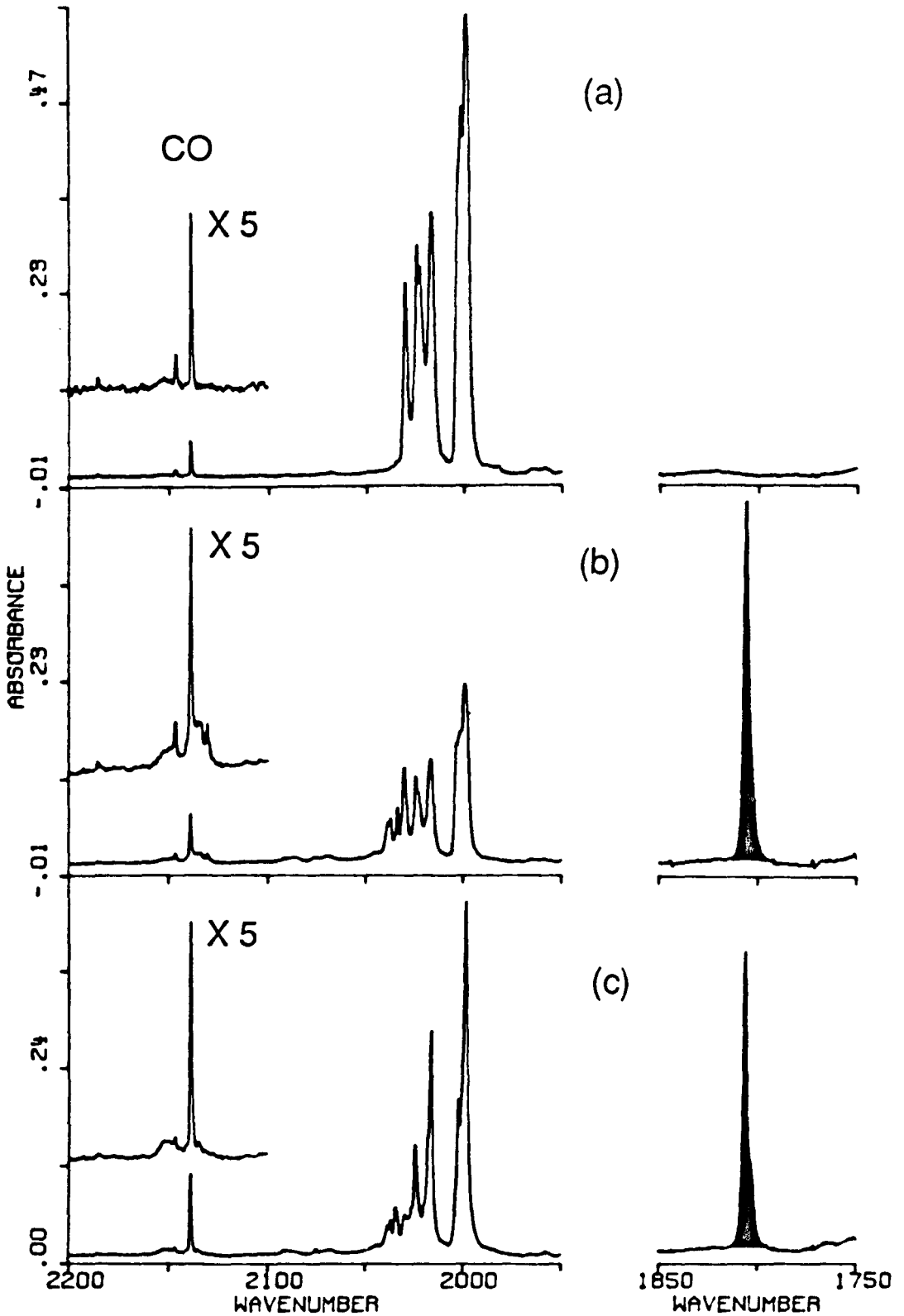


Figure 2.6: IR spectra illustrating the photochemistry of $(CpPt(CO))_2$ in an N_2 matrix at 20 K. (a) Before photolysis. (b) After 70 mins UV irradiation (230-345 nm); the band coloured black is due to $Cp_2Pt_2(\mu\text{-}CO)$. (c) After 210 mins visible photolysis (>400 nm). The absorption of CO is shown on an expanded absorbance scale.

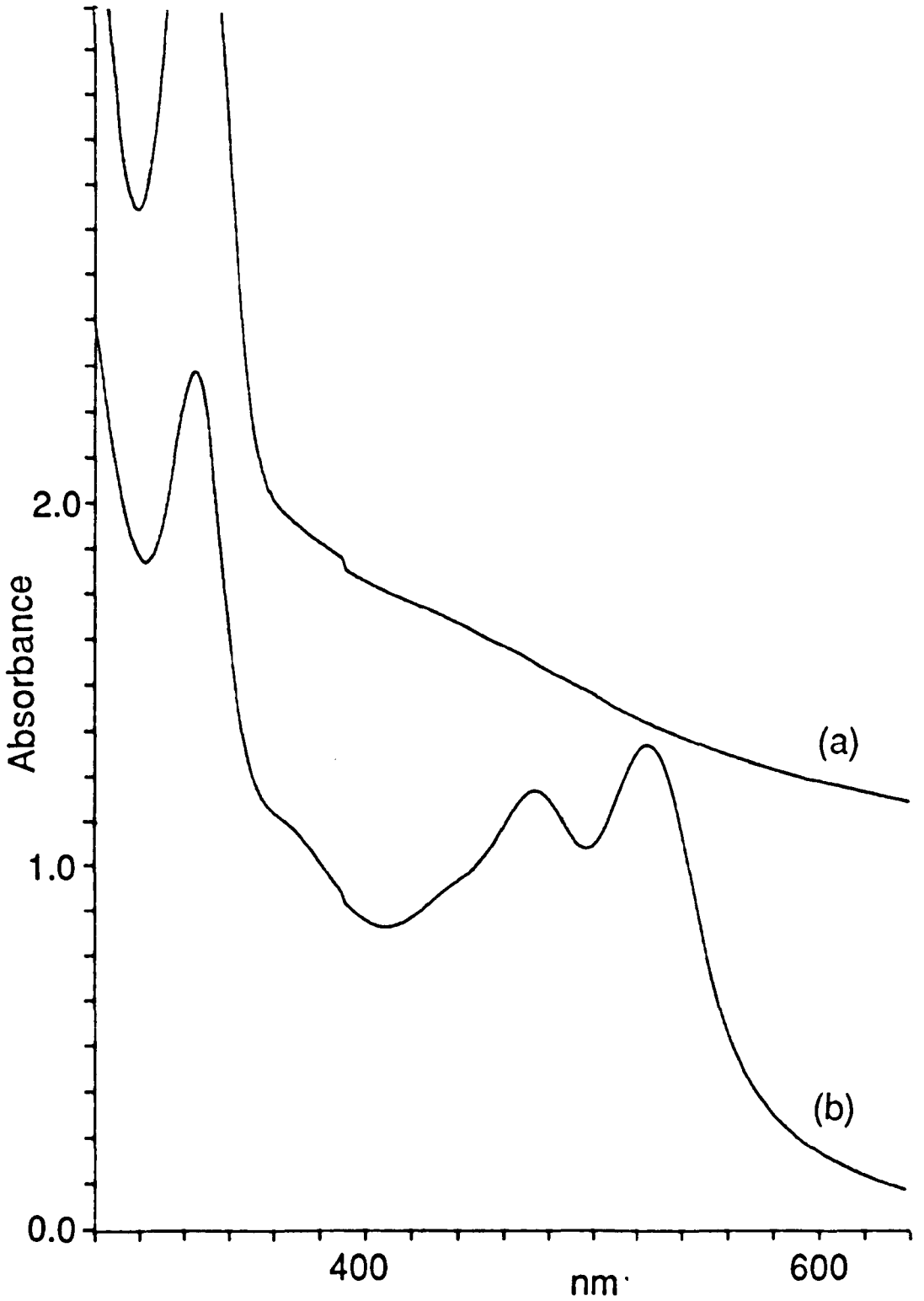


Figure 2.7: UV/visible spectra (a) before and (b) after 70 mins UV photolysis (230-345 nm) of $(CpPt(CO))_2$ in an N_2 matrix at 20 K. Note the growth of intense absorptions in the visible region due to formation of $Cp_2Pt_2(\mu\text{-}CO)$.

spectrum in Figure 2.7(c) shows depletion of the absorptions of both $Cp_2Pt_2(\mu\text{-}CO)$ and free CO, and regeneration of $(CpPt(CO))_2$.

At no time during this experiment were any bands observed in the N-N stretching region of the IR spectrum. The unsaturated species, $Cp_2Pt_2(\mu\text{-}CO)$, was thermally unreactive towards N_2, even when the matrix was warmed to 35 K. When the matrix was subjected to visible irradiation, the only reaction observed was recombination with CO. There was no evidence for coordination of a dinitrogen ligand to give a substitution product such as $Cp_2Pt_2(CO)(N_2)$.

Thus, the photochemistry observed for $(CpPt(CO))_2$ in an N_2 matrix, summarised in Equation 2.7, is identical to that in argon matrices.

$$(CpPt(CO))_2 \underset{> 400\ nm}{\overset{UV}{\rightleftharpoons}} Cp_2Pt_2(\mu\text{-}CO) + CO \qquad 2.7$$

Photolysis of $(CpPt(CO))_2$ in CO Matrices; A Case of Molecular Striptease!

In argon and nitrogen matrices, the sole photochemical process observed for $(CpPt(CO))_2$ is the ejection of a CO ligand. No evidence was obtained for mononuclear products resulting from Pt-Pt bond cleavage under these conditions. In principle it may be possible to prevent the rapid, in-cage recombination of bulky, mononuclear radicals by using more reactive host, such as CO.

Filtered UV irradiation (230-345 nm) of $(CpPt(CO))_2$, isolated in a CO matrix, produces results broadly similar to those observed in argon and nitrogen matrices. Figures 2.8(a) and 2.8(b) show a decrease in intensity of the ν(CO) bands of starting material and the growth of the bridging ν(CO) absorption of $Cp_2Pt_2(\mu\text{-}CO)$ (coloured black). Visible absorptions of $Cp_2Pt_2(\mu\text{-}CO)$, were again observed, giving the matrix a familiar pink colour. Figure 2.9 shows how the bridging ν(CO) band and visible electronic absorption of $Cp_2Pt_2(\mu\text{-}CO)$ retain the same relative intensities, indicating that they belong to the same species. Irradiation with visible light induces recombination of $Cp_2Pt_2(\mu\text{-}CO)$ with CO. However, the unsaturated photoproduct is thermally stable in a CO matrix, even when warmed to 30 K.

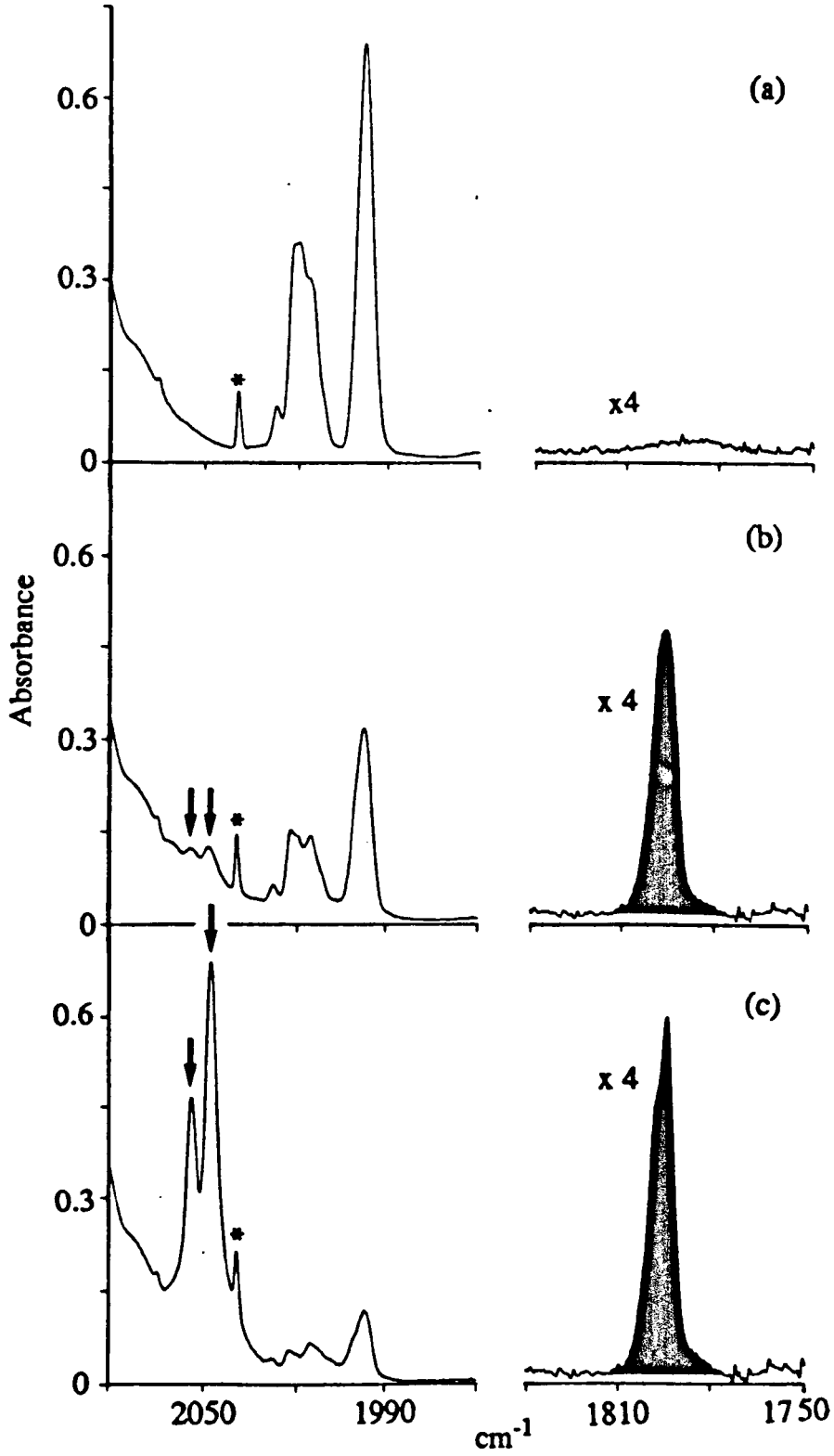


Figure 2.8: IR spectra illustrating the photochemistry of $(CpPt(CO))_2$ isolated in a CO matrix at 20 K. (a) Before photolysis; the band marked with an asterisk is due to a trace impurity of $Ni(CO)_4$ in the CO. (b) After 120 mins filtered UV photolysis (230-345 nm); the band coloured black is due to $Cp_2Pt_2(\mu\text{-}CO)$). (c) After 90 mins unfiltered UV photolysis; note the striking growth of the arrowed bands due to $Pt(CO)_4$. The bridging $\nu(CO)$ region is shown with an expanded absorbance scale.

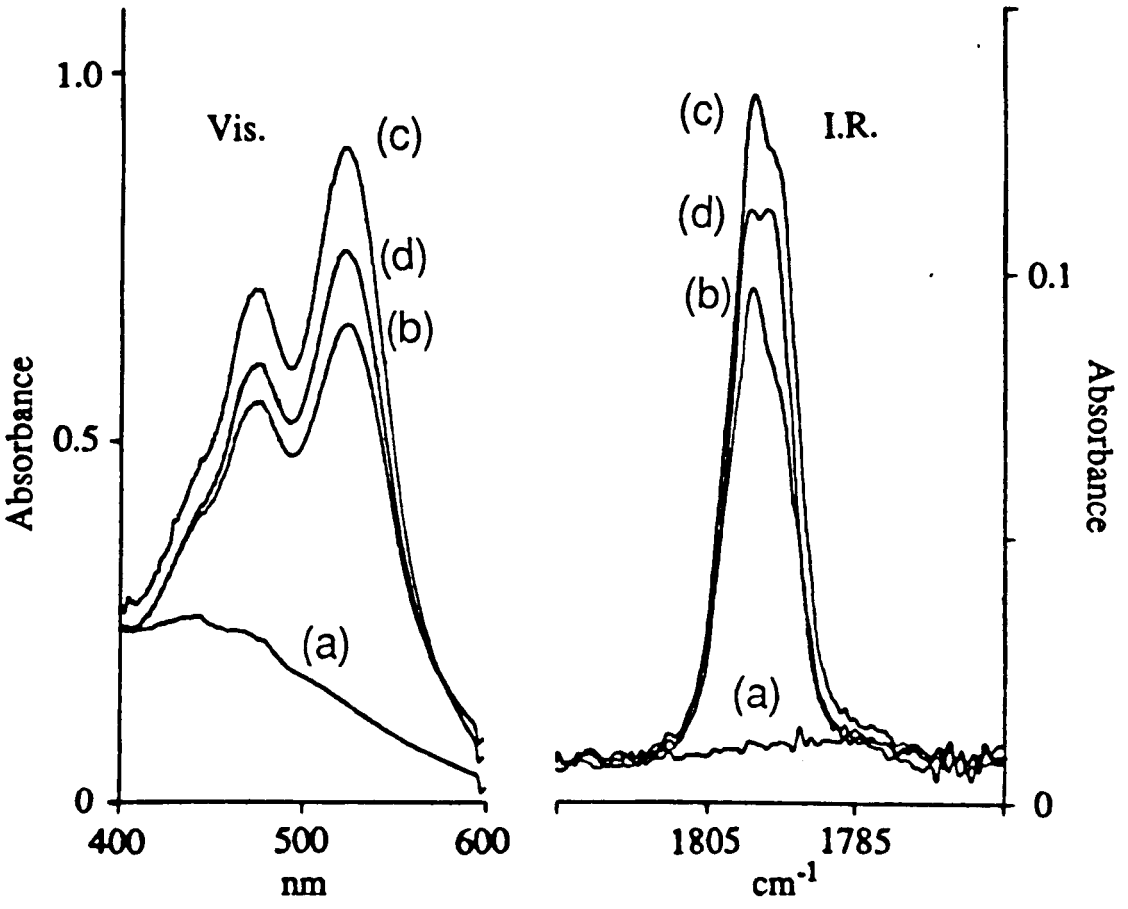
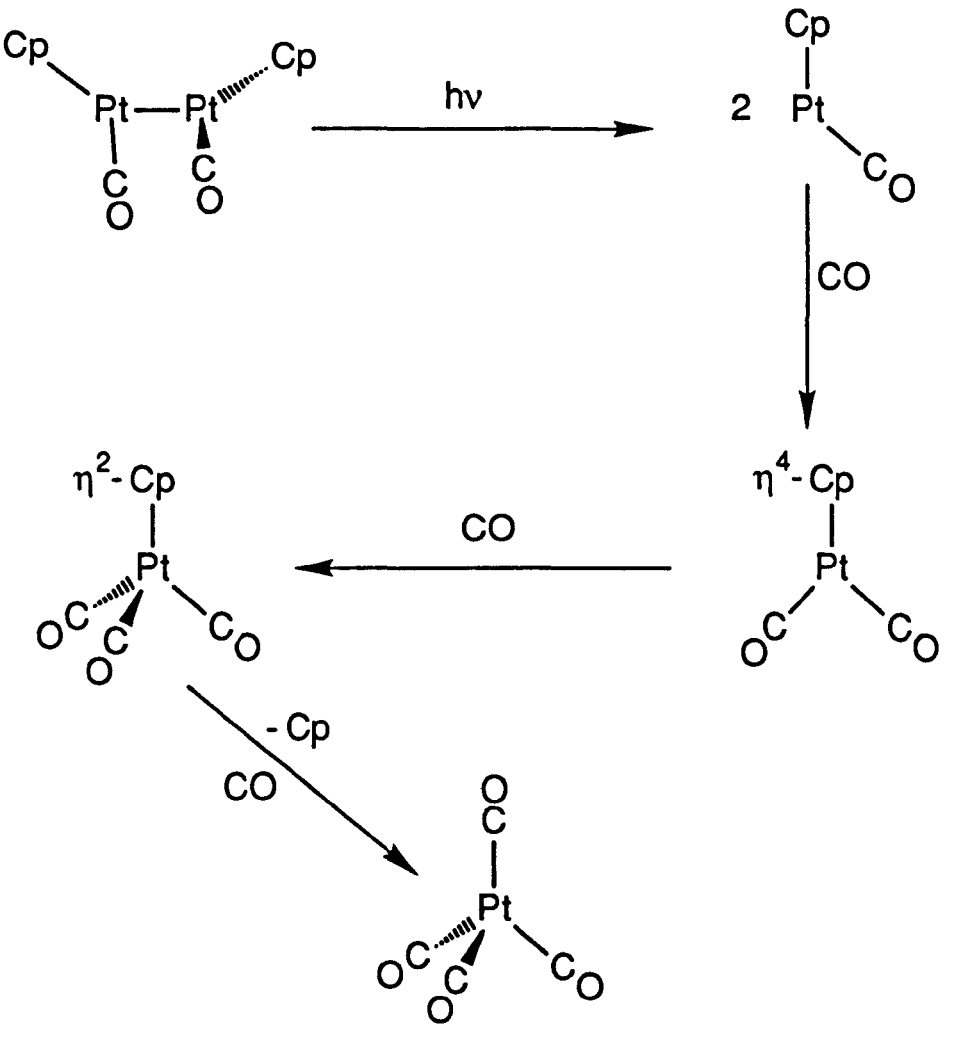


Figure 2.9: Spectra showing the similar behaviour of the visible and IR absorptions of $Cp_2Pt_2(\mu\text{-}CO)$. (a) Before photolysis of $(CpPt(CO))_2$ in a CO matrix at 20 K. (b) After 40 mins filtered UV irradiation (230-345 nm). (c) After 120 mins UV irradiation. (d) After 70 mins visible photolysis (>400 nm).

In addition to the bridging ν(CO) absorption, there are two weak absorptions in the terminal C-O stretching region, arrowed in Figure 2.8(b), which were not observed in Ar or N_2 matrices. After further photolysis of the matrix using unfiltered UV/Visible light, there is a striking increase in the intensity of these bands at 2053.9 and 2048.1 cm^{-1} (Figure 2.8(c)).

When Pt atoms are co-condensed with CO onto a matrix window terminal ν(CO) bands at 2055.0 and 2047.8 cm^{-1} are observed in the IR spectrum (Kundig 1973). These absorptions are assigned to the t_2 ν(CO) mode of the mononuclear tetracarbonyl species, $Pt(CO)_4$, split into a doublet by matrix site effects. Platinum tetracarbonyl, unlike its nickel analogue, has only been observed in low temperature matrices. The ν(CO) frequencies of $Pt(CO)_4$ prepared by this method correspond well with the bands arrowed in Figure 2.8(c). Therefore, it is reasonable to suggest that unfiltered UV photolysis of $(CpPt(CO))_2$ in a CO matrix leads to production of $Pt(CO)_4$.

It is clear that more than one step must be involved in this reaction. In view of the known solution photochemistry of $(CpPt(CO))_2$, in which Pt-Pt homolysis is implicated (Boag, 1988b), it is likely that the primary photochemical process involves formation of the metal centred mononuclear radical, CpPt(CO). A likely sequence of reactions following



Scheme 2.2: Possible mechanism for the photochemical conversion of $(CpPt(CO))_2$ to $Pt(CO)_4$ in a CO matrix.

this initial step is depicted in Scheme 2.2. The proposed mechanism involves stepwise addition of CO groups, along with dechelation of the cyclopentadienyl ligand, which is finally lost from the platinum complex on formation of $Pt(CO)_4$. No IR absorptions were observed which could be assigned to intermediate species in this reaction sequence. This would seem to imply that the steps in the mechanism leading from CpPt(CO) to $Pt(CO)_4$, occur much more rapidly than Pt-Pt bond homolysis. (However, a similar experiment with $(CpNi(CO))_2$ gives evidence for mononuclear products in which the Cp ligand is retained, as described later in this Chapter)

2.3 THE MATRIX PHOTOCHEMISTRY OF $(Cp^*Pt(CO))_2$

Identical experiments to those described above were performed on the pentamethylcyclopentadienyl platinum carbonyl dimer, $(Cp^*Pt(CO))_2$. Similar photochemistry was observed for this closely related complex in Ar, N_2 and CO matrices, as outlined in the following section. The IR and UV/Visible absorptions of all the species observed in these experiments are given in Tables 2.1 and 2.2 respectively.

Photolysis of $(Cp^*Pt(CO))_2$ in Argon Matrices

The IR spectrum of $(Cp^*Pt(CO))_2$ isolated in an argon matrix at 20 K is shown in Figure 2.10(a). The two bands in the terminal ν(CO) region are close to those observed in the hydrocarbon solution spectra (Figure 2.3(b)), corresponding to the symmetric and antisymmetric terminal C-O stretching modes of the molecule. Hence, the spectrum of $(Cp^*Pt(CO))_2$ isolated in argon matrix at 20 K is consistent with the structure determined by X-ray crystallography for this complex (Boag 1988b).

The two ν(CO) bands of $(Cp^*Pt(CO))_2$ are shifted to low frequency by about 30 cm^{-1}, compared to the corresponding absorptions of $(CpPt(CO))_2$ (see Table 2.1). This is due to the differing electronic

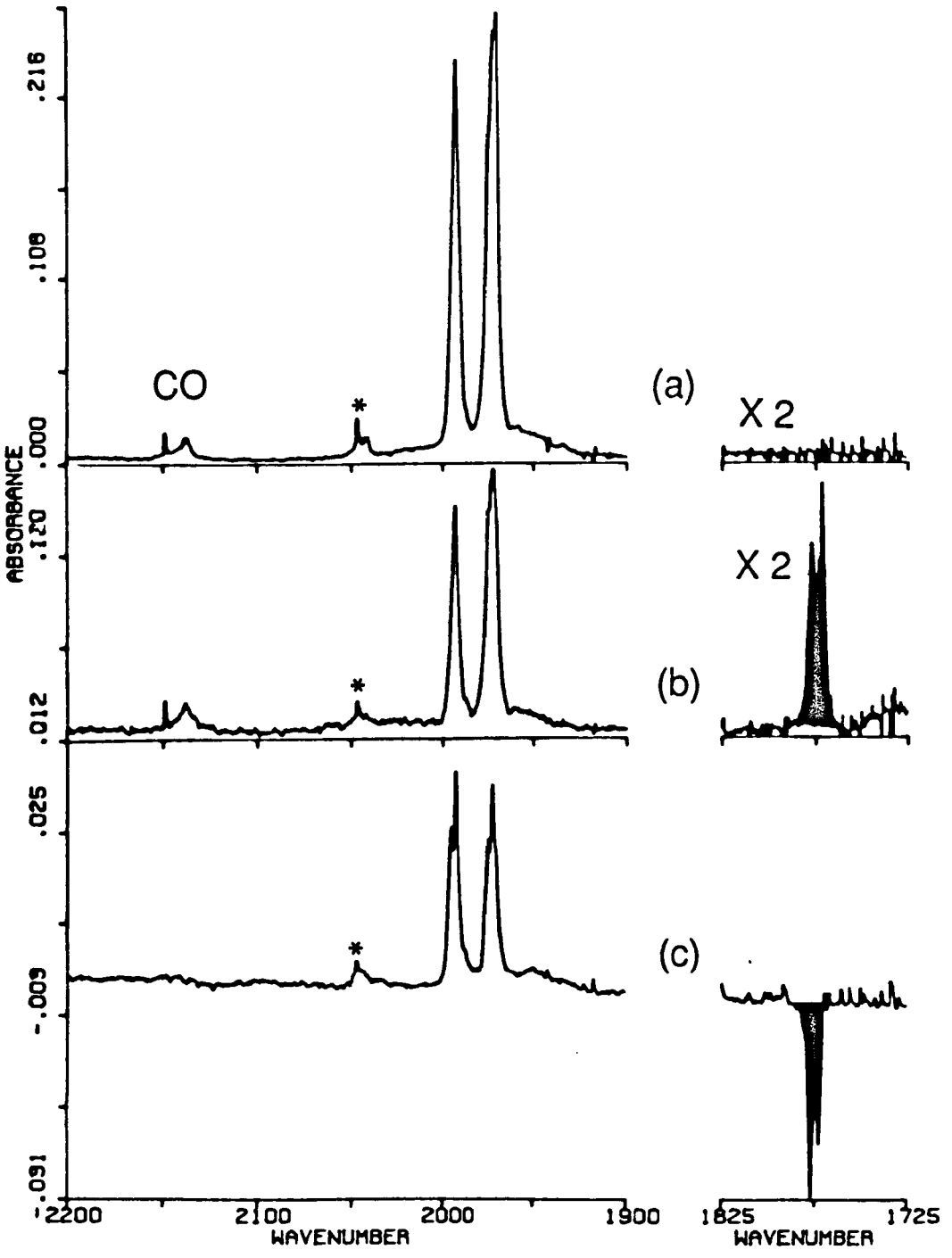


Figure 2.10: (a) IR spectrum of $(Cp^*Pt(CO))_2$ isolated in an argon matrix at 20K; the band marked with an asterisk is due to an impurity. (b) After 155 mins filtered UV irradiation (230-345 nm); the band coloured black is due to $Cp^*_2Pt_2(\mu\text{-}CO)$. (c) IR difference spectrum illustrating the effect of 75 mins photolysis with visible light (>400 nm). Note the absorbance scale expansion factors.

requirements of the Cp and Cp^* ligands in these complexes. Cp^* groups are better electron donors, leading to a higher electron density on the platinum atoms. This in turn causes a larger degree of back donation of electrons into the CO π^* orbitals, thus lowering the observed ν(C-O) frequencies.

UV photolysis of the matrix causes depletion of the parent absorptions and production of a new band near 1770 cm^{-1}, in the bridging ν(CO) region of the IR spectrum, shown in Figure 2.10(b). There is also an increase in intensity of the absorption due to free CO in the matrix. During the course of this photoreaction, the matrix acquired an intense pink colour, similar to that observed for the corresponding Cp species, $Cp_2Pt_2(\mu\text{-CO})$. The electronic absorption spectrum revealed the growth of an intense electronic absorption band at 540 nm, not present before photolysis. These changes in the IR and UV/Visible spectra indicate that UV photolysis causes dissociative loss of a CO ligand from $(Cp^*Pt(CO))_2$ to give the CO bridged photoproduct, $Cp^*_2Pt_2(\mu\text{-CO})$.

The IR difference spectrum shown in Figure 2.10(c) indicates that visible irradiation promotes the recombination of $Cp^*_2Pt_2(\mu\text{-CO})$ with CO to regenerate $(Cp^*Pt(CO))_2$. The photochemistry observed for $(Cp^*Pt(CO))_2$ in an argon matrix is summarised in Equation 2.8.

$$(Cp^*Pt(CO))_2 \xrightleftharpoons[> 400\ nm]{UV} Cp^*_2Pt_2(\mu\text{-}CO) + CO \qquad 2.8$$

Photolysis of $(Cp^*Pt(CO))_2$ in N_2 Matrices

The photochemistry observed for $(Cp^*Pt(CO))_2$ isolated in a N_2 at 20 K is identical to that in an argon matrix, shown in Equation 2.8. The IR and UV/visible spectra obtained in this experiment are shown in Figures 2.11 and 2.12. As in the case of the Cp complex, there was no evidence for the formation of any products containing coordinated N_2 during this experiment.

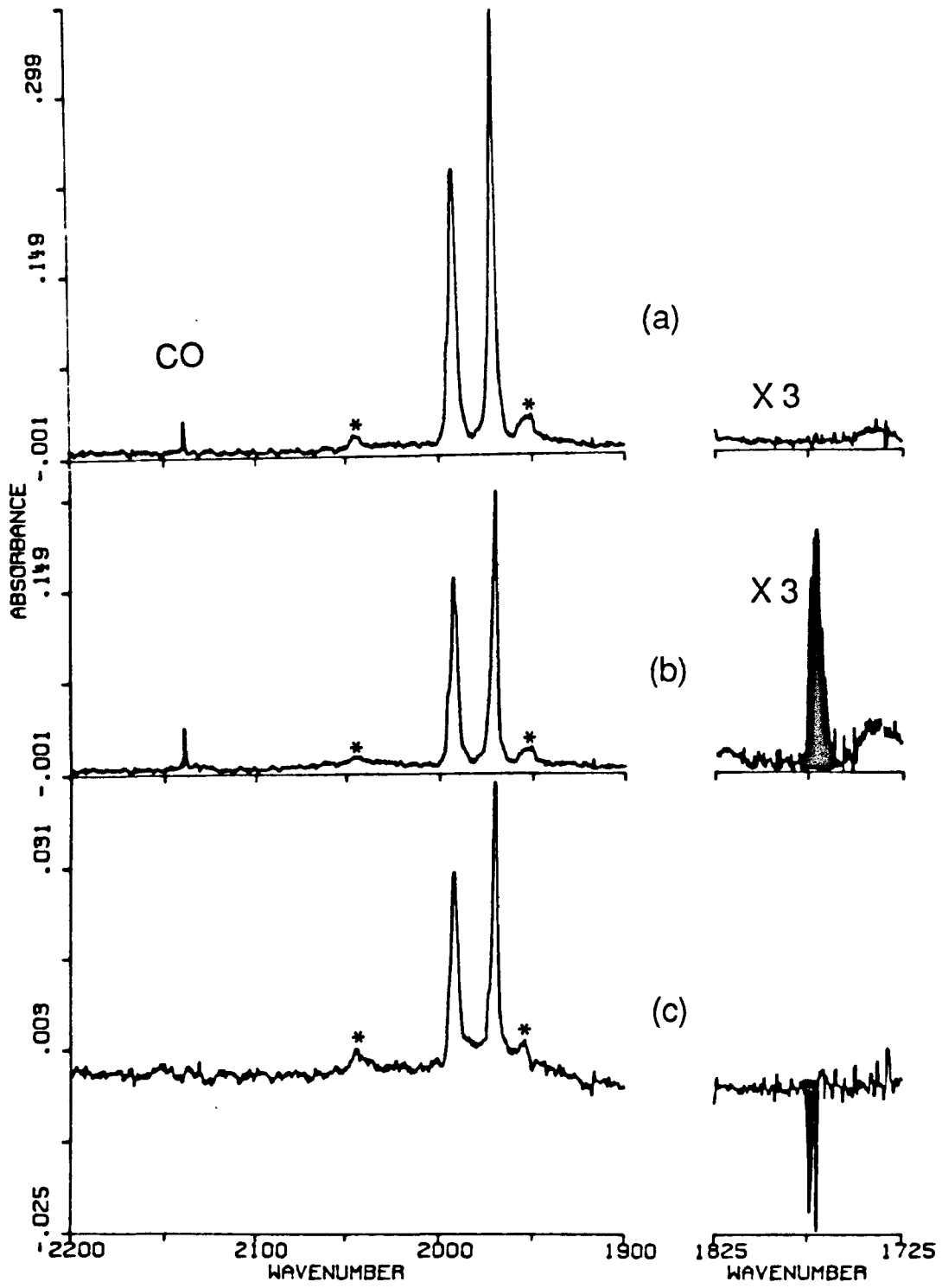


Figure 2.11: (a) IR spectrum of $(Cp^*Pt(CO))_2$ isolated in an N_2 matrix at 20K; the bands marked with asterisks are due to impurities. (b) After 120 mins filtered UV irradiation (230-345 nm); the band coloured black is due to $Cp^*_2Pt_2(\mu\text{-}CO)$. (c) IR difference spectrum illustrating the effect of 105 mins photolysis with visible light (>400 nm). Note the absorbance scale expansion factors.

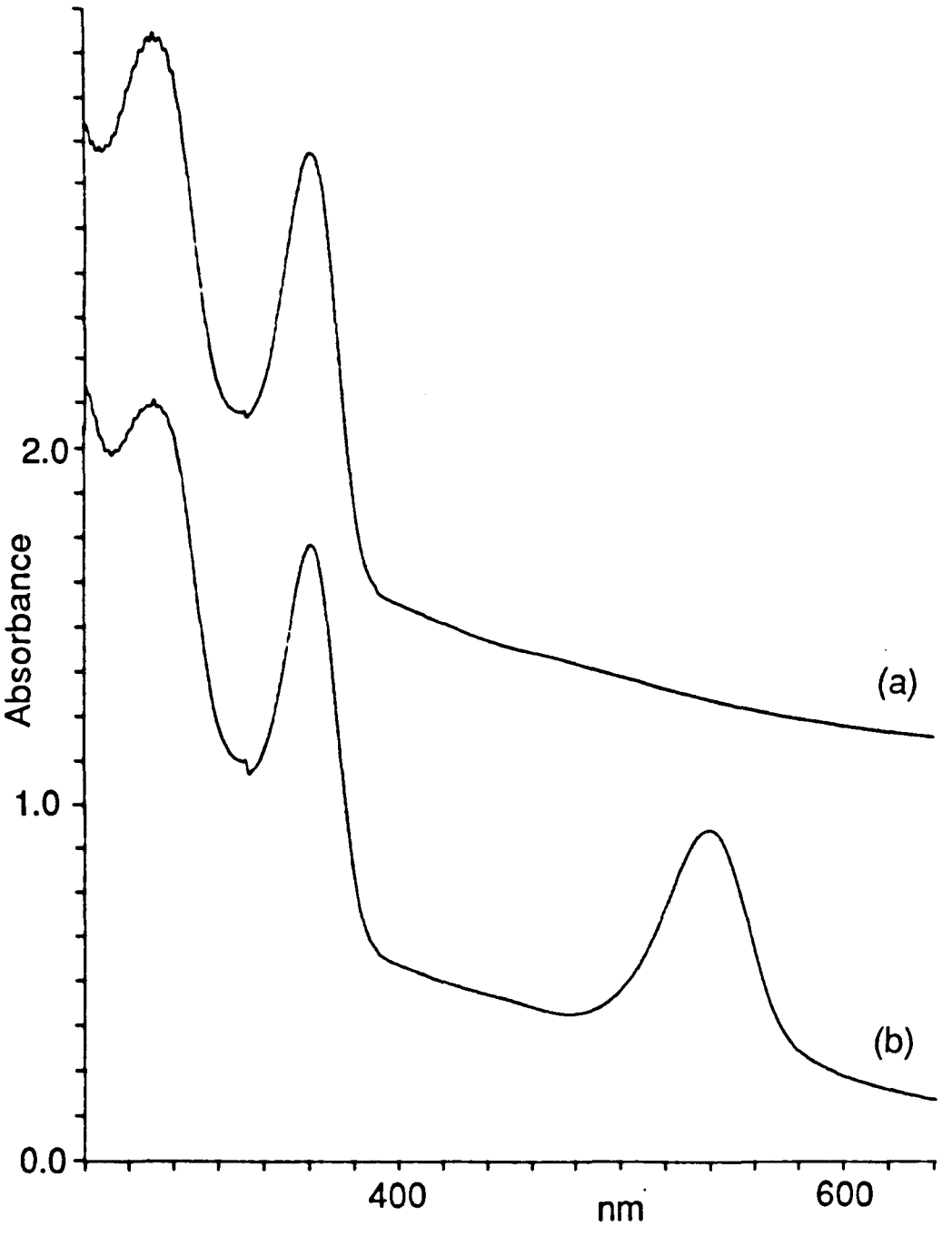


Figure 2.12: UV/visible spectra recorded (a) before and (b) after 120 mins UV photolysis (230-345 nm) of $(Cp^*Pt(CO))_2$ in an N_2 matrix at 20 K. Note the growth of an intense visible absorption in due to formation of $Cp^*_2Pt_2(\mu\text{-}CO)_2$.

Photolysis of $(Cp^*Pt(CO))_2$ in CO Matrices

It has already been described how photolysis of $(CpPt(CO))_2$ in a CO matrix leads to Pt-Pt bond cleavage and loss of the Cp rings, giving the mononuclear product, $Pt(CO)_4$. It is of interest whether a similar photochemical transformation can be achieved for the analogous Cp^* complex.

The IR spectra obtained from an experiment in which $(Cp^*Pt(CO))_2$ was photolysed in a CO matrix at 20 K are shown in Figure 2.13. Filtered UV irradiation (230-345 nm) leads to loss of starting material and production of a bridging ν(CO) band, coloured black in Figure 2.13(b), which is assigned to $Cp^*_2Pt_2(\mu\text{-}CO)$. A visible absorption at 540 nm is attributed to the same photoproduct. Subsequent visible photolysis promotes the recombination of $Cp^*_2Pt_2(\mu\text{-}CO)$ with CO to regenerate starting material.

Irradiation using the unfiltered medium pressure Hg arc lamp leads to further loss of the parent dimer and a small increase in the amount of $Cp^*_2Pt_2(\mu\text{-}CO)$. However, two weak bands are produced in the terminal ν(CO) region at 2054.0 and 2047.6 cm^{-1} (see Figure 2.13(c)). These frequencies correspond well with those assigned to $Pt(CO)_4$, generated either by co-condensation of Pt atoms with CO (Kundig 1973) or photochemically from $(CpPt(CO))_2$ in a CO matrix (see

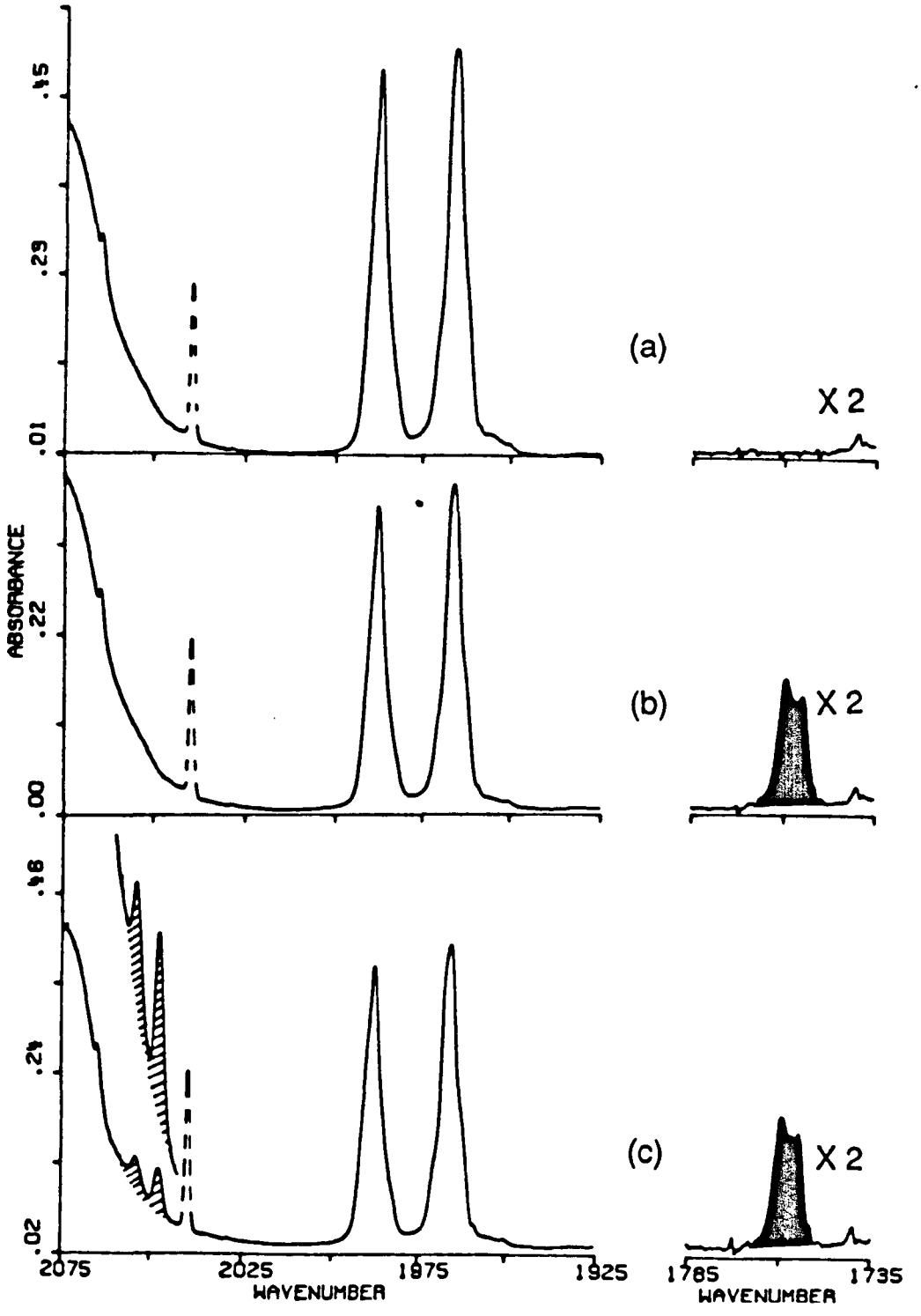


Figure 2.13: IR spectra illustrating the photochemistry of $(Cp^*Pt(CO))_2$ isolated in a CO matrix at 20 K. (a) Before photolysis; the band shown with a broken line is due to trace impurity of $Ni(CO)_4$ in the CO. (b) After 110 mins filtered UV photolysis (230-345 nm); the band coloured black is due to $Cp^*_2Pt_2(\mu\text{-}CO)$. (c) After 7.5 hrs unfiltered UV photolysis; the crosshatched bands are due to $Pt(CO)_4$. The bridging $\nu(CO)$ region is shown with an expanded absorbance scale.

above). The extreme similarity of the ν(CO) frequencies of $Pt(CO)_4$ produced from $(CpPt(CO))_2$ and $(Cp^*Pt(CO))_2$ provides strong evidence that cyclopentadienyl ligands are not present in the products giving rise to these bands. A shift of ca. 30 cm^{-1} is observed between the ν(CO) bands of the parent species, $(CpPt(CO))_2$ and $(Cp^*Pt(CO))_2$ and likewise between the dinuclear photoproducts, $Cp_2Pt_2(\mu\text{-}CO)$ and $Cp^*_2Pt_2(\mu\text{-}CO)$ (Table 2.1).

As in the case of $(CpPt(CO))_2$, no intermediate species in the reaction were observed. Generation of $Pt(CO)_4$ occurred much more slowly for the Cp^* complex. A likely explanation for this observation is that the $Cp^*Pt(CO)$ radicals, formed by homolysis of the Pt-Pt bond of $(Cp^*Pt(CO))_2$, recombine much more rapidly in the matrix cage than the corresponding Cp species, due to their larger steric bulk. Thus, there is a smaller chance that such radicals are trapped by CO, leading to mononuclear products. Also, ejection of a Cp ligand may occur more easily than a bulkier Cp^* group.

Table 2.1: Frequencies (cm^{-1}) of ν(CO) bands of $(CpPt(CO))_2$ and $(Cp^*Pt(CO))_2$ and their photoproducts in matrices at 20 K, and in room temperature hydrocarbon solution.

	Matrix Gas			
Species	**Ar**	**N_2**	**CO**	**Solution[b]**
$(CpPt(CO))_2$	2023.1[a]	2017.0[a]	2015.2[a]	2019
	2003.1	1999.5[a]	1996.9	1999
$(Cp^*Pt(CO))_2$	1992.8	1992.1	1987.8	1989
	1971.8[a]	1970.3	1966.4	1968
$Cp_2Pt_2(\mu\text{-}CO)$	1810.4[a]	1806.1	1796.9	1802[c]
$Cp^*_2Pt_2(\mu\text{-}CO)$	1772.0[a]	1770.0[a]	1759.6[a]	1765[c]
$Pt(CO)_4$			2053.9	
			2048.1	

a Average wavenumber of bands split by matrix effects.

b n-heptane solution.

c Observed using fast TRIR spectroscopy in cyclohexane solution - see section 2.6.

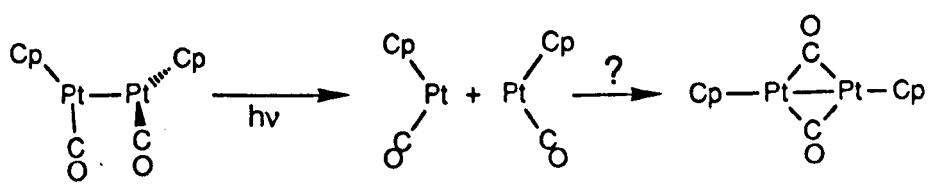
Table 2.2: Wavelengths (nm) of UV/vis absorption bands of $(CpPt(CO))_2$ and $(Cp^*Pt(CO))_2$ and their photoproducts in matrices at 20 K, and in room temperature cyclohexane solution.

	Matrix Gas			
Species	**Ar**	**N_2**	**CO**	**Solution**
$(CpPt(CO))_2$				222
		260		270
		325		337
				465
$(Cp^*Pt(CO))_2$				250
	290	290	295	307
	360	360	364	378
				499
$Cp_2Pt_2(\mu\text{-}CO)$	470	474	478	
	522	525	528	
$Cp^*_2Pt_2(\mu\text{-}CO)$	540	540	545	

2.4 ^{13}CO ISOTOPIC ENRICHMENT STUDIES ON $(Cp^*Pt(CO))_2$

The results described above provide strong evidence that photolysis of $(CpPt(CO))_2$ or $(Cp^*Pt(CO))_2$ in low temperature frozen gas matrices can cause dissociative loss of CO, giving the unsaturated dinuclear monocarbonyl products, $Cp_2Pt_2(\mu\text{-}CO)$ and $Cp^*_2Pt_2(\mu\text{-}CO)$ respectively.

However, these conclusions involve interpreting the relatively weak IR absorption of photoejected CO. It is possible that doubly CO-bridged species could give rise to the single bridging $\nu(CO)$ bands observed in these experiments. For a planar $Pt_2(\mu\text{-}CO)_2$ core, the symmetric $\nu(CO)$ vibration would be IR inactive, and only the antisymmetric $\nu(CO)$ mode would be observed in the IR spectrum.. The production of such doubly CO-bridged species can be envisaged via a reaction sequence such as that shown in Equation 2.9. In this scheme, the mononuclear radicals produced by photochemical cleavage of the Pt-Pt bond recombine in such a way as to give a bridged isomer of the parent complex.



2.9

In order to rule out the possibility of an isomerisation of this type taking place, experiments were carried out using a sample of $(Cp^*Pt(CO))_2$ which was isotopically enriched with ca. 50% ^{13}CO. A solution spectrum of this sample is compared with that of an unenriched sample of $(CpPt(CO))_2$ in Figure 2.14.

The isotopic $\nu(CO)$ band patterns predicted for either a monocarbonyl or linear dicarbonyl photoproduct are shown schematically in Figure 2.15. If the photoproduct contained a single bridging CO group, one would expect two $\nu(CO)$ bands of almost equal intensity, corresponding to the μ-^{12}CO and μ-^{13}CO groups of the two possible isotopomers.

If, however, the product contained two co-linear bridging CO groups, the arguments of Darling (1972) would predict four $\nu(CO)$ bands. Two of these bands would arise from the antisymmetric C-O stretching modes of the $(Cp^*Pt(\mu\text{-}^{12}CO))_2$ and $(Cp^*Pt(\mu\text{-}^{13}CO))_2$ isotopomers. The antisymmetric $\nu(CO)$ mode of the $(Cp^*Pt)2(\mu\text{-}^{12}CO)(\mu\text{-}^{13}CO)$ would occur at an intermediate frequency. The statistical probability of formation of the mixed isotopomer is twice that of the all-^{12}CO or all-^{13}CO species, leading to an IR band of greater intensity for this species. In addition, the symmetric $\nu(CO)$ mode becomes IR active for $(Cp^*Pt)_2(\mu\text{-}^{12}CO)$-$(\mu\text{-}^{13}CO)$, due to the loss of a centre of symmetry. This is responsible for the weak band at higher

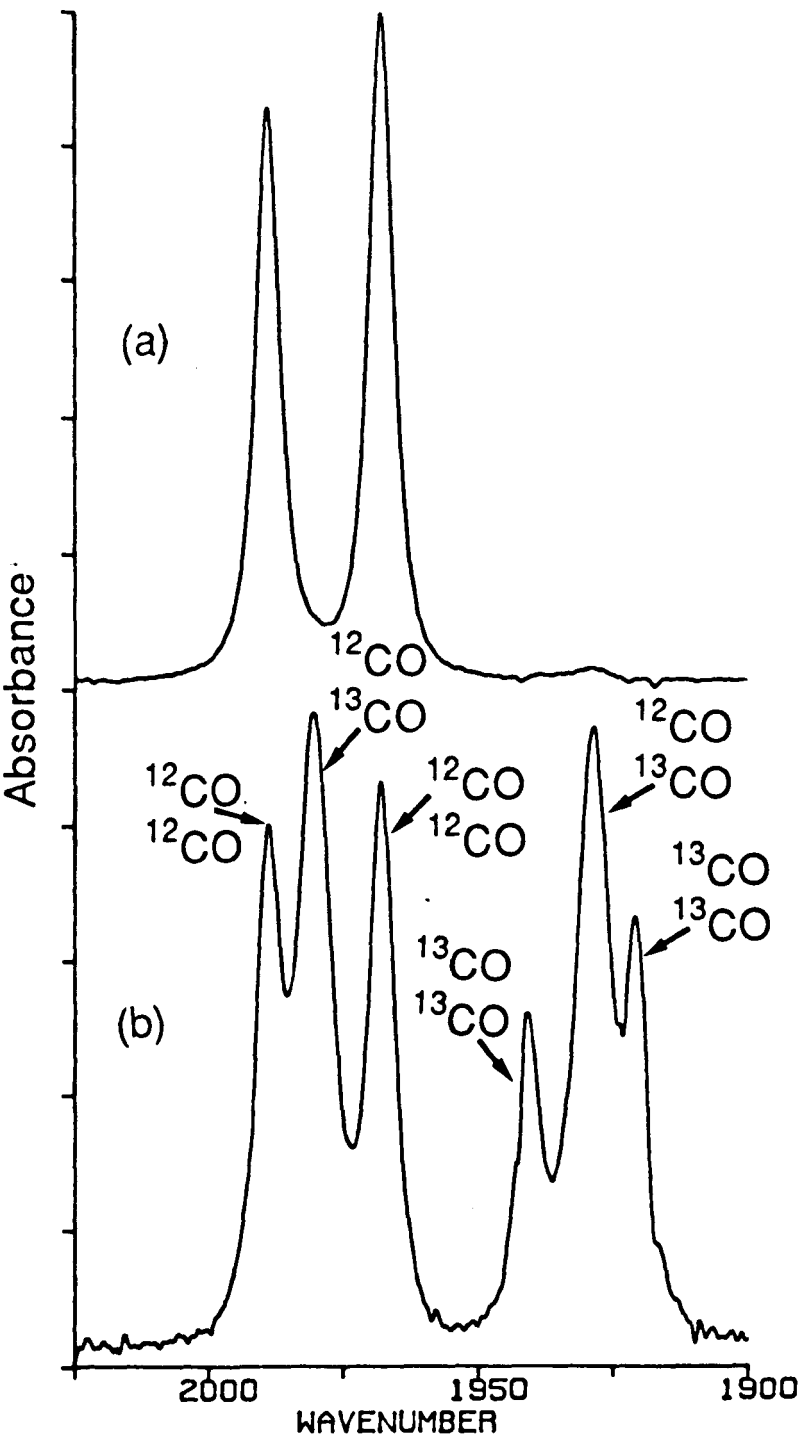


Figure 2.14: IR spectra of (a) unenriched and (b) ca. 50% ^{13}CO isotopically enriched samples of $(Cp^{*}Pt(CO))_2$ in n-heptane solution at room temperature. The bands in (b) are labelled according to the composition of the isotopomer responsible.

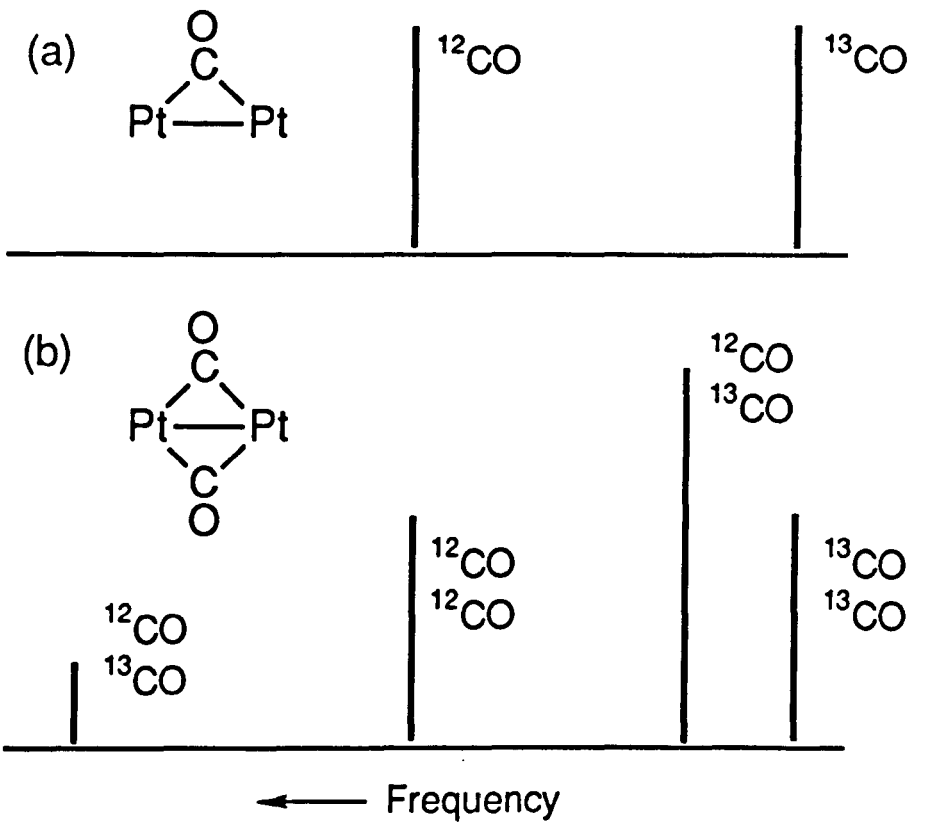


Figure 2.15: Relative ν(CO) band positions and intensities predicted for 50% isotopically enriched samples of (a) $Cp^*_2Pt_2(\mu\text{-}CO)$ and (b) $(Cp^*Pt(\mu\text{-}CO))_2$, based on the arguments of Darling (1972). Each band is labelled according to the composition of the isotopomer responsible.

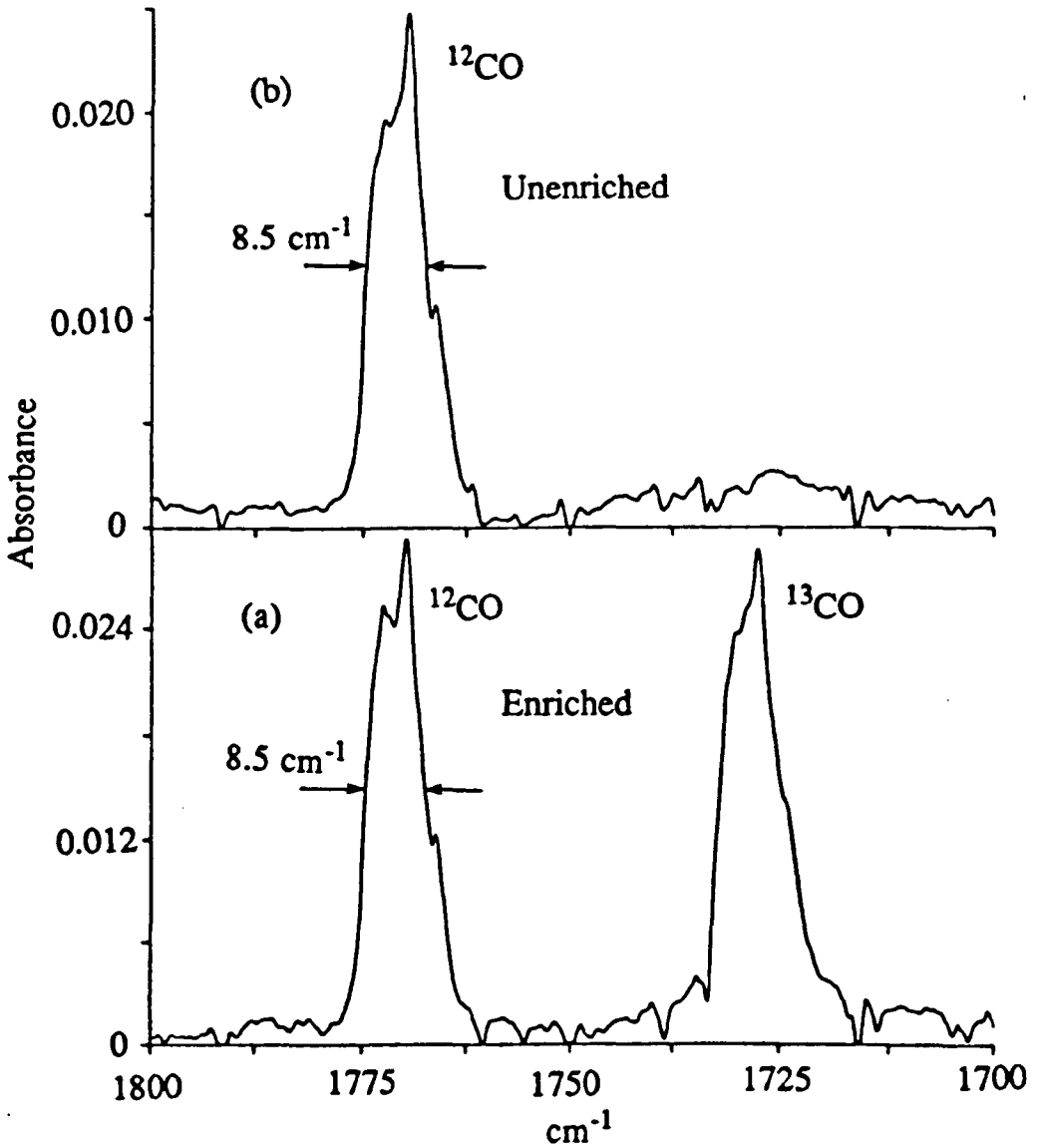


Figure 2.16: IR spectra showing how ^{13}CO enrichment establishes the number of bridging CO groups in $Cp^*_2Pt_2(\mu\text{-CO})$. (a) Bridging ν(CO) bands observed after 30 minutes filtered UV photolysis (230-345 nm) of ca. 50% ^{13}CO enriched $(Cp^*Pt(CO))_2$ isolated in a N_2 matrix at 20 K. The two bands are assigned to $Cp^*_2Pt_2(\mu\text{-}^{12}CO)$ and $Cp^*_2Pt_2(\mu\text{-}^{13}CO)$ as indicated. (b) The spectrum observed when an unenriched sample of $(Cp^*Pt(CO))_2$ was photolysed under similar conditions.

frequency shown in Figure 2.15(b). The frequencies and relative intensities of these absorptions depend on the relative values of the C-O stretching and interaction force constants (Darling 1972).

Figure 2.16(a) shows the bridging ν(CO) region of the IR spectrum obtained after UV photolysis of ca. 50% ^{13}CO enriched $(Cp^*Pt(CO))_2$, isolated in an N_2 matrix at 20 K. Two ν(CO) bands of equal intensity are observed. These can be assigned to the two isotopomers of a photoproduct with one bridging CO group. The band at higher frequency, due to $Cp^*_2Pt_2(\mu\text{-}^{12}CO)$, has the same half-width, 8.5 cm^{-1} as in the experiments without isotopic enrichment, see Figure 2.16(b). The difference in wavenumber of the two absorptions is 42.4 cm^{-1}, consistent with the shift expected when ^{12}CO is substituted by ^{13}CO. A doubly bridged structure, $(Cp^*Pt(\mu\text{-}CO))_2$, could only give rise to the spectra in Figure 2.16 if the interaction force constant between the two CO groups was negligible. This seems most improbable in view of the non-zero interaction constants found in related molecules such as $(CpNi(\mu\text{-}CO))_2$ and $Cp(CO)Fe(\mu\text{-}CO)_2NiCp$ (McArdle 1971, Crichton 1980)

Weak IR bands at 2139 and 2090 cm^{-1} are also produced on photolysis of the isotopically enriched sample. These correspond to the absorptions of the photoejected molecules of ^{12}CO and ^{13}CO respectively.

The data obtained from these isotopic substitution studies were used to calculate C-O stretching and interaction force constants for $(Cp^*Pt(CO))_2$ and $Cp^*_2Pt_2(\mu\text{-}CO)$. The program used for these calculations was adapted for the VAX computer by Thompson and Walters (1986). The observed and calculated frequencies are given in Table 2.3, along with the derived force constants.

Further evidence that UV photolysis of these platinum dimers causes dissociation of CO was provided by the results obtained from an experiment in which ca. 50% ^{13}CO enriched $(Cp^*Pt(CO))_2$ was irradiated in a ^{12}CO matrix. The IR difference spectrum shown in Figure 2.17 shows the effect of two cycles of UV followed by visible irradiation. It can be seen that the absorptions due to $(Cp^*Pt(^{12}CO))_2$ have increased in intensity, but those of $(Cp^*Pt)_2(^{12}CO)(^{13}CO)$ and $(Cp^*Pt(^{13}CO))_2$ have decreased after the two photolysis cycles. Also, the yield of $Cp^*_2Pt_2(\mu\text{-}^{12}CO)$ is greater than that of $Cp^*_2Pt_2(\mu\text{-}^{13}CO)$.

The explanation of these observations is as follows: UV photolysis is equally likely to cause dissociation of a ^{12}CO or ^{13}CO ligand, to a first approximation. However, during visible photolysis, the unsaturated species $Cp^*_2Pt_2(\mu\text{-}CO)$ is much more likely to combine with a molecule of ^{12}CO from the surrounding matrix cage, than with the CO to which it was

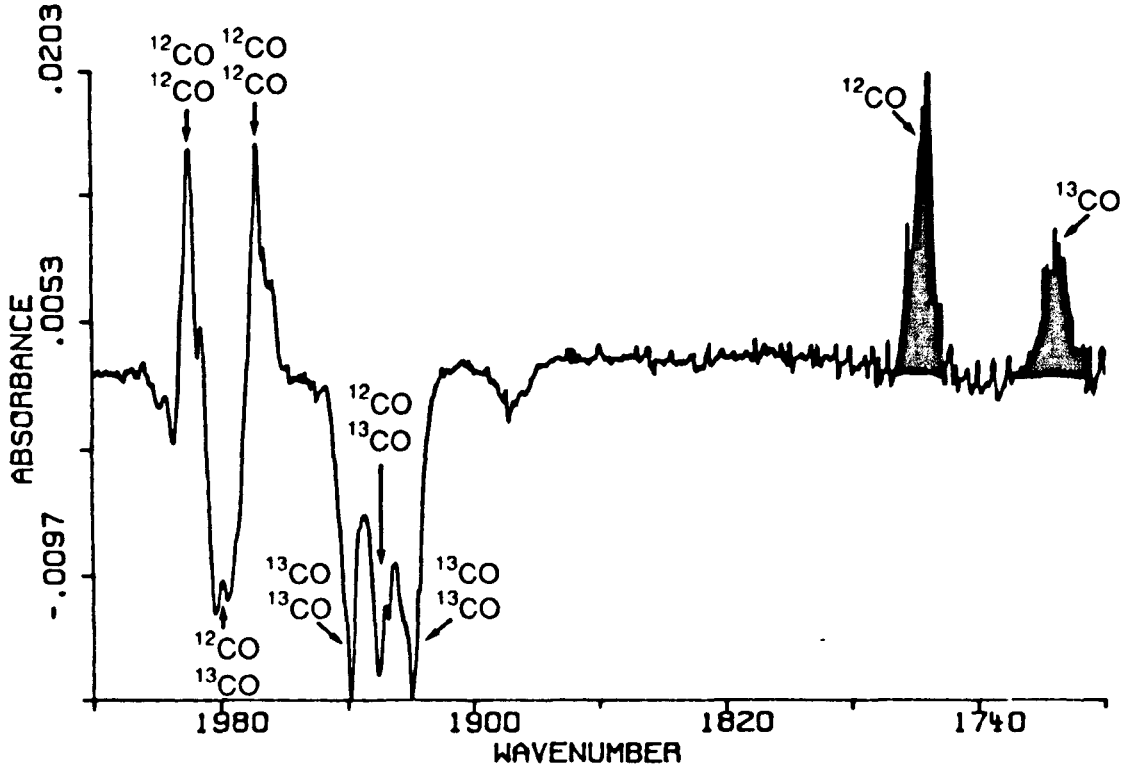
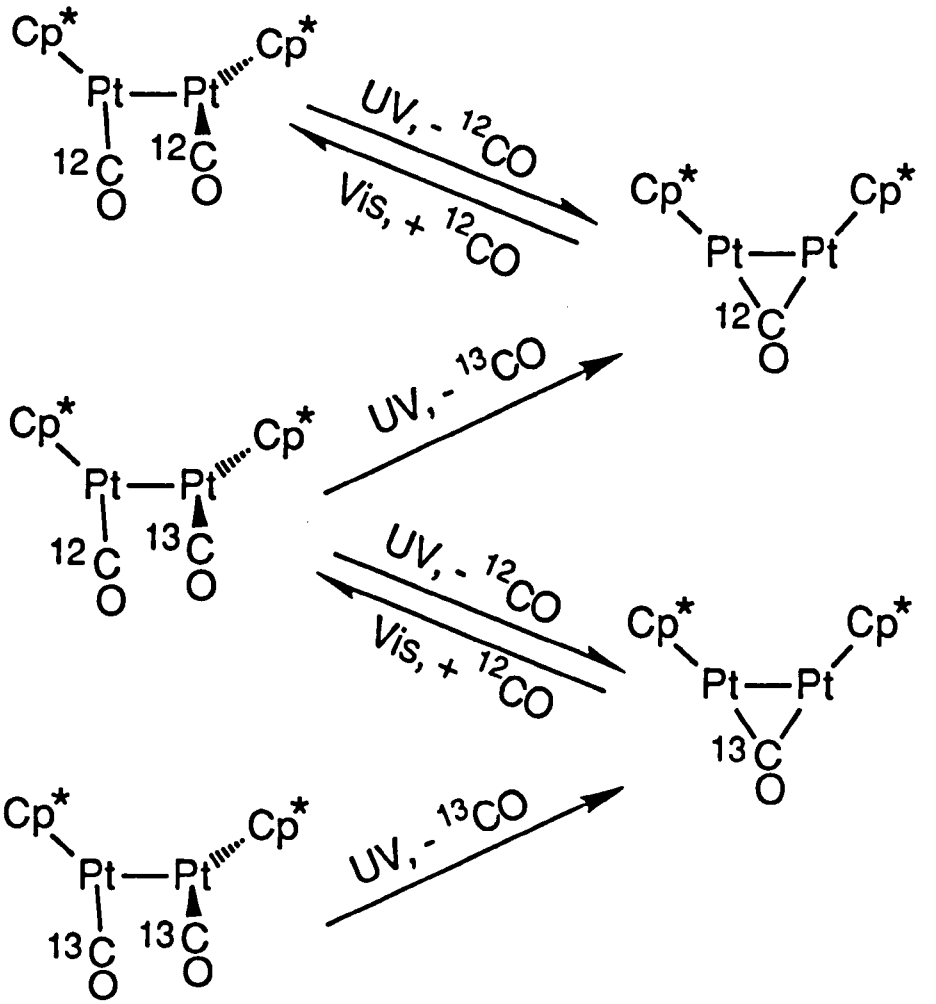


Figure 2.17: IR difference spectrum illustrating the photoinduced exchange of CO between 50% ^{13}CO enriched $(Cp^*Pt(CO))_2$ and a ^{12}CO matrix. The spectrum recorded before photolysis has been subtracted from that obtained after two cycles of 2 hrs UV (230-345 nm) followed by 6 hrs visible photolysis (>400 nm)). Bands are labelled according to the composition of the isotopomer responsible. The bands coloured black are due to isotopomers of $Cp^*_2Pt_2(\mu\text{-}CO)$.



Scheme 2.3: Photochemistry of ^{13}CO enriched $(Cp^*Pt(CO))_2$ in a pure ^{12}CO matrix.

originally bonded. This essentially lowers the percentage ^{13}CO enrichment of the matrix isolated sample of $(Cp^*Pt(CO))_2$ via photochemical exchange with the ^{12}CO matrix. The results of this experiment are summarised in Scheme 2.3. This scheme is slightly simplified, since the back reaction of $Cp^*_2Pt_2(\mu\text{-}CO)$ with ^{13}CO is assumed to have a probability of zero.

The results of these isotopic enrichment studies have proved that UV photolysis of $(Cp^*Pt(CO))_2$ generates the monocarbonyl species, $Cp^*_2Pt_2(\mu\text{-}CO)$, containing a bridging CO group. The photoproduct observed from the analogous Cp complex can similarly be assigned as $Cp_2Pt_2(\mu\text{-}CO)$.

Table 2.3: Data for isotopic enrichment experiments; observed and calculated frequencies (cm^{-1}) of the ν(CO) bands for the isotopomers of $(Cp^*Pt(CO))_2$ and $Cp^*_2Pt_2(\mu\text{-}CO)$ isolated in an N_2 matrix at 20 K.

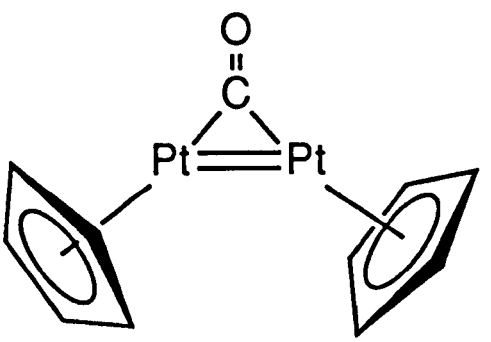
Species	Observed	Calculated
$Cp^*_2Pt_2(^{12}CO)_2$	1970.3	1970.4
	1992.1	1991.6
$Cp^*_2Pt_2(^{12}CO)(^{13}CO)$	1930.8	1930.8
	1982.8	1983.2
$Cp^*_2Pt_2(^{13}CO)_2$	1922.8	1922.6
	1943.2	1943.4
$Cp^*_2Pt_2(\mu\text{-}^{12}CO)$	1770.0	1770.0
$Cp^*_2Pt_2(\mu\text{-}^{13}CO)$	1727.6	1730.6

Frequencies calculated for $(Cp^*Pt(CO))_2$ using the C-O stretching force constant k = 1585.4 Nm^{-1} and interaction constant k_i = 17.03 Nm^{-1}.

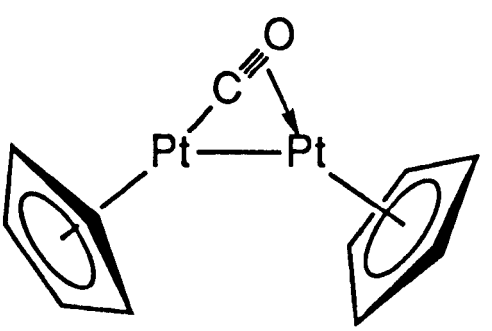
Frequencies calculated for $Cp^*_2Pt_2(\mu\text{-}CO)$ using the C-O stretching force constant k = 1265.6 Nm^{-1}.

2.5 STRUCTURAL CHARACTERISATION OF $Cp^*_2Pt_2(\mu\text{-}CO)$

It has now been established that the dinuclear photoproducts generated from $(CpPt(CO))_2$ and $(Cp^*Pt(CO))_2$ each have a single carbonyl group, which occupies a position bridging the Pt-Pt bond. There are, however, several ways in which a bridging CO group can be coordinated in a dinuclear system, as reviewed by Crabtree (1986). For the system under study, the two structures illustrated below remain as possibilities.



A



B

Structure A has a symmetrically bridging CO group, like those found in the unsaturated iron species, $Cp^*_2Fe_2(\mu\text{-}CO)_3$, for which a crystal structure has been determined (Blaha 1985b). Such a ligand is considered to donate one electron to each metal atom. Therefore a formal double bond must be drawn between the two platinum atoms for this structure to obey the 18 electron rule. Structure B possesses a linear semibridging CO ligand, which can be regarded as a four electron donor. It is like a terminal CO group to one of the Pt atoms, but in an η^2, fashion to the other. Such a bonding mode has been identified in the complex $Mn_2(CO)_5(Ph_2PCH_2PPh_2)_2$, using X-ray diffraction (Colton 1975).

For matrix isolated species it is possible to distinguish between these bonding modes using the technique of polarised photochemistry, the theory of which has been described in the Introduction to Section 1 of this thesis. This method was used by Dunkin (1984) to identify a semibridging CO group in $Mn_2(CO)_9$, generated in a low temperature matrix by irradiation of $Mn_2(CO)_{10}$.

The symmetrically bridging CO group in Structure A is oriented at 90° to the Pt-Pt bond. In a sample of molecules with a preferential Pt-Pt alignment, the resultant ν(CO) band is expected to show linear dichroism perpendicular to plane containing the Pt-Pt

bonds. By contrast, the semibridging CO group in Structure B is oriented at approx. 45° to the Pt-Pt bond. The transition moment vector associated with the ν(CO) vibrational mode of this species can be resolved into roughly equal components, parallel and perpendicular to the Pt-Pt axis. Therefore, one would not expect the ν(CO) band of this complex to exhibit linear dichroism, for a similarly aligned sample. This argument enabled Dunkin to assign a structure with a semibridging CO group to $Mn_2(CO)_9$.

Polarised Photochemistry of $(Cp^*Pt(CO))_2$

In this experiment, an N_2 matrix containing $(Cp^*Pt(CO))_2$ was photolysed with plane polarised light (290 nm). Pairs of IR and UV/Visible spectra were recorded through polarisers parallel or perpendicular to the plane of the photolysing light, as described in Chapter 6. The resulting spectra are shown in Figure 2.18.

The dichroism observed in the bands of those molecules of $(Cp^*Pt(CO))_2$ which remain intact after polarised photolysis are considered first. The photoactive UV absorption will always display dichroism perpendicular to the plane of polarisation of the photolysing light. However, dichroism was not observable in the 290 nm absorption of $(Cp^*Pt(CO))_2$,

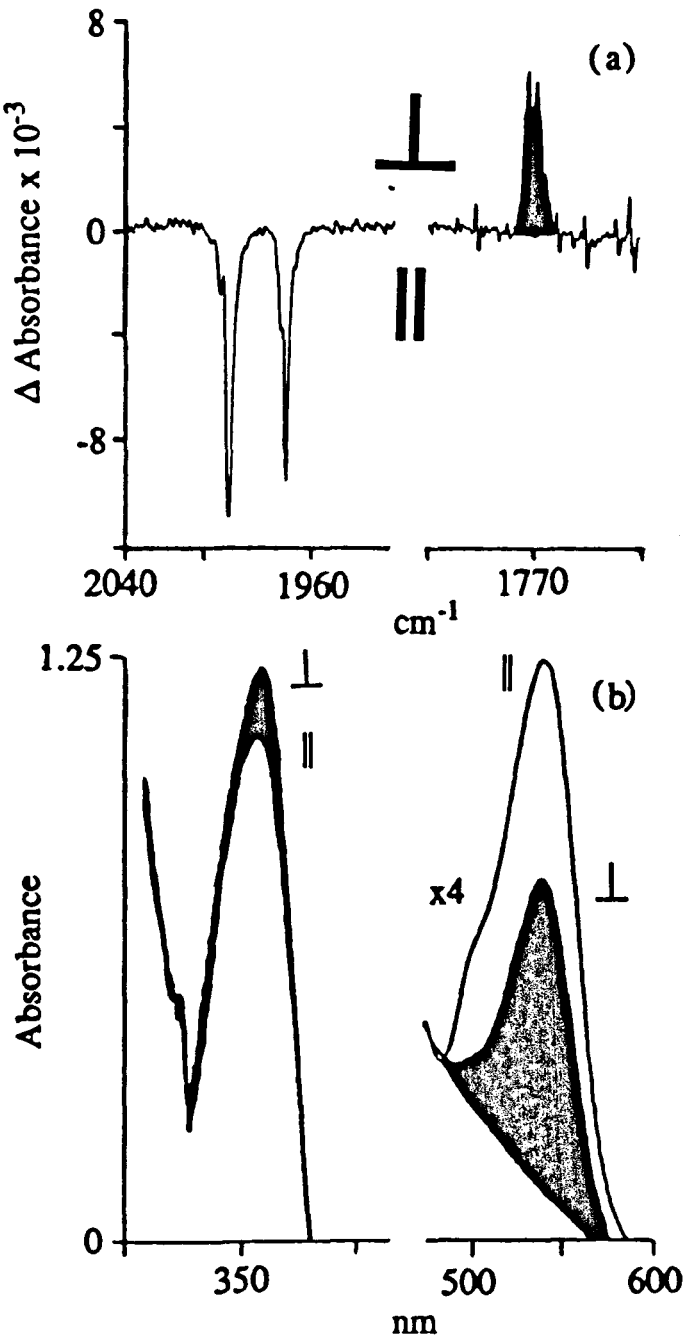


Figure 2.18: Spectra illustrating the dichroism generated by 60 hrs photolysis of $(Cp^*Pt(CO))_2$ in an N_2 matrix with plane polarised UV light (290 nm). (a) IR difference spectrum (Δ Absorbance = $A_\perp - A_\parallel$); the band coloured black is due to $Cp^*_2Pt_2(\mu\text{-}CO)$. (b) Superimposed UV/visible spectra; the spectra recorded with the polariser perpendicular to the plane of photolysis, ($A_\perp$) have been coloured black to distinguish them from $A_\parallel$. UV/visible and IR spectra were recorded on the same sample.

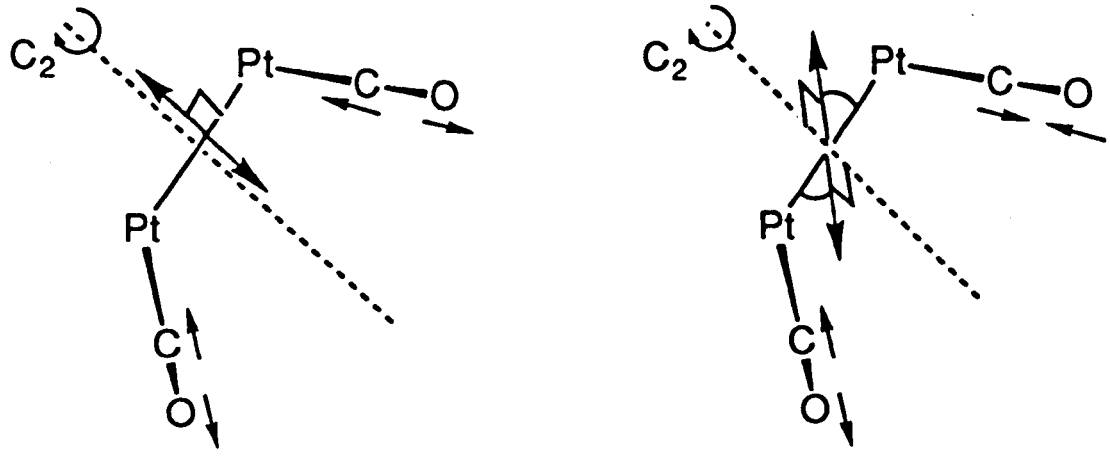


Figure 2.19: The ν(CO) vibrational modes of $(CpPt(CO))_2$ or $(Cp^*Pt(CO))_2$. Small arrows represent the relative motions of the carbon and oxygen atoms. Large arrows indicate the direction of the transition moment vector for each vibrational mode. The C_2 symmetry axis is indicated by a broken line and Cp groups are omitted for clarity.

due to the low throughput of short wavelength UV light by the matrix in this experiment.

The ν(CO) vibrational modes of $(Cp^*Pt(CO))_2$ are shown in Figure 2.19. The C_2 symmetry of this molecule requires that the transition moment vector for the symmetric (a) ν(CO) mode has an orientation exactly perpendicular to the Pt-Pt bond axis, along the C_2 axis. However, the transition moment vector for the antisymmetric (b) ν(CO) mode can be resolved into two components, the larger of which is in a direction orthogonal with both the C_2 axis and the Pt-Pt bond. The smaller component lies parallel to the Pt-Pt bond.

Figure 2.18(a) shows that both ν(CO) bands of $(Cp^*Pt(CO))_2$ exhibit dichroism parallel to the plane of the photolysing light (i.e. perpendicular to the photoactive UV transition moment vector of the remaining molecules). In conventional IR spectra of $(Cp^*Pt(CO))_2$, the low frequency absorption is more intense. However, the relative intensities of the two bands are reversed in the polarised IR spectrum.

The reduced relative intensity of the low frequency ν(CO) band can be explained if the transition moment responsible for this absorption is not exactly perpendicular to the photoactive UV transition moment. This band can, therefore, be readily assigned as the antisymmetric ν(CO) mode (see above). The high

frequency band must then be assigned as the symmetric ν(CO) mode, as expected if the interaction force constant between the two CO groups is positive. These assignments require that the photoactive UV transition moment at 290 nm, responsible for CO-loss from $(Cp^*Pt(CO))_2$, is parallel to the Pt-Pt bond.

The UV absorption of $(Cp^*Pt(CO))_2$ at 360 nm is also observed to be dichroic (Fig 2.28(b)), such that its transition moment vector must be parallel to that of the photoactive transition (290 nm), i.e. lying along the Pt-Pt bond. This is consistent with the assignment of the 360 nm band to a $\sigma \rightarrow \sigma^*$ transition.

The dichroism of the IR and visible bands of the photoproduct will now be considered. The most important observation to make from Figure 2.18(a) is that the IR band due to bridging CO group of $Cp^*_2Pt_2(\mu\text{-CO})$ shows significant dichroism in a direction perpendicular to the plane of the photolysing light. Therefore, the transition moment vector of the CO group must have an orientation perpendicular to the Pt-Pt bond (assuming that there is no rotation of the Pt-Pt bond within the matrix cage on ejection of CO). Such dichroism is consistent with a symmetrical bridging CO group oriented at 90° to the Pt-Pt vector (i.e. Structure A). A linear semibridging CO group would not be expected to display such dichroism, for the reasons explained above. Therefore, structure B

can be rejected as a possible structure for $Cp^*_2Pt_2(\mu\text{-}CO)$.

Dichroism is also observed in the intense visible absorption band of $Cp^*_2Pt_2(\mu\text{-}CO)$ at 540 nm, responsible for the colour of the photoproduct. This band is polarised parallel to the plane of the photolysing light indicating that its electronic transition moment must lie along the Pt-Pt bond.

Since the Cp analogue, $Cp_2Pt_2(\mu\text{-}CO)$, is observed to have similar properties to $Cp^*_2Pt_2(\mu\text{-}CO)$, it is reasonable to assign the same structure, with a symmetrically bridging CO group, to both species.

The Electronic Ground State of $(\eta^5\text{-}C_5R_5)_2Pt_2(\mu\text{-}CO)$ (R = H, Me)

It has now been established that UV photolysis of $(CpPt(CO))_2$ or $(Cp^*Pt(CO))_2$ in low temperature matrices leads to loss of CO and production of the coordinatively unsaturated dinuclear species, $Cp_2Pt_2(\mu\text{-}CO)$ and $Cp^*_2Pt_2(\mu\text{-}CO)$ respectively, each with a single, symmetrically bridging carbonyl group. Since such a CO ligand is considered to donate one electron to each platinum atom, a formal Pt=Pt double bond must be drawn to fulfil the 18 electron rule for this structure.

It is much more difficult to determine the exact details of the electronic ground state of these species. Magnetic susceptibility measurements on the analogous 32-electron species, $Cp^*_2Fe_2(\mu\text{-}CO)_3$, which can be isolated as a crystalline solid, have shown that it has a triplet electronic ground state (Blaha 1985). However, in this case the D_{3h} symmetry of the $Fe_2(\mu\text{-}CO)_3$ core means that the HOMO is a doubly occupied, doubly degenerate e" (π^*) orbital, leading to the observed triplet ground state.

One method by which the electronic ground state of matrix isolated species can be determined is by the measurement of magnetic circular dichroism spectra. This technique allowed the assignment of a triplet state for matrix isolated $Fe(CO)_4$ (Barton 1977).

The principle behind this approach is that a paramagnetic species should exhibit a temperature-dependence in its MCD spectrum, whereas that of a diamagnetic species is independent of temperature. MCD measurements record the difference in the absorption of left and right circular polarised light. The sample under study is placed in a strong magnetic field, which causes a Zeeman splitting in degenerate electronic states. It is known that right circularly polarised light can only cause excitation of an electron from one of these Zeeman split levels, whereas left circularly polarised light can only cause excitation from the

other level. An energy difference between these states, induced by the magnetic field, causes a population difference which is temperature dependent. Since the MCD effect senses the relative populations of the two states, the magnitude of the MCD signal from a paramagnetic species is also temperature dependent.

Both $Cp_2Pt_2(\mu\text{-}CO)$ and $Cp^*_2Pt_2(\mu\text{-}CO)$ have intense visible electronic absorption bands on which MCD measurements could be made, so this technique would appear to be an ideal method to determine their electronic ground states. Experiments were carried out using the MCD matrix apparatus developed at the University of East Anglia (Graham 1986). $(Cp^*Pt(CO))_2$ was isolated in an argon matrix at 15 K using a similar spray-on method to that used in the experiments at Nottingham. The presence of the platinum complex in the matrix was confirmed by its UV/Visible spectrum. However, the amount of $(Cp^*Pt(CO))_2$ isolated was much smaller than in the experiments at Nottingham. This was thought to be due to the condensation of the compound on other cold surfaces between the sample tube and the matrix window.

The matrix was irradiated with UV light (230-345 nm) to generate $Cp^*_2Pt_2(\mu\text{-}CO)$ which was detected by its absorption at 540 nm in the UV/visible spectrum. However, no pink colour of the matrix could not be observed with the naked eye, indicating that only a

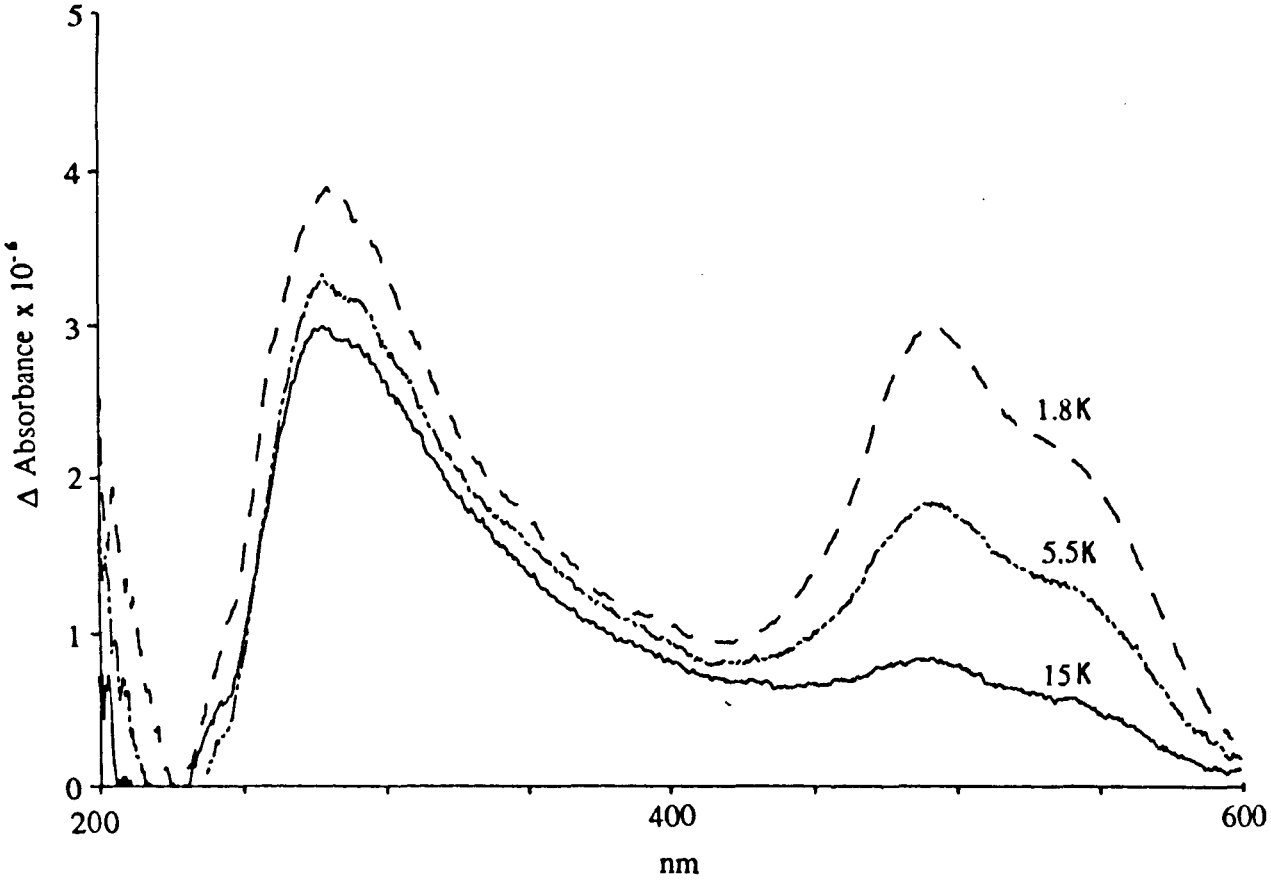


Figure 2.20: MCD spectra, recorded at 15, 5.5 and 1.8 K, after 25 mins filtered UV photolysis of $(Cp^{*}Pt(CO))_2$ isolated in an argon matrix, using a magnetic field strength of 8 Tesla. (Δ Absorbance is the difference in Absorbance of left and right circularly polarised light).

small amount of this species had been formed. (This colour was easily visible after only short periods of photolysis in the experiments at Nottingham). After irradiation, MCD spectra of the matrix were recorded at temperatures of 15, 5.0 and 1.8 K (shown in Figure 2.20). These spectra show a temperature dependence, particularly in the wavelength range 450-550 nm. This might be thought to indicate the presence of a paramagnetic species in the matrix. However, these results could not be reproduced in subsequent experiments and are considered unreliable, in view of the small amount of matrix isolated platinum complex. It is possible that the temperature dependence observed in these MCD spectra is due to an instrumental effect.

2.6 FLASH PHOTOLYSIS OF $((\eta^5\text{-}C_5R_5)Pt(CO))_2$ (R = H, Me)

Flash photolysis experiments on the platinum dimers were performed in collaboration with Dr. A. J. Dixon. Figure 2.21 shows a transient IR absorption band centred at 1765 cm^{-1}, generated by UV flash photolysis of $(Cp^*Pt(CO))_2$ in cyclohexane solution at room temperature. The frequency of this band is very close to the absorption observed for $Cp^*_2Pt_2(\mu\text{-}CO)$ in low temperature matrices (see Table 2.1) and can be reasonably assigned to the same species. The kinetic trace shown inset in Figure 2.21 illustrates that no significant decay of the IR absorption at 1765 cm^{-1}

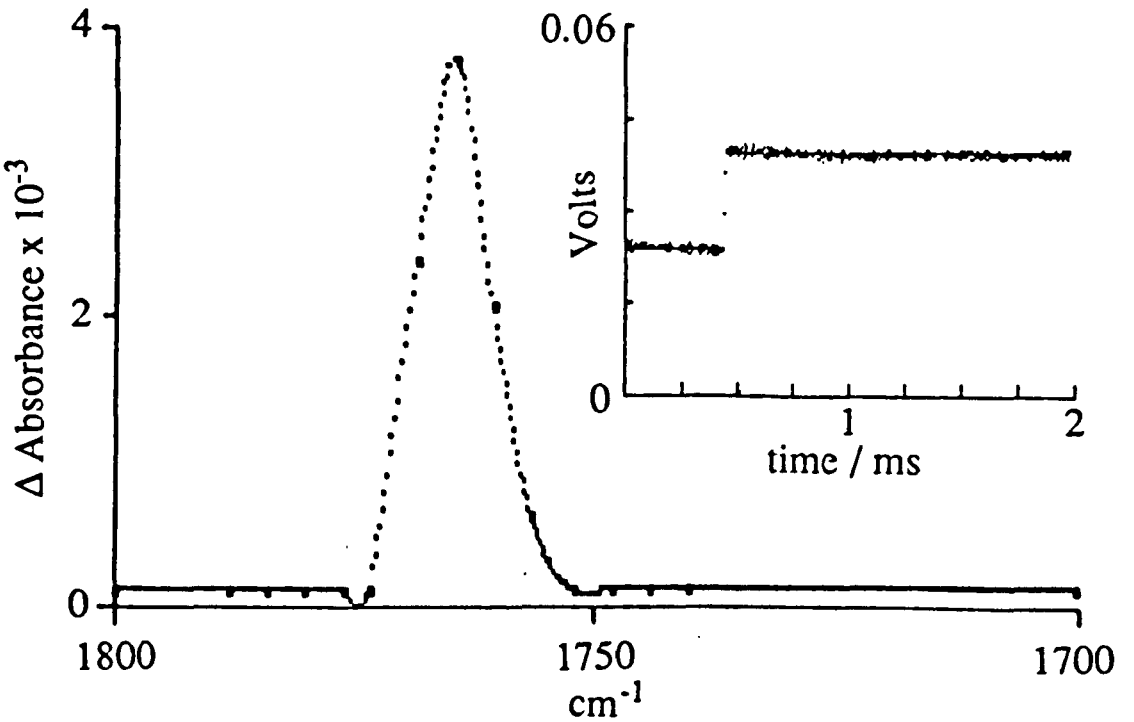


Figure 2.21: Transient IR absorption band due to $Cp^*_2Pt_2(\mu\text{-}CO)$ observed 250 μs after UV laser flash photolysis of $(Cp^*Pt(CO))_2$ in cyclohexane solution at room temperature. The inset illustrates the kinetic trace obtained at 1764.7 cm^{-1} showing no decay of the transient nearly 2 ms after the laser pulse.

is observable nearly 2 ms after the laser pulse, indicating that $Cp^*_2Pt_2(\mu\text{-}CO)$ is relatively long-lived in room temperature solution. Even in the presence of potential reactants such as CO or acetonitrile in solution, no change in the lifetime of $Cp^*_2Pt_2(\mu\text{-}CO)$ can be detected. TRIR experiments with $(CpPt(CO))_2$ give similar results to those with the Cp^* complex. A transient absorption centred at 1802 cm^{-1} is produced, very close to that of $Cp_2Pt_2(\mu\text{-}CO)$ isolated in low temperature matrices (see Table 2.1). This productive appears to similarly unreactive on a millisecond timescale

It is known that when a hydrocarbon solution containing an equimolar mixture of $(CpPt(CO))_2$ and $(Cp^*Pt(CO))_2$ is irradiated, the mixed dimer, containing both Cp and Cp^* rings is obtained (Equation 2.3) (Boag 1988b). In CO matrices, photolysis of either of the parent dimers leads to generation of the mononuclear species, $Pt(CO)_4$. Both of these reactions are likely to proceed via photochemical Pt-Pt cleavage. The radicals generated by such a reaction, $CpPt(CO)$ and $Cp^*Pt(CO)$, can combine to form the crossover product, or react with CO in a matrix, leading to $Pt(CO)_4$. In TRIR studies on the related iron dimer, $(CpFe(CO)_2)_2$, signals are observed due to the $\nu(CO)$ bands of the metal centred radical, $CpFe(CO)_2$, formed by homolysis of the Fe-Fe bond.

By contrast, flash photolysis of the platinum dimers gave no evidence for mononuclear products. It is possible that the ν(CO) bands of the radical species, $(C_5R_5)Pt(CO)$, lie outside the tuning range of the CO laser used to monitor IR absorption changes. However, kinetic traces due to the ν(CO) absorptions of the parent compounds show no evidence for rapid regeneration of starting material from any other photoproducts, such as mononuclear radicals. It is possible that for photolysis at 308 nm, the quantum yield for Pt-Pt bond homolysis is negligible compared with that for CO-loss. Generally, the relative quantum yield for M-M bond fission decreases compared with that for CO-loss with shorter wavelength irradiation (Turner 1988, Dixon 1989)). Under the conditions of these experiments, therefore, the yield of $(C_5R_5)Pt(CO)$ radicals may be negligible. It might be possible to detect the products of Pt-Pt bond fission using flash photolysis at a longer wavelength.

2.7 THE MATRIX PHOTOCHEMISTRY OF $(CpNi(\mu\text{-}CO))_2$

The low temperature photochemistry of the methylcyclopentadienyl nickel carbonyl dimer, $(Cp'Ni(\mu\text{-}CO))_2$, has been investigated by Hooker (1986). UV irradiation of $(Cp'Ni(\mu\text{-}CO))_2$ in a PVC film at 77 K causes depletion of the parent $\nu(CO)$ bands at 1877 and 1829 cm^{-1}, and generation of a photoproduct with an IR absorption at 1804 cm^{-1}, together with free CO. The photoproduct was assigned as a species with a single bridging CO ligand, $Cp'_2Ni_2(\mu\text{-}CO)$. Recombination of the unsaturated species with CO could be promoted by warming the film to ca. 150 K

There have also been reports of the isolation of the Cp complex, $(CpNi(\mu\text{-}CO))_2$, in frozen gas matrices. Crichton (1977) noted that photolysis of $(CpNi(\mu\text{-}CO))_2$ in a CO matrix results in formation of the mononuclear species CpNi(CO) and $CpNi(CO)_2$. In a separate study, the isolation of ^{13}CO enriched $(CpNi(\mu\text{-}CO))_2$ in an N_2 matrix enabled the calculation of an energy factored CO force field for this complex, for comparison with that of the related cobalt complex, $(CpCo(\mu\text{-}CO))_2$ (Crichton 1980).

Photolysis of $(CpNi(\mu\text{-}CO))_2$ in Argon Matrices

The $\nu(CO)$ region of the IR spectrum of $(CpNi(\mu\text{-}CO))_2$, isolated in an argon matrix at 12 K is shown in Figure 2.23(a). It has two matrix split bridging $\nu(CO)$ absorptions, centred near 1900 and 1850 cm^{-1} respectively. The spectrum is consistent with the IR spectrum of $(CpNi(\mu\text{-}CO))_2$ shown in Figure 2.22. The IR frequencies of all the species observed in this experiment are given in Table 2.4, along with their values in solution and in other matrices.

The intense low frequency absorption is assigned as the antisymmetric C-O stretching mode of the two bridging carbonyl groups, and the weaker high frequency band is attributed to the symmetric $\nu(CO)$ mode. This vibration is IR active because the molecule has C_{2v} symmetry with a non-planar $Ni_2(\mu\text{-}CO)_2$ core. The relative intensities of the two $\nu(CO)$ bands of $(CpNi(\mu\text{-}CO))_2$ in various solvents have been used to give an estimate of ca. 140° for the angle between the two CO groups (McArdle 1971). The crystal structure reveals that, in the solid state, two independent molecules with differently bent $Ni_2(\mu\text{-}CO)_2$ cores are present, with OC-CO angles of 146.8° and 139.9° respectively (Byers 1980).

Figure 2.23(b) shows the IR spectrum obtained after UV photolysis of the matrix containing

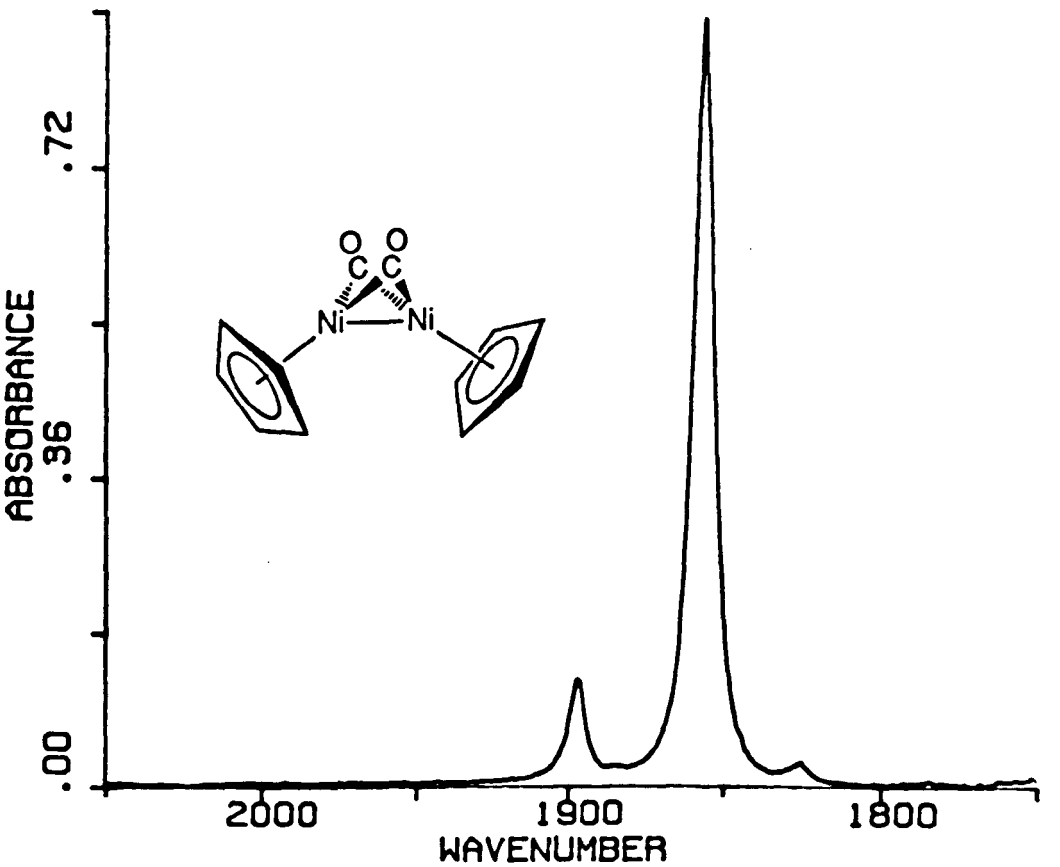


Figure 2.22: IR spectrum of $(CpNi(\mu\text{-}CO))_2$ in n-heptane solution at room temperature.

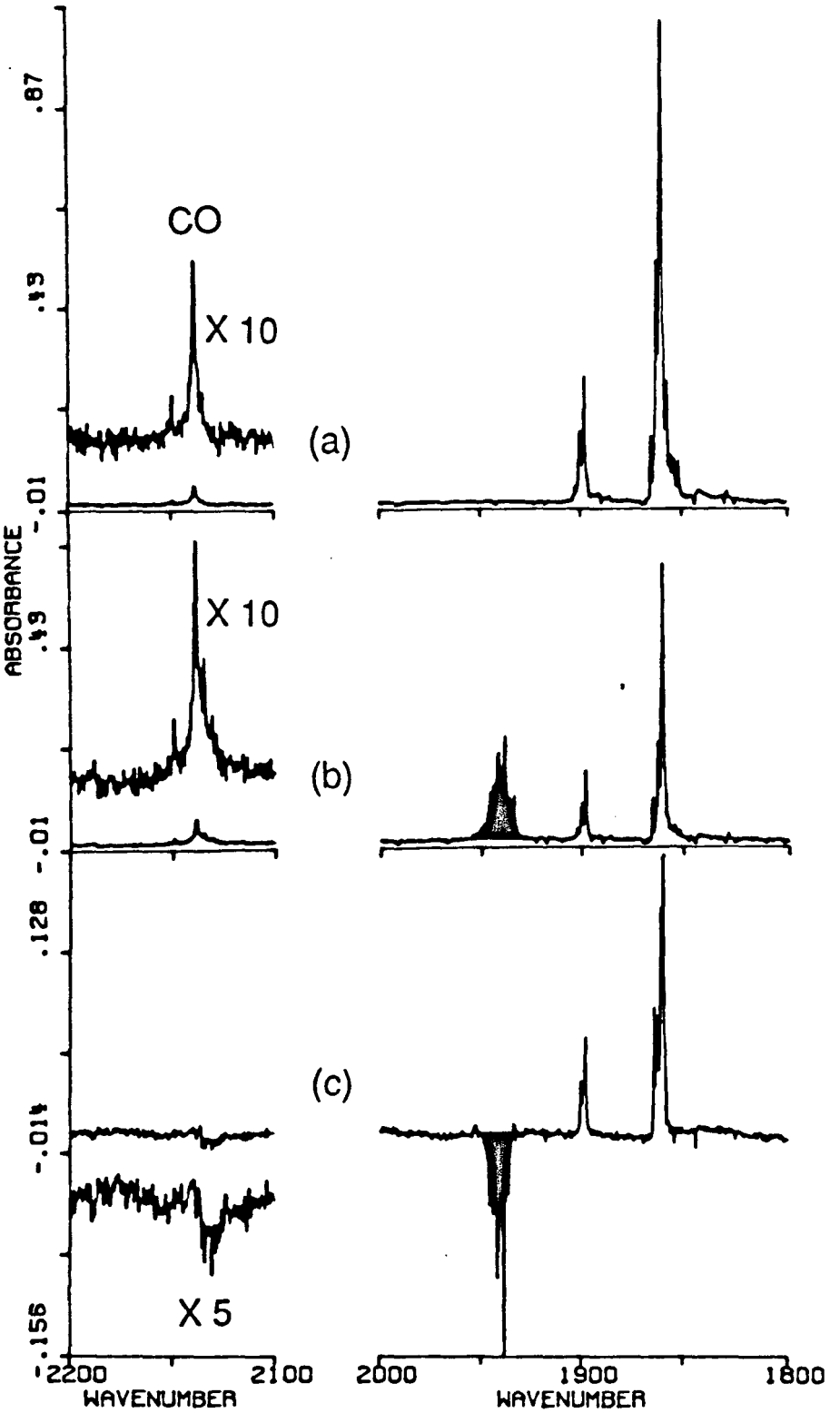


Figure 2.23: (a) IR spectrum of $(CpNi(\mu\text{-}CO))_2$ isolated in an argon matrix at 12 K. (b) After 90 mins filtered UV photolysis (230-345 nm); the band coloured black is due to $Cp_2Ni_2(CO)$. (c) IR difference spectrum showing the effects of 17 hrs photolysis with visible light (>375 nm). The absorption of CO is shown with an expanded absorbance scale.

$(CpNi(\mu\text{-}CO))_2$. The two bands of the starting material have decreased in intensity, and a new, matrix slit absorption has appeared to higher frequency, near 1940 cm^{-1}. There is also an increase in the band due to free CO at 2139 cm^{-1}. These changes in the IR spectrum are consistent with photoejection of CO from $(CpNi(\mu\text{-}CO))_2$ yielding a photoproduct with a terminal CO group, $Cp_2Ni_2(CO)$.

Clearly, there is an inconsistency between the results of this experiment and the observation of a CO-bridged species, $Cp'_2Ni_2(\mu\text{-}CO)$, on irradiation of $(Cp'Ni(\mu\text{-}CO))_2$ in a PVC film at 77 K (Hooker 1986). However, the difference in experimental conditions used may be significant. This will be discussed later in the Chapter.

By contrast with the results obtained for the platinum dimers, UV photolysis of matrices containing $(CpNi(\mu\text{-}CO))_2$ does not produce any visible colouration. However, irradiation with visible light promotes the reverse photochemical reaction, in a similar manner to the platinum dimers. The IR difference spectrum shown in Figure 2.23(c) shows that visible photolysis leads to depletion of the bands due to $Cp_2Ni_2(CO)$, and uncomplexed CO, and the regeneration of starting material. The photochemistry observed for $(CpNi(\mu\text{-}CO))_2$ in an argon matrix is summarised in Equation 2.10.

$$(CpNi(\mu\text{-}CO))_2 \underset{VIS}{\overset{UV}{\rightleftharpoons}} Cp_2Ni_2(CO) + CO \qquad 2.10$$

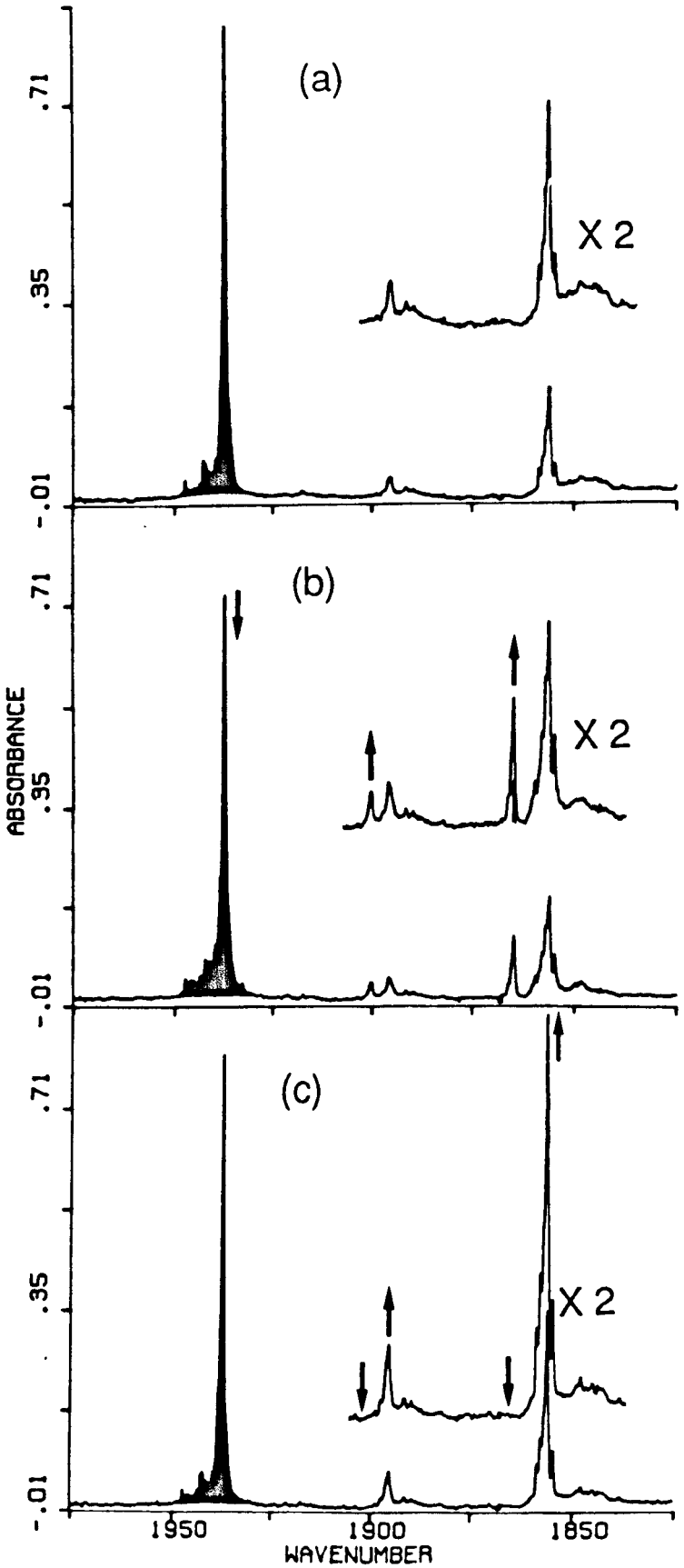
Annealing an argon matrix containing $Cp_2Ni_2(CO)$ to 30 - 35 K does not result in any thermal reaction of the unsaturated species.

Photolysis of $(CpNi(\mu\text{-}CO))_2$ in N_2 Matrices

UV photolysis of $(CpNi(\mu\text{-}CO))_2$ in an N_2 matrix at 12 K leads to similar changes in the IR spectrum as those observed using an argon matrix. A decrease in intensity of the parent $\nu(CO)$ bands is accompanied by the growth of a new absorption at 1937.3 cm^{-1} (Figure 2.24(a)), close to that assigned to $Cp_2Ni_2(CO)$ in argon matrices, and a weaker band at 2139 cm^{-1}, due to free CO. Annealing the matrix to 35 K causes a sharpening of the photoproduct band at 1937.3 cm^{-1}, but does not result in any thermal reaction of $Cp_2Ni_2(CO)$ with CO or N_2.

Visible irradiation causes the $\nu(CO)$ absorptions of the monocarbonyl, $Cp_2Ni_2(CO)$, and free CO to diminish. Figure 2.24(b) shows the growth of two new absorptions, close to the $\nu(CO)$ bands of remaining starting material. These new absorptions, at 1864.8

Figure 2.24: (Overleaf) IR spectra illustrating the photochemistry of $(CpNi(\mu\text{-}CO))_2$ isolated in an N_2 matrix at 12 K. (a) After 75 mins filtered UV photolysis (230-345 nm); the band coloured black is due to $Cp_2Ni_2(CO)$. (b) After 3 hrs visible photolysis (>375 nm). (c) After annealing the matrix to 30 K for 5 mins. Arrows represent the growth or depletion of absorptions. The bridging $\nu(CO)$ region is shown with an expanded absorbance scale.


(a)
(b)
(c)
X 2
X 2
X 2
.71
.35
-.01
ABSORBANCE
1950
1900
1850
WAVENUMBER

and 1900.3 cm^{-1}, resemble the two parent ν(CO) bands in relative intensity, but are shifted several cm^{-1} to higher frequency (see Table 2.4). Annealing the matrix to 30 K results in depletion of the new absorptions and growth of those of the starting material (Figure 2.24(c)).

In an argon matrix, photolysis with visible light was found to promote recombination of $Cp_2Ni_2(CO)$ with CO (see above). It is likely that the same reaction occurs in an N_2 matrix, the new absorptions being due to molecules of $(CpNi(\mu\text{-}CO))_2$ which are perturbed in some way. It appears that some interaction with the N_2 matrix causes the ν(CO) absorptions of the regenerated $(CpNi(\mu\text{-}CO))_2$ to be slightly shifted from those of the molecules not destroyed by photolysis. After warming the matrix the ν(CO) bands of the reformed molecules of $(CpNi(\mu\text{-}CO))_2$ shift back to the frequencies observed after deposition of the matrix.

Two possible explanations for these observations are given below:-

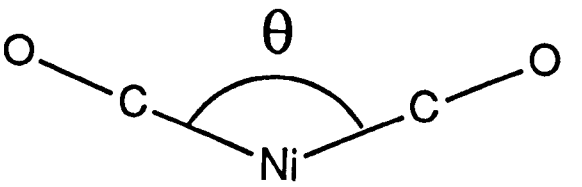
1) The shift in frequency could be due to site effects in the N_2 matrix. Ejection followed by recoordination of a CO ligand presumably causes reorganisation of the N_2 molecules of the matrix cage around each molecule of the nickel dimer. A molecule of $(CpNi(\mu\text{-}CO))_2$ which has undergone this process might occupy a different

site in the crystalline host than a molecule which has remained intact. This may explain the difference in ν(CO) frequencies for the molecules with different photochemical histories. Reversion to the original frequencies on annealing the matrix can be explained by further reorganisation of the crystal lattice.

2) Molecules of $(CpNi(\mu\text{-}CO))_2$ formed by recombination of $Cp_2Ni_2(CO)$ with CO might have a slightly different structure than those which remain intact during irradiation of the matrix. It has already been noted that crystals of $(CpNi(\mu\text{-}CO))_2$ are comprised of two independent molecules, which differ slightly in the degree of non-planarity of their $Ni_2(CO)_2$ cores (Byers 1980). It is possible that this type of structural isomerism also occurs in a solid N_2 matrix. An estimate of the OC-CO angles in each molecule can be obtained from the relative intensities of the two ν(CO) bands of each species, using Equation 2.11

$$\tan^2 (\theta/2) = I_{antisymm'}/I_{symm'} \qquad 2.11$$

θ is the angle between the two C-O bonds of the molecule, as shown below. The molecule is viewed along the Ni-Ni bond, and the Cp rings are omitted for clarity.



Using this relationship, OC-CO angles of 134° for $(CpNi(\mu\text{-}CO))_2$ before photolysis, and 128° for $(CpNi(\mu\text{-}CO))_2$ regenerated from the CO-loss product are obtained. The difference between these values is similar to the difference between the OC-CO angles of the two independent molecules of $(CpNi(\mu\text{-}CO))_2$ observed by X-ray crystallography (146.0° and 139.2°). This may indicate that the phenomenon is not just a matrix site effect, as suggested in (1), but that small differences in molecular geometry are induced photochemically. The fact that annealing the matrix to 30 K causes a shift back to the original ν(CO) frequencies implies a small energy of activation for conversion back to the more thermodynamically stable structure.

This effect is only observed in N_2 matrices, which may indicate that that a matrix site effect as described in (1) is operating. However, host-solute interactions, which vary depending on the matrix employed, might be strong enough to cause a small

structural perturbation of matrix isolated species, as suggested in (2).

No absorptions attributable to species containing N_2 ligands were observed at any stage in this experiment.

Photolysis of $(CpNi(u\text{-}CO))_2$ in CO Matrices

In a study of the photochemistry of CpNi(NO), Crichton and Rest (1977) reported briefly that photolysis of $(CpNi(\mu\text{-}CO))_2$ in a CO matrix leads to the production of small amounts of two mononuclear species, CpNi(CO) and $CpNi(CO)_2$.

Figure 2.25 shows the IR spectra recorded when this experiment was repeated during the current study. The initial spectrum of $(CpNi(\mu\text{-}CO))_2$ in a CO matrix (Figure 2.25(a)) shows the two characteristic bridging ν(CO) absorptions of the starting material, split by matrix effects. Filtered UV photolysis (230-345 nm) caused these bands to decrease in intensity, and the growth of a new band at 1932.7 cm^{-1} (Figure 2.25(b)). The similarity of the wavenumber of this band with that of the photoproduct observed for $Cp_2Ni_2(CO)$ in argon and nitrogen matrices suggests that it is due to the same monocarbonyl species. Annealing the matrix

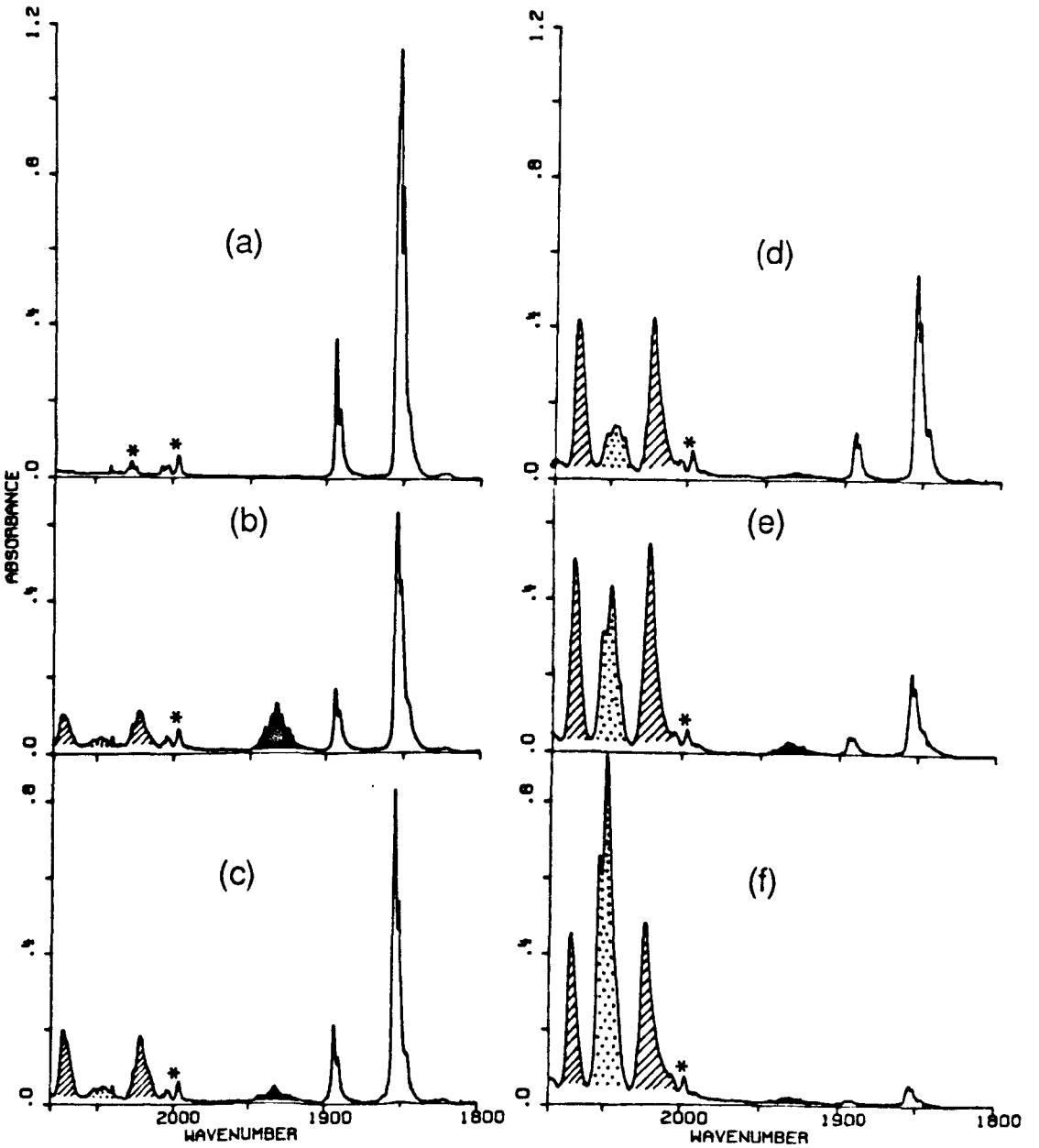


Figure 2.25: IR spectra illustrating the photochemistry of $(CpNi(\mu\text{-}CO))_2$ isolated in a CO matrix at 12 K. (a) Before photolysis; bands marked with asterisks are due to a trace impurity of $Fe(CO)_5$ in the CO. (b) After 170 mins filtered UV photolysis (230-345 nm). (c) After 40 mins visible photolysis (>400 nm) (d) After 300 mins visible photolysis. (e) After 75 mins unfiltered photolysis. (f) After 225 mins unfiltered photolysis. Photoproduct bands are marked: $Cp_2Ni_2(CO)$-black; $CpNi(CO)_2$-crosshatched; $Ni(CO)_4$-dotted.

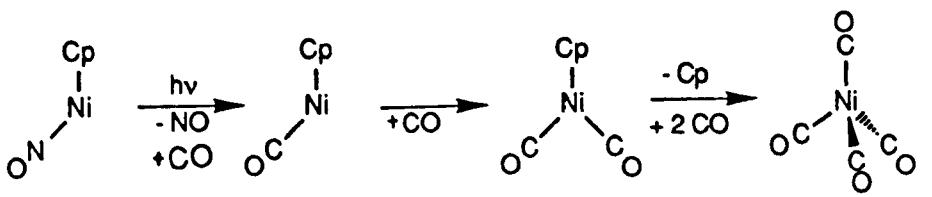
containing $Cp_2Ni_2(CO)$ to 30 K causes slow recombination with CO to regenerate starting material, as well as narrowing of the IR absorptions of matrix isolated species. Figure 2.25(c) shows that photolysis with visible light (> 375 nm) also leads to recombination of $Cp_2Ni_2(CO)$ with CO. This reaction occurs at a faster rate than observed in Ar or N_2 matrices, as might be expected.

Several weak features are also produced above 2000 cm^{-1} in the IR spectra shown in Figures 2.25(b) and (c). These absorptions are not observed in argon or nitrogen matrices. On further visible photolysis, the parent ν(CO) bands begin to decrease in intensity once more, whilst the terminal ν(CO) bands above 2000 cm^{-1} continue to grow (Figure 2.25(d)). The two crosshatched bands correspond well with those previously assigned to the mononuclear nickel species, $CpNi(CO)_2$, generated from either CpNi(NO) or$(CpNi(\mu\text{-}CO))_2$ in a CO matrix (Crichton 1977). The weaker (dotted) absorption between these two bands is close to that previously observed for $Ni(CO)_4$ in CO matrices (Perutz 1973).

Continued photolysis with the unfiltered medium pressure Hg arc lamp leads to further loss of starting material, accompanied by growth of all of the terminal ν(CO) absorptions above 2000 cm^{-1} due to mononuclear products (Figures 2.25(e) and (f)). The ν(CO) band of

$Ni(CO)_4$ becomes resolved into a doublet, corresponding to the matrix split t_2 vibrational mode previously observed for this species (Perutz 1973, Crichton 1977). In Figure 2.25(f), virtually all the starting material has been destroyed and the absorption of $Ni(CO)_4$ is the dominant feature of the spectrum. The bands of $CpNi(CO)_2$ have decreased in intensity, indicating that the dicarbonyl is an intermediate in the production of $Ni(CO)_4$.

The previously reported photochemical transformation of CpNi(NO) to $Ni(CO)_4$ in a CO matrix was proposed to proceed via the 17 electron radical, CpNi(CO) and the 19 electron species, $CpNi(CO)_2$, as shown in Equation 2.12 (Crichton 1977).



2.12

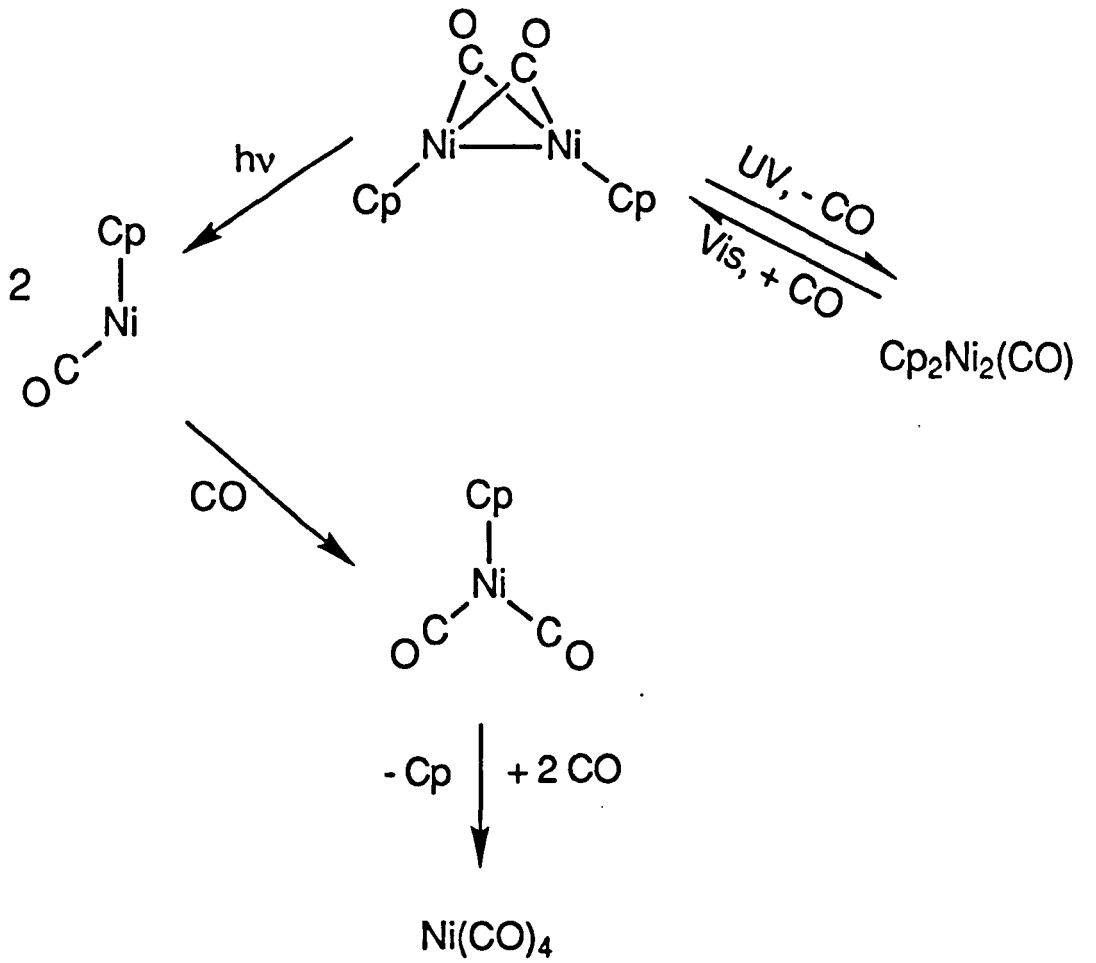
Isotopic enrichment with ^{13}CO led to the conclusion that the ν(CO) absorption of the monocarbonyl, CpNi(CO) is coincident with the high frequency band of the dicarbonyl, $CpNi(CO)_2$. This explained the variability in the observed relative intensities of the bands at 2070 and 2021 cm^{-1} during the experiment. In Figure 2.25, these two absorptions again show small changes in relative intensity. In spectrum (c) the high frequency band is the more

intense but this is reversed in spectra (d),(e)and (f). This suggests that small amounts of CpNi(CO) are present in the early stages of photolysis.

The photochemistry of $(CpNi(\mu\text{-}CO))_2$ in a CO matrix is summarised in Scheme 2.4. The two primary photochemical processes are CO loss and Ni-Ni bond homolysis. Recombination of $Cp_2Ni_2(CO))$ with CO can be promoted photochemically with visible irradiation, or thermally by annealing the matrix to 30 K. In this, and previous studies, there is evidence for small amounts of the primary product of Ni-Ni bond cleavage, CpNi(CO). It appears that the mononuclear 17-electron radicals react readily with CO to give $CpNi(CO)_2$, thus preventing rapid recombination in the matrix cage. Subsequent loss of the cyclopentadienyl ring and coordination of two more CO ligands leads to the final product, $Ni(CO)_4$.

These results provide an interesting contrast to the photochemistry of $(CpPt(CO))_2$ and $(Cp^*Pt(CO))_2$ in CO matrices. No mononuclear intermediate species such as CpPt(CO) or $CpPt(CO)_2$ were observed during the photochemical conversion of the platinum dimers to $Pt(CO)_4$. However, it is likely that these reactions follow a similar course.

The reaction of CpNi(CO) with CO, yielding $CpNi(CO)_2$, is analogous to that of the $CpFe(CO)_2$



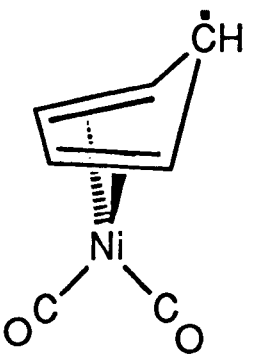
Scheme 2.4: Photochemistry of $(CpNi(\mu\text{-}CO))_2$ in a pure CO matrix.

radical, formed by photochemical homolysis of the Fe-Fe bond of $(CpFe(CO)_2)_2$ in CO matrices (Firth 1987b, Equation 2.13)

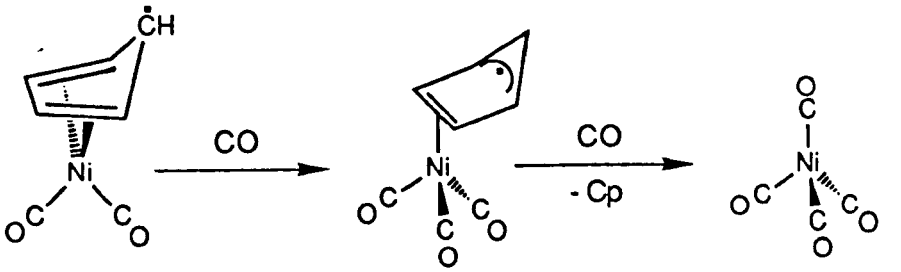
$$CpFe(CO)_2 \xrightarrow{+\ CO} CpFe(CO)_3 \qquad 2.13$$

$CpFe(CO)_3$ was proposed to have a structure with an $(\eta^4\text{-}C_5H_5)$ ligand, similar to that found in $(\eta^4\text{-}C_5R_4CH_2Ph)Fe(CO)_3$ (R = H, Me) (Blaha 1985a). This mode of coordination for the C_5R_5 ligand enables the metal atom to obey the 18 electron rule.

A structure with an $(\eta^4\text{-}C_5H_5)$ ligand can also be envisaged for $CpNi(CO)_2$, as illustrated below.

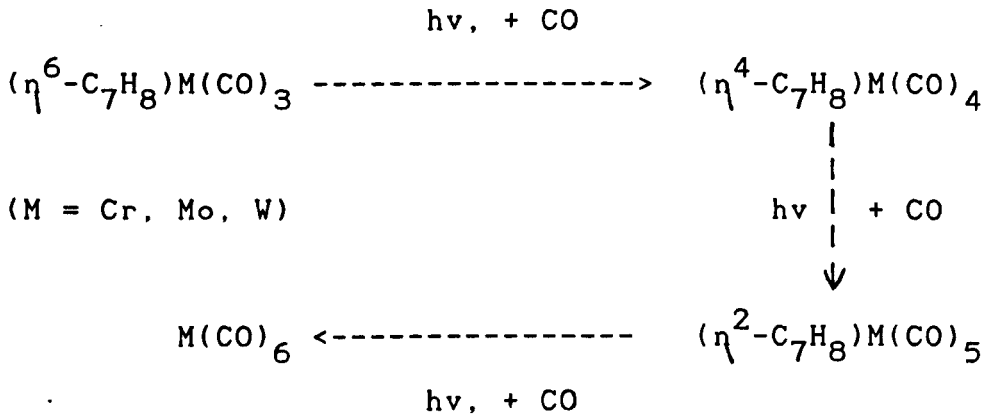


Subsequent reaction with CO to yield $Ni(CO)_4$ requires loss of the cyclopentadienyl ring. This could occur via an intermediate tricarbonyl species with an $(\eta^2\text{-}C_5H_5)$ group (Equation 2.14).

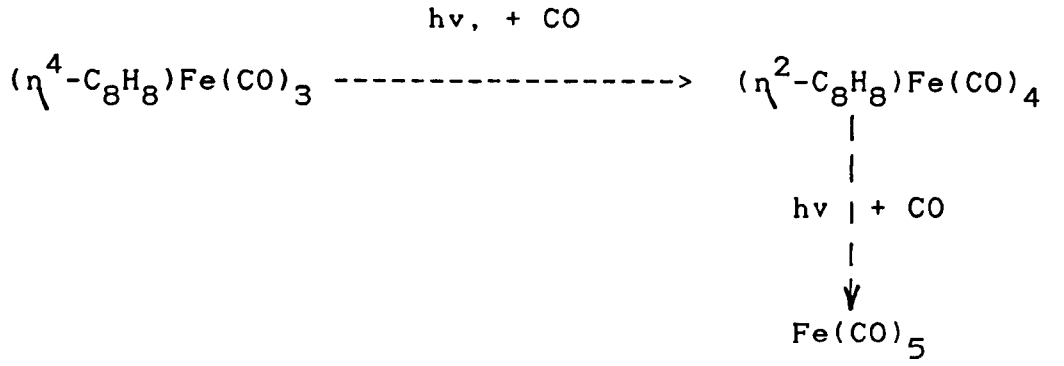


2.14

A similar reaction sequence can be envisaged for the production of $Pt(CO)_4$ from $((\eta^5\text{-}C_5R_5)Pt(CO))_2$ (R = H, Me). Such ring dechelation processes have been observed in several other systems as exemplified in Equations 2.15 and 2.16 (Hitam 1984).



2.15



2.16

In each of these cases, the final product is a binary metal carbonyl, $M(CO)_n$, resulting from stepwise ring ejection and addition of CO.

Table 2.4: Frequencies (cm^{-1}) of ν(CO) bands of $(CpNi(\mu\text{-}CO))_2$ and its photoproducts in matrices at 12 K, and in room temperature n-heptane solution. Frequencies bracketed together are assigned to matrix split bands.

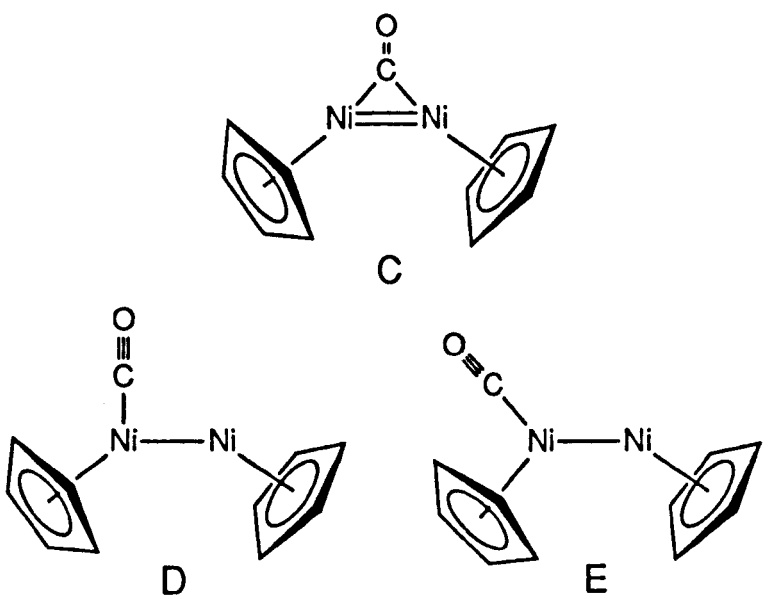
	Matrix Gas			
Species	**Ar**	**N_2**	**CO**	**Solution**
$(CpNi(\mu\text{-}CO))_2$	1859.9 1862.2	1856.3 1857.8	1851.4 1853.7	1856
	1897.9 1900.2	1896.0	1891.1 1894.0	1897
$Cp_2Ni_2(CO)$	1938.8 1942.1	1937.3	1932.7	1941[b]
$CpNi(CO)$			2071[a]	
$CpNi(CO)_2$			2021.8 2071.2	
$Ni(CO)_4$			2047.0 2051.8	

a This assignment is tentative, since it coincides with the high frequency band of $CpNi(CO)_2$ (see text).

b Observed by fast TRIR spectroscopy - see section 2.9.

2.8 STRUCTURAL CHARACTERISATION OF $Cp_2Ni_2(CO)$

The photochemistry observed for $(CpNi(\mu\text{-}CO))_2$ in low temperature matrices indicates that CO-loss and Ni-Ni cleavage are the primary photochemical processes, as observed for many other dinuclear metal carbonyls. The monocarbonyl species resulting from CO-loss has an IR absorption in the terminal $\nu(CO)$ region. This result conflicts with a previous observation of a bridged monocarbonyl product generated by irradiation of the closely related species, $(Cp'Ni(\mu\text{-}CO))_2$, in a PVC film at 77 K (Hooker 1986). Singly CO-bridged photoproducts have also been generated from $(CpPt(CO))_2$ and $(Cp^*Pt(CO))_2$ during the current study as described above. Three possible structures for a complex with the formula $Cp_2Ni_2(CO)$ are shown below.



Structure C contains a bridging CO group, as observed for $Cp_2Pt_2(\mu\text{-}CO)$, $Cp^*_2Pt_2(\mu\text{-}CO)$ and $Cp'_2Ni_2(\mu\text{-}CO)$. This structure can be ruled out due to observation of an IR band in the terminal $\nu(CO)$ region for $Cp_2Ni_2(CO)$ in low temperature matrices. D and E each contain a terminal CO ligand, oriented respectively at ca. 90° and 45° to the Ni-Ni bond. In principle, polarised photochemistry can be used to distinguish between such orientations. The arguments used to distinguish between a symmetric and semibridging CO group for $Cp^*_2Pt_2(\mu\text{-}CO)$ are equally applicable in this case.

Polarised Photochemistry of $(CpNi(\mu\text{-}CO))_2$

An experiment was carried out in which an N_2 matrix containing $(CpNi(\mu\text{-}CO))_2$ was irradiated with plane polarised light (230-345 nm). IR spectra were recorded through polarisers parallel or perpendicular to the plane of the photolysing light, as described in Chapter 6. The resulting dichroic spectrum is shown in Figure 2.26(b).

The bands of the starting material remaining after photolysis will be considered first. $(CpNi(\mu\text{-}CO))_2$ is known to possess C_{2v} symmetry, with two symmetrically bridging CO groups. The transition moment vectors for the symmetric (a_1) and antisymmetric (b_2) $\nu(CO)$

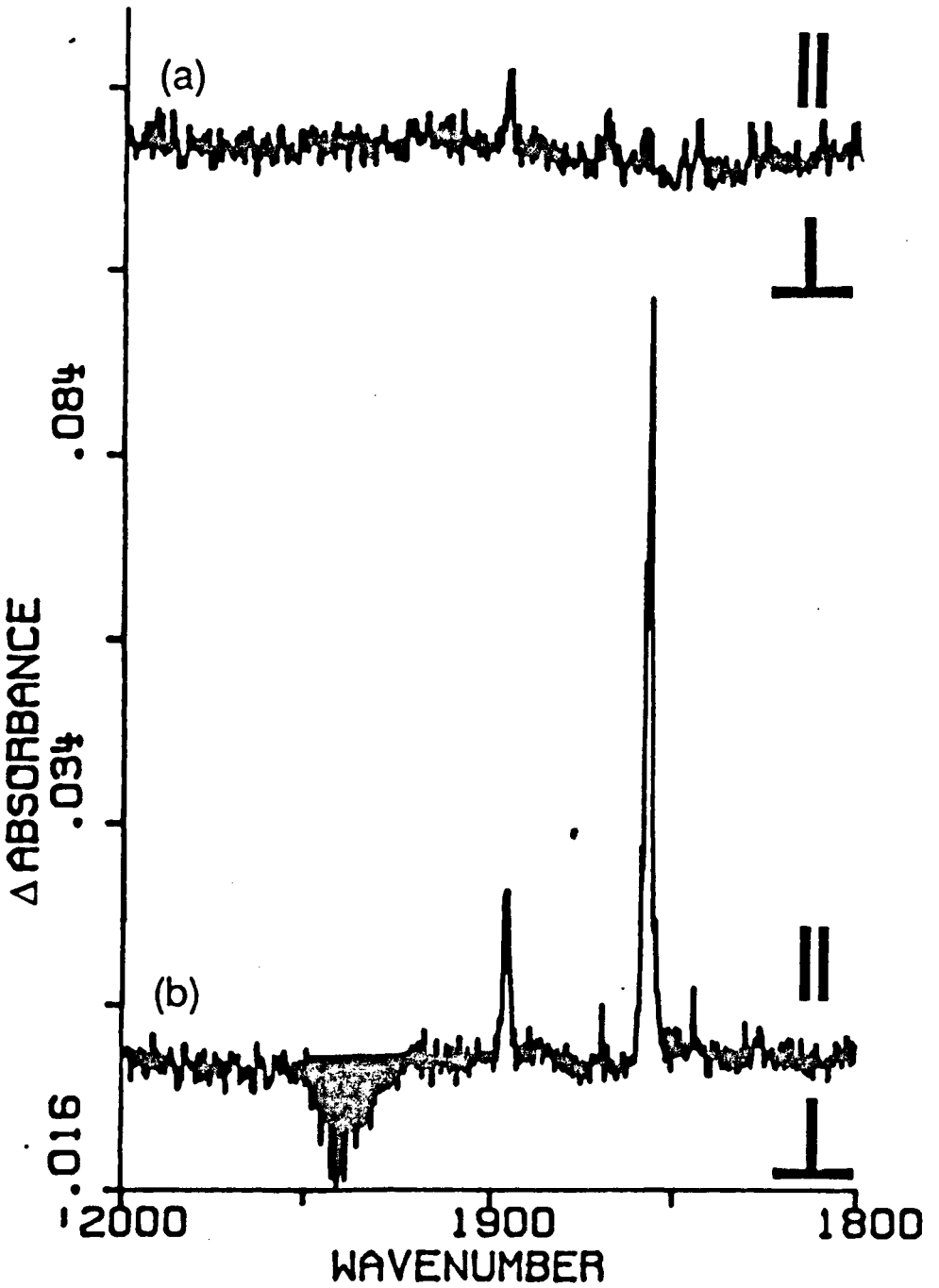


Figure 2.26: IR spectra illustrating the dichroism generated by plane polarised photolysis of $(CpNi(\mu\text{-}CO))_2$ isolated in an N_2 matrix at 12 K; Absorbance = $A_{\parallel} - A_{\perp}$. (a) Before photolysis; essentially a non-dichroic spectrum. (b) After 85 mins plane polarised photolysis (230-345 nm). The band coloured black is due to $Cp_2Ni_2(CO)$.

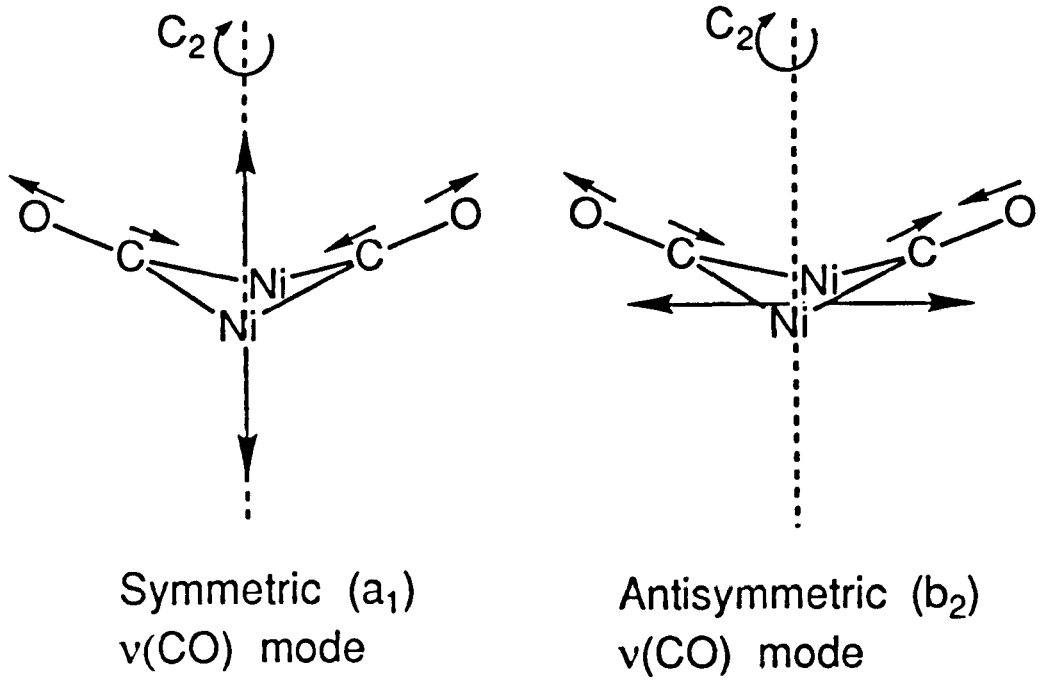


Figure2.27: The ν(CO) vibrational modes of $(CpNi(\mu\text{-}CO))_2$. Small arrows represent the relative motions of the carbon and oxygen atoms. Large arrows indicate the direction of the transition moment vector for each vibrational mode. The C_2 symmetry axis is indicated by a broken line and Cp groups are omitted for clarity.

vibrational modes of this molecule are orthogonal, each lying in a plane perpendicular to the Ni-Ni bond, as shown in Figure 2.27.

Both ν(CO) bands of $(CpNi(\mu\text{-}CO))_2$ exhibit linear dichroism parallel to the plane of photolysis (i.e. perpendicular to the photoactive transition moment vector of those molecules of starting material remaining intact after photolysis). The relative intensity of the two absorptions is identical to that in conventional IR spectra. Therefore, the photoactive UV transition moment vector must be parallel to the Ni-Ni bond.

The ν(CO) band of $Cp_2Ni_2(CO)$ produced by plane polarised photolysis exhibits dichroic photoproduction perpendicular to the plane of photolysis. Assuming no rotation of the Ni-Ni bond on loss of a CO group, this implies that that the remaining CO ligand has an orientation approximately perpendicular to the Ni-Ni axis. This observation is consistent with structure D, in which the Ni-Ni-CO bond angle is ca. 90°. No dichroism would be expected for structure E, with an Ni-Ni-CO bond angle of ca. 45°.

2.9 FLASH PHOTOLYSIS OF $(CpNi(\mu\text{-}CO))_2$

Figure 2.28 shows three transient IR absorption traces obtained in a preliminary solution flash photolysis experiment on $(CpNi(\mu\text{-}CO))_2$, performed in collaboration with Mr. M. W. George. The signal to noise ratio in these traces is not of the best quality, possibly due to scattering of light by small particles of undissolved material.

The signal obtained at 1856 cm^{-1} (Figure 2.28(a)) indicates a depletion of the low frequency parent ν(CO) band by the UV pulse, which is not regenerated. The trace recorded at 1941 cm^{-1} (Figure 2.28(b)), shows the production and rapid decay of a photoproduct absorption which corresponds well with the terminal ν(CO) band assigned to $Cp_2Ni_2(CO)$ in low temperature matrices (see Table 2.4). This absorption decays rapidly (half life ca. 100 μs) in room temperature solution. At 1837 cm^{-1}, in the bridging ν(CO) region, the growth of an IR absorption of a secondary product is apparent (Figure 2.28(c)). The rate at which this absorption is generated is similar to the rate of decay of the primary photoproduct, although the poor signal to noise ratio makes kinetic measurements difficult. The secondary product does not decay on the timescale of this experiment.

When the flash photolysis of $(CpNi(\mu\text{-}CO))_2$ was

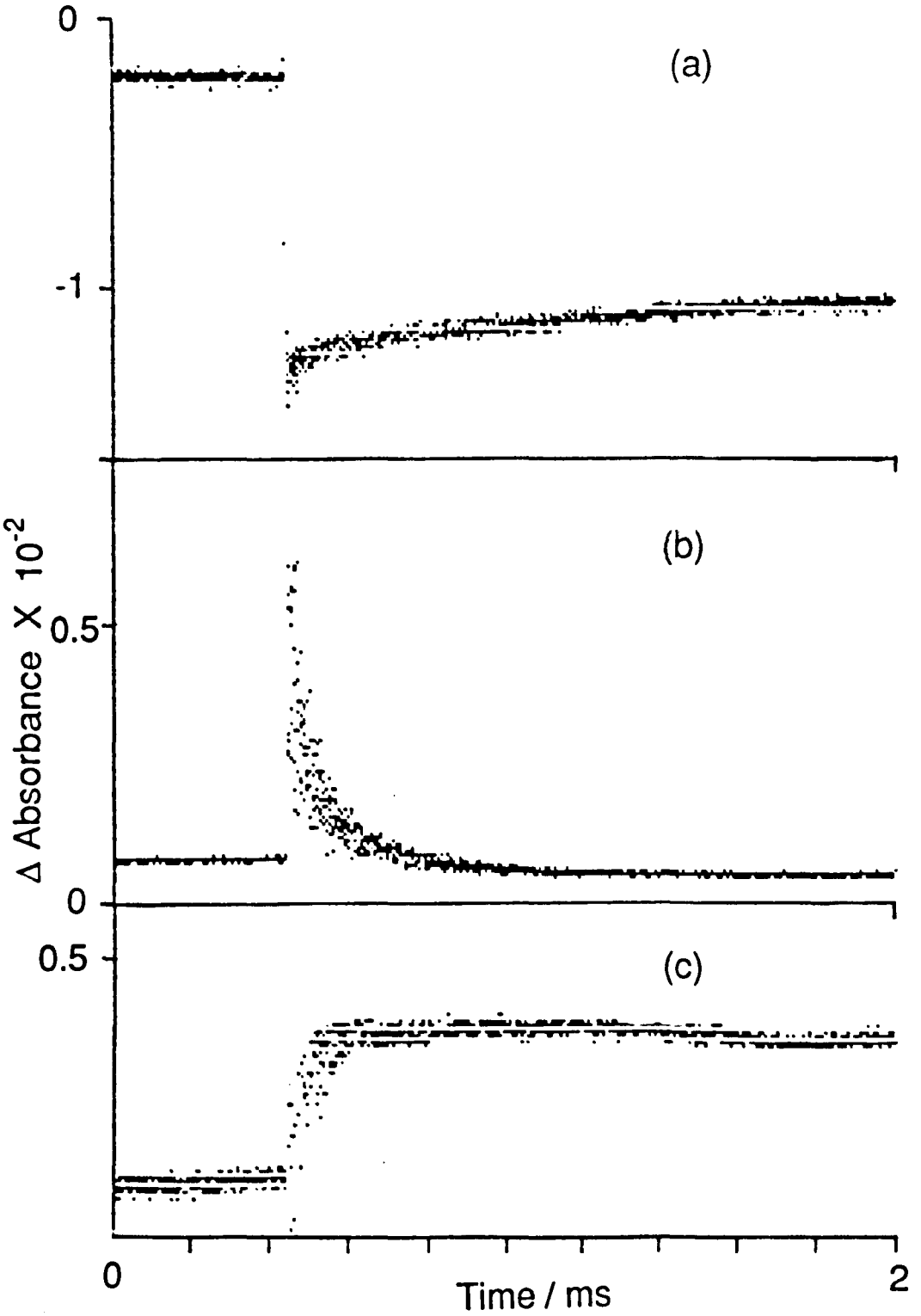


Figure 2.28: Transient IR absorption traces obtained on flash photolysis of $(CpNi(\mu\text{-}CO))_2$ in n-heptane at room temperature.

(a) 1856 cm^{-1}; depletion of low frequency parent ν(CO) band.

(b) 1941 cm^{-1}; formation and decay of $Cp_2Ni_2(CO)$.

(c) 1837 cm^{-1}; growth of secondary product, assigned as $Cp_2Ni_2(\mu\text{-}CO)$.

repeated under a pressure of 2 atm CO, no photoreaction was observed. Neither loss of parent nor generation of any photoproduct could be detected after the UV pulse.

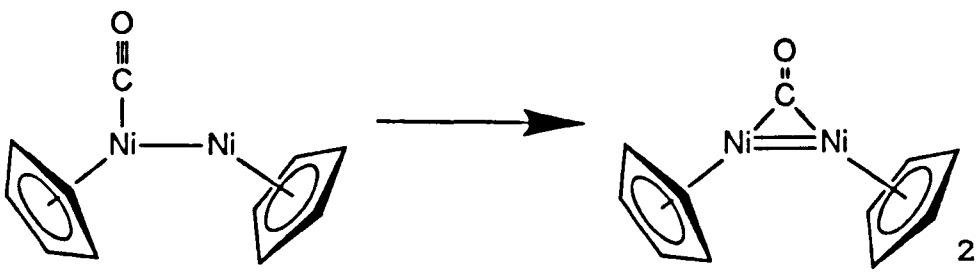
No evidence was obtained for radicals resulting from Ni-Ni bond homolysis on flash photolysis of $(CpNi(\mu\text{-}CO))_2$ in solution. However, the quantum yield for Ni-Ni cleavage may be small at 308 nm. Irradiation into the visible absorption band of $(CpNi(\mu\text{-}CO))_2$ in a CO matrix results in formation of mononuclear products, whereas UV photolysis leads predominantly to CO-loss (see above).

2.10 DISCUSSION

Flash photolysis of $(CpNi(\mu\text{-}CO))_2$ in room temperature solution results in formation of the same primary photoproduct as observed in low temperature matrices. The fact that this species cannot be detected in the presence of added CO in solution is consistent with its assignment as a CO-loss product. Presumably, rapid recombination with CO occurs under these conditions to regenerate parent. The thermal reaction of $Cp_2Ni_2(CO)$ with CO in matrices has already been noted.

In the absence of added CO, $Cp_2Ni_2(CO)$ decays rapidly by another route, to generate a secondary

product with an IR absorption in the bridging ν(CO) region. This absorption occurs to low frequency of the parent ν(CO) bands, and is reminiscent of the bridging ν(CO) band of $Cp'_2Ni_2(\mu\text{-}CO)$ observed in PVC films at 77 K. This suggests that the terminal CO group of $Cp_2Ni_2(CO)$ can migrate to a bridging position in room temperature solution (Equation 2.17).



2.17

The CO-bridged product of this reaction exhibits stability in solution similar to that of the isostructural platinum complexes (see section 2.6)

The observation of a terminal CO group in the primary photoproduct shows that photodissociation of CO from $(CpNi(\mu\text{-}CO))_2$ is accompanied by migration of the remaining CO group to a terminal position. Photo-induced CO-bridge opening has previously been observed for the ruthenium dimer, $(CpRu(CO)_2)_2$, although simultaneous CO-loss did not occur in this case (Hooker 1986).

The previous observation of $Cp'_2Ni_2(\mu\text{-}CO)$ in PVC films at 77 K can be explained by the different experimental conditions employed (Hooker 1986). Presumably, terminal-bridging CO migration occurs

readily even at 77 K. The limited temperature range of frozen gas matrices means that little information can be obtained about the thermal stability of $Cp_2Ni_2(CO)$ under these conditions.

$Cp_2Ni_2(CO)$ is assigned an asymmetrical structure with a vacant coordination site at one Ni atom. Therefore, it is a little surprising that this complex is thermally unreactive in N_2 matrices. However, N_2 complexes cannot be generated from either $Cp_2Pt_2(\mu\text{-}CO)$ (section 2.2) or $Cp_2Fe_2(\mu\text{-}CO)_3$ (Firth 1987b), even on excitation of their visible electronic absorption bands. It is not clear why unsaturated dinuclear complexes containing Cp ligands appear to be unreactive towards N_2.

2.11 CONCLUSIONS

The results presented in this Chapter have shown that photolysis of the platinum dimers, $((\eta^5\text{-}C_5R_5)Pt(CO))_2$ (R = H, Me), in frozen gas matrices results in dissociation of CO and formation of $(\eta^5\text{-}C_5R_5)_2Pt_2(\mu\text{-}CO)$. Polarised photochemistry has enabled identification of a symmetrically bridging CO group with its C-O vector perpendicular to the Pt-Pt bond. These 32 electron dinuclear photoproducts, with formal Pt=Pt double bonds are relatively long-lived in room temperature hydrocarbon solution. This stability

is a common feature amongst unsaturated cyclopentadienyl transition metal carbonyl dimers (Winter 1989).

The nickel dimer, $(CpNi(\mu\text{-}CO))_2$, also undergoes photodissociation of CO in frozen gas matrices. However, the carbonyl ligand remaining in the photoproduct occupies a terminal coordination site, indicating that CO loss is accompanied by bridge opening. The results of flash photolysis of $(CpNi(\mu\text{-}CO))_2$ in room temperature solution suggest rapid CO migration in the primary photoproduct, to give the more stable CO-bridged species, $Cp_2Ni_2(\mu\text{-}CO)$. In a previous investigation into the photochemistry of $(CpNi(\mu\text{-}CO))_2$ in PVC films at 77 K, the analogous bridged species, $Cp'_2Ni_2(\mu\text{-}CO)$ was the only photoproduct to be observed. The contrast between these results indicates the importance of the temperature and matrix medium employed in the study of unstable molecules.

For both the platinum and nickel dimers, irradiation in a CO matrix leads to formation of mononuclear fragments, resulting from M-M bond cleavage. In each case, the final product is the tetracarbonyl, $M(CO)_4$. For the nickel dimer, there is evidence for the intermediate mononuclear species, $CpNi(CO)$ and $CpNi(CO)_2$.

CHAPTER 3

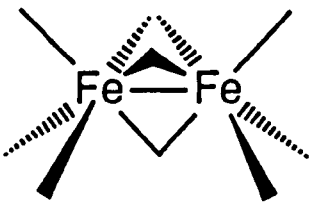
THE PHOTOCHEMISTRY OF DINUCLEAR OSMIUM CARBONYL COMPLEXES

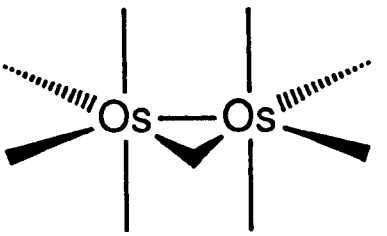
3.1 INTRODUCTION

A year after publication of his discovery of $Ni(CO)_4$, Ludwig Mond reported the photochemical decomposition of $Fe(CO)_5$, yielding free CO and a solid product (Mond 1891). This product was later formulated by Dewar and Jones (1905) as $Fe_2(CO)_9$, the first known dinuclear metal carbonyl complex. $Fe_2(CO)_9$ has since been the subject of considerable study and is amongst the most widely known and well characterised dinuclear metal carbonyls.

By contrast, the dinuclear carbonyl complexes of ruthenium and osmium have proved elusive until much more recent times. The synthesis of $Os_2(CO)_9$ was first achieved by Moss and Graham in 1970, using UV photolysis of $Os(CO)_5$ in n-heptane solution at -40°C. The product is a yellow, light sensitive solid which decomposes both in solution and the solid state at room temperature. The infrared and mass spectra of $Os_2(CO)_9$ are consistent with the complex having the structure of C_{2v} symmetry shown below, with four terminal CO groups on each osmium atom, and one CO group bridging the osmium-osmium bond. X-ray crystallographic studies

have shown that, by contrast, $Fe_2(CO)_9$ possesses a structure of D_{3h} symmetry with 3 symmetrically bridging CO groups (Powell 1939, Cotton 1974).

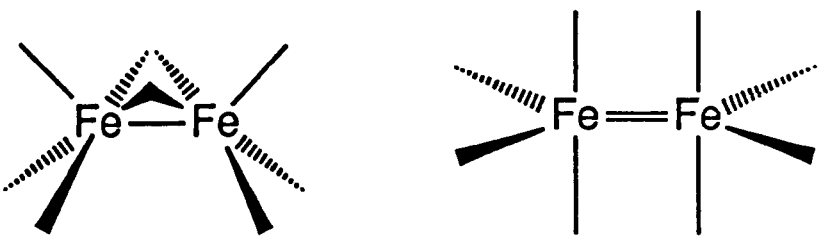




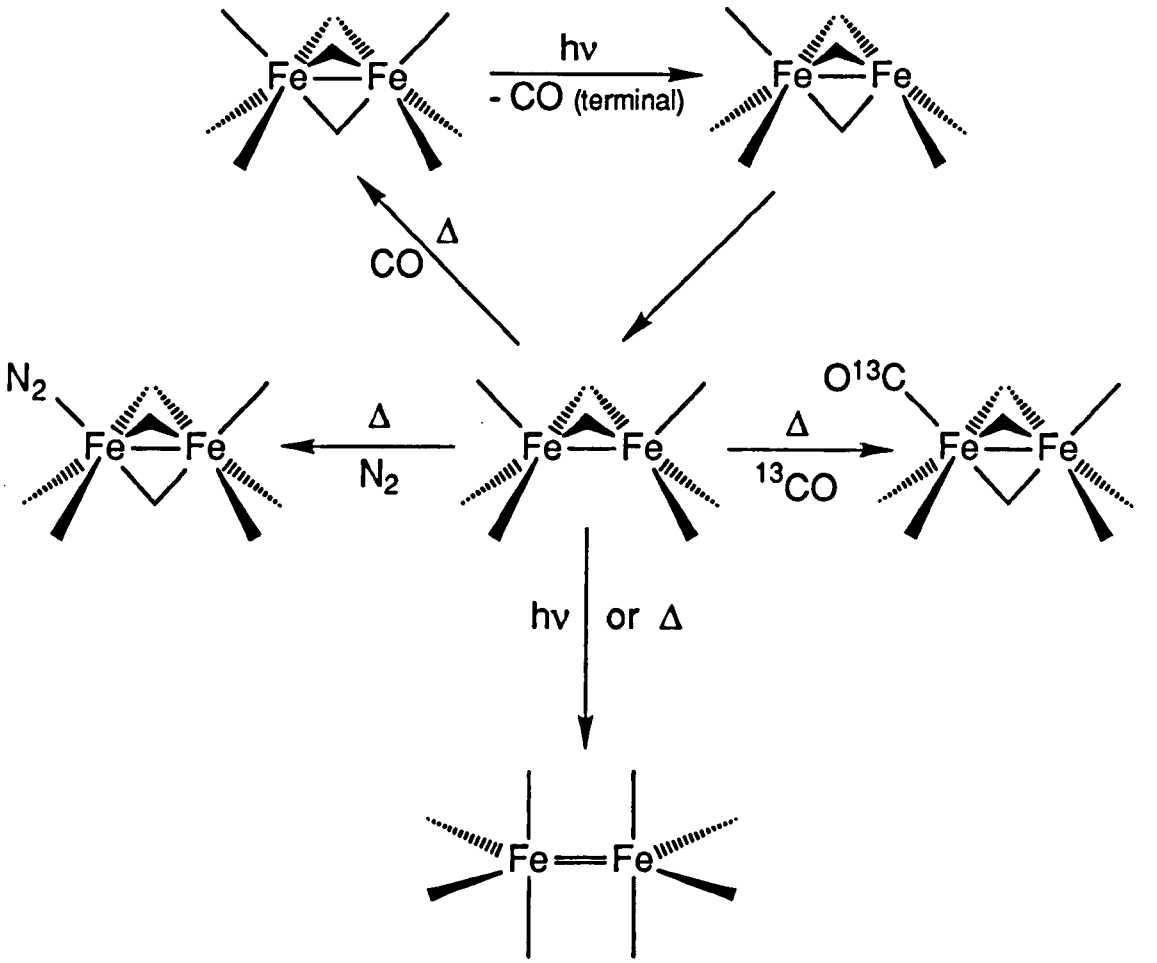
The difference in structure between these molecules is thought to be due to the longer metal-metal bond in the third row transition metal complex, which make it less energetically favourable for carbonyl groups to occupy a bridging position. Further studies by Moss and Graham (1977) gave evidence for the photochemical production of the dinuclear ruthenium analogue from $Ru(CO)_5$ in low temperature solution experiments. However, $Ru_2(CO)_9$ was found to be less stable than $Os_2(CO)_9$, and rapid decomposition made it difficult to obtain the solution IR spectrum. Thus, a definite structure could not be assigned for $Ru_2(CO)_9$.

The iron analogue, $Fe_2(CO)_9$, is insoluble in all common solvents. In this case, matrix isolation proved invaluable for carrying out vibrational studies on both

the parent and its photoproducts (Poliakoff 1971, Fletcher 1985, 1986). These studies provided evidence for photodissociation of CO and formation of the coordinatively unsaturated dinuclear species, $Fe_2(CO)_8$. It was found that $Fe_2(CO)_8$ could exist in two isomeric forms, with either two bridging CO groups or an unbridged structure, reminiscent of the isomerism known to occur in $Co_2(CO)_8$ (Bor 1974, Sweany 1977a).



The details of the matrix photochemistry of $Fe_2(CO)_9$ are shown in Scheme 3.1. Polarised photochemistry gave evidence for primary photodissociation of a terminal CO group. This must be followed by rapid CO migration to give the doubly CO-bridged isomer of $Fe_2(CO)_8$, which is the primary observable photoproduct. This species undergoes thermal recombination with CO in competition with an isomerisation to the thermodynamically more stable unbridged form of $Fe_2(CO)_8$. The same isomerisation can also be brought about photochemically. Annealing an N_2 or ^{13}CO doped matrix containing bridged $Fe_2(CO)_8$ leads to coordination of the dopant in a terminal position,

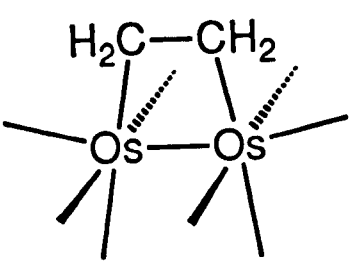


Scheme 3.1: The matrix photochemistry of $Fe_2(CO)_9$ (Adapted from Fletcher (1985)).

to give the substitution products $Fe_2(CO)_8(N_2)$ or $Fe_2(CO)_8(^{13}CO)$ respectively. Prolonged unfiltered photolysis of $Fe_2(CO)_9$ in a pure CO matrix results in the slow production of $Fe(CO)_5$, indicating that photo-induced Fe-Fe cleavage is an alternative photochemical process.

A study of the matrix photochemistry of $Os_2(CO)_9$ provides the opportunity to characterise the analogous unsaturated diosmium species, $Os_2(CO)_8$. In view of the effect that the difference in metal-metal bond length has on structures of the precursor molecules, $Fe_2(CO)_9$ and $Os_2(CO)_9$, it is of interest whether or not $Os_2(CO)_8$ shows similar structural isomerism to $Fe_2(CO)_8$.

The unsaturated dinuclear species, $Os_2(CO)_8$, has been proposed as a reactive intermediate in several recent studies (Burke 1983, Hembre 1987, Takats 1988). The formation and reactivity of 1,2-diosmacyclobutane complexes is of particular relevance. The structure of the simplest of these compounds, $Os_2(CO)_8(\mu\text{-}\eta^1,\eta^1\text{-}C_2H_4)$ (F), is illustrated below.



F

This complex is closely related to $Os_2(CO)_9$, which also contains four terminal CO ligands bound to each osmium atom. The bridging CO group of $Os_2(CO)_9$ is replaced by an ethylene unit bridging the Os-Os bond, which forms one side of the four membered ring in the 1,2-diosmacyclobutane. The two main synthetic routes to 1,2-diosmacyclobutanes are shown in Equations 3.1 and 3.2.

$$Na_2(Os_2(CO)_8) \xrightarrow{ICR_2CR_2I} Os_2(CO)_8(\mu\text{-}C_2R_4) \qquad 3.1$$

(Motyl 1982)

$$Os_3(CO)_{12} \xrightarrow[C_2R_4]{h\nu} Os(CO)_4(\eta^2\text{-}C_2R_4) + Os_2(CO)_8(\mu\text{-}C_2R_4) \qquad 3.2$$

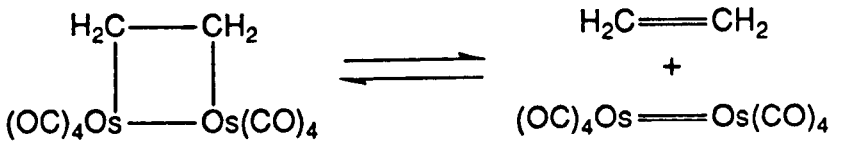
(Burke 1983, Takats 1988)

The ethylene unit of F undergoes exchange with other olefins and acetylenes in solution under mild, thermal conditions to provide a convenient route to other 1,2-diosmacycles. Similarly, the ethylene unit can be replaced by CO to give $Os_2(CO)_9$ in a reversible thermal reaction (Equation 3.3).

$$Os_2(CO)_8(\mu\text{-}C_2H_4) \underset{C_2H_4}{\overset{CO}{\rightleftharpoons}} Os_2(CO)_9 \qquad 3.3$$

Preliminary kinetic studies on these reactions indicate a dissociative mechanism (Equation 3.4) and

implicate $Os_2(CO)_8$ as a common reactive intermediate (Norton 1989).



3.4

The reactions shown in Equation 3.4 are ($2\pi + 2\pi$) processes and as such are formally forbidden as concerted processes by orbital symmetry rules. However, the olefin exchange reaction is highly stereospecific, which suggests a concerted mechanism (rather than a diradical one) for the fragmentation of F into C_2H_4 and $Os_2(CO)_8$ (Hembre 1987). A concerted mechanism is more plausible if $Os_2(CO)_8$ has a singlet ground state, although calculations suggest that the HOMO and LUMO of $Os_2(CO)_8$ are very close in energy, and thus make either a singlet or a triplet ground state imaginable (Bender 1989).

UV irradiation of an alkane solution of F under a CO atmosphere also results in production of $Os_2(CO)_9$. This implies that elimination of ethylene, to give the reactive $Os_2(CO)_8$ fragment, can occur photochemically, as well as thermally. In principle, however, an alternative photochemical process for F might be CO-loss. A low temperature matrix provides the ideal

environment in which to identify the primary photoproducts formed on irradiation of F. Comparison with the results of a similar study on $Os_2(CO)_9$ would be particularly illuminating. Observation of the same photoproduct from each complex would provide strong evidence for the intermediacy of $Os_2(CO)_8$ in the photochemistry of these complexes. Assignment of a structure for $Os_2(CO)_8$ may also give evidence for the nature of the electronic ground state of this species.

In this Chapter the results of an investigation into the matrix photochemistry of $Os_2(CO)_9$ and F are described. For $Os_2(CO)_9$, irradiation with plane polarised light is used, in order to probe the structural details of both starting material and photoproduct. Reference is also made to two recent studies of particular relevance, each using fast TRIR spectroscopy to identify $Os_2(CO)_8$.

3.2 THE MATRIX PHOTOCHEMISTRY OF DINUCLEAR OSMIUM CARBONYL COMPLEXES

Photolysis of $Os_2(CO)_9$ in Argon Matrices

The ν(CO) region of the IR spectrum of $Os_2(CO)_9$ in n-heptane solution, shown in Figure 3.1(a), exhibits four strong absorptions in the terminal ν(CO) region and one bridging ν(CO) band. This spectrum is in agreement with that previously reported by Moss and Graham (1970, 1977), and supports a C_{2v} structure for $Os_2(CO)_9$.

The electronic absorption spectrum of $Os_2(CO)_9$ shown in Figure 3.2(a) displays an absorption maximum at 275 nm, which tails into the visible region of the spectrum, giving the compound its yellow colour.

The IR spectrum of $Os_2(CO)_9$ isolated in an argon matrix at 12 K (Figure 3.3(a)) is essentially identical to the spectrum recorded in n-heptane solution, with four strong terminal ν(CO) bands and one bridging ν(CO) band. The frequencies of these bands show small shifts from the solution spectrum (see Table 3.1) and some of the bands are split into two or more narrow components. These splittings, which vary according to the type of matrix used are assigned to site effects in the crystal lattice of the solid matrix. The weak absorption at 2139 cm^{-1} is due to a small amount of uncoordinated CO

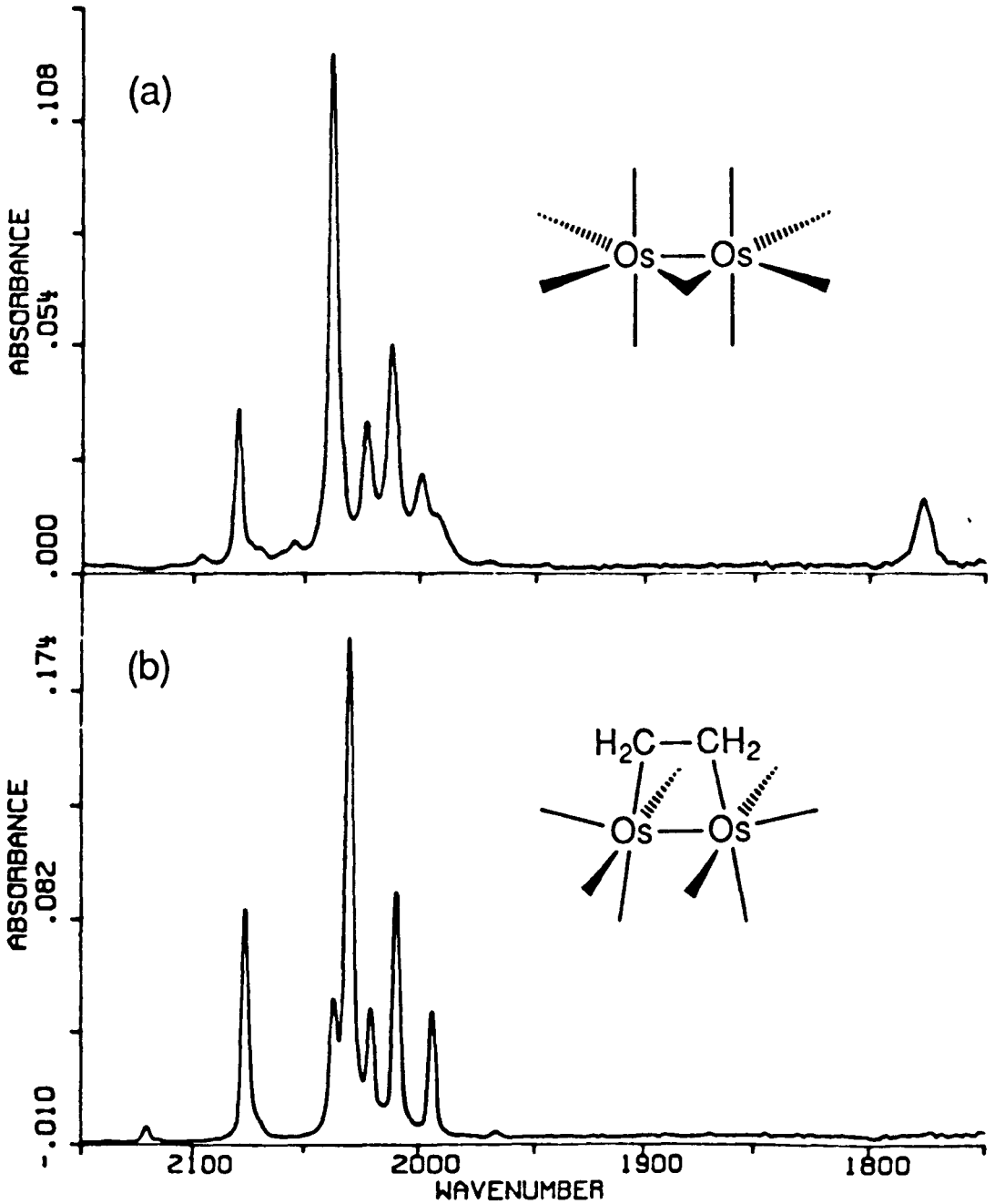


Figure 3.1: IR spectra of (a) $Os_2(CO)_9$ and (b) $Os_2(CO)_8(\mu\text{-}C_2H_4)$ (F) in n-heptane solution (1.2×10^{-4} M) at room temperature. The spectrum of $Os_2(CO)_9$ was obtained after 15 mins photolysis (230-345 nm) of F under 1 atm of CO.

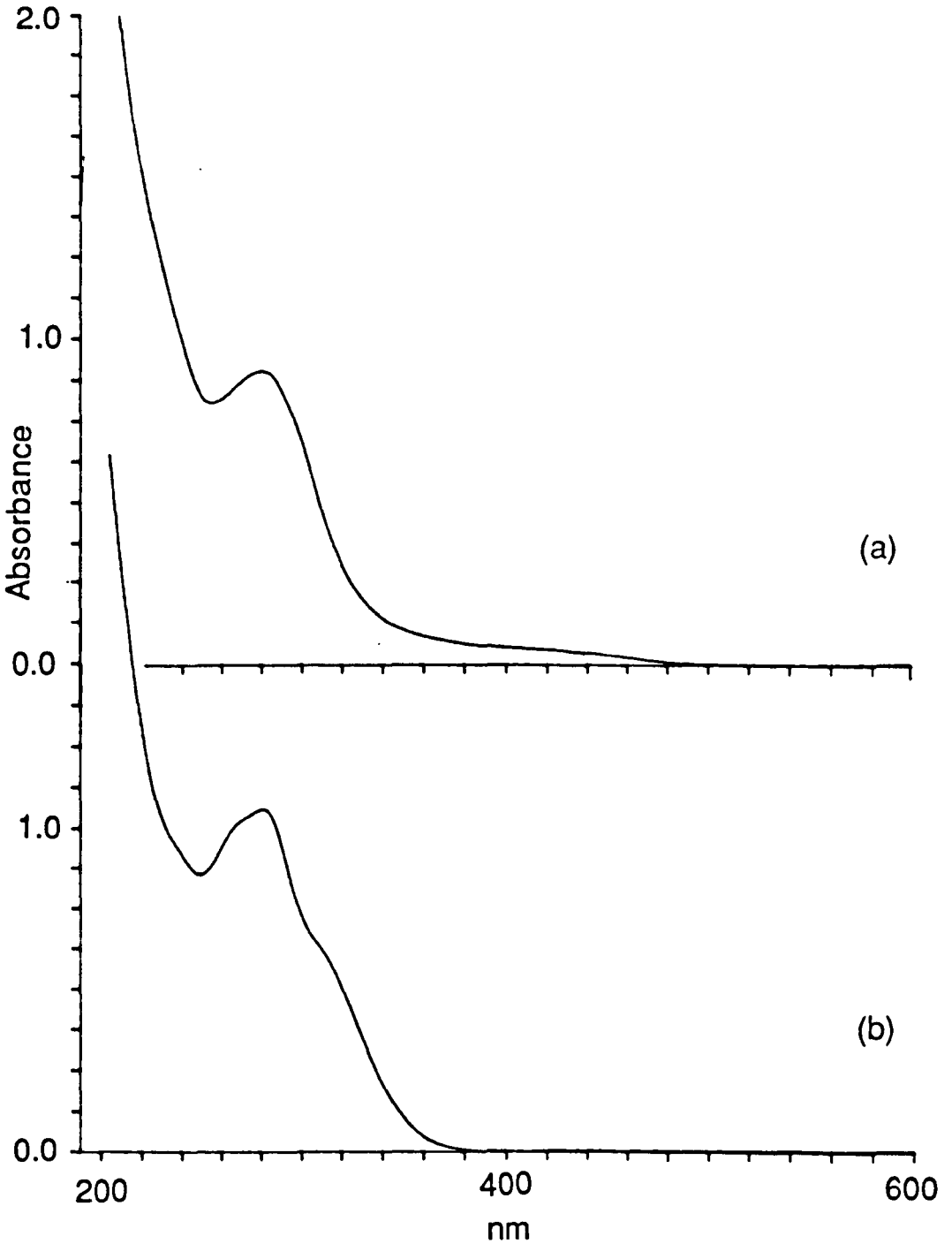


Figure 3.2: Electronic absorption spectra of (a) $Os_2(CO)_9$ and (b) $Os_2(CO)_8(\mu\text{-}C_2H_4)$ (F) in n-heptane solution (1.2×10^{-4} M) at room temperature. The spectrum of $Os_2(CO)_9$ was obtained in the same manner as the IR spectrum shown in Figure 3.1(a)

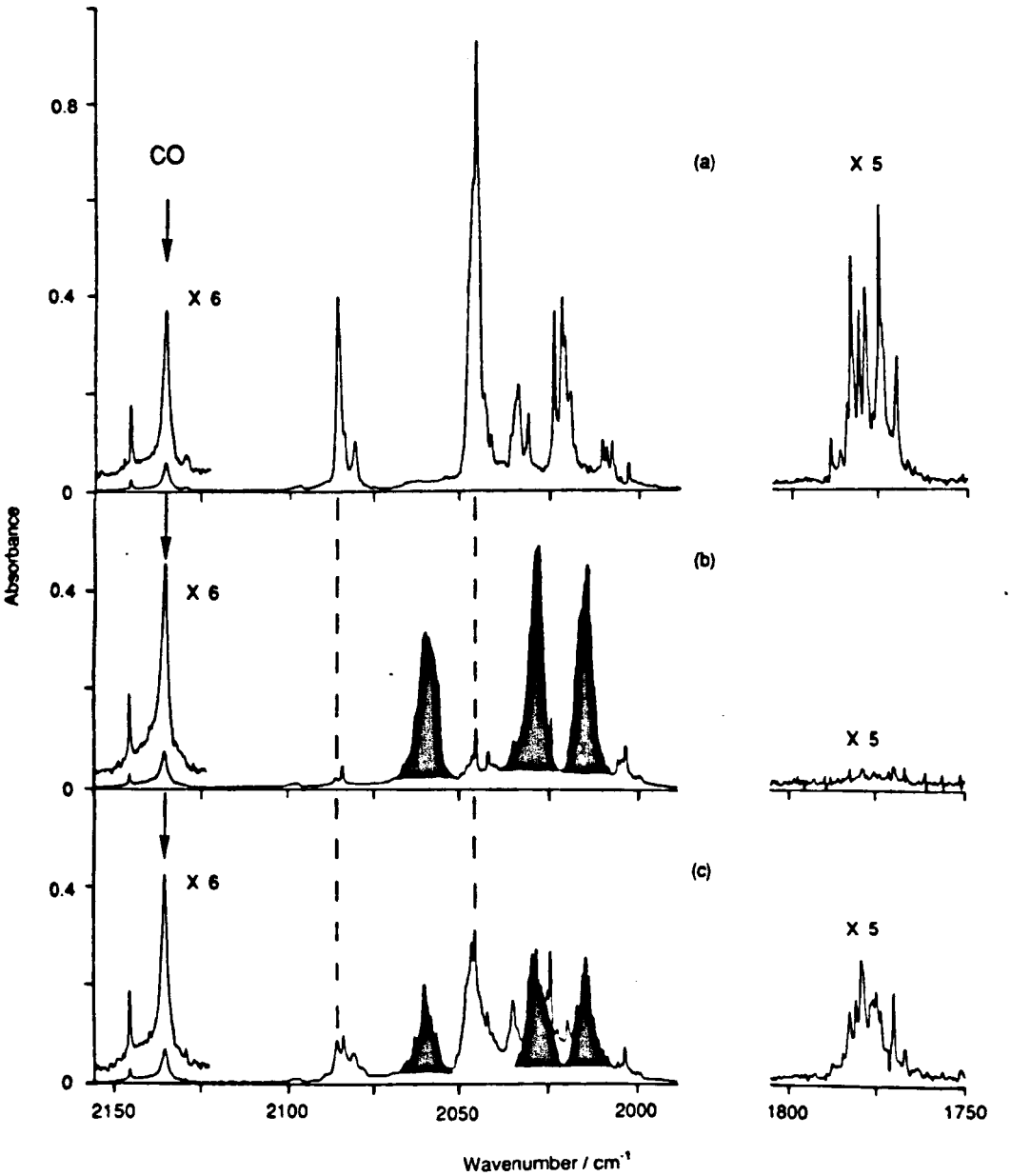


Figure 3.3: IR absorption spectra illustrating the photochemistry of $Os_2(CO)_9$ in an argon matrix at 12 K. (a) Before photolysis. (b) After 30 mins near UV irradiation (>375 nm). Bands due to the photoproduct, $Os_2(CO)_8$, are coloured black. (c) After 110 mins long wavelength (>525 nm) photolysis, showing reappearance of bands of $Os_2(CO)_9$ and depletion of $Os_2(CO)_8$ and CO. Note the absorbance scale expansion factors for the bridging CO and free CO regions.

trapped in the matrix. This probably originates from a slight decomposition of the $Os_2(CO)_9$ sample under vacuum, during deposition of the matrix. The matrix IR spectrum is thus in agreement with the C_{2v} structure proposed for $Os_2(CO)_9$ (Moss 1970, 1977).

Near UV irradiation (> 375 nm) of the matrix leads to a decrease in intensity of all of the ν(CO) bands of $Os_2(CO)_9$ and the growth of three new intense bands in the terminal ν(C-O) region, coloured black in Figure 3.3(b). After 30 min UV photolysis the bands of $Os_2(CO)_9$ have virtually disappeared. There is also an increase in the amount of uncoordinated CO in the matrix as shown by the growth of the absorption at 2139 cm^{-1}.

Since the starting material contains nine CO groups, it is possible that more than one is ejected upon photolysis. In order to determine the stoichiometry of the photoproduct, it is necessary to determine the relative concentrations of starting material and free CO produced by photolysis. However, it is difficult to measure the extinction coefficients of matrix isolated species accurately. A reasonable approximation can be made by using data recorded in other conditions. In this case, the values used are 2.0×10^4 M^{-1} cm^{-1} for the most intense ν(C-O) band of $Os_2(CO)_9$ (2038 cm^{-1}, measured in room temperature n-heptane solution) and 4.0×10^2 M^{-1} cm^{-1} for CO in an

alkane matrix at 77 K (Pope 1985). The ratio of these two values is 50:1 which is almost exactly the ratio of the changes in absorbance of the corresponding bands observed in an argon matrix. Therefore, the amount of free CO produced by photolysis is consistent with the liberation of one CO ligand for each molecule of $Os_2(CO)_9$ destroyed.

The spectrum in Figure 3.3(b) shows that the photoproduct has no absorptions which could be assigned to bridging CO groups. However it is unlikely that any mononuclear species are formed, since the observed IR spectrum corresponds to neither of the potential mononuclear products, $Os(CO)_5$ or $Os(CO)_4$, which have previously been observed in low temperature matrices (Poliakoff 1974).

The observations are readily explained by dissociation of CO, leading to the formation of an unsaturated dinuclear product with the formula $Os_2(CO)_8$ (Equation 3.5).

$$Os_2(CO)_9 \xrightarrow[Ar\ /\ 12K]{UV} Os_2(CO)_8 + CO \qquad 3.5$$

To be consistent with the spectrum in Figure 3.3(b), $Os_2(CO)_8$ must have a structure with only terminal CO ligands. The analogous iron species was

found to exist in two isomeric forms, with or without bridging CO groups, as described in the Introduction to this Chapter. The unbridged structure was found to be more thermodynamically stable than the structure with two CO bridges. For $Os_2(CO)_8$, which has a longer metal-metal bond, one would expect a bridged isomer to be even less energetically favourable, which is consistent with the observations described above.

In many previous matrix studies on similar systems, it has been found that unsaturated dinuclear metal carbonyl complexes have electronic absorption bands at longer wavelengths than their saturated precursors. Excitation of these absorptions with visible light, can induce the unsaturated species to recombine with the photoejected CO, or with other potential two electron donor ligands.

When the argon matrix containing $Os_2(CO)_8$ is irradiated with visible light of wavelength > 525 nm, the IR absorptions of $Os_2(CO)_8$ and free CO decrease in intensity and those of $Os_2(CO)_9$ grow (Figure 3.3(c)). This indicates that recombination of $Os_2(CO)_8$ with CO is indeed promoted under these photolysis conditions (Equation 3.6).

$$Os_2(CO)_8 + CO \xrightarrow[Ar\ /\ 12\ K]{> 525\ nm} Os_2(CO)_9 \qquad 3.6$$

Repeating the photolysis of $Os_2(CO)_9$ in an argon matrix using UV light of wavelength 230-345 nm results in similar changes in the IR spectrum to those observed when using a light of wavelength > 375 nm. $Os_2(CO)_9$ is destroyed and the bands assigned to the photoproducts, $Os_2(CO)_8$ and free CO, grow in. Under these photolysis $Os_2(CO)_9$ is consumed more rapidly. This could indicate a higher quantum yield for CO loss at shorter wavelengths, or that competition with the reverse reaction occurs when longer wavelength irradiation is used.

Table 3.1: Frequencies (cm^{-1}) of ν(CO) bands of $Os_2(CO)_9$, $Os_2(CO)_8$ and $Os(CO)_5$ in different matrices at 12 K. Weak bands assigned as ^{13}CO satellites are not included.

	Matrix Gas				
Species	**Ar**	**N_2**	**CO**	**CH_4**	**Solution**
$Os_2(CO)_9$	2085.2[a]	2087.0[a]	c	2084.3	2080[d]
	2041.9[a]	2046.5[a]	2046.0[a]	2045.1[a]	2038
	2028.8[a]	2026.8	2026.0	2027.5[a]	2023
	2018.4[a]	2013.0[a]	2011.1[a]	2011.3[a]	2012
	1778.5[b]	1771.6[b]	1759.9[b]	1766.3	1778
$Os_2(CO)_8$	2056.8	2059.3[a]	2055.5[a]	2055.7[a]	2058[e]
	2023.4	2025.0	2022.4	2023.5	2018
	2007.1	2007.6[a]	2005.3	2004.1	2003
$Os(CO)_5$			2046.2		
			1995.3		
			1985.6		

a Strongest component of band split by matrix effects.

b Average frequency of band split into multiplet.

c High frequency band obscured by absorption of CO matrix.

d IR spectrum of $Os_2(CO)_9$ recorded in n-heptane.

e IR spectrum of $Os_2(CO)_8$ observed by fast TRIR spectroscopy in cyclohexane (Grevels 1989 - see section 3.4).

Photolysis of $Os_2(CO)_8(\mu\text{-}\eta^1,\eta^1\text{-}C_2H_4)$ (F) in Argon Matrices

As reviewed in the Introduction to this Chapter, $Os_2(CO)_8$ has been proposed as an intermediate in both the thermal and photochemical reactions of 1,2-diosmacyclobutanes. Since the IR spectrum of matrix isolated $Os_2(CO)_8$ has been observed in experiments on $Os_2(CO)_9$, it should be a simple matter to determine whether the same photoproduct is generated from F under similar conditions.

Figure 3.4(a) shows the IR spectrum of F isolated in an argon matrix at 12 K. It agrees well with the spectrum recorded in hydrocarbon solution shown in Figure 3.1(b).The electronic absorption spectrum of F in n-heptane solution displays a maximum at 280 nm (Figure 3.2(b)). Photolysis of the argon matrix containing F was carried out using broad band filtered UV light of wavelength 230-345 nm.

The IR spectrum obtained after 3 minutes UV photolysis can be seen in Figure 3.4(b). The bands of F have virtually disappeared, and three new intense absorptions, coloured black, have grown in. The new absorptions correspond well with the bands of $Os_2(CO)_8$ produced by photolysis of $Os_2(CO)_9$ in an argon matrix (see above). (Slight differences in the relative band widths and intensities in the two experiments are

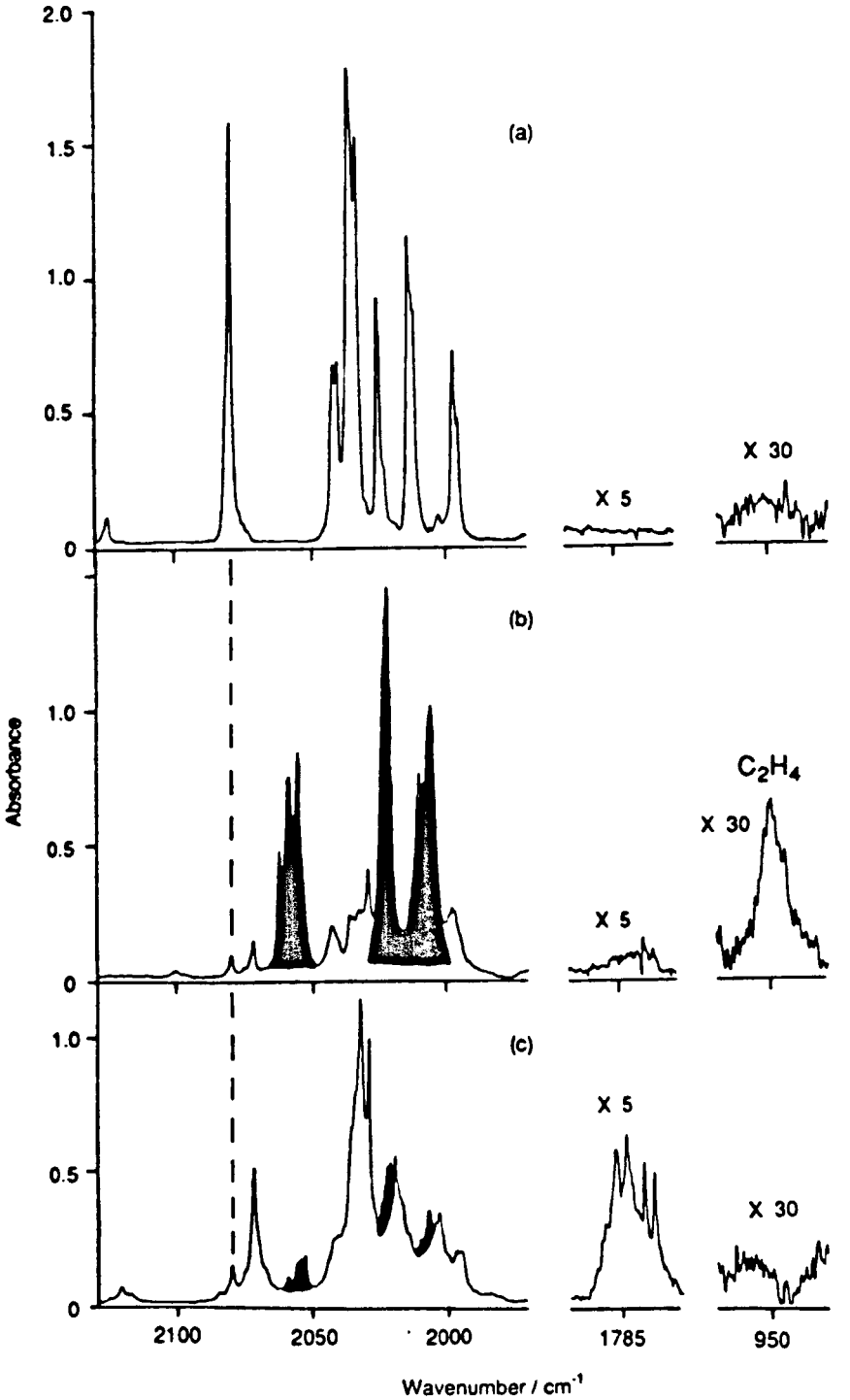


Figure 3.4: IR spectra illustrating the photochemistry of $Os_2(CO)_8(\mu\text{-}C_2H_4)$ (F) in an argon matrix at 12 K. (a) Before photolysis. (b) After 3 mins UV photolysis (230-345 nm). The bands coloured black are due to $Os_2(CO)_8$. Note the low frequency absorption due to the photoejected C_2H_4. (c) After 15.5 hrs long wavelength irradiation (> 525 nm). Note the growth of new absorptions due to G. The bridging ν(CO) and free C_2H_4 bands are shown with an expanded absorbance scale.

probably due to small variations in the matrix concentration or weak interactions of $Os_2(CO)_8$ with the photoejected CO or C_2H_4 molecules in the matrix cage).

A weak absorption at 950 cm-1, due to free ethylene in the matrix, is also observed, proving that UV photolysis causes ejection of C_2H_4 from F. (Equation 3.7). No absorption due to photoejected CO is produced in this experiment. The fact that the same photoproduct is observed, on both dissociation of CO from $Os_2(CO)_9$, and dissociation of C_2H_4 from F, gives clear evidence that the photoproduct is, indeed, $Os_2(CO)_8$.

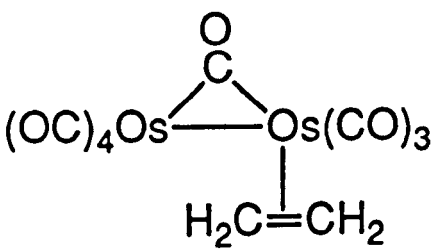
$$Os_2(CO)_8(\mu\text{-}C_2H_4) \xrightarrow[Ar\ /\ 12\ K]{UV} Os_2(CO)_8 + C_2H_4 \qquad 3.7$$

This photochemical reaction involves ejection of a bridging ethylene fragment. It is not clear whether a terminal or bridging CO group is ejected from $Os_2(CO)_9$.

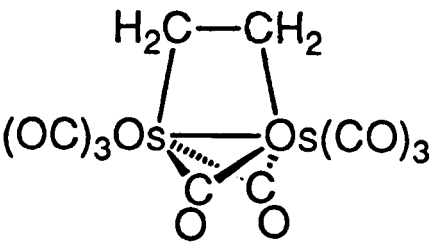
When a matrix containing $Os_2(CO)_8$ and free ethylene is photolysed with light of wavelength > 525 nm, the IR absorptions of both $Os_2(CO)_8$ and free C_2H_4 are depleted (Figure 3.4(c)). However, none of the starting complex, F, is regenerated. Instead, several new absorptions are observed, including a matrix-split band in the bridging ν(CO) region. The frequencies of

these absorptions are given in Table 3.2.

These observations lead to the conclusion that long wavelength photolysis induces the recombination of $Os_2(CO)_8$ with C_2H_4 to give an isomer of the parent diosmacyclobutane. Two possible structures, G and H, for this product are illustrated below.



G



H

Structure G possesses a single bridging CO group, with the the C_2H_4 ligand coordinated to one of the osmium atoms as an η^2-ligand. This can be regarded as a structural analogue of $Os_2(CO)_9$, with a terminal CO group replaced by an η^2-C_2H_4 ligand. The mononuclear species, $Os(CO)_4(C_2H_4)$ is known to include an ethylene ligand bound in this fashion (Carter 1982, Kiel 1987). Structure H is a doubly CO-bridged isomer of F, which retains a 1,2- diosmacyclobutane ring. The results obtained in this experiment favour structure G as the product of the photo-induced recombination of $Os_2(CO)_8$ with C_2H_4, for the following reasons:

(1) The intensity of the bridging ν(CO) band relative to the terminal ν(CO) bands is similar to that in $Os_2(CO)_9$, which has a single CO bridging group.

(2) Only one bridging ν(CO) band is observed. For structure C, two bridging ν(CO) absorptions are predicted (a_1 and b_2 in C_{2v} symmetry). However, the a_1 mode may have low intensity, by analogy with the bridged isomer of $Fe_2(CO)_8$ (Fletcher 1985).

(3) Third-row transition metals are generally reluctant to support CO bridges, due to the large metal-metal distance. For example, no CO-bridged isomer of $Os_2(CO)_8$ is observed. Therefore, C would be expected to be highly thermodynamically unstable with respect to bridge opening.

(3) The photochemical reaction of matrix isolated $Os_2(CO)_8$ with N_2 leads to coordination of N_2 as a terminally bound ligand (see below).

There is a precedent for the coordination of ethylene as an η^2 ligand to one metal atom in dinuclear systems. The complexes $Cp_2M_2(\mu\text{-}CO)_2(CO)(\eta^2\text{-}C_2H_4)$, where M = Fe or Ru are both known to exist, along with the hetero-dimer, in which the ethylene ligand is bound to the Ru centre (Gracey 1985). A recent flash photolysis study has also indicated that the unsaturated dinuclear complex, $Cp_2Fe_2(u\text{-}CO)_3$, reacts

with alkynes in solution, to give, initially, $Cp_2Fe_2(\mu\text{-}CO)_2(CO)(\eta^2\text{-alkyne})$, which subsequently rearranges to a dimetallacyclopentanone (Bursten 1989).

The evidence for structure G is therefore quite strong. UV irradiation of G leads to the regeneration of the IR bands of $Os_2(CO)_8$ and C_2H_4, indicating that ethylene can be photoejected from G.

Table 3.2: Frequencies (cm^{-1}) of ν(CO) bands of $Os_2(CO)_8$-ethylene complexes, in an argon matrix at 12 K and in room temperature hydrocarbon solution.

Species	Ar Matrix	Solution
$Os_2(CO)_8(\mu\text{-}\eta^1,\eta^1\text{-}C_2H_4)$	2125.6	2121[b]
(F)	2080.5	2076
	2042.2[a]	2037
	2034.9[a]	2030
	2025.5	2021
	2014.1	2010
	1997.2	1994
$Os_2(CO)_8(\eta^2\text{-}C_2H_4)$	2121.4	-
(G)	2072.2[a]	2068[c]
	2031.0[a]	2027
	2019.7	2016
	2003.4	2000
	1996.0[a]	1992
	1778.9	1780

a Average frequency of band split by matrix effects.

b IR spectrum of F measured in n-heptane solution

c IR spectrum of G observed using fast TRIR spectroscopy in cyclohexane solution (Grevels 1989 - see section 3.4)

Photolysis of $Os_2(CO)_9$ in N_2 Matrices

Figure 3.5(a) shows the spectrum of $Os_2(CO)_8$ produced by UV photolysis of $Os_2(CO)_9$ in a N_2 matrix at 12 K. Photolysis with light of wavelength > 525 nm leads to a decrease in the bands of $Os_2(CO)_8$ but unlike in argon matrices, no regeneration of $Os_2(CO)_9$ is observed. Instead several new bands appear after long wavelength irradiation of the matrix, which are not observed in other matrices (Figure 3.5(b)). The most significant of these bands, arrowed near 2250 cm^{-1}, is in the region normally associated with the ν(NN) mode of a terminal N_2 ligand coordinated to a metal centre. This shows that photochemical excitation of $Os_2(CO)_8$ in a N_2 matrix can lead to the coordination of a dinitrogen ligand, in preference to the photoejected CO, presumably to give a complex with the formula $Os_2(CO)_8(N_2)$ (N) (Equation 3.8). (Reaction of unsaturated dinuclear metal carbonyls with N_2 in matrices has previously been observed for both $Fe_2(CO)_8$ and $Re_2(CO)_9$, from which, respectively, $Fe_2(CO)_8(N_2)$ and $Re_2(CO)_9(N_2)$ can be produced (Poliakoff 1971, Fletcher 1985, 1986, Firth 1987a,b)

$$Os_2(CO)_8 \xrightarrow[N_2 \,/\, 12\ K]{> 525\ nm} Os_2(CO)_8(N_2) \qquad 3.8$$

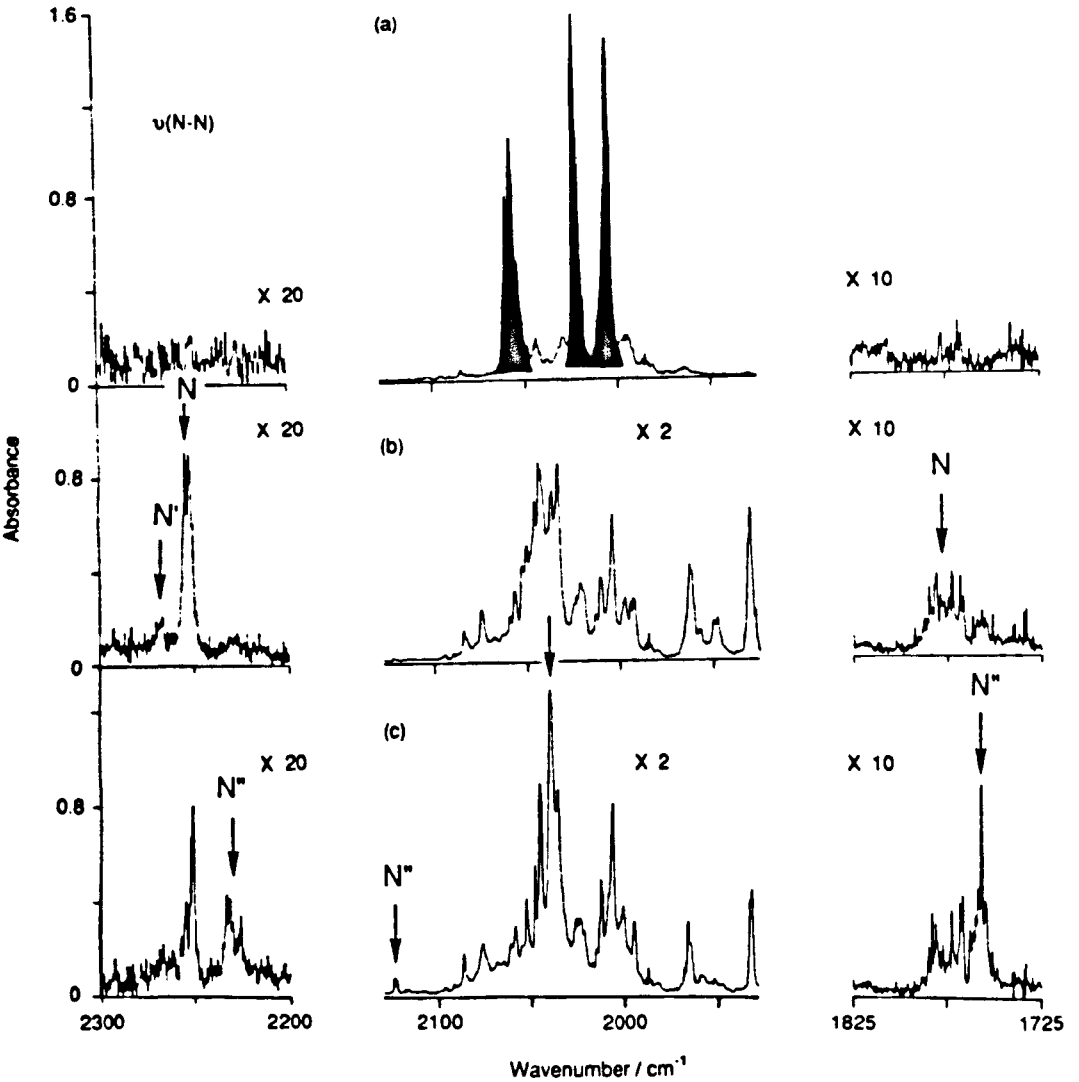


Figure 3.5: IR absorption spectra illustrating the reactivity of $Os_2(CO)_8$ towards N_2. (a) ν(CO) bands of $Os_2(CO)_8$ (coloured black) generated by 6 mins UV photolysis (230-345 nm) of $Os_2(CO)_9$ in a N_2 matrix at 12 K. (b) After 50 mins long wavelength irradiation (>525 nm). New bands in the ν(NN) and bridging ν(CO) regions, assigned to N and N' are arrowed (see text). (c) After annealing the matrix to 30 K for 10 mins. New bands assigned to N" are arrowed. Note the absorbance scale expansion factors.

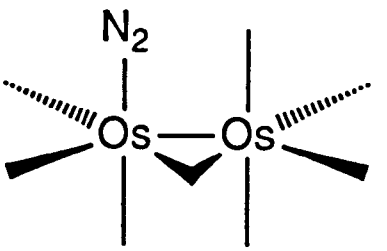
This behaviour is entirely analogous with the recombination of $Os_2(CO)_8$ and CO under the same photolysis conditions. Several terminal ν(CO) bands of N can be seen in Figure 3.5(b) and these are listed in Table 3.3. There is also a weak new absorption marked with an arrow in the bridging ν(CO) region at higher frequency than the bridging ν(CO) band of $Os_2(CO)_9$. This can be assigned to a bridging carbonyl group in N.

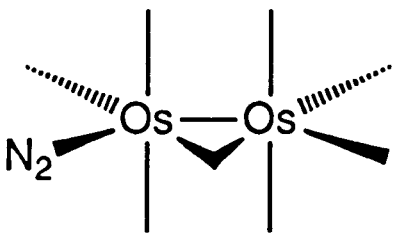
As well as the principal ν(NN) band produced after long wavelength photolysis, a second, much weaker band is produced near 2270 cm^{-1} (arrowed in Figure 3.5(b)), which can also be attributed to the stretch of a terminal N_2 ligand. This may be assigned to N', a structural isomer of N where the N_2 ligand is bound in a different coordination site (see below).

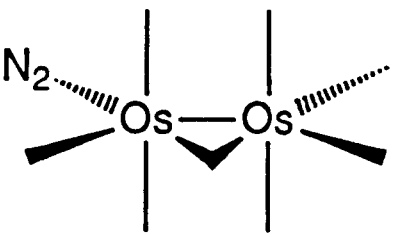
Figure 3.5(c) shows the IR spectrum obtained after annealing the matrix containing N to 30 K. Annealing causes considerable modification to the IR spectrum and several new absorptions, indicated by arrows, have appeared. The terminal ν(C-O) region is very complicated and it is difficult to make definite assignments. However the changes in the ν(NN) region are much simpler. The ν(NN) band of N has diminished and a previously unobserved band near 2230 cm^{-1} has appeared. This is assigned to the ν(NN) mode of a new species N", containing a terminal N_2 ligand. Bands

assigned to N" are listed in Table 3.3, including a new bridging ν(CO) band at 1756.6 cm^{-1}. The weak new absorption at 2124.2cm^{-1} could be assigned to either a high frequency terminal ν(CO) mode or a low frequency ν(NN) mode. Since several dinuclear osmium carbonyl complexes possess a band near 2130cm^{-1} (e.g. $ROs_2(CO)_8R'$ (R,R' = H, CH_3) (Carter 1982)), the assignment of this absorption to a ν(CO) mode is preferred.

It is probable that N" is another structural isomer of $Os_2(CO)_8(N_2)$ with a bridging CO group formed by a thermal rearrangement of N, in which the N_2 ligand shifts to occupy a different coordination site. Therefore there is evidence for three structural isomers of $Os_2(CO)_8(N_2)$. Previous studies have shown the N_2 ligand in $Re_2(CO)_9(N_2)$ can occupy either an axial or equatorial coordination site (Firth 1987a,b). Three possible structures for $Os_2(CO)_8(N_2)$ are shown below. These are based on the replacement of each of the non-equivalent terminal CO groups of $Os_2(CO)_9$ with an N_2 ligand. The evidence does not indicate which of the three possible positions is occupied by the N_2 ligand in each of the observed species.







None of these dinitrogen complexes could be formed by merely annealing a N_2 matrix containing $Os_2(CO)_8$ to 35 K, indicating that $Os_2(CO)_8$ is not thermally reactive towards N_2 under these conditions. (The unbridged isomer of $Fe_2(CO)_8$ was also found to be unreactive when annealed in a N_2 matrix (Fletcher 1985, 1986)).

UV irradiation of a matrix containing these dinitrogen complexes leads to the depletion of all their absorptions and the reappearance of the bands of $Os_2(CO)_8$, indicating that UV photolysis can cause dissociation of N_2 from these species (Equation 3.9).

$$Os_2(CO)_8(N_2) \xrightarrow[N_2 \,/\, 12\ K]{UV} Os_2(CO)_8 + N_2 \qquad 3.9$$

Table 3.3: Frequencies (cm^{-1}) of IR bands observed for dinitrogen containing complexes. Bands bracketed together are assigned to a single absorption split by matrix effects.

	Species		
	N	**N'**	**N"**
ν(NN)	2254.4	2269.2	2233.3
	2252.3		
ν(CO) (terminal)[a]	2077.5		2124.2
	2059.5		2039.5
	2053.1		
	2048.9		
	2045.3		
	2036.1		
	2024.5		
	2013.9		
	2007.2		
	1966.3		
	1951.8		
	1934.2		
ν(CO) (bridging)	1780.5		1756.6

a Assignment of bands in the terminal ν(C-O) region is made difficult by the complex nature of the spectrum. All the bands observed in this region before annealing the matrix are arbitrarily assigned to N. Some of these are probably due to N' or matrix splittings.

Photolysis of $Os_2(CO)_9$ in CO Matrices: Evidence for Photochemical Cleavage of the Os-Os Bond

Filtered UV irradiation (230-345 nm) of $Os_2(CO)_9$ in a pure CO matrix gives results similar to those in other matrices, with $Os_2(CO)_9$ being destroyed and the bands of $Os_2(CO)_8$ growing in (Figures 3.6(a) and 3.6(b)). Similarly, long wavelength (> 525 nm) photolysis of $Os_2(CO)_8$ in a pure CO matrix results in regeneration of $Os_2(CO)_9$, the reaction proceeding more rapidly than in an argon matrix, as might be expected. The recombination of $Os_2(CO)_8$ with CO in a CO matrix can also be promoted by annealing the matrix to 30 K, indicating that $Os_2(CO)_8$ is thermally more reactive towards CO than towards C_2H_4 or N_2.

These results do not show whether the incoming CO ligand enters a terminal or bridging position. However, preliminary results from ^{13}CO isotopic labelling experiments on $Os_2(CO)_9$ in solution indicate that the ^{13}CO ligand enters a terminal position (Norton 1989). In these experiments, the rate of CO dissociation from $Os_2(CO)_9$ was measured as 1.3×10^{-4} s^{-1} in hexane solution at 298 K, using methyl methacrylate to trap the transient $Os_2(CO)_8$. In the thermal exchange reaction of $Os_2(CO)_9$ with ^{13}CO, an IR band due to a bridging ^{13}CO group, at 1734 cm^{-1} did not appear until several half lives of CO dissociation were complete, indicating initial coordination of ^{13}CO in a

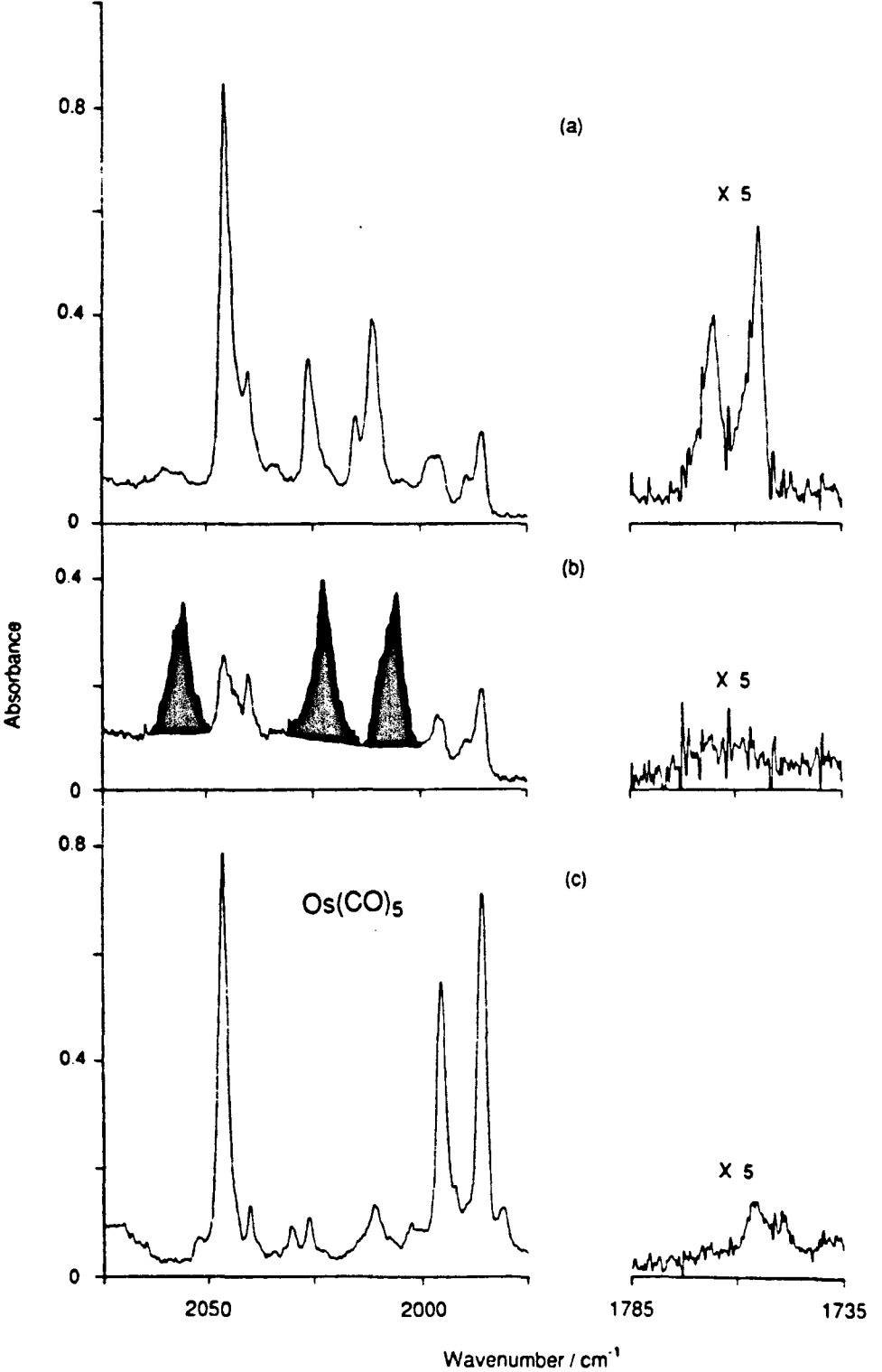


Figure 3.6: IR spectra illustrating the photochemistry of $Os_2(CO)_9$ isolated in a CO matrix at 12 K. (a) Before photolysis; the region above 2075 cm^{-1} is masked by the absorption of the CO matrix. (b) After 21.5 mins near UV/visible photolysis (380-550 nm). Bands due to $Os_2(CO)_8$ are coloured black. (c) After 15 hrs unfiltered UV/visible photolysis. The three intense new absorptions are due to $Os(CO)_5$. The bridging ν(CO) region is shown with an expanded absorbance scale.

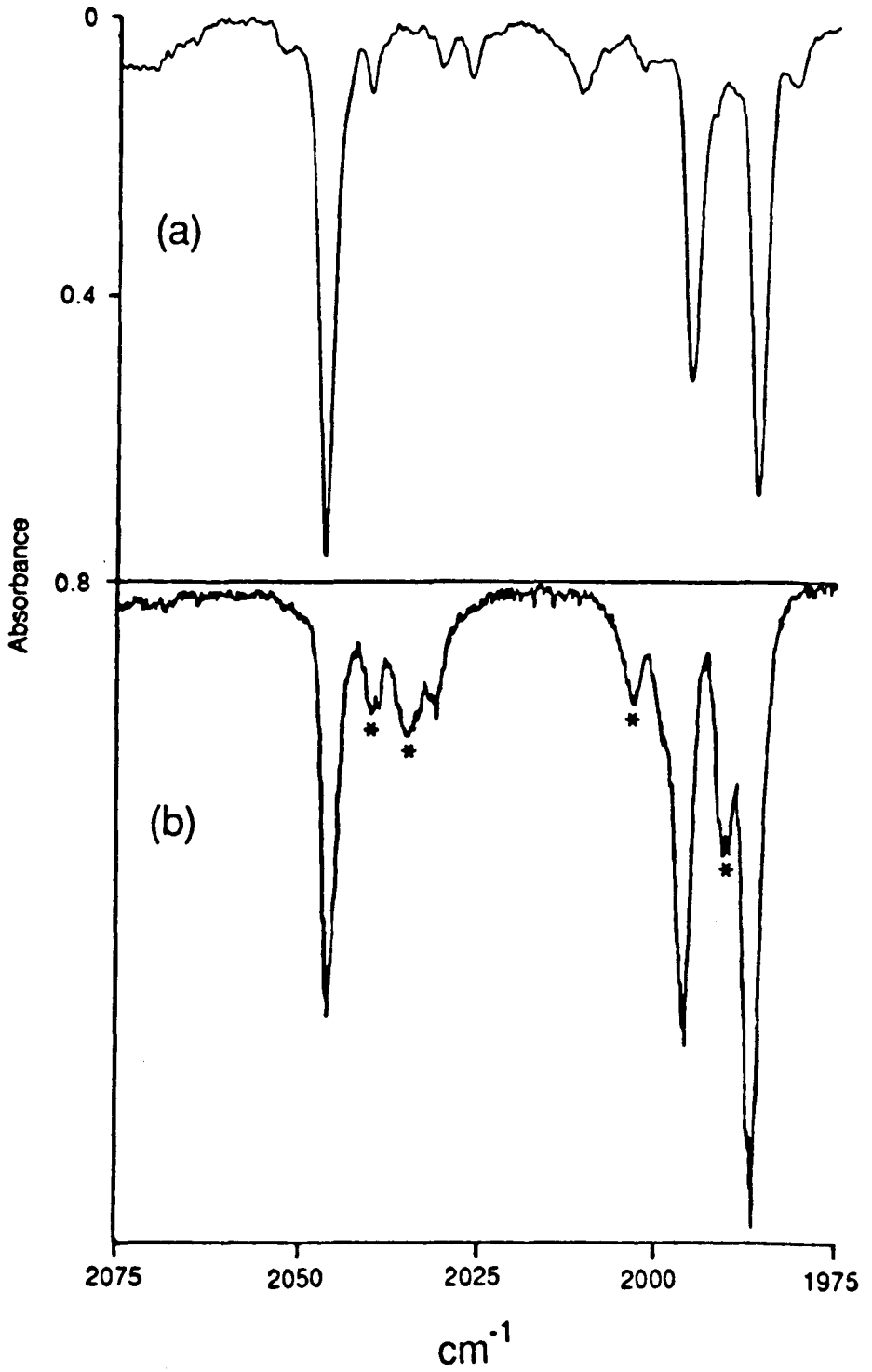


Figure 3.7: (a) IR spectrum of $Os(CO)_5$ generated by 15 hrs unfiltered UV/visible photolysis of $Os_2(CO)_9$ in a CO matrix at 12 K. (b) IR spectrum of a genuine sample of $Os(CO)_5$ isolated in a CO matrix (spectrum obtained by M. Poliakoff, 1972, reproduced by permission). The difference in relative intensities is probably due to overlapping bands of remaining $Os_2(CO)_9$ in (a). Bands marked with asterisks in (b) are due to impurities.

terminal position.

Further photolysis of the CO matrix was carried out with an unfiltered medium pressure Hg arc lamp, in order to promote all possible photochemical processes. Prolonged unfiltered photolysis led to destruction of most of the $Os_2(CO)_9$ and $Os_2(CO)_8$ and the growth of three intense new absorptions in the terminal ν(CO) region (Figure 3.6(c)). This spectrum corresponds well with that of $Os(CO)_5$ isolated in a CO matrix in a previous study by Poliakoff (1972). The terminal ν(CO) regions of the IR spectra of $Os(CO)_5$ obtained by the two methods are compared in Figure 3.7. Two infrared active ν(CO) modes (a_2'' + e') are predicted for $Os(CO)_5$ on the basis of D_{3h} symmetry but the low frequency (e') mode is split into a doublet by matrix effects. The ν(CO) frequencies of $Os(CO)_5$ in a CO matrix are given in Table 3.1.

The formation of a mononuclear product proves that photolysis can lead to cleavage of the metal-metal bond in this system. The same process was observed when $Fe_2(CO)_9$ was subjected to prolonged unfiltered photolysis in a CO matrix, giving $Fe(CO)_5$ (Fletcher 1986).

It is not clear whether the Os-Os bond of an $Os_2(CO)_9$ or $Os_2(CO)_8$ molecule is broken initially (i.e. Equations 3.10 or 3.11 below).

$$Os_2(CO)_9 \xrightarrow{h\nu} Os(CO)_5 + Os(CO)_4 \xrightarrow{CO} 2\ Os(CO)_5 \qquad 3.10$$

$$Os_2(CO)_8 \xrightarrow{h\nu} 2\ Os(CO)_4 \xrightarrow{2\ CO} 2\ Os(CO)_5 \qquad 3.11$$

This result again illustrates how the use of a pure CO matrix and unfiltered UV/visible photolysis can make CO loss easily reversible and an alternative photochemical pathway, such as metal-metal bond cleavage, irreversible. The unsaturated mononuclear species, $Os(CO)_4$, implied in Equations 3.10 and 3.11 is trapped by a CO molecule from the surrounding matrix to give the stable mononuclear product, $Os(CO)_5$, preventing reformation of dinuclear species.

Photolysis of $Os_2(CO)_9$ in Methane Matrices

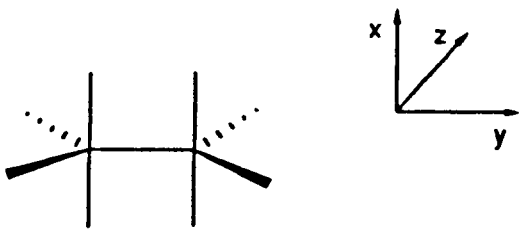
An experiment was performed in which $Os_2(CO)_8$ was generated in a methane matrix at 12 K by in situ photolysis of $Os_2(CO)_9$. Subsequent irradiation with light of wavelength > 525 nm promoted the recombination of $Os_2(CO)_8$ with CO. However, some weak features were observed in the terminal $\nu(CO)$ region of the IR spectrum after long wavelength photolysis, at 2117, 2068, 1949 and 1929 cm^{-1}. These absorptions do not occur in other matrices and may be due to a species in which CH_4 interacts in some way with the unsaturated $Os_2(CO)_8$ complex. At present there is insufficient evidence to suggest what this interaction might be. Previously it has been suggested that the unsaturated mononuclear species, $Fe(CO)_4$ and $Os(CO)_4$ can interact with methane in low temperature matrices (Poliakoff 1974)

3.3 STRUCTURAL CHARACTERISATION OF $Os_2(CO)_8$

There are several possible structures for an unbridged $M_2(CO)_8$ system, as illustrated in Figure 3.8, together with their predicted ν(C-O) vibrational modes.

Hoffmann's isolobal analogy (1982) predicts that the most likely structure is the one with D_{2h} symmetry, consisting of two trigonal bipyramidal metal centres joined through equatorial coordination sites. This is expected to have a singlet electronic ground state and is the structure proposed for unbridged $Fe_2(CO)_8$ in earlier studies (Fletcher 1985, 1986). It can be produced, formally at least, by removal of the bridging CO group from $Os_2(CO)_9$. A closely related structure is one of D_{2d} symmetry where one of the equatorially linked $M(CO)_4$ units is twisted through 90° with respect to the other. Alternatively, two trigonal bipyramidal metal centres can be joined through axial coordination sites, giving a dimer with D_{3d} symmetry. Three other structures, based on square pyramidal metal environments are shown in Figure 3.8. These are considered less likely candidates.

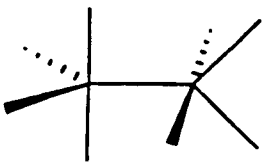
If $Os_2(CO)_8$ had D_{3d} symmetry it would be required to possess a triplet ground state. The HOMO and LUMO of $Os_2(CO)_8$, which are calculated to be close in energy if a D_{2h} structure is assumed, become degenerate in D_{3d} symmetry and a triplet ground state is the



D_{2h}

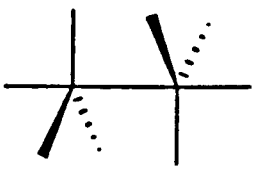
$2\,a_g + b_{1g} + b_{3g} +$

$b_{1u}(z) + 2\,b_{2u}(y) + b_{3u}(x)$



D_{2d}

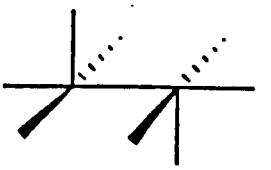
$2\,a_1 + 2\,b_2(y) + 2\,e(x,z)$



D_{3d}

$2\,a_{1g} + e_g +$

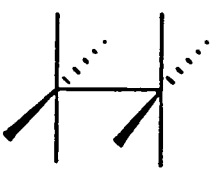
$2\,a_{2u}(y) + e_u(x,z)$



C_{2h}

$3\,a_g + b_g +$

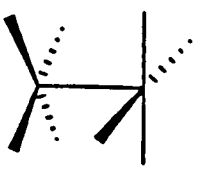
$a_u(z) + 3\,b_u(x,y)$



D_{4h}

$a_{1g} + b_{1g} + e_g +$

$a_{2u}(y) + b_{2u} + e_u(x,z)$



D_{4d}

$a_1 + b_2(y) +$

$e_1(x,z) + e_2 + e_3$

Figure 3.8: Six possible structures for an unbridged $M_2(CO)_8$ molecule. The point group and predicted normal ν(CO) vibrational modes are given for each structure, using the same set of cartesian axes in each case (as illustrated). The directions of the transition moment vectors for IR active modes are given in brackets.

inevitable result (Bender 1989). The 32-electron dimer, $Cp^*Fe_2(\mu\text{-}CO)_3$, the core of which has D_{3h} symmetry, has a triplet ground state for similar reasons (Blaha 1985).

Photochemistry and spectroscopy with polarised light has proved extremely valuable in the structural characterisation of dinuclear metal carbonyls trapped in low temperature matrices (Dunkin 1984, Fletcher 1985, 1986, Firth 1987). The application of this technique to cyclopentadienyl nickel and platinum carbonyl dimers has already been described in Chapter 2 of this thesis. It will now be shown how polarised photochemistry has been used to rule out the D_{3d} structure for $Os_2(CO)_8$.

Polarised Photochemistry of $Os_2(CO)_9$

Figure 3.9(b) shows the dichroism induced in the ν(CO) bands of $Os_2(CO)_9$ and $Os_2(CO)_8$ by 7 minutes polarised photolysis (380-550 nm) of $Os_2(CO)_9$ isolated in a N_2 matrix. The polarisation of each band relative to the plane of photolysis is also given in Table 3.4. The bands of those molecules of $Os_2(CO)_9$ remaining intact after photolysis will be considered first, followed by those of the photoproduct, $Os_2(CO)_8$.

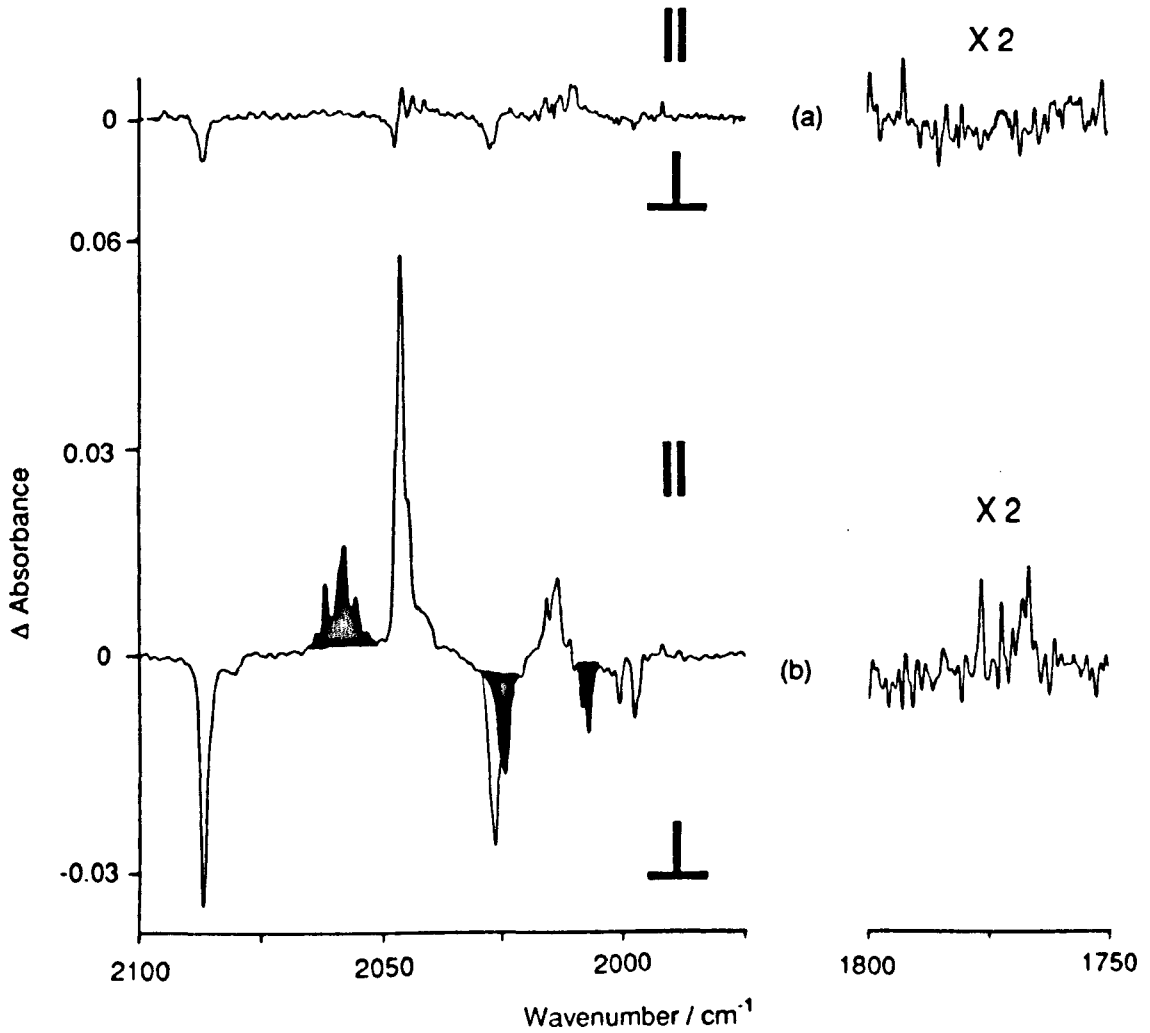


Figure 3.9: IR spectra illustrating the dichroism generated by near UV photolysis of $Os_2(CO)_9$ in an N_2 matrix with plane polarised light. These are subtraction spectra showing the difference in absorbance between spectra measured through a polariser either parallel or perpendicular to the plane of photolysis. (ΔAbsorbance = $A_{||} - A_{\perp}$). (a) Before photolysis; essentially a non-dichroic spectrum indicating a randomly oriented sample. (b) After 7 min plane polarised photolysis (380-550 nm); bands due to $Os_2(CO)_8$ are coloured black. The bridging ν(CO) region is shown with an expanded absorbance scale.

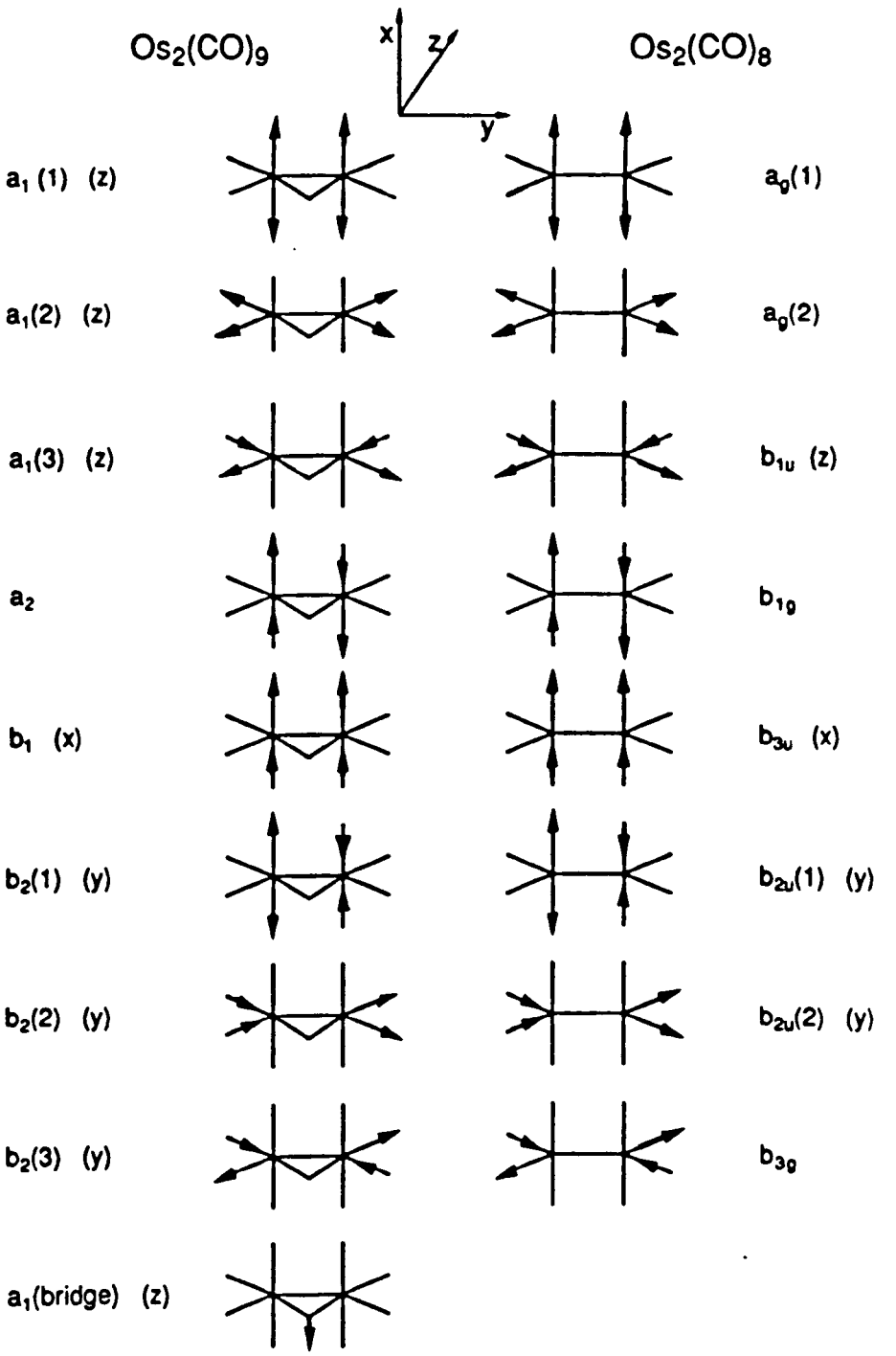


Figure 3.10: Normal ν(CO) vibrational modes for C_{2v} $Os_2(CO)_9$ and D_{2h} $Os_2(CO)_8$. The directions of the transition moment vectors for IR active modes are given in brackets. The same set of cartesian axes have been used in each case to illustrate the correlation between the symmetry modes of the two species. Coupling between axial and equatorial CO groups is ignored.

Table 3.4: Linear dichroism observed in ν(CO) bands of $Os_2(CO)_9$ and $Os_2(CO)_8$ after plane polarised photolysis of $Os_2(CO)_9$ in a N_2 matrix at 12 K. Assignments are based on C_{2v} symmetry for $Os_2(CO)_9$ and D_{2h} symmetry for $Os_2(CO)_8$. The ν(CO) vibrations for these species are illustrated in Figure 3.10. The Os-Os bonds of $Os_2(CO)_9$ molecules have a preferred orientation perpendicular to the plane of photolysis, and those of $Os_2(CO)_9$ parallel to the plane of photolysis (see text).

Species	ν(CO) (cm^{-1})	Polarisation Relative to Plane of Photolysis	Polarisation Relative to Os-Os Bond	Assignment
$Os_2(CO)_9$	2087.0	⊥	∥	$b_2(1)$
	2046.5	∥	⊥	b_1
	2026.8	⊥	∥	$b_2(2)$
	2013.0	∥	⊥	$a_1(3)$
	1771.6	∥	⊥	a_1(bridge)
$Os_2(CO)_8$	2059.3	∥	∥	$b_{2u}(1)$
	2025.0	⊥	⊥	$b_{3u} + b_{2u}(2)$
	2007.6	⊥	⊥	b_{1u}

The Dichroic IR Spectrum of $Os_2(CO)_9$ After Plane Polarised Photolysis

The ν(C-O) modes of $Os_2(CO)_9$, assuming the C_{2v} structure proposed by Moss and Graham (1970, 1977), are illustrated in Figure 3.10. As long as the bridging carbonyl group does not cause any large departure from D_{2h} symmetry for the terminal CO groups, the $a_1(1)$, $a_1(2)$ and $b_2(3)$ vibrations, although formally IR active for C_{2v} symmetry, are likely to be very weak.

Both the bridging ν(CO) band and the most intense terminal ν(CO) absorption of $Os_2(CO)_9$ exhibit dichroism parallel to the plane of the photolysing light (i.e. perpendicular to the photoactive UV transition in those molecules of $Os_2(CO)_9$ remaining intact after photolysis). By analogy with studies on the infrared spectrum of $Os_3(CO)_{12}$ (Huggins 1965, Battiston 1980), the most intense ν(CO) absorption is expected to arise from the b_1 vibrational mode of the axial CO groups of C_{2v} $Os_2(CO)_9$. The changes in dipole moment for the a_1(bridging) and b_1 vibrational modes are orthogonal both with each other and with the Os-Os bond. Therefore, the photoactive UV transition moment responsible for CO-loss from $Os_2(CO)_9$ must have a direction parallel to the Os-Os bond.

The highest frequency band of $Os_2(CO)_9$ shows dichroism perpendicular to the photolysis plane. This

polarisation is in the opposite sense from that observed for the a_1(bridging) and b_1 vibrational modes. Thus, the high frequency band can be assigned to a ν(CO) mode for which the change in dipole moment is parallel to the Os-Os bond. This is consistent with an assignment to the $b_2(1)$ vibration of the axial CO ligands, again in agreement with studies on $Os_3(CO)_{12}$.

The two lower frequency terminal ν(C-O) bands are due to vibrations predominantly of the equatorial CO groups. The higher of these bands exhibits dichroism perpendicular to the plane of photolysis, and is assigned to the $b_2(2)$ vibration which has an associated dipole moment change parallel to the Os-Os bond. The lower frequency band is polarised in the opposite sense and is assigned to the $a_1(3)$ vibration of the equatorial CO groups.

Thus the polarised IR spectrum of $Os_2(CO)_9$ is consistent with the C_{2v} structure proposed for this molecule. This is an example of how polarised photochemistry can be give evidence for the structure of a stable molecule for which no crystallographic data are available.

The Dichroic IR Spectrum of $Os_2(CO)_8$ Generated by Plane Polarised Photolysis

Matrix isolated $Os_2(CO)_8$ exhibits three intense terminal ν(CO) absorptions in its IR spectrum. At first sight this seems to point towards a D_{3d} structure for this species, since three ν(CO) bands are predicted for D_{3d} symmetry, whereas four are expected for D_{2h} or D_{2d} symmetry. However, the intensity pattern in the observed spectrum differs from that for complexes of known D_{3d} structure, such as the unbridged isomer of $Co_2(CO)_8$ (Bor 1974) and $Hg(Co(CO)_4)_2$ (Ziegler 1972). The IR spectra of these complexes exhibit strong high and low frequency ν(CO) absorptions, with a less intense band at intermediate frequency. This relationship is reversed in the spectrum of $Os_2(CO)_8$, in which the middle absorption of the three is the most intense. It is possible that weak or overlapping ν(CO) bands of $Os_2(CO)_8$ are not observed, so further evidence is required to make a structural assignment for $Os_2(CO)_8$.

The polarisations of the bands of $Os_2(CO)_8$ produced in the early stages of plane polarised photolysis of $Os_2(CO)_9$ in a N_2 matrix can be seen in Fig 3.9(b) and are listed in Table 3.4. It has already been shown that the photoactive transition moment responsible for CO loss from $Os_2(CO)_9$ has a direction parallel to the Os-Os bond. If it is assumed that

$Os_2(CO)_8$ is produced from $Os_2(CO)_9$ without rotation of the Os-Os bond, then the molecules of $Os_2(CO)_8$ produced should exhibit a preferred orientation with their Os-Os bonds parallel to the plane of photolysis.

The high frequency band of $Os_2(CO)_8$ is polarised parallel to the plane of photolysis, so the dipole moment change for this vibration must be parallel to the Os-Os bond if the above assumption is correct. The two lower frequency absorptions are polarised in the opposite direction i.e. with dipole moment changes perpendicular to the Os-Os bond.

By analogy with complexes of known D_{3d} symmetry, such as $Hg(Co(CO)_4)_2$ (Ziegler 1972), a D_{3d} $M_2(CO)_8$ complex would be expected to have two higher frequency bands of a_{2u} symmetry polarised in the same sense, parallel to the Os-Os bond. The lower frequency e_u band would be polarised in the opposite sense, perpendicular to the Os-Os bond. Clearly, the observations are not consistent with a D_{3d} structure, since the two highest frequency ν(CO) absorptions of $Os_2(CO)_8$ are polarised in opposite senses. Therefore a D_{3d} structure can definitely be ruled out for $Os_2(CO)_8$.

As already stated, the IR spectrum of $Os_2(CO)_8$ with a D_{2h} structure should have four bands in the terminal ν(C-O) region. The vibrational modes responsible for these bands and their correlations with

those of $Os_2(CO)_9$ are shown in Figure 3.10. If the Os-Os bonds of molecules of $Os_2(CO)_8$ have a preferred orientation, the two vibrations of b_{2u} symmetry should be polarised in the opposite direction to the b_{1u} and b_{3u} vibrations. By analogy with the previous assignments for $Os_2(CO)_9$, the high frequency band of $Os_2(CO)_8$ can be assigned as the $b_{2u}(1)$ vibration of the axial CO groups, polarised parallel to the Os-Os bond. Similarly the low frequency band is the radial b_{1u} mode, polarised in a perpendicular direction. If the intense axial b_{3u} and weak radial $b_{2u}(2)$ absorptions were coincident at an intermediate frequency, this would lead to the observed 1:2 (parallel:perpendicular) ratio of band polarisations. (The polarisation of the intense b_{3u} band would easily outweigh that of the weak b_{2u} absorption).

Hence, these observations could be consistent with a D_{2h} structure for $Os_2(CO)_8$. It is impossible to rule out the closely related D_{2d} structure which would have similar IR polarisation properties. However, the former structure is favoured due to its very close relationship with the parent molecule, $Os_2(CO)_9$.

Figure 3.11(b) shows the polarised IR spectrum obtained after plane polarised photolysis (> 525 nm) of a randomly oriented sample of $Os_2(CO)_8$ in a N_2 matrix. It shows that each ν(CO) band of $Os_2(CO)_8$ exhibits the opposite dichroism to that observed on production of

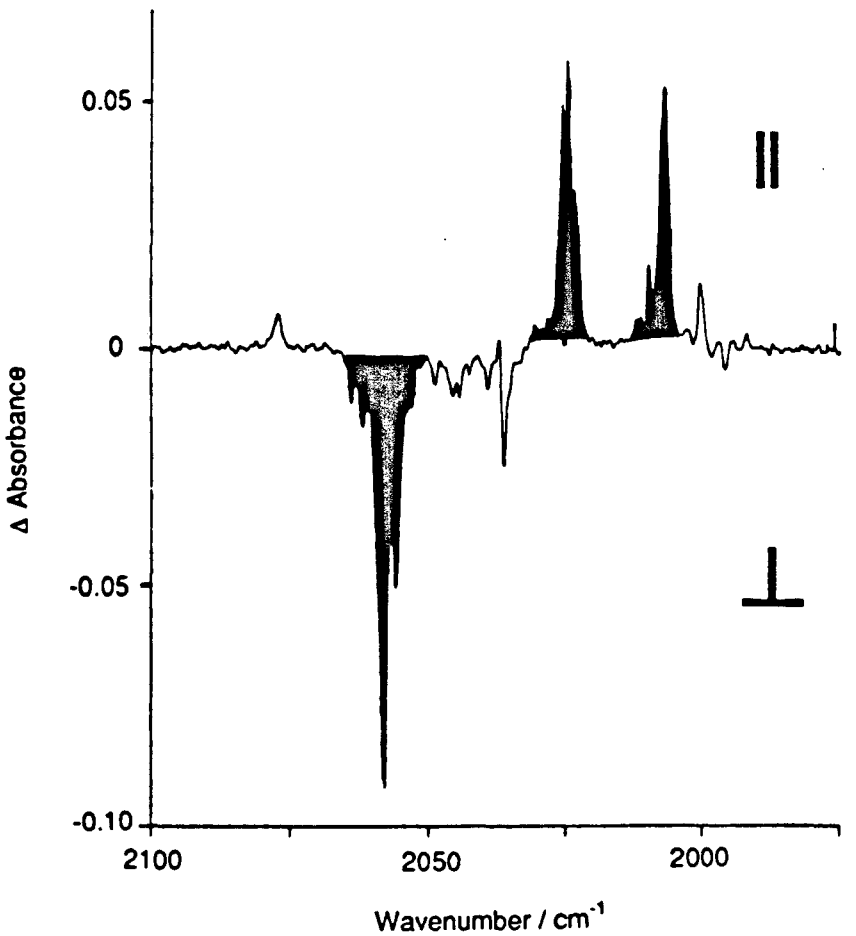


Figure 3.11: IR difference spectrum (ΔAbsorbance = $A_{\parallel} - A_{\perp}$) showing the dichroism generated by 10 min irradiation of a randomly oriented sample of $Os_2(CO)_8$ in an N_2 matrix with plane polarised light (> 525 nm). The polarisations of the bands of the remaining $Os_2(CO)_8$ are the opposite to those of $Os_2(CO)_8$ generated by plane polarised UV photolysis of $Os_2(CO)_9$ (Figure 3.9).

$Os_2(CO)_8$ from $Os_2(CO)_9$ (see Figure 3.9). This implies that molecules of $Os_2(CO)_8$ with their Os-Os bonds aligned parallel to the plane of photolysis have been preferentially destroyed. Therefore, the electronic transition of $Os_2(CO)_8$ excited by long wavelength irradiation has a transition moment vector along the Os-Os bond.

3.4 ROOM TEMPERATURE SOLUTION AND GAS PHASE IDENTIFICATION OF $Os_2(CO)_8$

Two recent investigations using fast TRIR spectroscopy have given direct evidence for the formation of $Os_2(CO)_8$ in room temperature hydrocarbon solutions and in the gas phase. The findings of these studies will now be outlined

Flash Photolysis of $Os_2(CO)_8(\mu\text{-}\eta^1,\eta^1\text{-}C_2H_4)$ (F) in Room Temperature Solution

Recent results obtained independently by Grevels and co-workers show that $Os_2(CO)_8$ can be generated by flash photolysis of F in cyclohexane solution at room temperature (Grevels 1989).

Figure 3.12(a) shows the transient IR difference spectrum recorded ca. 3 μs after the photolysing UV pulse of an excimer laser (308 nm). It can be seen that three intense photoproduct bands are generated in the terminal ν(CO) region. The frequencies of these bands show gratifying agreement with those assigned to $Os_2(CO)_8$ in an argon matrix (see Table 3.1). The relative intensities of the ν(CO) absorptions of $Os_2(CO)_8$ in Figure 3.12(a) appear different from those of matrix isolated $Os_2(CO)_8$ recorded in this study. (Figures 3.3(b), 3.4(b)). This is due to overlap with

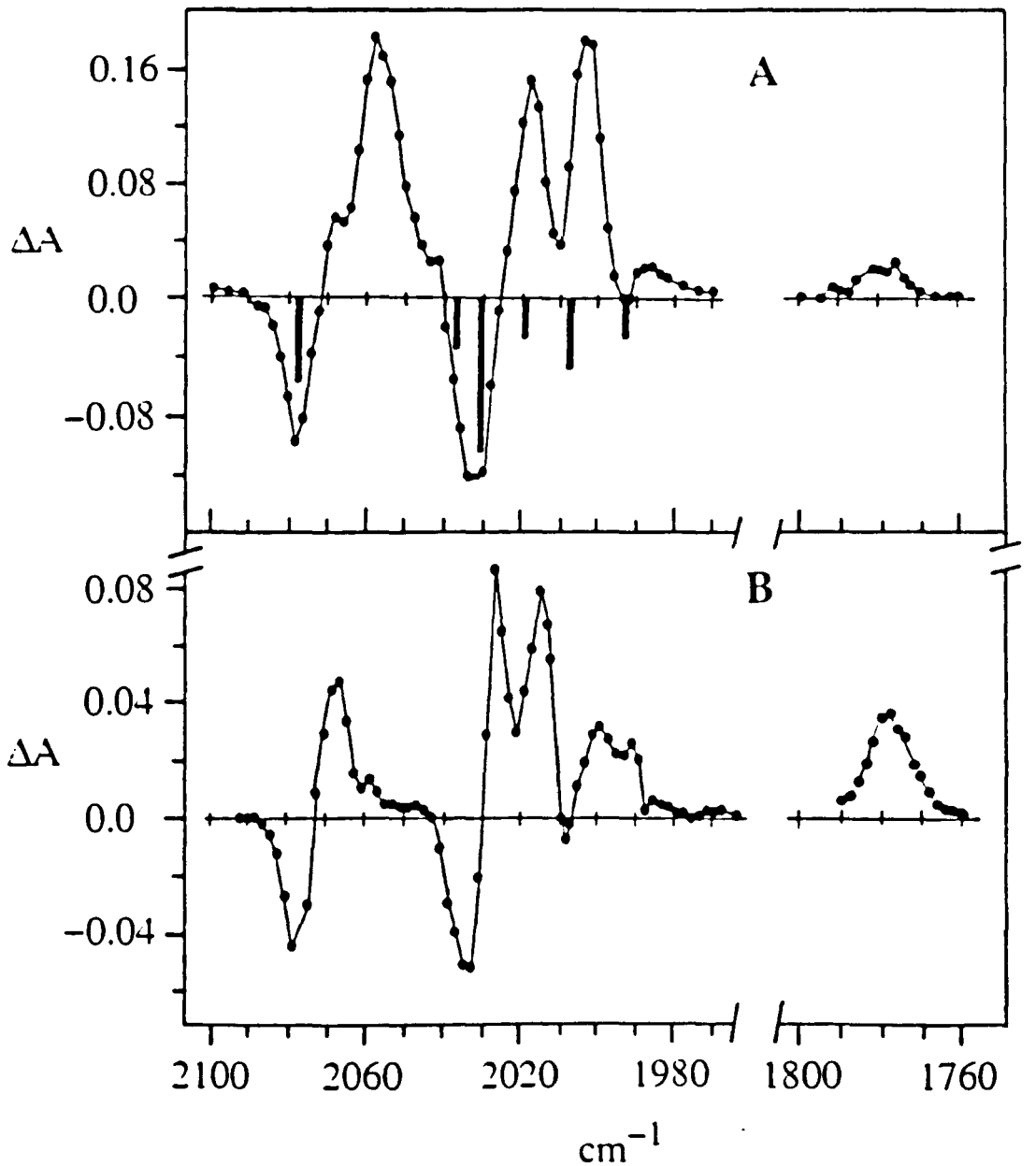


Figure 3.12: Transient ν(CO) IR difference spectra from flash photolysis (308 nm) of $Os_2(CO)_8(u\text{-}C_2H_4)$ (F) (8 X 10^{-4}M) in cyclohexane at room temperature. (A) After ca. 3 μs under argon (the vertical bars represent the ν(CO) pattern of F. (B) After 100 μs in the presence of added ethylene (ca. 10^{-2} M); note the difference in scales. (Adapted from Grevels (1989)).

negative signals due to photolysed starting material, in the transient difference spectrum.

In room temperature solution, $Os_2(CO)_8$ is observed to decay with a half-life of ca. 40 μs under an argon atmosphere. The decay involves partial reformation of F along with production of a secondary, longer lived product with a bridging ν(CO) absorption. When the experiment is performed with ca. 10^{-2} M free ethylene in solution, the decay of $Os_2(CO)_8$ is much more rapid (half life < 5 μs), leaving behind the spectrum of the longer lived product (Figure 3.12(b). In an ethylene saturated solution, $Os_2(CO)_8$ cannot not be detected. Under these conditions, only the secondary product is observed. This species decays slowly with first order kinetics to reform starting material ($k = 8\ (+/-3)\ s^{-1}$) independent of the concentration of added ethylene.

The ν(CO) absorptions of the secondary product are quoted in Table 3.2. It can be seen that the IR spectrum of this product in room temperature solution corresponds excellently with that of G in an argon matrix at 12 K (the weak high frequency band at 2121.4 cm^{-1} was not observed by Grevels et al). These results indicate that G, with a terminally bound η^2-C_2H_4 ligand and a bridging CO group, can be formed by a thermal reaction of $Os_2(CO)_8$ with ethylene in solution.

Grevels et al also report the photochemical

production of $Os_2(CO)_8$ from F in a mixed argon-ethylene matrix (ratio 5:1) at 10 - 12 K (ν(CO): 2057, 2023, 2006 cm^{-1}). A new absorption attributed to $Os_2(CO)_8$ is also observed at 525 nm in the UV/visible spectrum. Annealing causes slight broadening and shifts of the ν(CO) bands of $Os_2(CO)_8$, but no reaction with the large excess of ethylene in the matrix. Irradiation at 546 nm results in destruction of $Os_2(CO)_8$ with the concomitant growth of ν(CO) absorptions at 2071, 2032, 2014 and 1765 cm^{-1}, assigned to G.

This study has confirmed $Os_2(CO)_8$ as an important reactive intermediate in the solution photochemistry of dinuclear osmium carbonyl systems. The thermal recombination of $Os_2(CO)_8$ with ethylene in solution results in the formation of G, which is also formed by photochemical excitation of $Os_2(CO)_8$ in low temperature matrices in the presence of ethylene. The solution study suggests that G can undergo a relatively slow rearrangement to regenerate F. Therefore, it appears that the thermal reaction of $Os_2(CO)_8$ with olefins to yield 1,2-diosmacyclobutanes occurs via initial coordination of the olefin as an η^2 ligand at one end of the di-osmium complex. This is followed by slow exchange of the bridging CO group and terminal ethylene ligand to give the 1,2-diosmacyclobutane.

$Os_2(CO)_8$ in the Gas Phase

In another recent investigation, fast TRIR spectroscopy has been used to monitor the products of flash photolysis of $Os(CO)_5$ in the gas phase (Bogdan 1989). The primary photoproducts, resulting from photoejection of either one or two CO ligands from $Os(CO)_5$, are the unsaturated mononuclear fragments, $Os(CO)_4$ and $Os(CO)_3$. Both of these species are observed to recombine with CO. However, both $Os(CO)_4$ and $Os(CO)_3$ also react with the parent pentacarbonyl, to yield dinuclear products (Equations 3.12 and 3.13)

$$Os(CO)_4 + Os(CO)_5 \text{ ----------> } Os_2(CO)_9 \qquad 3.12$$

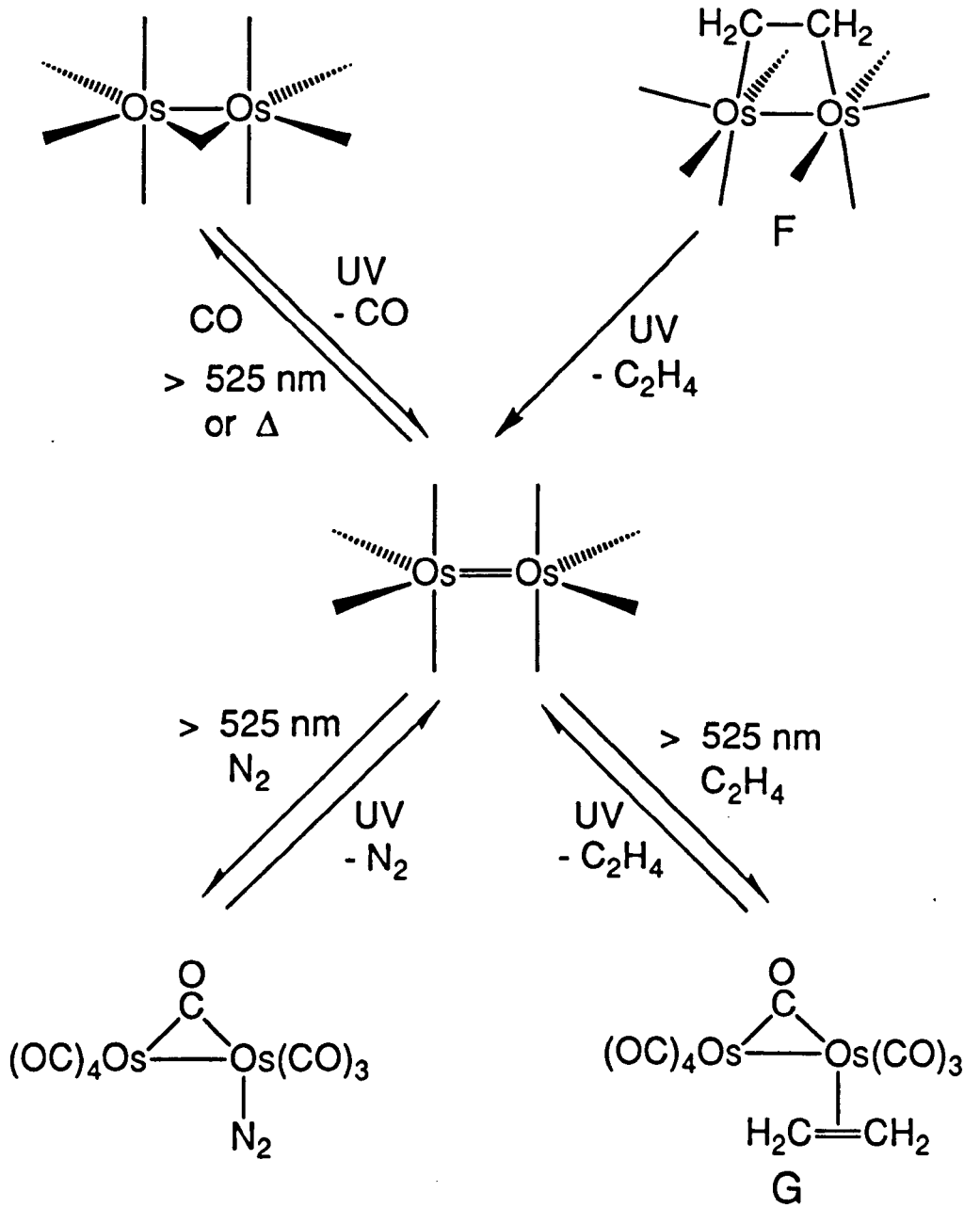
$$Os(CO)_3 + Os(CO)_5 \text{ ----------> } Os_2(CO)_8 \qquad 3.13$$

The broad IR bands inherent in gas phase studies make it difficult to resolve all the terminal ν(CO) bands. However, an absorption at 2014 cm^{-1}, together with a bridging ν(CO) band at 1794 cm^{-1} can be assigned to $Os_2(CO)_9$. More significantly, in terms of the current study, bands at 2024 and 2005 cm^{-1} are assigned to $Os_2(CO)_8$, corresponding well with the two lowest frequency absorptions attributed to $Os_2(CO)_8$ in low temperature matrices (Table 3.1). Apparently, $Os_2(CO)_8$ formed in this manner in the gas phase can subsequently react with $Os(CO)_5$, yielding larger clusters, including $Os_3(CO)_{12}$.

3.5 CONCLUSIONS

The photochemistry observed for $Os_2(CO)_9$ and $Os_2(CO)_8(\mu\text{-}\eta^1,\eta^1\text{-}C_2H_4)$ (F) is summarised in Scheme 3.2. Photolysis of $Os_2(CO)_9$ in a variety of frozen gas matrices leads to dissociation of CO and the formation of the unsaturated dinuclear photoproduct, $Os_2(CO)_8$ which contains only terminal CO groups. The same product, which has been implicated as a reactive intermediate in several previous studies, can also be generated by photoejection of the bridging ethylene ligand from F. It is of interest that $Os_2(CO)_9$ and $Os_2(CO)_8$ each contain two less bridging CO groups than their iron analogues, $Fe_2(CO)_9$ and its primary photoproduct, bridged $Fe_2(CO)_8$ (Poliakoff 1971, Fletcher 1985, 1986). This is attributable to the fact that the third row transition metal complex has a longer metal-metal bond which makes it more difficult for a CO group to occupy a bridging position.

The results do not show whether a terminal or a bridging carbonyl group is ejected from a molecule of $Os_2(CO)_9$ excited by UV light. However, previous studies on $Fe_2(CO)_9$ indicated that a terminal CO group was ejected. If this were also the case for $Os_2(CO)_9$, the primary photoproduct, $(OC)_4Os(\mu\text{-}CO)Os(CO)_3$ would have an asymmetrical structure with inequivalent osmium atoms. Subsequent rapid migration of a CO group from a bridging to a terminal position would give the observed



Scheme 3.2: The matrix photochemistry of $Os_2(CO)_9$ and $Os_2(CO)_8(\mu\text{-}\eta^1,\eta^1\text{-}C_2H_4)$ (F).

symmetrical structure. If the bridging CO group was ejected from $Os_2(CO)_9$, then no rearrangement would be necessary to give the observed structure.

The recombination of $Os_2(CO)_8$ with CO has been shown to occur both thermally and photochemically in matrices. Irradiation with long wavelength light can also induce $Os_2(CO)_8$ to react with N_2 or C_2H_4. In each case the incoming ligand coordinates in a terminal site, with a CO group migrating to a bridging position. $Os_2(CO)_8(N_2)$ is thought to undergo thermal isomerisation at ca. 30 K

Polarised photochemistry has given further evidence for the C_{2v} structure of $Os_2(CO)_9$ and enabled a D_{3d} structure, which would have required a triplet electronic ground state, to be ruled out for $Os_2(CO)_8$. A D_{2h} structure is favoured for $Os_2(CO)_8$, which is expected to possess a singlet electronic ground state. The concerted, thermal reaction of ethylene with singlet $Os_2(CO)_8$ (or the reverse fragmentation) is "forbidden" by orbital symmetry by analogy with the $2\pi + 2\pi$ dimerisation of cyclobutane (Hoffmann 1982, Trinquier 1984). It has been shown that matrix isolated $Os_2(CO)_8$ reacts with ethylene photochemically to give a diosmium species with a terminally bound olefin (G). The same species has also been identified as the product of the thermal reaction of $Os_2(CO)_8$ with ethylene in room temperature solution, using fast TRIR

spectroscopy (Grevels 1989). It is likely that such a species plays an important role in the thermal elimination and exchange of olefins involving diosmacyclobutanes.

The alternative photochemical process normally found for dinuclear metal carbonyls, namely metal-metal bond cleavage, is again observed in this system. Thus, unfiltered photolysis of $Os_2(CO)_9$ in a pure CO matrix leads to production of $Os(CO)_5$.

THE PHOTOCHEMISTRY OF DINUCLEAR METAL CARBONYL COMPLEXES

SUMMARY

THE STRUCTURE OF UNSATURATED DINUCLEAR PHOTOPRODUCTS

For each of the dinuclear metal carbonyl complexes described above, two commonly observed photochemical processes are again encountered:

a) dissociation of CO
b) metal-metal bond homolysis

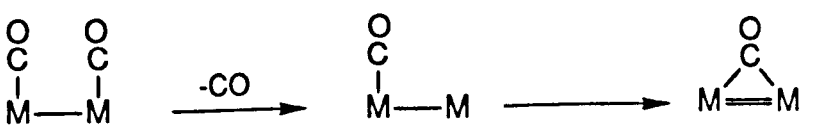
The structures of the unsaturated products arising from CO loss are of particular interest. The table below lists all the homodinuclear transition metal carbonyl complexes for which photodissociation of CO has been observed in a low temperature matrix. Each species listed has been observed in a gas matrix, hydrocarbon glass or cooled PVC film. Some reactions have been studied using more than one of these methods. The table gives the number of bridging CO groups, n(μ-CO), in both starting material and photoproduct, and the change in n(μ-CO) for each pair of complexes.

Parent Complex	n(μ-CO)	CO-loss Product	n(μ-CO)	Change n(μ-CO)
Binary carbonyls				
$Mn_2(CO)_{10}$	0	$Mn_2(CO)_9$	1	+1
$Re_2(CO)_{10}$	0	$Re_2(CO)_9$	0	0
$Fe_2(CO)_9$	3	$Fe_2(CO)_8$	2,0	-1,-3
$Os_2(CO)_9$	1	$Os_2(CO)_8$	0	-1
$Co_2(CO)_8$	0,2	$Co_2(CO)_7$	0	0,-2
Cyclopentadienyl complexes				
$Cp_2Mo_2(CO)_6$	0	$Cp_2Mo_2(CO)_5$	3	+3
$Cp^*_2Mo_2(CO)_6$	0	$Cp^*_2Cr_2(CO)_5$	3	+3
$Cp_2W_2(CO)_6$	0	$Cp_2W_2(CO)_5$	3	+3
$Cp_2Cr_2(CO)_4$	4	$Cp_2Cr_2(CO)_3$	3	-1
$Cp^*_2Cr_2(CO)_4$	4	$Cp^*_2Cr_2(CO)_3$	3	-1
$Cp_2Fe_2(CO)_4$	2	$Cp_2Fe_2(CO)_3$	3	+1
$Cp^*_2Fe_2(CO)_4$	2	$Cp^*_2Fe_2(CO)_3$	3	+1
$Cp"_2Fe_2(CO)_4$	2	$Cp"_2Fe_2(CO)_3$	3	+1
$Cp_2Ru_2(CO)_4$	0,2	$Cp_2Ru_2(CO)_3$	3	+3,+1
$Cp_2Co_2(CO)_3$	1	$(CpCo(CO))_2$	2	+1
$Cp_2Rh_2(CO)_3$	1	$(CpRh(CO))_2$	2	+1
$Cp_2Ni_2(CO)_2$	2	$Cp_2Ni_2(CO)$	0	-2
$Cp'_2Ni_2(CO)_2$	2	$Cp'_2Ni_2(CO)$	1	-1
$Cp_2Pt_2(CO)_2$	0	$Cp_2Pt_2(CO)$	1	+1
$Cp^*_2Pt_2(CO)_2$	0	$Cp^*_2Pt_2(CO)$	1	+1

(Cp" = η^5-$C_5H_4CH_2Ph$)

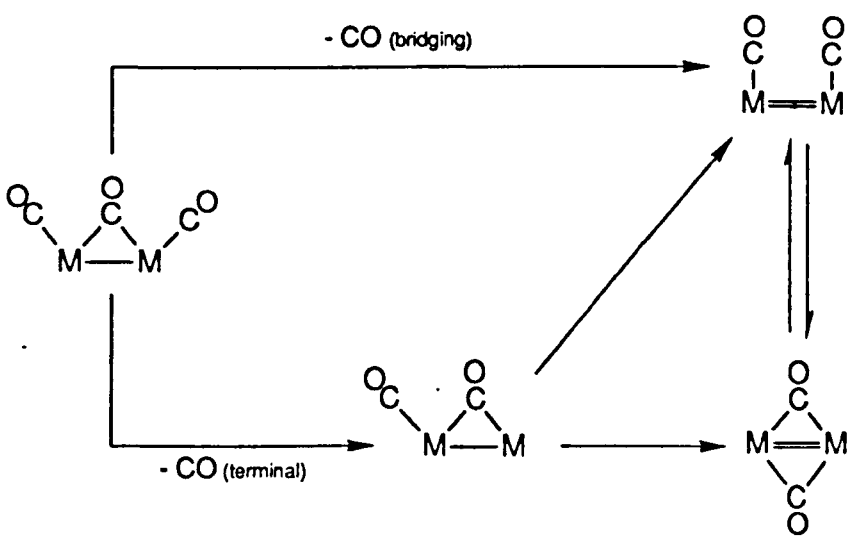
It can be seen that on loss of CO, the change in the number of bridging CO groups is generally +/- 1 or +/-3. Each of the parent dimers listed has a symmetrical structure with two chemically equivalent metal atoms. An odd-numbered change in n(μ-CO) enables the CO-loss product to possess similar equivalent metal centres.

Several of the CO-loss processes shown involve an unbridged precursor, which gives a photoproduct with an odd number of CO bridges (e.g. $Cp_2Pt_2(CO)_2$). Since, in these cases, the parent possesses only terminal CO ligands, the primary photoprocess must involve ejection of a terminal CO group. This results in an asymmetrical structure with inequivalent metal atoms, as illustrated below. To achieve the structure of the observed photoproduct (e.g. $Cp_2Pt_2(\mu$-CO) the remaining CO group must migrate from a terminal to a bridging position.

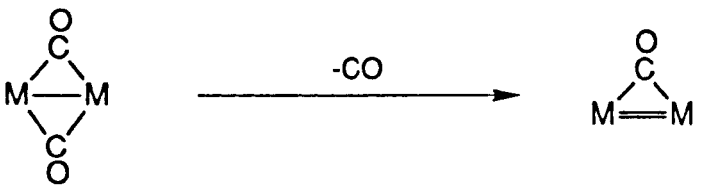


Such a process would be expected to occur rapidly, since it is known that migration of CO ligands between terminal and bridging sites is a facile process in polynuclear systems (Cotton 1976, Crabtree 1986).

In other examples, the starting complex contains both terminal and bridging CO groups (e.g. $Os_2(CO)_9$). In such cases the primary photochemical step could involve loss of either type of CO ligand, as shown below. Loss of a bridging CO group results in a symmetrical dimeric structure. However, loss of a terminal ligand gives an asymmetrical product, for which there are two alternative rearrangements leading to a symmetrical structure. These involve either a bridging->terminal or terminal->bridging CO migration, to give, respectively, an unbridged or doubly bridged product. Isomerism between these two species can be envisaged and is observed for $Fe_2(CO)_8$ (Poliakoff 1971, Fletcher 1985, 1986).



Finally there are examples which contain only bridging CO groups in the parent complex (e.g. $Cp'_2Ni_2(\mu\text{-}CO)_2$, $Cp_2Cr_2(\mu\text{-}CO)_4$). In these cases a bridging CO ligand must be ejected as the primary photochemical step, as illustrated below. No CO migration is necessary to give a symmetrical structure.



In the case of $Cp_2Ni_2(\mu\text{-}CO)_2$, it appears that CO loss in frozen gas matrices is accompanied by bridge opening to give $Cp_2Ni_2(CO)$, with a terminal CO ligand, In room temperature solution, terminal->bridging CO migration occurs rapidly to form $Cp_2Ni_2(\mu\text{-}CO)$ (see Chapter 3).

It seems that migration of CO groups between terminal and bridging positions on photodissociation of a terminal CO ligand results from the desire of the photoproduct to have a symmetrical structure with equal electron counts for the two metal atoms. An unsaturated 32 electron dimer would prefer to have two 16 electron metal centres than to have 15 and 17 electron counts (ignoring the contribution from M-M bonding). Rearrangement of the primary photoproduct to

give a symmetrical structure is generally rapid, even in low temperature matrices. Room temperature flash photolysis experiments with very fast IR detection have yet to detect an intermediate species in the conversion of $Cp_2Fe_2(CO)_4$ to $Cp_2Fe_2(\mu\text{-}CO)_3$.

There are only three examples known where $n(\mu\text{-}CO)$ changes by an even number on dissociation of CO in a low temperature matrix. The case of $(CpNi(\mu\text{-}CO))_2$ has already been discussed. Both $Re_2(CO)_{10}$ and its photoproduct, $Re_2(CO)_9$, have unbridged structures (Firth 1987). In $Re_2(CO)_9$, five terminal CO ligands are bound to one rhenium atom, and four to the other, with either an axial or equatorial vacant coordination site. Likewise, $Co_2(CO)_7$, which can be produced from the doubly bridged or unbridged isomers of $Co_2(CO)_8$, is thought to have an unbridged structure (Sweany 1977b). The absence of a bridging CO group in $Re_2(CO)_9$ is probably a consequence of the length of the Re-Re bond, which precludes CO bridging. The explanation of the unbridged structure of the first row transition metal complex, $Co_2(CO)_7$, is less obvious

A symmetrical electronic structure may confer enhanced stability on an unsaturated dinuclear complex. For example, $Os_2(CO)_8$ is found to be thermally unreactive towards N_2 in matrices, whereas coordination of N_2 to the asymmetrical $Re_2(CO)_9$ occurs even at 15-20 K (Firth 1977). In $Re_2(CO)_9$ there is an empty

coordination site at one of the rhenium atoms, to which a ligand can bind. This is essentially identical to the vacant coordination site in a mononuclear species such as $Cr(CO)_5$, formed by photolysis of $Cr(CO)_6$. In an N_2 matrix, formation of both $Cr(CO)_5(N_2)$ and $Re_2(CO)_9(N_2)$ is rapid. By contrast, in symmetrical species such as $Os_2(CO)_8$, the unsaturation caused by loss of CO is effectively shared between both metal atoms. This can be represented as a double M=M bond.

The enhanced stability of symmetrical unsaturated dinuclear complexes is reflected in the fact that several cyclopentadienyl complexes of this type can be isolated at room temperature e.g. $Cp^*_2Fe_2(\mu\text{-}CO)_3$ (Blaha 1985b, Winter 1989). Flash photolysis experiments on $(CpPt(CO))_2$ and $(Cp^*Pt(CO))_2$ have indicated that the CO-bridged photoproducts, $Cp_2Pt_2(\mu\text{-}CO)$ and $Cp^*_2Pt_2(\mu\text{-}CO)$ are also relatively stable in room temperature solution. However, attempts to isolate these species by Dr. N. M. Boag (University of Salford), have so far been unsuccessful.

Section Two

The Photochemistry of Cyclopentadienyl Iron Dicarbonyl Silyl Complexes

SECTION TWO

THE PHOTOCHEMISTRY OF CYCLOPENTADIENYL IRON DICARBONYL SILYL COMPLEXES

INTRODUCTION

The $(\eta^5\text{-}C_5H_5)CpFe(CO)_2$ fragment (Fp) and its pentamethyl analogue $(\eta^5\text{-}C_5Me_5)CpFe(CO)_2$ (Fp^*) are frequently encountered in organometallic chemistry. In order for the iron atom to fulfil the 18 electron rule, the 17 valence electron Fp radical must form a single covalent bond with another chemical entity. The simplest such molecule is the hydride, FpH, resulting from formation of an Fe-H bond.

Many complexes of the general type FpR are known, where R is a one electron donating organic ligand such as an alkyl or acetyl group. Alternatively, dimerisation can occur, giving the Fe-Fe bonded species, $(CpFe(CO)_2)_2$, which is closely related to the platinum and nickel dimers discussed in Chapter 2 of this Thesis.

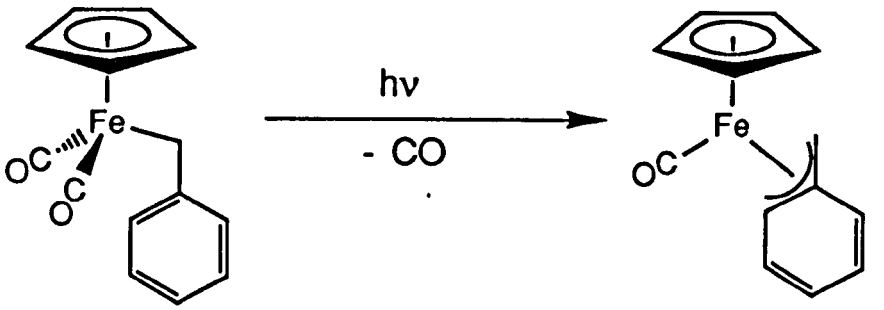
The photochemistry of complexes with the formula FpR has been the subject of considerable research. Solution studies suggest that primary dissociation of CO is by far the most important photochemical process in these systems. This conclusion has been confirmed

in several cases by using matrix isolation to characterise reactive photoproducts at low temperature (Kazlauskas 1982a, Hooker 1984, Mahmoud 1985, Blaha 1985a, Belmont 1986).

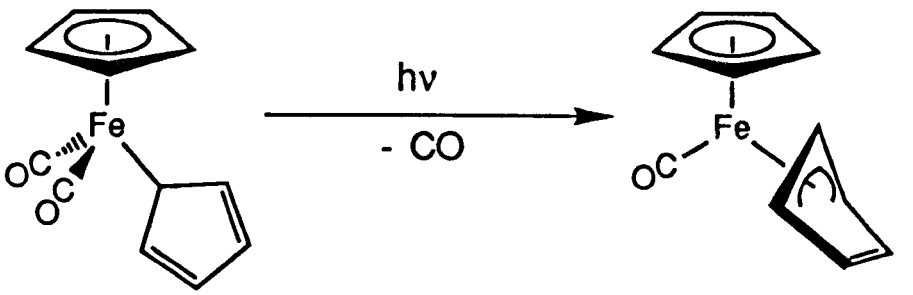
Accumulation of a CO-loss product, CpFe(CO)R, generally occurs extremely slowly, if at all, in low temperature matrices, unless the ligand R can act as an intramolecular trap for the 16 electron species. For example, CpFe(CO)Me, which is implicated in the solution photochemistry of FpMe, cannot be detected after irradiation of FpMe in frozen gas or hydrocarbon glass matrices (Kazlauskas 1982a, Mahmoud 1985). However there is evidence of a CO-loss product from this complex in PVC films (Hooker 1984) where, it is believed, photoejected CO can diffuse more readily. In this case recombination of CpFe(CO)Me with CO is observed when the film was warmed to 40 K, indicating the high reactivity of the unsaturated complex.

Shown below are several examples where a ligand R has been chosen which can act as an intramolecular trap for the 16 electron CO-loss product. In both (1) and (2), η^1-η^3 changes in ligand hapticity occur (Blaha 1985, Belmont 1986), whereas (3) and (4) involve intramolecular oxidative additions, resulting in β-H transfer to the iron atom (Kazlauskas 1982, Mahmoud 1985,Randolph 1986).

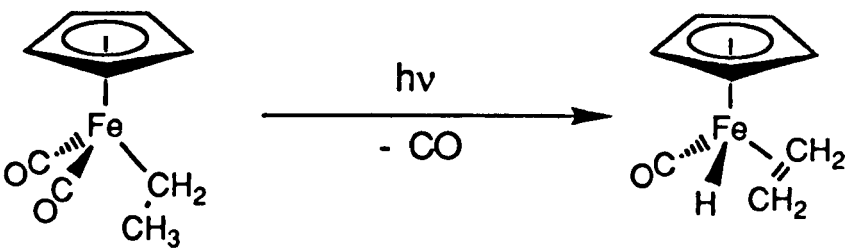
(1)



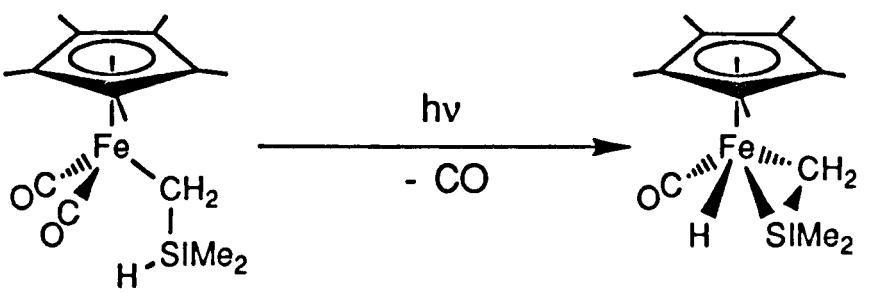
(2)



(3)



(4)



The reaction shown in example (4) involves a ligand R containing a silyl group. In this molecule there is no direct Fe-Si bond, the Fe and Si atoms

being separated by a methylene group. However, a number of compounds are known which contain an Fp fragment bonded directly to a silyl ligand. The first molecule of this type to be isolated, $FpSiMe_3$, was also the first example of a compound with a transition metal-silicon bond (Piper 1956).

The photochemistry of $FpSiMe_3$ has been widely studied, leading to similar conclusions as for other FpR complexes. In solution, irradiation in the presence of added ligands leads to substitution of CO, suggesting CO-loss as the primary photochemical step (King 1968, Chan 1978, Cerveau 1981, Treichel 1981). Photolysis of the pentamethyl analogue, Fp^*SiMe_3, in a hydrocarbon glass at 77 K, results in slow formation of the 16 electron species, $Cp^*Fe(CO)SiMe_3$, confirming proposed mechanism for the solution photochemistry (Randolph 1986).

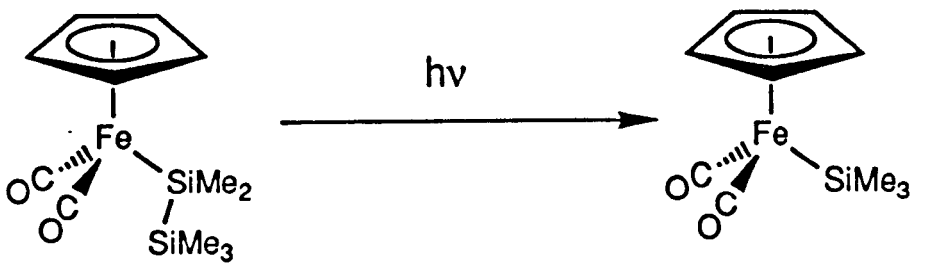
Section Two of this Thesis is concerned with the photochemistry of Fp-disilyl complexes, in which the silyl group is extended to two silicon atoms in length. Chapter 4 deals with the complex $FpSiMe_2SiMe_3$, which is known to undergo an intriguing photoinduced deoligomerisation, losing an "$SiMe_2$" group to yield $FpSiMe_3$. Chapter 5 describes a study of the photochemistry of Fp-disilyl complexes containing hydrogen atoms bonded to the β-Si atom.

CHAPTER 4

THE PHOTOINDUCED DEOLIGOMERISATION OF DISILYL IRON COMPLEXES

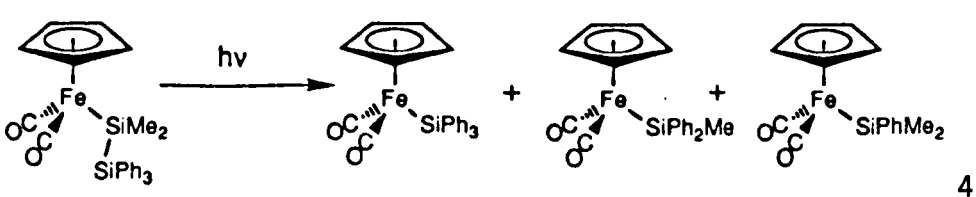
4.1 INTRODUCTION

The photochemical conversion of a disilyl iron complex to the corresponding monosilyl iron species was first reported by Pannell (1974), who observed the deoligomerisation of $FpSiMe_2SiMe_3$ to form $FpSiMe_3$ (Equation 4.1)



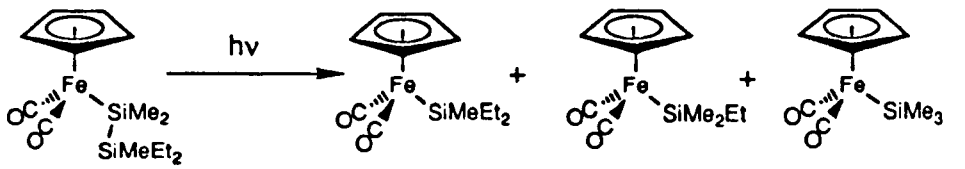
4.1

Recently, there has been considerable interest in the mechanism of this, and other closely related photochemical transformations. Pannell (1986) reported that photolysis of a hexane solution of $FpSiMe_2SiPh_3$ leads to the formation of a mixture of monosilyl iron complexes (Equation 4.2).



4.2

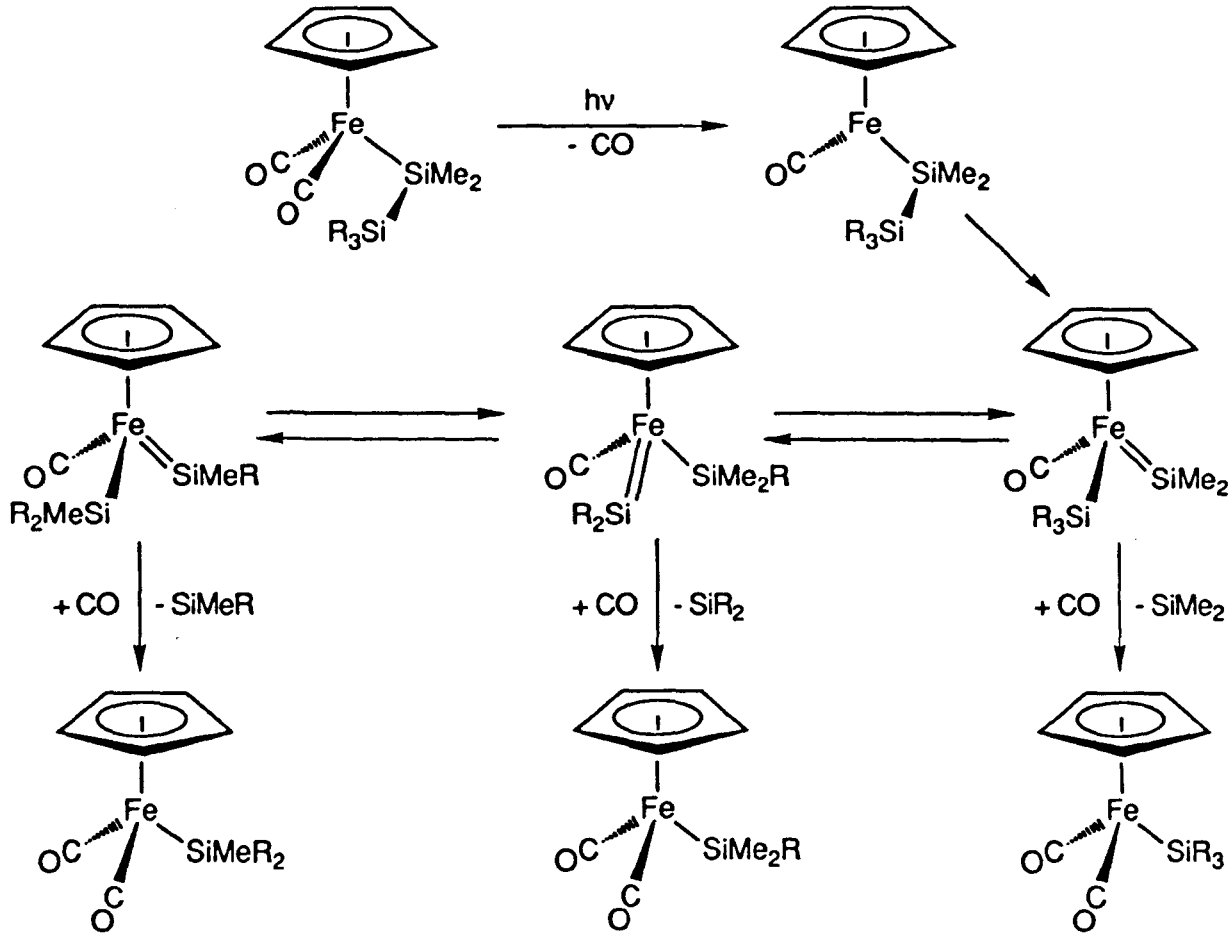
A similar reaction has also been observed for $FpSiMe_2SiMeEt_2$ (Tobita 1988) (Equation 4.3).



4.3

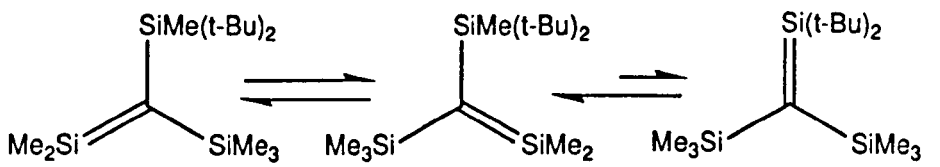
The mixtures of products obtained in these reactions suggest an intramolecular mechanism. For example, irradiation of $FpSiMe_2SiMeEt_2$ does not lead to any of the complex, $FpSiEt_3$, (which could only be generated by an intermolecular process). Tobita also showed that the products obtained from photolysis of a mixture of $FpSiMe_2SiMeEt_2$ and $Fp'SiMe_2SiMe_3$ (Fp' = η^5-C_5H_4Me) are consistent with an intramolecular mechanism.

From these results, both Pannell and Tobita were able to propose essentially identical reaction mechanisms, which are summarised in Scheme 4.1. The primary photoprocess is thought to be dissociative loss of a CO group, creating a coordinatively unsaturated 16 electron metal centre, as observed for many FpR-type complexes. Subsequent migration of the SiR_3 moiety from silicon to iron results in the formation of the key intermediate in this mechanism: a silyl(silylene) iron complex. This step can be thought of as an oxidative addition of a Si-Si bond to an unsaturated metal centre.



Scheme 4.1: The mechanism proposed by both Pannell and Tobita for the deoligomerisation of Fp-disilyl complexes

The mixture of products obtained when different R groups are present in the disilyl ligand of the starting complex is explained by the third step proposed in Scheme 4.1, the rapid scrambling of R groups between silicon atoms in the silyl(silylene) iron intermediate. The mechanism proposed for this scrambling is successive [1,3] sigmatropic shift of alkyl groups. A similar process is thought to occur in silaolefins (Eaborn 1979, Wiberg 1984, 1985). In the example shown in Equation 4.4, rearrangement occurs rapidly enough to cause broadening of bands in the ^1H NMR spectrum at 30°C.

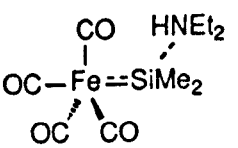


4.4

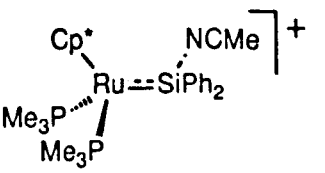
The mechanism is completed by the loss of an SiR_2 group and recoordination of CO, to generate the monosilyl complexes $FpSiR_3$. A recent investigation has provided further evidence that the rate of scrambling of R groups is fast compared to the rate at which an SiR_2 is expelled from the silylene intermediate. This study involved analysis of the product distributions resulting from photolysis of a series of isomeric pairs with the general formula $FpSi_2Ph_{3-n}Me_{2+n}$ (n = 0, 1, 2). (Pannell 1989b).

Both Pannell and Tobita employed trapping agents designed to capture free SiR_2 fragments released in the final step of the proposed mechanism, but were unable to obtain the expected products from the reaction of the trapping agent with silylene.

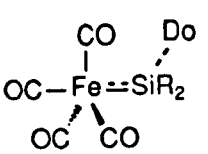
Silylene complexes have often been proposed as intermediates in the reactions of silicon containing transition metal systems (Aylett 1982). However, unlike the analogous, well known class of carbene compounds, very few silylene complexes have been isolated. The only mononuclear transition metal complexes known to contain an $M{=}SiR_2$ unit have been stabilised by interaction with the lone pair of electrons from an adjacent molecule of a Lewis base. Some examples of these base (or donor) stabilised silylene complexes are illustrated below. Currently there are no examples of monomeric silylene complexes existing without base-stabilisation.



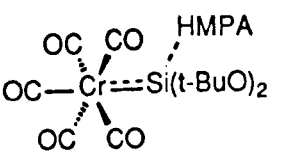
(Schmid 1977)



(Straus 1987)

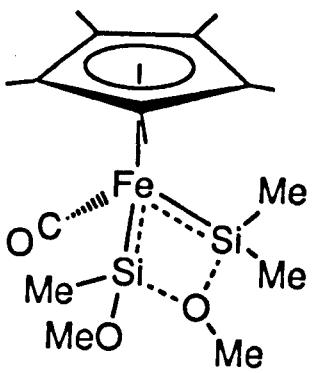


R = Me or t-BuO
Do = HMPA or THF
(Zybill 1988)

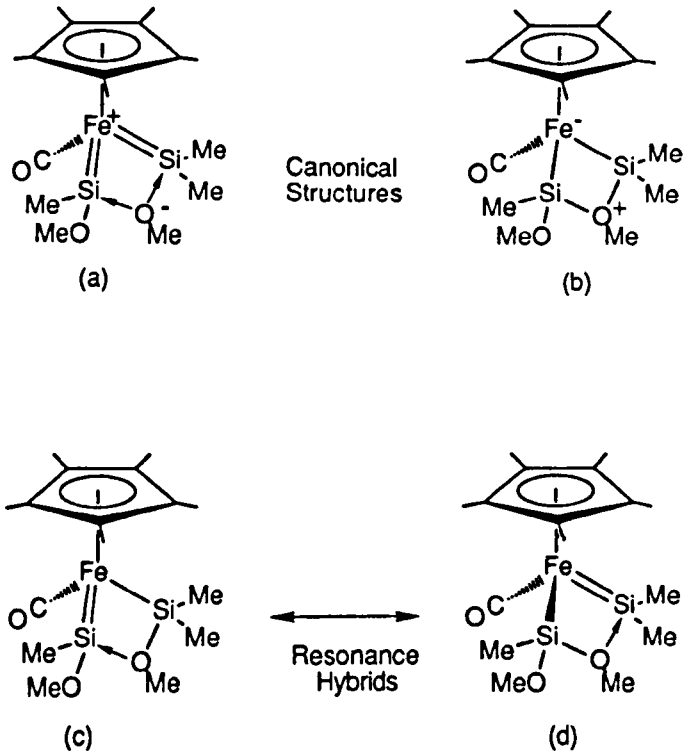


(Zybill 1988)

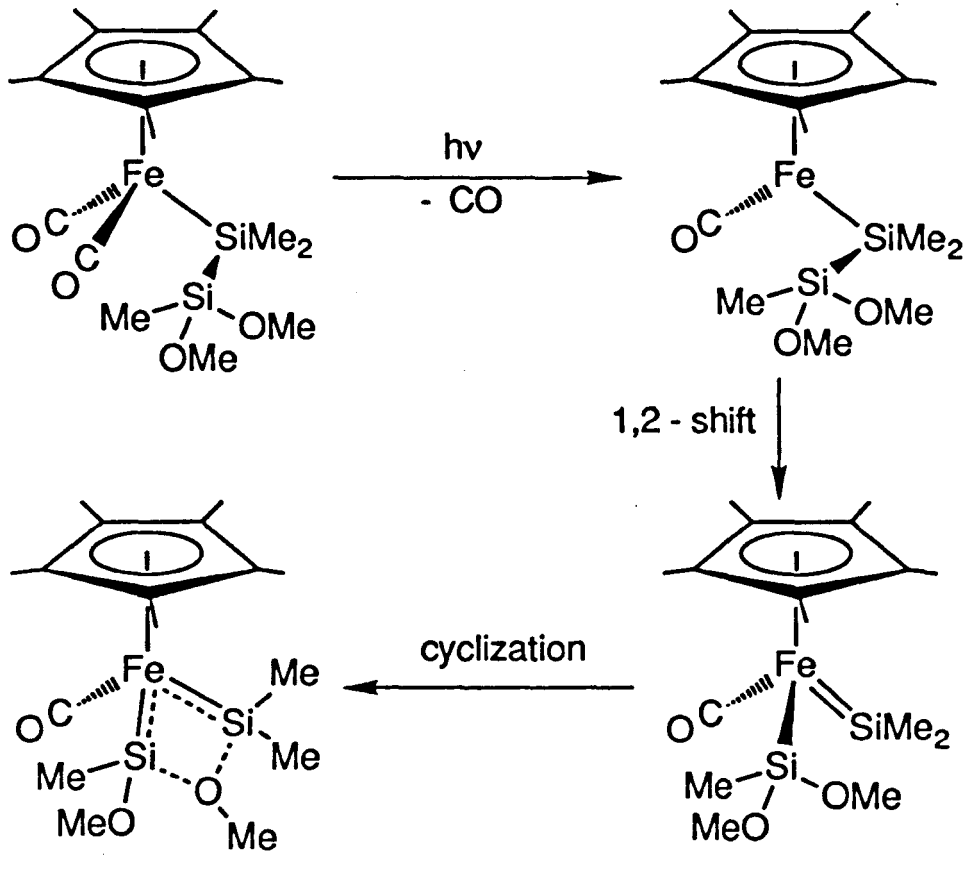
The base stabilisation approach has recently been used to provide further evidence for the intermediacy of $CpFe(CO)(=SiR_2)SiR_3$, in the deoligomerisation of $FpSiR_2SiR_3$ (Ueno 1988). Photolysis of $Fp^*SiMe_2SiMe(OMe)_2$ in deuterobenzene or toluene, results in the product illustrated below.



The X-ray crystal structure of this product reveals that cleavage of the Si-Si bond has occurred, with both Si atoms bonded to the Fe atom. The two Fe-Si bonds are very short, suggesting bond orders greater than one. The molecule is considered to be an intramolecularly base-stabilised bis(silylene) complex. The donor is a methoxy group originating from the β-Si atom in the starting compound. The two Si-O bonds are significantly longer than those generally found for Si-O single bonds. The bonding in this molecule is considered to lie between the two extreme canonical forms, (a) and (b), shown below. Two resonance hybrids of the structure, (c) and (d), can also be drawn.



Scheme 4.2 shows the mechanism proposed for the photochemical production of this complex. Primary photodissociation of CO yields an unsaturated 16 electron species. Migration of an SiR_3 unit from silicon to metal (i.e. Si-Si oxidative addition) then forms a silyl(silylene) complex. This species is then stabilised by intramolecular electron donation from a methoxy group on the silyl ligand to the silicon atom of the silylene ligand. Exactly analogous reactions were observed for a series of similar complexes: $Fp^*SiMe_2SiMe_2(OMe)$, $Fp^*SiMe_2SiMe_2(O\text{-}t\text{-}Bu)$, $FpSiMe_2SiMe(O\text{-}t\text{-}Bu)_2$ and $FpSiMe_2SiMe_2(O\text{-}t\text{-}Bu)$.



Scheme 4.2: Formation and structure of an intramolecularly Base- Stabilised bis(silylene) complex (Adapted from Ueno 1988).

Thus, introduction of alkoxy substituents on the β-Si atom of the disilyl ligand can lead to stabilisation of products resulting from Si-Si oxidative addition. This suggests strongly that β-migration of an SiR_3 group also occurs for the complexes with only alkyl or aryl substituents, for which intramolecular base stabilisation is not possible. In an attempt to observe the silyl(silylene)iron intermediate supposedly generated from $FpSiMe_2SiMe_3$, Tobita et al irradiated the starting complex isolated in a methylcyclohexane matrix at 77 K, but observed "little net photoreaction" (Tobita 1988).

This Chapter describes how a variety of techniques have been applied in an attempt to understand the photochemistry of $FpSiMe_2SiMe_3$. Experiments have been carried out at low temperature, using both matrix isolation and liquid xenon solution techniques. Room temperature studies have also been undertaken, employing both "slow" detection with FTIR spectroscopy and flash photolysis coupled with fast TRIR spectroscopy.

A principal feature of this research is the comparison of the photochemistry of $FpSiMe_2SiMe_3$ with that of the closely related monosilyl complex, $FpSiMe_3$,

the solution photochemistry of which is well known (King 1968, Chan 1978, Cerveau 1981, Treichel 1981, Randolph 1986). Any differences in photochemistry due to extension of the silyl chain from one to two silicon atoms should be made apparent by these control experiments. The results are discussed with reference to previous observations of the photochemistry of FpR complexes.

4.2 THE MATRIX PHOTOCHEMISTRY OF $FpSiMe_2SiMe_3$

Photolysis of $FpSiMe_2SiMe_3$ in N_2 Matrices

Figure 4.1(a) shows the infrared spectrum in the terminal C-O stretching region of a sample of $FpSiMe_2SiMe_3$ isolated at high dilution in a nitrogen matrix at 12 K. The spectrum is essentially identical to that observed for $FpSiMe_2SiMe_3$ in alkane solvents (Pannell 1980), apart from slight shifts and small splittings due to matrix effects. There are two intense absorptions, corresponding to the in-phase and out of phase ν(CO) vibrational modes expected for a non-linear dicarbonyl structure. The frequencies of the ν(CO) absorptions of $FpSiMe_2SiMe_3$ are compared with those observed in other matrices and solvents in Table 4.1.

The electronic spectrum of $FpSiMe_2SiMe_3$ in n-hexane solution has been reported previously (Tobita 1988), and is in agreement with the spectrum recorded in n-heptane, shown in Figure 4.2(a). It exhibits two maxima, at 284 and 330 nm, with the low energy band tailing into the visible region, giving the compound its yellow colour. Irradiation of the matrix was carried out into the near UV/visible region, using a medium pressure Hg arc lamp and a > 300 nm filter. Figure 4.1(b) shows the IR spectrum obtained after photolysis. The two ν(CO) bands of $FpSiMe_2SiMe_3$ have

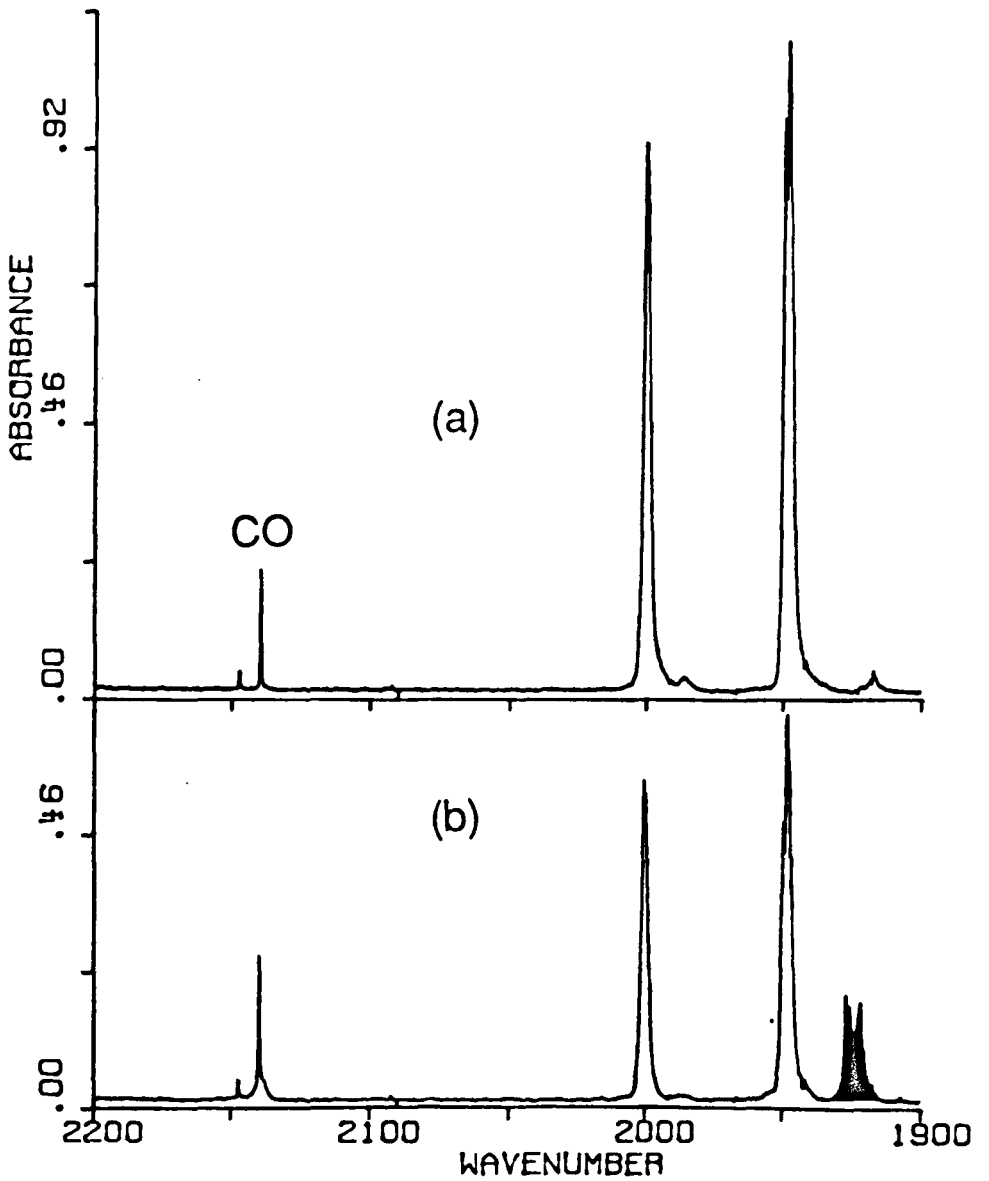


Figure 4.1: IR spectra illustrating the photochemistry of $FpSiMe_2SiMe_3$ isolated in an N_2 matrix at 12 K. (a) Before photolysis. (b) After 230 mins near UV irradiation (>300 nm); the band coloured black is due to $CpFe(CO)SiMe_2SiMe_3$.

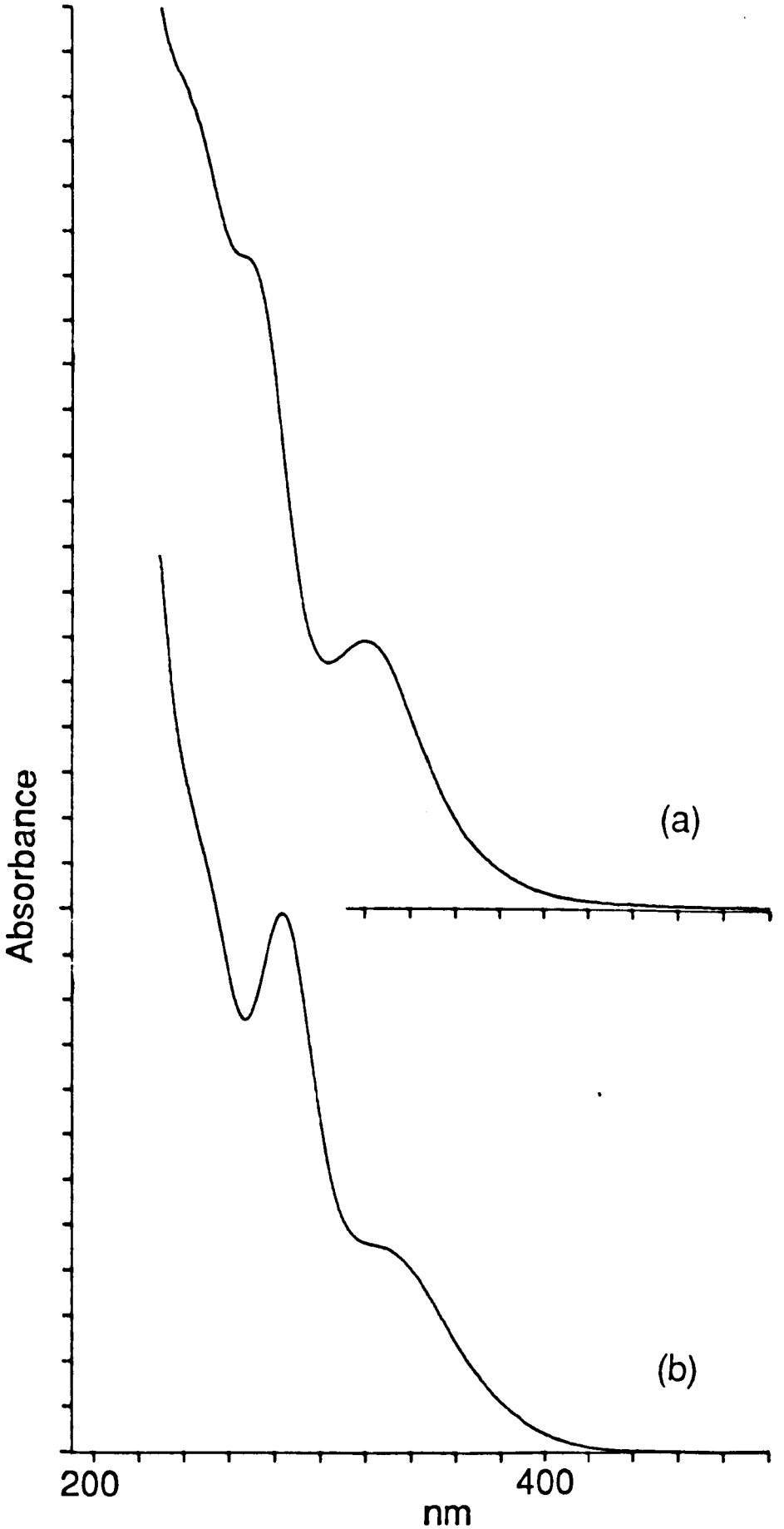
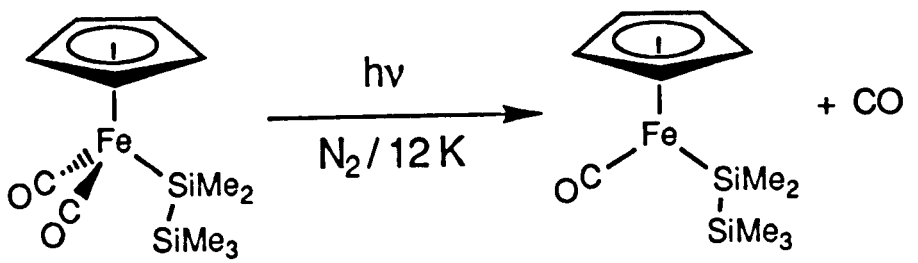


Figure 4.2: Electronic absorption spectra of (a) $FpSiMe_3$ and (b) $FpSiMe_2SiMe_3$ in n-heptane at room temperature.

decreased in intensity, showing that some of the parent has been destroyed. A new absorption due to a photoproduct has appeared at lower frequency, near 1925 cm^{-1}. An increase in intensity of the weaker absorption 2139 cm^{-1} indicates generation of free CO in the matrix.

These observations suggest that UV photolysis of $FpSiMe_2SiMe_3$ causes dissociative loss of CO to give a monocarbonyl photoproduct (Equation 4.5).



4.5

The frequency of the ν(CO) band of this species is in the expected position for a CO-loss product. For Fp^*SiMe_3, the frequency of the ν(CO) band of the CO loss product, observed in an alkane matrix, is shifted 48 cm^{-1} to low frequency relative to the mean position of the parent ν(CO) modes (Randolph 1986). In this case the equivalent shift is 51 cm^{-1}.

The terminal ν(CO) absorption of the photoproduct is split into two major components separated by ca. 5 cm^{-1}. Figure 4.3 shows that annealing the matrix to 30 K results in a change in the relative intensities of

the two components of the doublet. Subsequent photolysis with visible light (> 400 nm) reverses this effect. These changes in band shape may be simply due to site effects in the solid matrix. Another possibility is that visible photolysis or annealing of the matrix may cause subtle changes in the structure of the photoproduct itself. Such effects have been suggested for the 16 electron species formed on CO-loss from $CpW(CO)_3CH_2CH_3$ in an alkane glass at 77 K (Kazlauskas 1982b). The electronic absorption spectrum of $CpW(CO)_2CH_2CH_3$ indicated the presence of two species. These were assigned as the truly unsaturated complex and an isomer with an agostic interaction between the tungsten atom and a β-hydrogen. Evidence for these isomers was also obtained in flash photolysis experiments on $CpW(CO)_3CH_2CH_3$ in room temperature solution (Yang 1986).

Prolonged photolysis of the matrix using visible light leads to very slow recombination of $CpFe(CO)SiMe_2SiMe_3$ with CO to regenerate starting material. Throughout this experiment, no absorptions were observed in the region of the IR spectrum associated with N-N stretching modes. This implies that the N_2 matrix essentially acts as an inert host in this system, there being no photoproducts containing dinitrogen as a ligand.

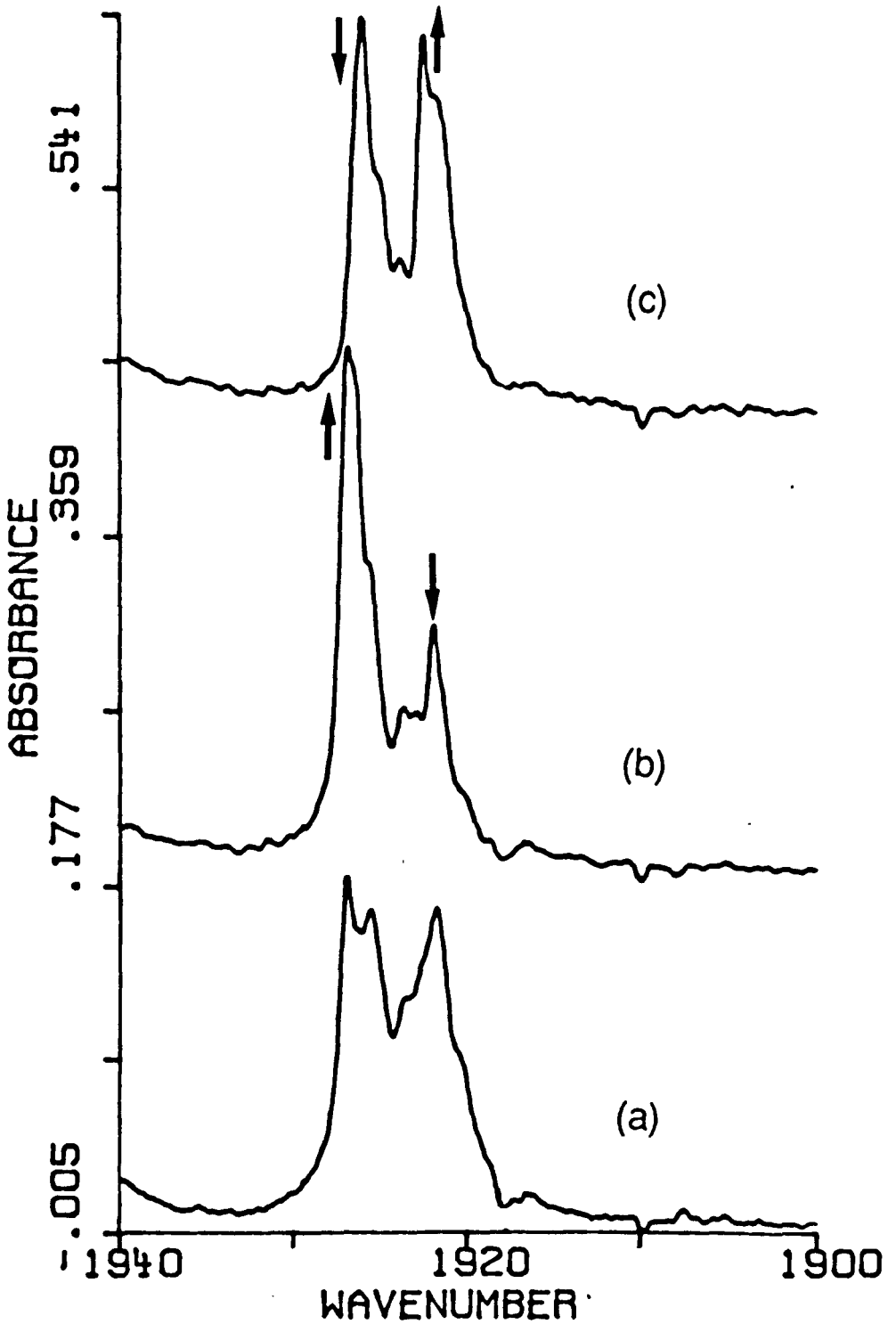


Figure 4.3: IR spectra illustrating the behaviour of the ν(CO) band of $CpFe(CO)SiMe_2SiMe_3$ in an N_2 matrix. (a) After 230 mins >300 nm irradiation of $FpSiMe_2SiMe_3$ (see Figure 4.1). (b) After 18 hrs visible photolysis (> 400 nm). (c) After annealing the matrix to 27 K for 150 mins. Arrows indicate the growth and depletion of absorptions.

Photolysis of $FpSiMe_2SiMe_3$ in Argon Matrices

Similar photochemistry is observed for $FpSiMe_2SiMe_3$ isolated in an argon matrix at 12 K. UV photolysis leads to loss of parent, and growth of a terminal ν(CO) band at 1928.5 cm^{-1}, assigned to $CpFe(CO)SiMe_2SiMe_3$. However, this species was only generated in small amounts under these conditions. It is not clear why the yields are different in Ar and N_2 matrices. The IR frequencies of $FpSiMe_2SiMe_3$ and the photoproduct $CpFe(CO)SiMe_2SiMe_3$ in an argon matrix are given in Table 4.1.

Photolysis of $FpSiMe_2SiMe_3$ in CO Matrices

Irradiation of $FpSiMe_2SiMe_3$ in a CO matrix at 12 K results in similar photochemistry to that observed in Ar and N_2 matrices. Loss of parent is accompanied by production of a single terminal ν(CO) band at 1918.9 cm^{-1}, which can be assigned to the CO-loss product, $CpFe(CO)SiMe_2SiMe_3$. Irradiation of $CpFe(CO)SiMe_2SiMe_3$ with visible light under these conditions causes regeneration of the starting complex. This reaction occurs substantially faster in a pure CO matrix, as might be expected.

4.3 THE MATRIX PHOTOCHEMISTRY OF $FpSiMe_3$

Photolysis of $FpSiMe_3$ in an Argon Matrices

The frequencies of the two ν(CO) bands of $FpSiMe_3$ isolated in an argon matrix at 12 K are given in Table 4.1. Apart from slight solvent shifts and splittings of the bands due to matrix effects, the IR spectrum is identical to that obtained in hydrocarbon solvents at room temperature (Pannell 1980). The electronic absorption spectrum of $FpSiMe_3$ in n-heptane (Figure 4.2(b)) shows absorption maxima at 270 and 322 nm, agreeing well with the spectrum recorded in n-hexane (Tobita 1988). Irradiation into the near UV band of $FpSiMe_3$ (> 300 nm) results in no net photochemistry. Even prolonged photolysis using the unfiltered medium pressure Hg arc lamp does not lead to any change in the IR spectrum.

Photolysis of $FpSiMe_3$ in N_2 Matrices

Figure 4.4(a) shows the IR spectrum of $FpSiMe_3$, isolated in a N_2 matrix at 12 K. The frequencies of the two intense ν(CO) bands of the starting compound are given in Table 4.1. On UV photolysis of the matrix, depletion of the parent ν(CO) absorptions occurred at a very slow rate, even under extremely strong photolysis conditions (Xe lamp with 230-345 nm

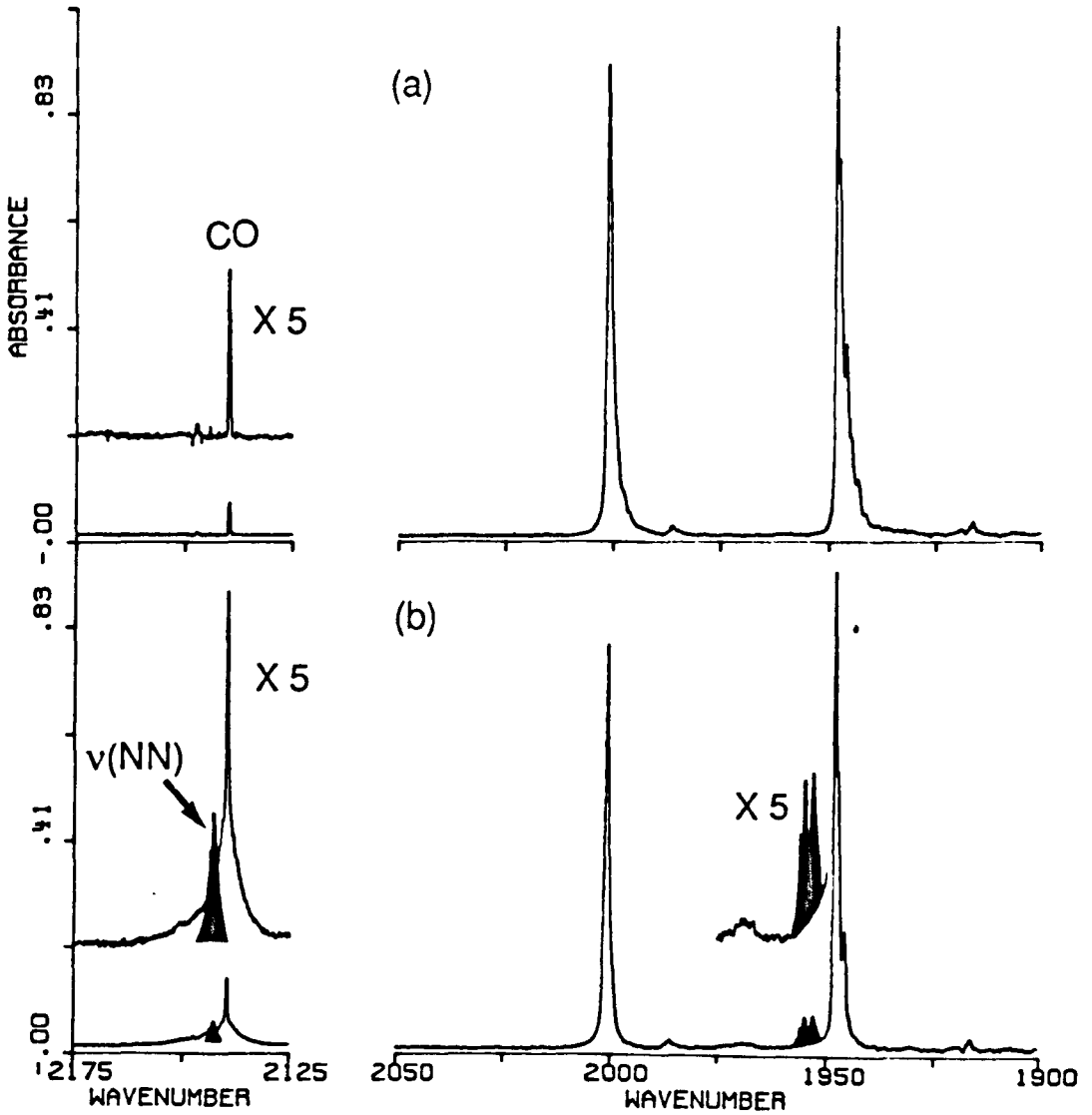


Figure 4.4: IR spectra illustrating the photochemistry of $FpSiMe_3$ isolated in an N_2 matrix at 12 K. (a) Before photolysis. (b) After 15 hrs UV irradiation (230-345 nm); the bands coloured black and shown on an expanded absorbance scale are due to the ν(CO) and ν(NN) modes of $CpFe(CO)(N_2)SiMe_3$.

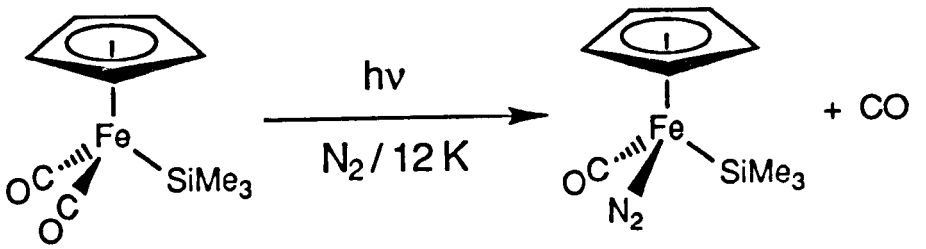
filter) Figure 4.4(b) shows the IR spectrum obtained after a total of 17 hr irradiation of the matrix. Loss of parent is accompanied by the growth of two new absorptions, shaded black, neither of which were observed in an argon matrix. The frequencies of these bands are listed in Table 4.1.

The absorption centred near 1955 cm^{-1} is assigned as a matrix split terminal C-O stretching mode. The frequency of this band is higher than that predicted for a simple CO-loss product, since it is only 19 cm^{-1} lower in frequency than the mean position of the parent ν(CO) bands. A significantly larger shift is expected for an unsaturated CO loss product, by comparison with the equivalent shifts of 51 cm^{-1} for $FpSiMe_2SiMe_3$ (see Table 4.1) and 48 cm^{-1} for Fp^*SiMe_3 (Randolph 1986).

The other new absorption is very close to the C-O stretching frequency of matrix isolated CO. However, the absorption of uncoordinated CO is very narrow in N_2 matrices, and the new absorption shows a definite shift from this band. Inspection of spectra recorded during other photoreactions involving CO loss in N_2 matrices revealed that an absorption had never previously been observed at the frequency of the new band.

However, the new absorption occurs in the N-N stretching region of the IR spectrum. Since it is not observed in an argon matrix, assignment to a ν(NN) mode

is reasonable. These results are consistent with the production of a species containing both CO and N_2 ligands, as illustrated in Equation 4.6.



4.6

Further evidence for the formation of $CpFe(CO)(N_2)SiMe_3$ was obtained by irradiation of $FpSiMe_3$ in low temperature liquid xenon and room temperature hydrocarbon solutions doped with N_2. These experiments are described later in the Chapter.

At no time in argon or N_2 matrices, was any absorption observed which might be attributable to a coordinatively unsaturated monocarbonyl species. The solution photochemistry of $FpSiMe_3$ is readily explained in terms of efficient primary loss of CO so it is unlikely that the quantum yield for CO-loss is small in low temperature matrices. It is more probable that recombination of $CpFe(CO)SiMe_3$ with photoejected CO within the matrix cage is extremely rapid, even at 12 K. Thus, in an argon matrix, no net photochemistry is observed and in an N_2 matrix the dinitrogen complex is produced very slowly, since the photoejected CO recombines more quickly than a N_2 molecule can co-ordinate to the unsaturated iron centre.

Discussion

There are two distinct differences between the matrix photochemistry of the disilyl and monosilyl iron complexes. For $FpSiMe_2SiMe_3$, UV photolysis in Ar, N_2 or CO matrices causes dissociative loss of CO, and generation of $CpFe(CO)SiMe_2SiMe_3$. There is no evidence for formation of an N_2 complex. By contrast, $FpSiMe_3$ undergoes no photoreaction in argon matrices, whereas in N_2 matrices, small amounts of $CpFe(CO)(N_2)SiMe_3$ are formed. The intermediate unsaturated species implicated in this reaction, $CpFe(CO)SiMe_3$, was not observed.

The differences in the low temperature matrix photochemistry of $FpSiMe_2SiMe_3$ and $FpSiMe_3$ indicate that the disilyl ligand of $FpSiMe_2SiMe_3$ can block the vacant co-ordination site caused by photodissociation of CO from the iron centre in a way that is not possible for the monosilyl ligand of $FpSiMe_3$. In this way, the coordinative unsaturation of $CpFe(CO)SiMe_2SiMe_3$ is alleviated, preventing rapid combination with CO or N_2.

In the Introduction to Section 2 of this Thesis, it was noted that photodissociation of CO from matrix-isolated FpR species is normally very slow unless the ligand R can act as an intramolecular trap for the 16 electron iron centre. For instance, CO loss from

Fp^*SiMe_3 in an alkane matrix at 77 K occurs only to the extent of 1% after one hour's photolysis (Randolph 1986). Several examples were cited where intramolecular trapping can occur, due to a change in ligand hapticity or by β-hydrogen transfer.

The ease with which a CO loss product from $FpSiMe_2SiMe_3$ is generated suggests that Si_2Me_5 can be added to the list of ligands which can block an empty co-ordination site after photodissociation of CO. The exact nature of the interaction between the disilyl ligand and the 16 electron metal centre is not apparent from the matrix isolation results. However, the mode of interaction is clearly not one which is available to the monosilyl ligand in $FpSiMe_3$. Therefore, any interactions of the iron centre with an α-Si-CH_3 unit can be ruled out. It is unlikely the interaction is particularly strong, since the ν(CO) frequency of $CpFe(CO)SiMe_2SiMe_3$ is close to that expected for a truly unsaturated monocarbonyl species. This seems to rule out the complete oxidative addition of a covalent bond in the disilyl ligand to the iron centre. It is more likely that the stabilisation takes the form of a relatively weak three centre electronic interaction. Modes of interaction which might stabilise the photoproduct are considered in the Discussion at the end of this Chapter.

Table 4.1: IR frequencies (cm^{-1}) of species observed in low temperature matrices. Solution data is included for comparison. Matrix-split bands are bracketed.

	Matrix/Solvent			
Complex	**Ar**	**N_2**	**CO**	**n-heptane[a]**
$FpSi_2Me_5$	1949.4 1950.6	1948.4 1949.7	1945.0 1947.7	1946.3
	2001.6 2002.7	2000.7	1997.6	1997.6
$FpSiMe_3$	1949.4 1950.6	1945.9 1947.9	-	1945.3
	2002.5 2004.7	2000.8	-	1998.5
$CpFe(CO)Si_2Me_5$	1928.5	1921.8 1925.6 1927.0	1918.9	1924[b]
$CpFe(CO)(N_2)SiMe_3$	-	1953.0 1954.9 1955.8		1952.6
	-	2142.8		2139.4

a Error +/- 0.2 cm^{-1}

b Measured using fast TRIR spectroscopy.

4.4 FLASH PHOTOLYSIS OF Fp-SILYL COMPLEXES

Matrix isolation has enabled the monocarbonyl photoproduct generated by the irradiation of $FpSiMe_2SiMe_3$ to be trapped and observed. However this low temperature technique provides little information about the reactivity of this species and the role it may play in the room temperature solution photochemistry of this system. Flash photolysis, coupled with fast TRIR spectroscopy has recently been applied extensively to mechanistic problems in organometallic photochemistry, and provides an ideal tool for monitoring the reactions of unstable transition metal carbonyl species. The following section describes how fast TRIR spectroscopy has complemented matrix isolation studies on the photochemistry of the Fp-silyl system. These experiments were carried out in collaboration with Mr. M. W. George, in whose Ph.D. Thesis these results will also be presented.

Flash Photolysis of $FpSiMe_2SiMe_3$

Figure 4.5(a) shows the transient IR absorption trace obtained at 1950 cm^{-1}, generated by flash photolysis of $FpSiMe_2SiMe_3$ in n-heptane under an argon atmosphere. It indicates a depletion of the low frequency parent ν(CO) band which is irreversible on the timescale of this experiment. (The slight recovery

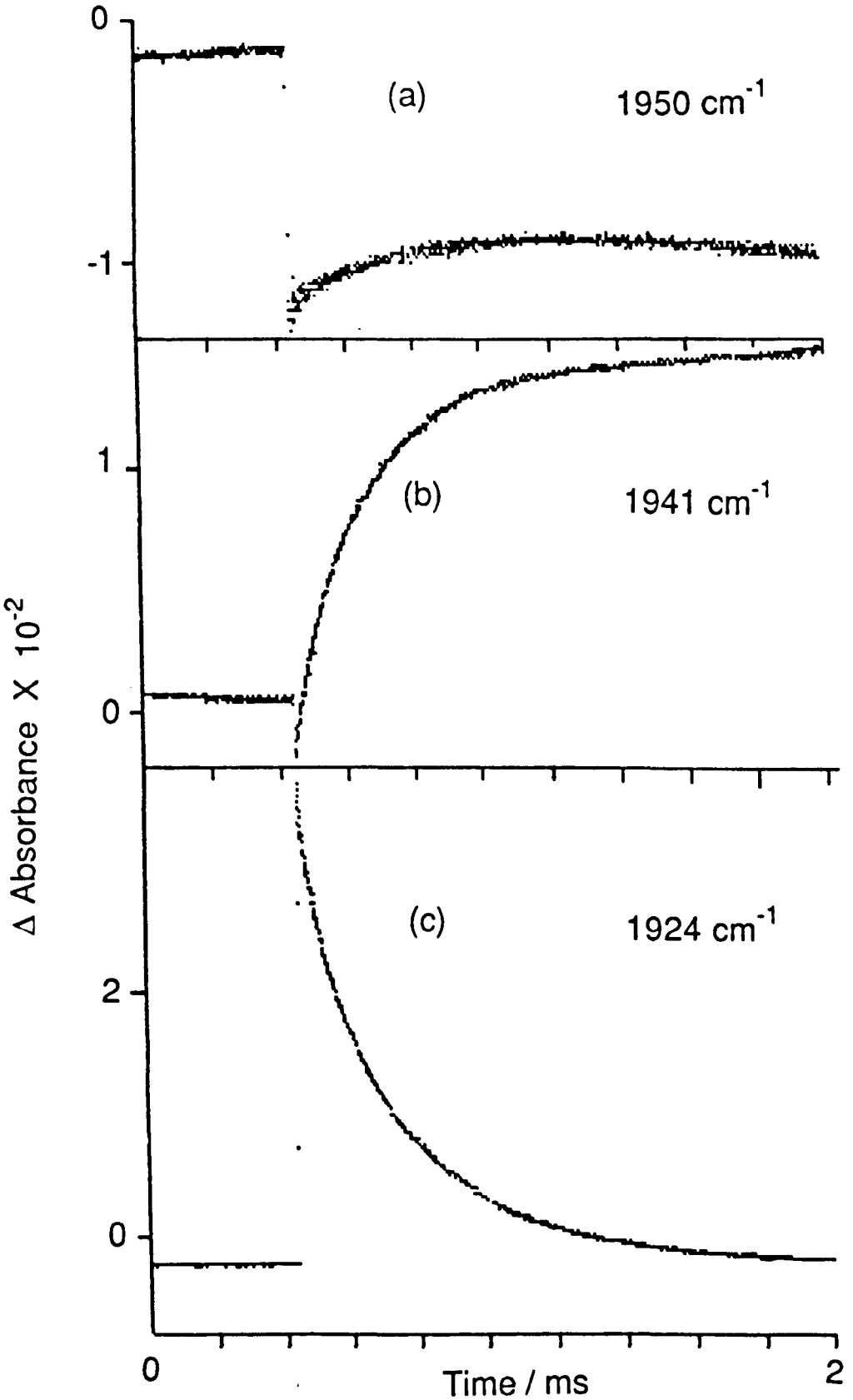


Figure 4.5: Transient IR absorption traces recorded on flash photolysis (308 nm) of $FpSiMe_2SiMe_3$ (2 X 10^{-3} M) in n-heptane at room temperature under argon. (a) 1950 cm^{-1}; depletion of low frequency parent ν(CO) band. (b) 1941 cm^{-1}; growth of ν(CO) band of secondary product, X. (c) 1924 cm^{-1}; formation and decay of ν(CO) band of primary product, $CpFe(CO)SiMe_2SiMe_3$.

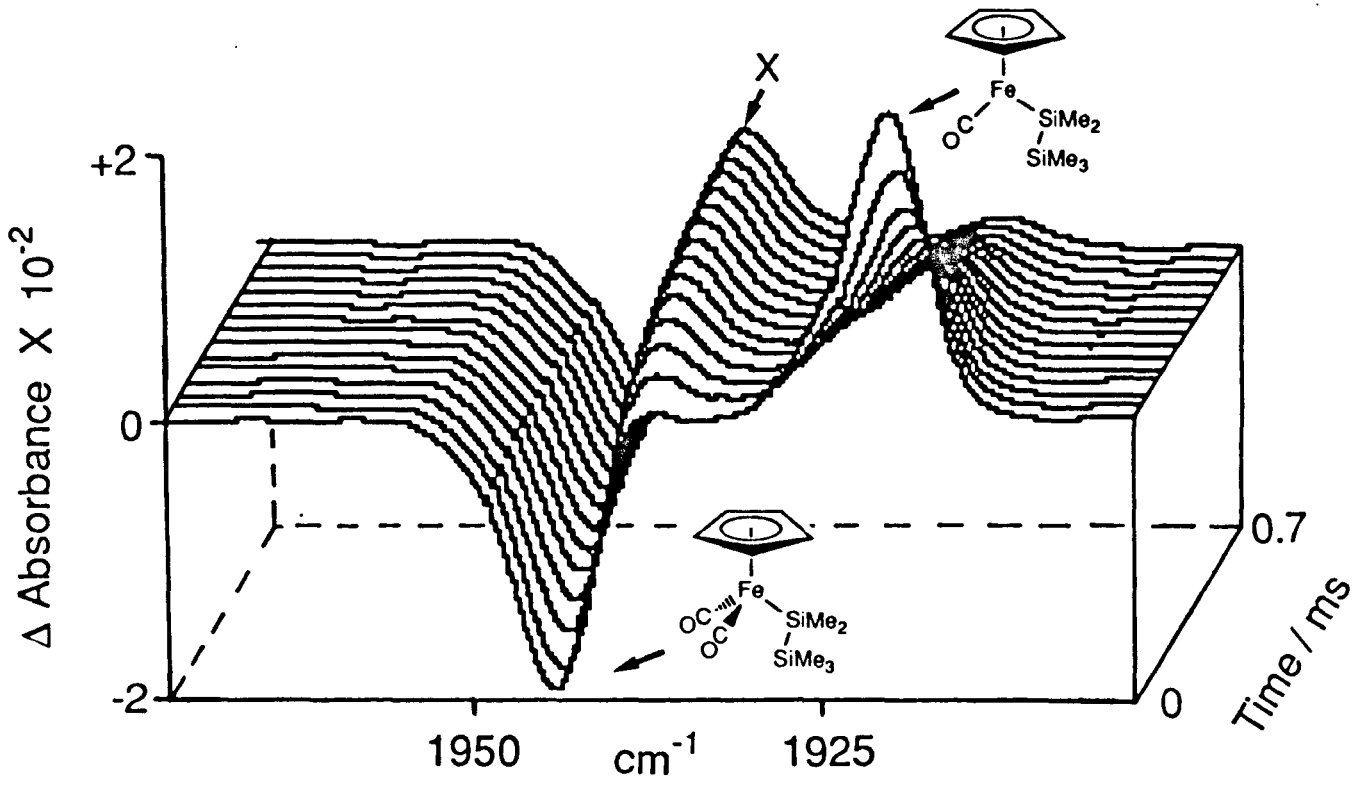


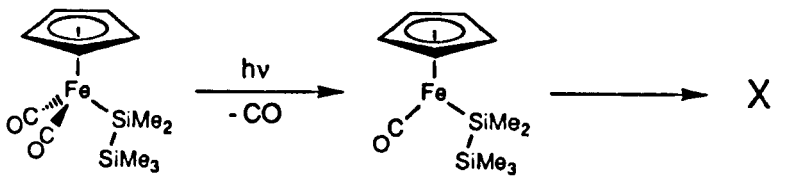
Figure 4.6: A series of time-resolved IR spectra obtained after flash photolysis of $FpSiMe_2SiMe_3$ (2 X 10^{-3} M) in n-heptane at room temperature under argon. The time delay between each spectrum is 50 μs. Bands are labelled according to the species responsible.

of IR absorption in this trace is assigned to the edge of a ν(CO) band which grows in due to a secondary product (see below). The trace in Figure 4.5(c) indicates that a primary photoproduct with an IR absorption at 1924 cm^{-1} is generated by the UV flash This absorption decays with a half life of ca. 200 μs. The trace obtained at 1941 cm^{-1} (Figure 4.5(b)) shows an initial small depletion in IR absorption due to the edge of the of the low frequency parent ν(CO) band, centred at 1946 cm^{-1}. An IR absorption then grows at 1941 cm^{-1}, which exactly mirrors the decay of the transient absorption at 1924 cm^{-1}.

The changes in the IR spectrum caused by flash photolysis are illustrated excellently by the "stack plot" of time-resolved IR spectra shown in Figure 4.6. Depletion of the low frequency parent ν(CO) absorption at 1946 cm^{-1} is accompanied by the generation of the single ν(CO) band of a primary photoproduct at 1924 cm^{-1}. This absorption is close to that of $CpFe(CO)SiMe_2SiMe_3$ in low temperature matrices (Table 4.1) and can reasonably be assigned to the same species. The decay of the primary photoproduct results in the generation of a secondary product, X, with a ν(CO) band at 1941 cm^{-1} (The peak position of this band may be distorted by the adjacent negative signal due to starting material destroyed by photolysis). The ν(CO) absorption at 1941 cm^{-1} exhibits no decay even 10 ms after the UV laser pulse, indicating that X is stable

on the timescale of these experiments.

The photochemistry observed in this experiment is summarised in Equation 4.7.



4.7

The decay of $CpFe(CO)SiMe_2SiMe_3$ and production of X both obey first order kinetics with a first order rate constant of $3.5(+/-0.2) \times 10^{3}\ s^{-1}$. The single $\nu(CO)$ absorption band suggests that X is a monocarbonyl species. These observations are consistent with the generation of X via an intramolecular reaction of $CpFe(CO)SiMe_2SiMe_3$. It should be possible to confirm that this reaction is intramolecular by varying the conditions of the experiment in the following ways:

1) Changing the concentration of $FpSiMe_2SiMe_3$ in solution; If X is produced by the combination of two molecules of $CpFe(CO)SiMe_2SiMe_3$ or by reaction of $CpFe(CO)SiMe_2SiMe_3$ with starting material, then an increase in the concentration of parent compound would cause an increase in the rate of the reaction.

2) Dissolving carbon monoxide in the solution; If the reaction involves combination of $CpFe(CO)SiMe_2SiMe_3$ with CO, then an increase in the concentration of CO in solution would increase the rate of reaction.

The results of experiments with double the concentration of $FpSiMe_2SiMe_3$, or a pressure of 2 atm of CO above the solution are identical to those described above. The rate of conversion of $CpFe(CO)SiMe_2SiMe_3$ to X is unaffected by either of these changes in conditions, within the limits of experimental error ($3.5(+/-0.2) \times 10^3\ s^{-1}$). (By contrast, the presence of 2 atm of CO in experiments on $FpSiMe_3$ has a pronounced effect - see below).

It is concluded that the decay of $CpFe(CO)SiMe_2SiMe_3$ to give X is an intramolecular process. It is likely that rearrangement of $CpFe(CO)SiMe_2SiMe_3$ occurs, to form a thermodynamically more stable structure. No such decay is observed in a matrix at 12 K, indicating that there is a significant activation energy for this process. The observation of no rapid recombination of $CpFe(CO)SiMe_2SiMe_3$ with CO in solution suggests that this reaction can be blocked by an interaction of the disilyl ligand with the unsaturated iron atom can block this reaction. This is in agreement with the results of matrix isolation studies on $FpSiMe_2SiMe_3$.

Flash Photolysis of $FpSiMe_3$

Figure 4.7(a) shows the IR absorption trace obtained at 1928 cm^{-1}, on flash photolysis of a solution of $FpSiMe_3$ in n-heptane under an atmosphere of argon. It shows that a transient IR absorption is produced immediately after the UV flash, which then decays rapidly, with a half life of ca. 9 μs.

The transient IR spectrum shown in Figure 4.8(a) corresponds to a time interval 5 μs after the UV laser pulse. It shows depletion of the low frequency parent ν(CO) band at 1946 cm^{-1}, and the appearance of a photoproduct absorption at 1928 cm^{-1}. Figure 4.8(b) shows the spectrum obtained 45 μs after the UV flash, by which time the the photoproduct absorption at 1928cm^{-1} has disappeared. Some of the starting material destroyed by the flash has been regenerated but there is also a weak new absorption at 1911 cm^{-1}, not present after 5 μs, which is presumably due to a secondary product.

The frequency of the single primary photoproduct band is in the region expected for a monocarbonyl species formed by dissociative loss of CO from $FpSiMe_3$. The matrix isolation results on $FpSiMe_3$ suggest that recombination of the monocarbonyl with CO is a facile process. A certain amount of rapid regeneration of $FpSiMe_3$ is observed after flash photolysis, but not all

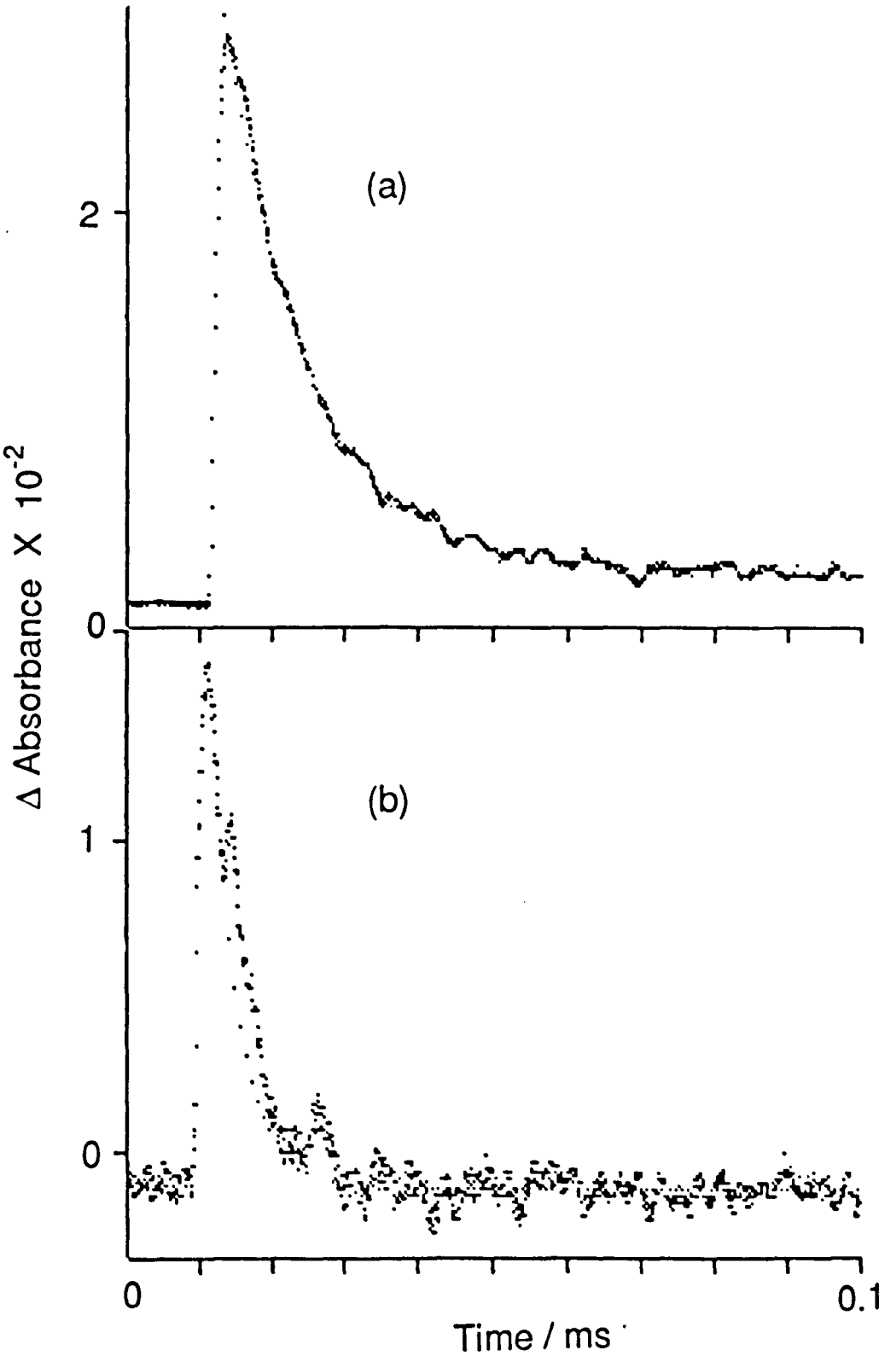


Figure 4.7: Transient IR absorption traces recorded at 1928 cm^{-1} on flash photolysis (308 nm) of $FpSiMe_3$ (2 X 10^{-3} M) in n-heptane at room temperature. (a) Under 2 atm argon. (b) Under 0.1 atm CO/1.9 atm argon. Note the increase in decay rate of the absorption due to $CpFe(CO)SiMe_3$ in the presence of added CO.

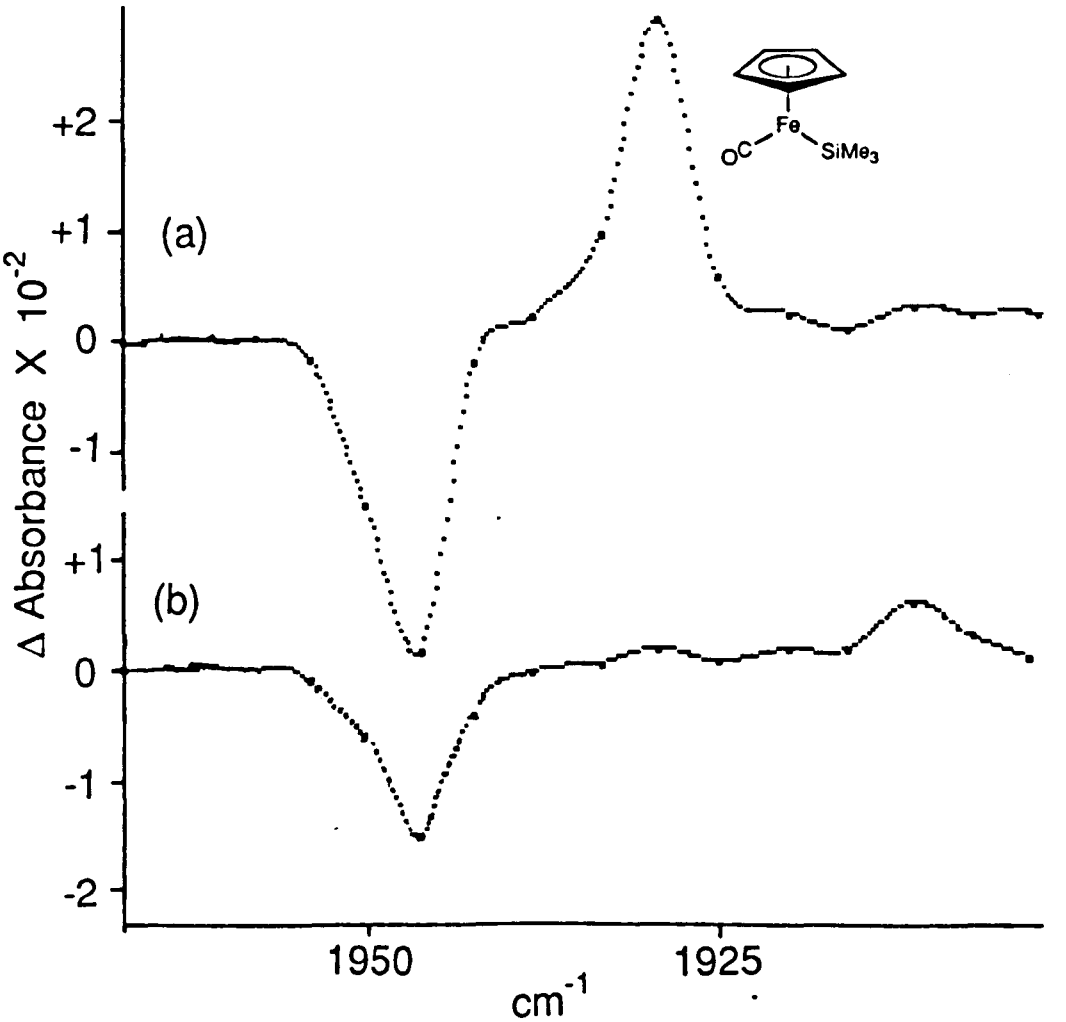


Figure 4.8: Time-resolved IR spectra obtained (a) 5 μs and (b) 45 μs after flash photolysis of $FpSiMe_3$ in n-heptane (2 X 10^{-3} M) at room temperature under argon.

of the starting material is recovered on this timescale. To probe whether the primary photoproduct is co-ordinatively unsaturated species resulting from CO-loss, the experiment was repeated with different pressures of CO above the solution.

Figure 4.7(b) shows the IR absorption trace obtained at 1928 cm^{-1} on introduction of a pressure of 0.1 atm of CO above the solution. Decay of the photoproduct ν(CO) band at 1928 cm^{-1} occurs approximately twice as fast as under a pure argon atmosphere (half-life ca. 4 μs) . In this experiment, the starting material destroyed by the UV flash is completely recovered during the decay of the 1928 cm^{-1} absorption. On increasing the pressure of CO to 2 atm, no photoreaction was detected on flash photolysis, suggesting that the photoproduct recombines with CO extremely rapidly. Hence, in the presence of added CO, the reversibility of the photoreaction on this timescale is greatly improved.

These results are consistent with rapid recombination of a monocarbonyl photoproduct with CO to regenerate $FpSiMe_3$ (Equation 4.8).

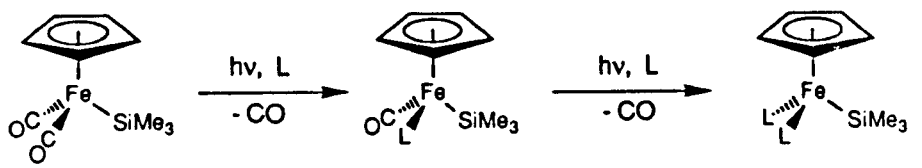
$$FpSiMe_3 \underset{+\ CO}{\overset{h\nu,\ -CO}{\rightleftharpoons}} CpFe(CO)SiMe_3 \qquad 4.8$$

The fact that the reaction is not completely reversible under a pure argon atmosphere may be due to some reaction of the unsaturated monocarbonyl photoproduct with starting material. When a solution of $FpSiMe_3$ in n-heptane under argon is photolysed with a medium pressure Hg arc lamp (> 300 nm), small amounts of the iron dimer, Fp_2, are produced. Under a CO atmosphere, similar irradiation causes no net photoreaction.

The results of fast TRIR spectroscopy are in excellent agreement with the photochemistry observed in low temperature matrices for $FpSiMe_3$. Matrix isolation studies suggest that the rapid in-cage recombination of $CpFe(CO)SiMe_3$ with CO prevents observation of the monocarbonyl species. However, this photoproduct can be detected in room temperature hydrocarbon solution with fast IR detection. The behaviour of $CpFe(CO)SiMe_3$ in these experiments confirms that its reaction with CO is extremely rapid.

Flash Photolysis of $FpSiMe_2SiMe_3$ or $FpSiMe_3$ in the Presence of PPh_3

The photochemical reaction of $FpSiMe_3$ with two electron donor ligands such as phosphines, phosphites and isocyanides is well known (King 1968, Chan 1978, Cerveau 1981, Treichel 1981). It has been found that either one or both of the carbonyl groups in the parent compound can be substituted photochemically, depending on the ligand L which is employed (Equation 4.9).



4.9

In the reaction with triphenylphosphine, only monosubstitution occurs, yielding $CpFe(CO)(PPh_3)SiMe_3$.

The results discussed so far suggest that the disilyl group of $FpSiMe_2SiMe_3$ can prevent reaction of the photochemically generated monocarbonyl with ligands such as CO or N_2. It is of interest whether TRIR spectroscopy can show any differences in the solution photochemistry of $FpSiMe_2SiMe_3$ and $FpSiMe_3$ in the presence of triphenylphosphine.

Flash photolysis experiments were carried out, in which TRIR spectra were recorded of solutions containing the particular Fp-silyl complex and a five-fold excess of triphenylphosphine. Four of the IR

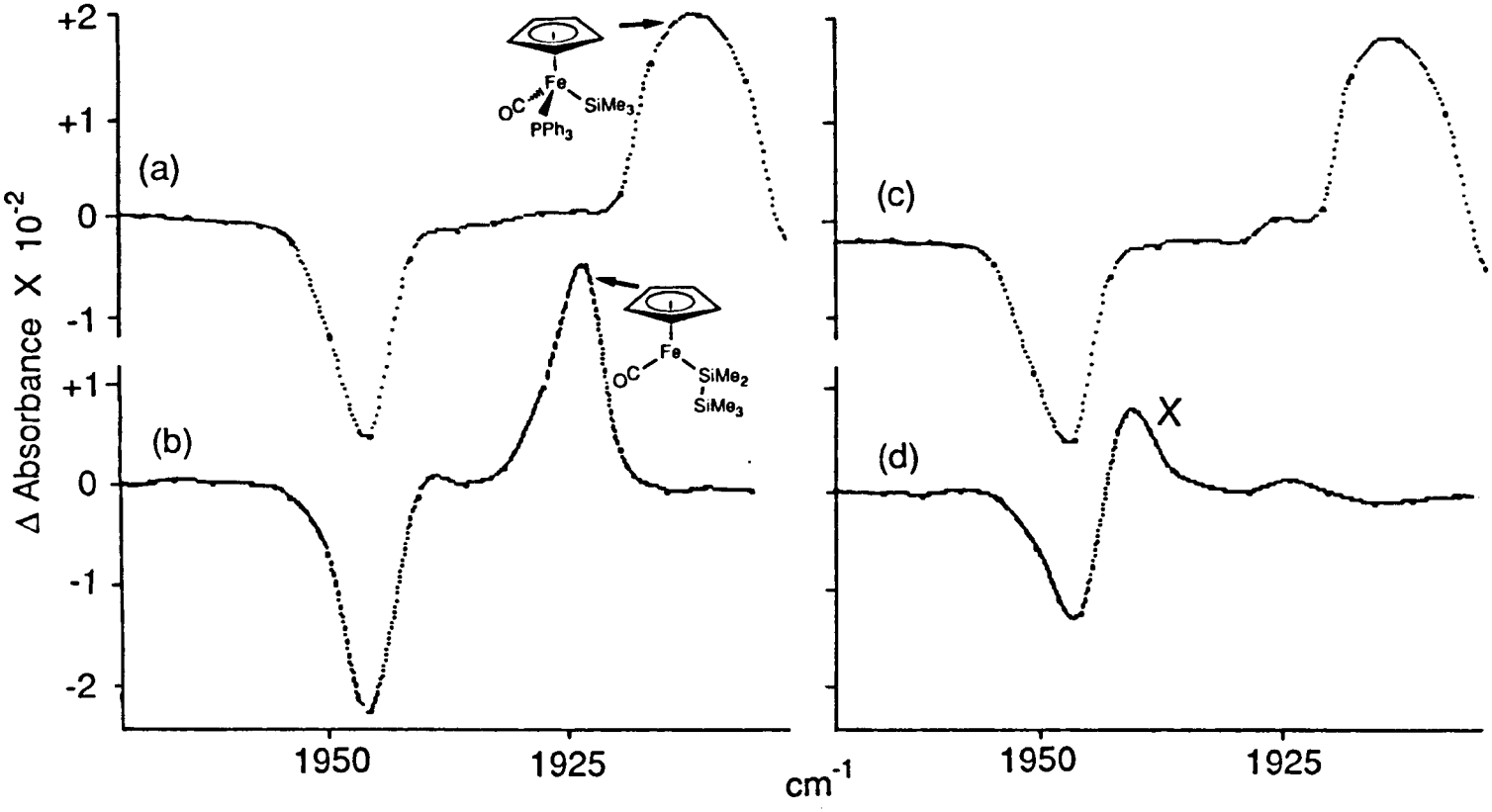


Figure 4.9: Time-resolved IR spectra obtained 5μs after flash photolysis of (a) $FpSiMe_3$ and (b) $FpSiMe_2SiMe_3$ (2×10^{-3} M) in n-heptane at room temperature containing PPh_3 (10^{-2} M). (c),(d) Time-resolved IR spectra of the same solutions 750 μs after the UV flash.

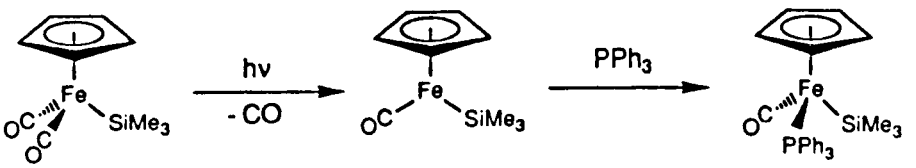
spectra recorded in these experiments are shown in Figure 4.9.

Spectra (a) and (b) correspond to a time interval 5 μs after the UV laser pulse in each experiment. Both spectra show negative bands at 1946 cm^{-1}, due to loss of starting material. In spectrum (a) there is a photoproduct IR absorption at 1912 cm^{-1}, which is not observed in the absence of phosphine. This absorption corresponds well with the ν(CO) band of $CpFe(CO)(PPh_3)SiMe_3$, in n-heptane solution (Table 4.2). However, in spectrum (b) there is no photoproduct absorption which can be assigned to a simple phosphine substitution product, $CpFe(CO)(PPh_3)SiMe_2SiMe_3$. Such a species would be expected to have a ν(CO) band very close to that of its monosilyl analogue. Instead, the same photoproduct IR band is observed as in the absence of phosphine, at 1924 cm^{-1}, assigned to $CpFe(CO)SiMe_2SiMe_3$. This suggests formation of the same monocarbonyl species in which the vacant co-ordination site is blocked by the disilyl ligand.

Figures 4.9(c) and (d) show spectra recorded 750 μs after the UV laser pulse. For $FpSiMe_3$, the spectrum is identical with that obtained after 5 μs. This is consistent with the production of the stable monocarbonyl phosphine substitution product, $CpFe(CO)(PPh_3)SiMe_3$. For $FpSiMe_2SiMe_3$, the photoproduct absorption at 1924 cm^{-1} observed after 5

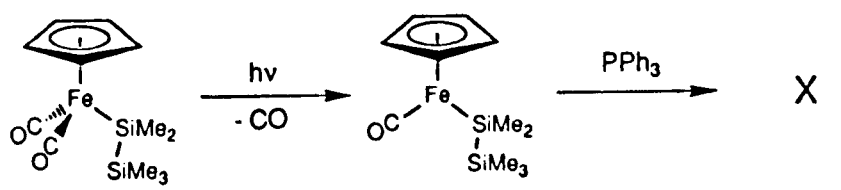
μs has almost disappeared, with the growth of a new ν(CO) band at 1941 cm^{-1}. This is assigned to the stable product, X, observed in the absence of phosphine. Kinetic traces show that the rate at which X is produced from the monocarbonyl is unaffected by the addition of phosphine.

The results of fast TRIR spectroscopy of the Fp-silyl complexes in the presence of added triphenylphosphine show that photodissociation of CO from $FpSiMe_3$ is followed by rapid uptake of phosphine to yield the stable complex, $CpFe(CO)(PPh_3)SiMe_3$ (Equation 4.10). The primary photoproduct, $CpFe(CO)SiMe_3$, is not detected under these conditions due to rapid reaction with phosphine.



4.10

The analogous reaction for $FpSiMe_2SiMe_3$ does not occur. Instead, the monocarbonyl species generated by flash photolysis decays in the same manner as in the absence of phosphine, to yield the stable, secondary product, X (Equation 4.11).



4.11

Discussion

Fast TRIR spectroscopy in room temperature solution has shown that CO-loss from $FpSiMe_2SiMe_3$, initiated by flash photolysis, is irreversible. The primary photoproduct, $CpFe(CO)SiMe_2SiMe_3$, is relatively stable, considering its formal 16 electron count, and is unreactive towards CO or PPh_3. It undergoes an intramolecular reaction to give a secondary product, X, which is stable on the timescale of these experiments. By contrast, $CpFe(CO)SiMe_3$, generated by flash photolysis of $FpSiMe_3$, reacts rapidly with CO or PPh_3.

The photochemical conversion of $FpSiMe_2SiMe_3$ to $FpSiMe_3$ in solution is well known. However, fast TRIR spectroscopy shows that the only stable product of flash photolysis is X, with no evidence for the production of $FpSiMe_3$ on this timescale. These results suggest that the monosilyl complex may be formed by a secondary photochemical process.

The ν(CO) frequency of X is higher than that of the primary photoproduct. Such a shift would be expected if formation of X involved an intramolecular oxidative addition of the disilyl ligand to the metal centre. Possible reactions of this type are considered in the Discussion at the end of this Chapter.

4.5 THE ROOM TEMPERATURE SOLUTION PHOTOCHEMISTRY OF Fp-SILYL COMPLEXES

The solution photochemistry of $FpSiMe_3$ is well known and provides a good reference with which to compare the solution photochemistry of $FpSiMe_2SiMe_3$. The following section describes experiments in which n-heptane solutions of $FpSiMe_3$ or $FpSiMe_2SiMe_3$ were irradiated, sometimes in the presence of potential reactants. The reactions were monitored using FTIR.

Photolysis of $FpSiMe_3$ or $FpSiMe_2SiMe_3$ with no Added Ligands

Irradiation (> 300 nm) of $FpSiMe_3$ in n-heptane under argon results in extremely slow destruction of starting material. Only ca. 2% of the parent is destroyed by 30 mins photolysis, and the only product observed by IR spectroscopy is a small quantity of the dinuclear iron complex, Fp_2.

Figure 4.10 shows a series of IR spectra recorded at intervals during the irradiation of $FpSiMe_2SiMe_3$ in n-heptane under an argon atmosphere. Loss of starting material is accompanied by the growth of a shoulder on the low frequency parent ν(CO) band, marked with an arrow. The effect of the first 60 seconds of photolysis is illustrated by the difference spectrum in Figure 4.11(a). The shoulder observed in the

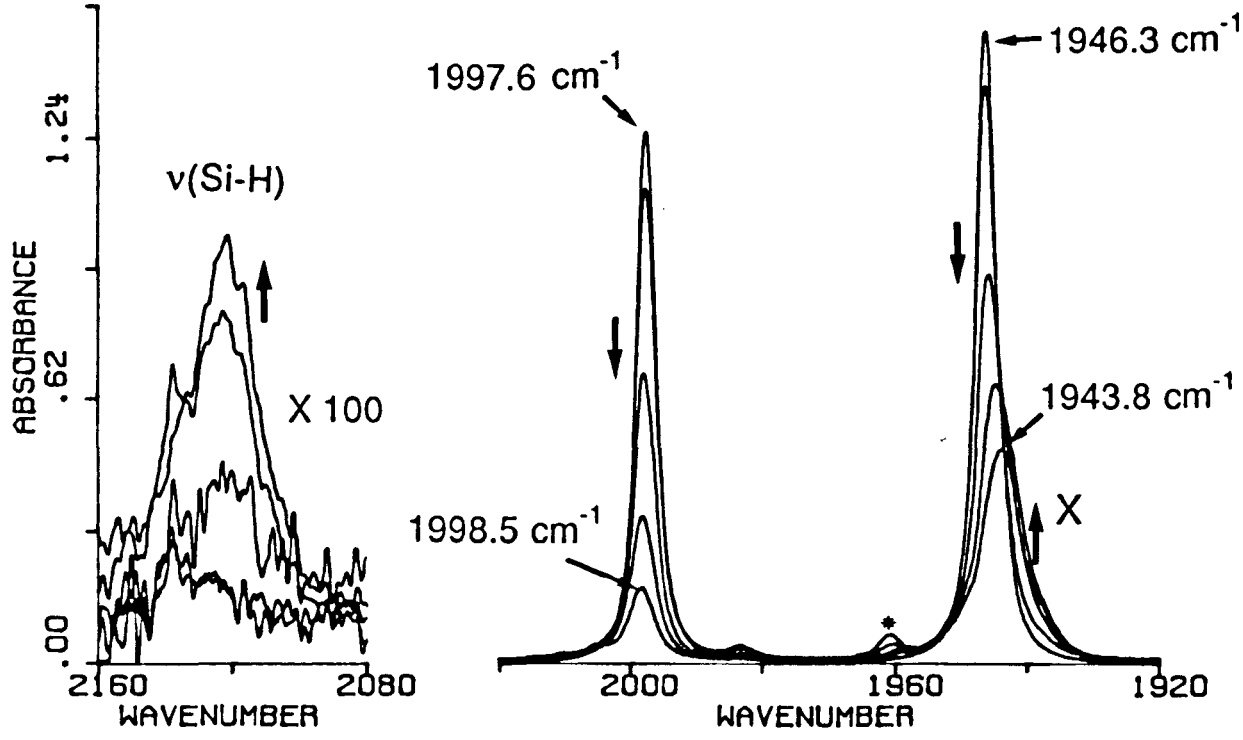


Figure 4.10: IR spectra obtained after 0, 1, 6, 21 and 56 minutes irradiation (>300 nm) of $FpSiMe_2SiMe_3$ (1.7×10^{-3} M) in n-heptane under argon at room temperature. Arrows indicate the growth and depletion of absorptions. The shoulder near 1940 cm^{-1} is due to X. Note the shifts in frequency due to formation of $FpSiMe_3$ (Peak position error +/- 0.2 cm^{-1}). The band marked with an asterisk is due to the minor product, Fp_2. The ν(Si-H) region is shown with an expanded absorbance scale.

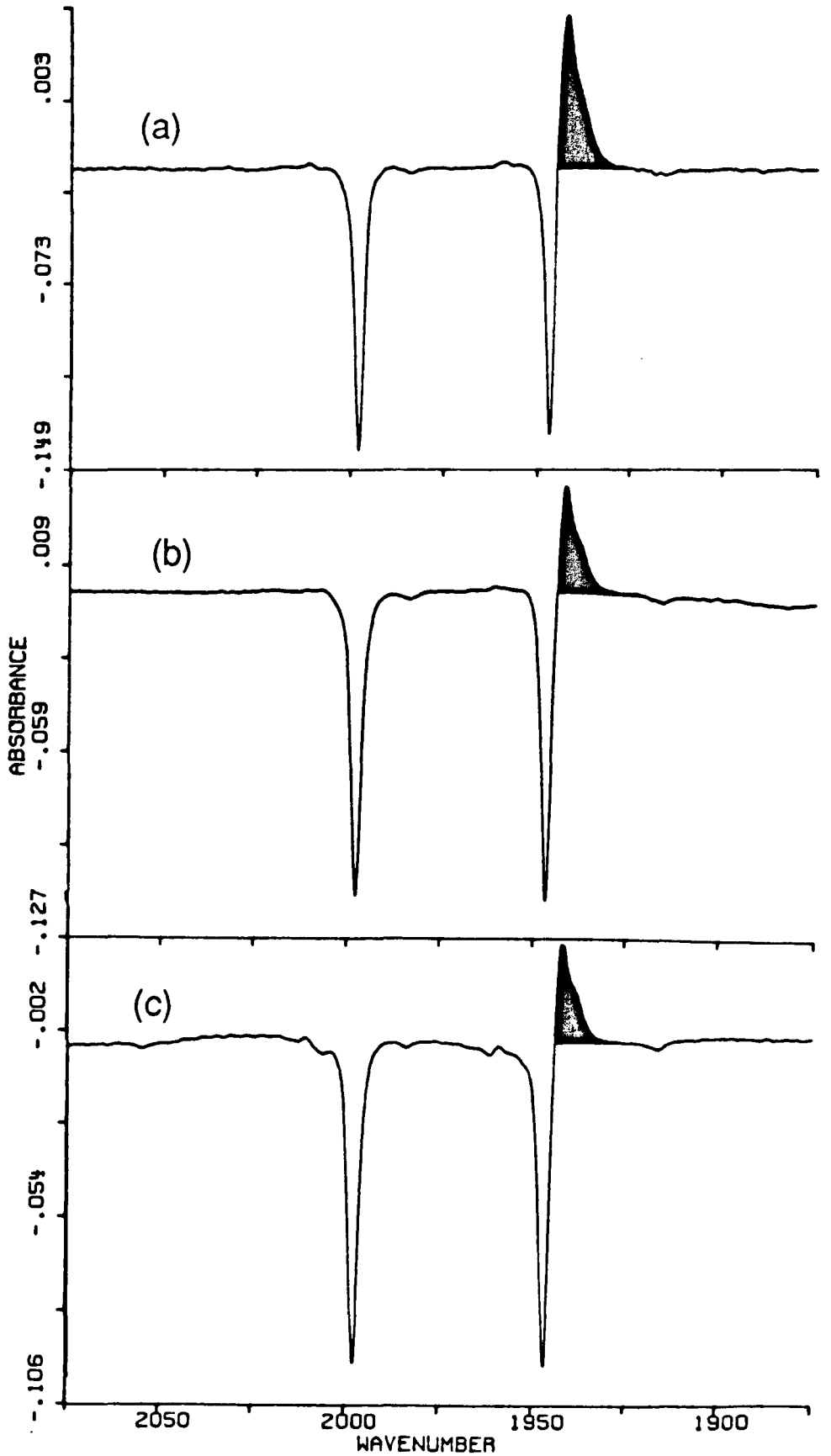


Figure 4.11: IR difference spectra obtained after 1 min irradiation (>300 nm) of $FpSiMe_2SiMe_3$ (1.7×10^{-3} M) in n-heptane under an atmosphere of (a) argon, (b) ethylene and (c) carbon monoxide. The band coloured black in each case is due to X.

conventional IR spectrum appears as a positive absorption in the difference spectrum. Scaled subtraction of the spectrum of the starting spectrum reveals a single photoproduct ν(CO) band centred at 1943 cm^{-1}. This corresponds to the absorption of X, the secondary product observed in flash photolysis experiments (see above). No decay of this species, or regeneration of starting material was observed after 90 minutes, during which time the solution was left in the dark at room temperature.

On continued photolysis, more starting material is consumed and the amount of X in solution increases. However, the concentration of X reaches a maximum value and then begins to decrease. At the same time, small but significant shifts in the ν(CO) absorptions of the "parent" are observed. The peak position of the low frequency parent band is distorted by the proximity of the absorption of X, but a shift is also apparent in the high frequency band, as indicated in Figure 4.10 This is consistent with the production of $FpSiMe_3$. The ν(CO) bands of $FpSiMe_2SiMe_3$ and $FpSiMe_3$ have very similar frequencies which are listed in Table 4.2. However, it is possible to distinguish the absorptions of these two complexes using FTIR spectroscopy, and it is clear that the monosilyl complex is produced in this experiment. The generation of $FpSiMe_3$ is in agreement with previous studies, in which NMR spectroscopy and Gas Chromatography were used to monitor the reaction

(Pannell 1986, Tobita 1988). These results suggest that a thermally stable, intermediate compound, X, is formed initially, and that $FpSiMe_3$ is generated by a secondary photochemical process. It was found that larger concentrations of X could be generated using filtered UV photolysis (300-345 nm). Presumably, the rate the of secondary photochemical process is reduced under these conditions. The intermediate species, X, has not been observed in previous studies on this system.

This experiment provides another interesting observation. On extended photolysis of $FpSiMe_2SiMe_3$, a weak, broad IR absorption is observed to grow at $2121cm^{-1}$, in the ν(SiH) region of the IR spectrum (Figure 4.10). The band is not apparent in the earliest stages of photolysis. Inspection of the spectra obtained during irradiation of $FpSiMe_3$ reveals that no such absorption is produced for the monosilyl complex under identical conditions.

Attempts to characterise X using ^1H NMR spectroscopy have so far been unsuccessful, since secondary photolysis prevents the formation of large concentrations of this species.

Photolysis of $FpSiMe_3$ or $FpSiMe_2SiMe_3$ in the Presence of Added CO

Irradiation (> 300 nm) of a solution of $FpSiMe_3$ in n-heptane under a pressure of 1 atm of CO results in no net photochemistry, indicating that the presence of excess CO in solution suppresses any photochemical reactions of this complex. This is in agreement with the results obtained from low temperature matrices and TRIR spectroscopy, from which it was concluded that photoejection of CO is followed by rapid recombination to regenerate starting material.

Tobita et al noted that the yield of $FpSiMe_3$ obtained from irradiation of $FpSiMe_2SiMe_3$ is increased when the reaction is carried out under an atmosphere of CO. Figure 4.11(c) shows the IR difference spectrum obtained after 60 seconds photolysis (> 300 nm) of a solution of $FpSiMe_2SiMe_3$ in in n-heptane under 1 atm CO. It is similar to the difference spectrum obtained when an argon atmosphere is used (Figure 4.11(a)). The relative amount of X generated by photolysis is reduced under a CO atmosphere. This suggests that the rate of consumption of X by a secondary photochemical process is increased in the presence of added CO.

In a separate experiment, a solution of $FpSiMe_2SiMe_3$ in n-heptane under argon, was initially irradiated with filtered UV light (300-345 nm) until a

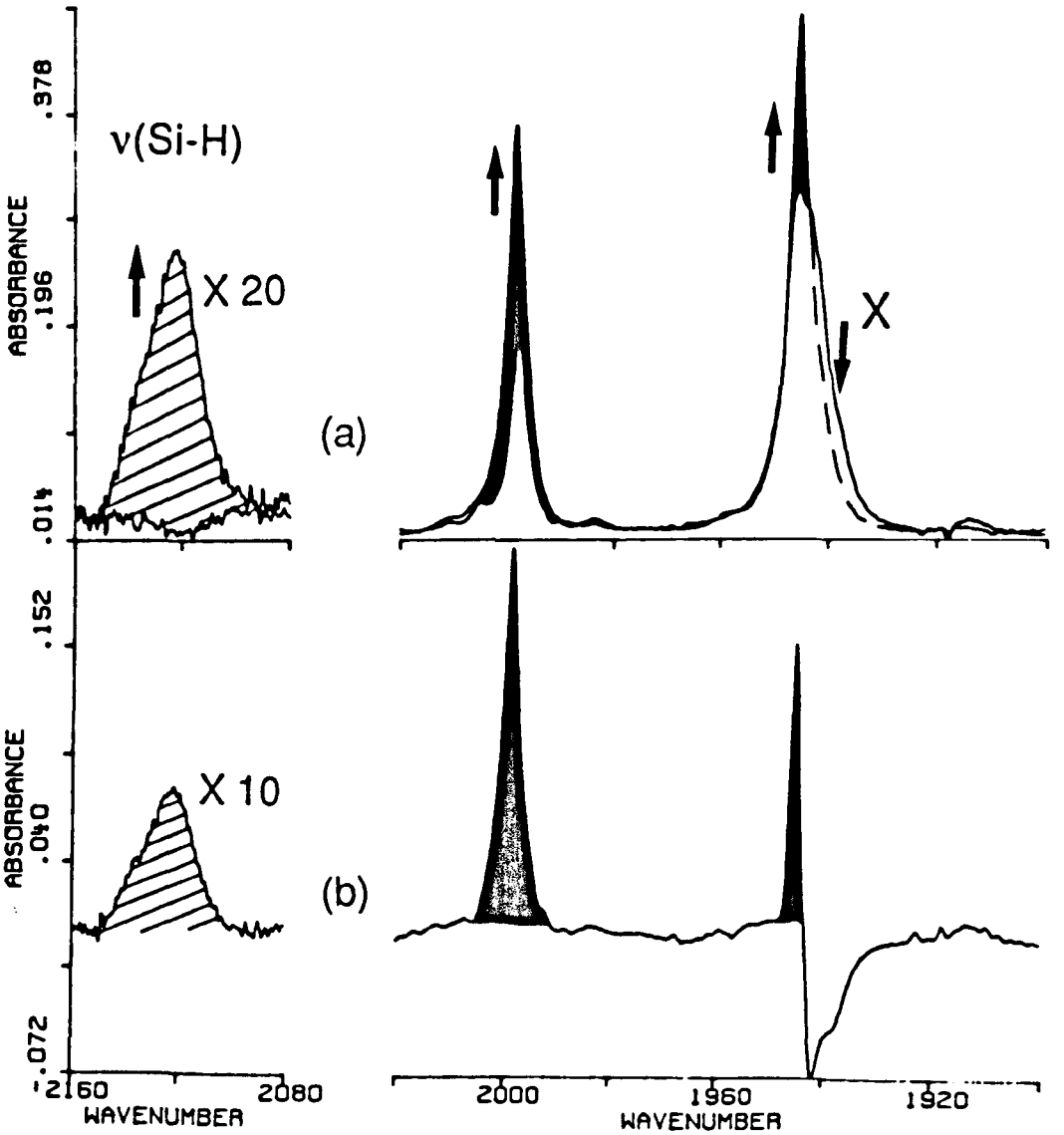
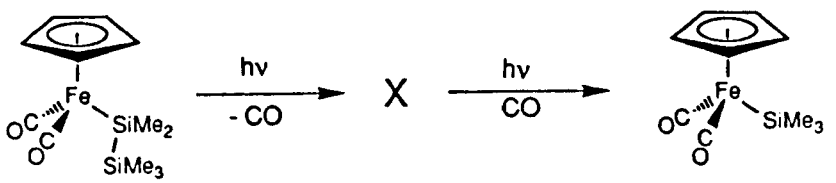


Figure 4.12: IR spectra illustrating the photochemical reaction of X with CO to give $FpSiMe_3$. (a) Starting spectrum obtained after 300 mins filtered UV irradiation (230-345 nm) of $FpSiMe_2SiMe_3$ in n-heptane under argon to generate X. The bands coloured black, due to $FpSiMe_3$, were produced after 345 mins further photolysis (>400 nm) under CO. Arrows indicate the behaviour of individual bands. (b) Difference spectrum showing depletion of shoulder at 1943 cm^{-1} due to X. Note the crosshatched ν(Si-H) band produced during this reaction, shown with an expanded absorbance scale.

significant concentration of X was generated. The solution was then placed under a CO atmosphere, and irradiated with visible light (> 400 nm). The spectra shown in Figure 4.12(a) illustrate that visible photolysis causes the depletion of the ν(CO) band of X at 1943 cm^{-1} and production of two new ν(CO) bands, coloured black, which are assigned to $FpSiMe_3$. Figure 4.12(b) shows the difference spectrum illustrating this reaction. This observation provides direct evidence that there are two distinct photochemical steps in the deoligomerisation of $FpSiMe_2SiMe_3$ to yield $FpSiMe_3$. The intermediate product, X, has been found to be thermally stable, even in the presence of CO in solution, and only reacts with CO to give $FpSiMe_3$ under photochemical conditions (Equation 4.12).



4.12

This reaction is accompanied by the growth of a broad absorption at 2121 cm^{-1}, in the ν(Si-H) region of the IR spectrum as observed on prolonged photolysis of $FpSiMe_2SiMe_3$ under an argon atmosphere. It may be due to an organosilicon fragment containing Si-H bond(s), produced when an "$SiMe_2$" unit is ejected from the transition metal complex. The identity of this species will be discussed in more detail later in this Chapter.

Photolysis of $FpSiMe_3$ or $FpSiMe_2SiMe_3$ in the Presence of PPh_3

Flash photolysis has already revealed that loss of a CO group from $FpSiMe_3$ is followed by the rapid uptake of phosphine to give $CpFe(CO)(PPh_3)SiMe_3$. No product containing a phosphine ligand was detected in an identical experiment on $FpSiMe_2SiMe_3$.

Figure 4.13 shows the IR difference spectra obtained after 60 seconds photolysis (> 300 nm) of $FpSiMe_3$ or $FpSiMe_2SiMe_3$ in n-heptane with a a five-fold excess of PPh_3. In Figure 4.13(a), loss of $FpSiMe_3$ is accompanied by the growth of an absorption at 1912 cm^{-1}, assigned to $CpFe(CO)(PPh_3)SiMe_3$. Identical irradiation of $FpSiMe_2SiMe_3$ results only in the production of X (Figure 4.13(b)). There is no absorption near 1912cm^{-1}, where one would expect the ν(CO) band of a phosphine substituted product, $CpFe(CO)(PPh_3)SiMe_2SiMe_3$, to appear. These observations resemble the transient difference spectra obtained 750 μs after flash photolysis of similar solutions (Figure 4.9).

Figure 4.14(a) shows the IR spectra recorded at intervals during irradiation of $FpSiMe_3$ in n-heptane in the presence of a five-fold excess of PPh_3. These spectra illustrate the clean photochemical conversion of $FpSiMe_3$ to $CpFe(CO)(PPh_3)SiMe_3$. A similar series of

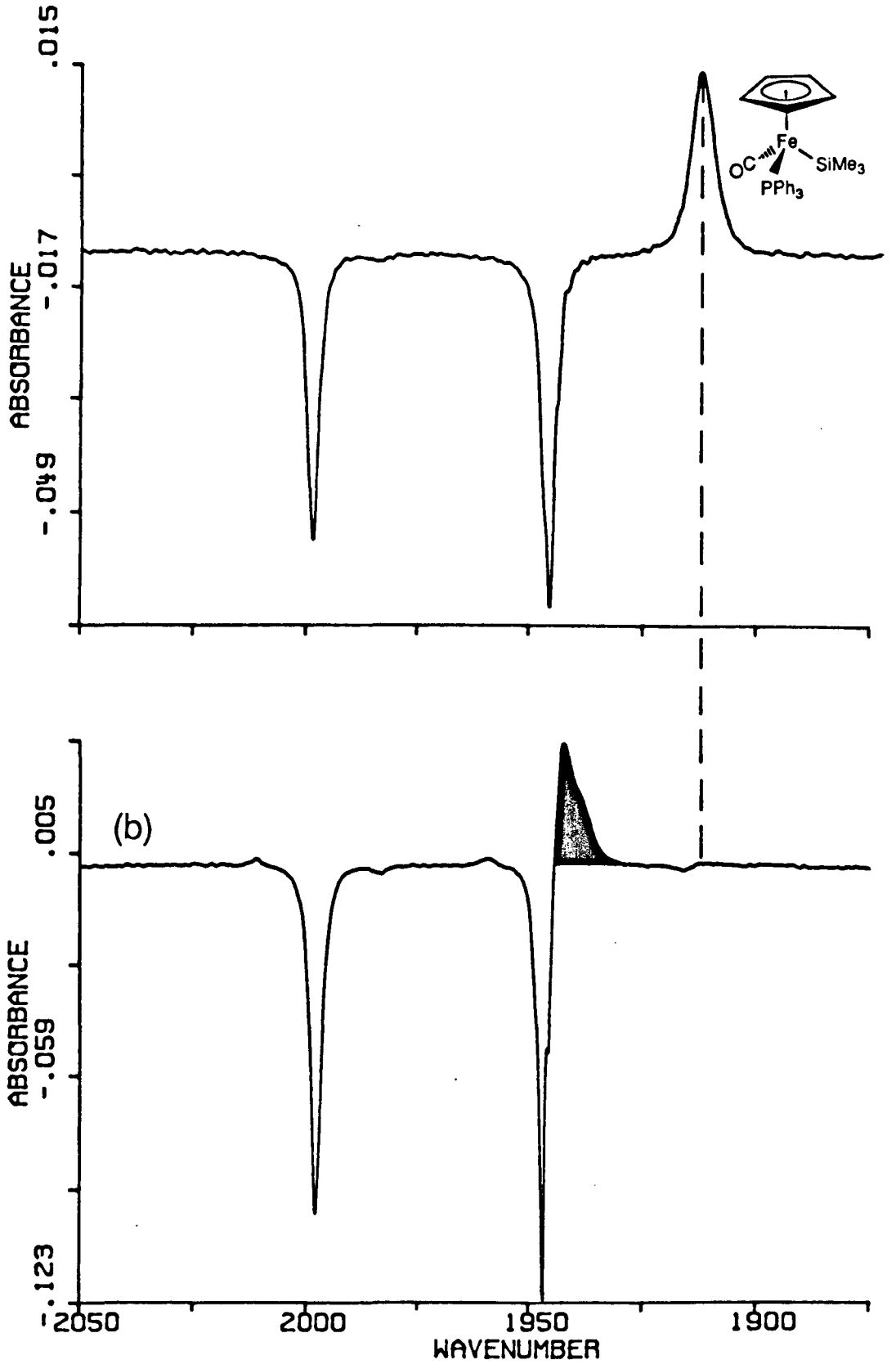


Figure 4.13: IR difference spectra obtained after 1 min irradiation of (a) $FpSiMe_3$ and (b) $FpSiMe_2SiMe_3$ (2.0×10^{-3} M) in n-heptane in the presence of excess PPh_3 (10^{-2} M). The band coloured black in (b) is due to X. Note the absence of any ν(CO) band due to a phosphine substitution product on brief photolysis of $FpSiMe_2SiMe_3$.

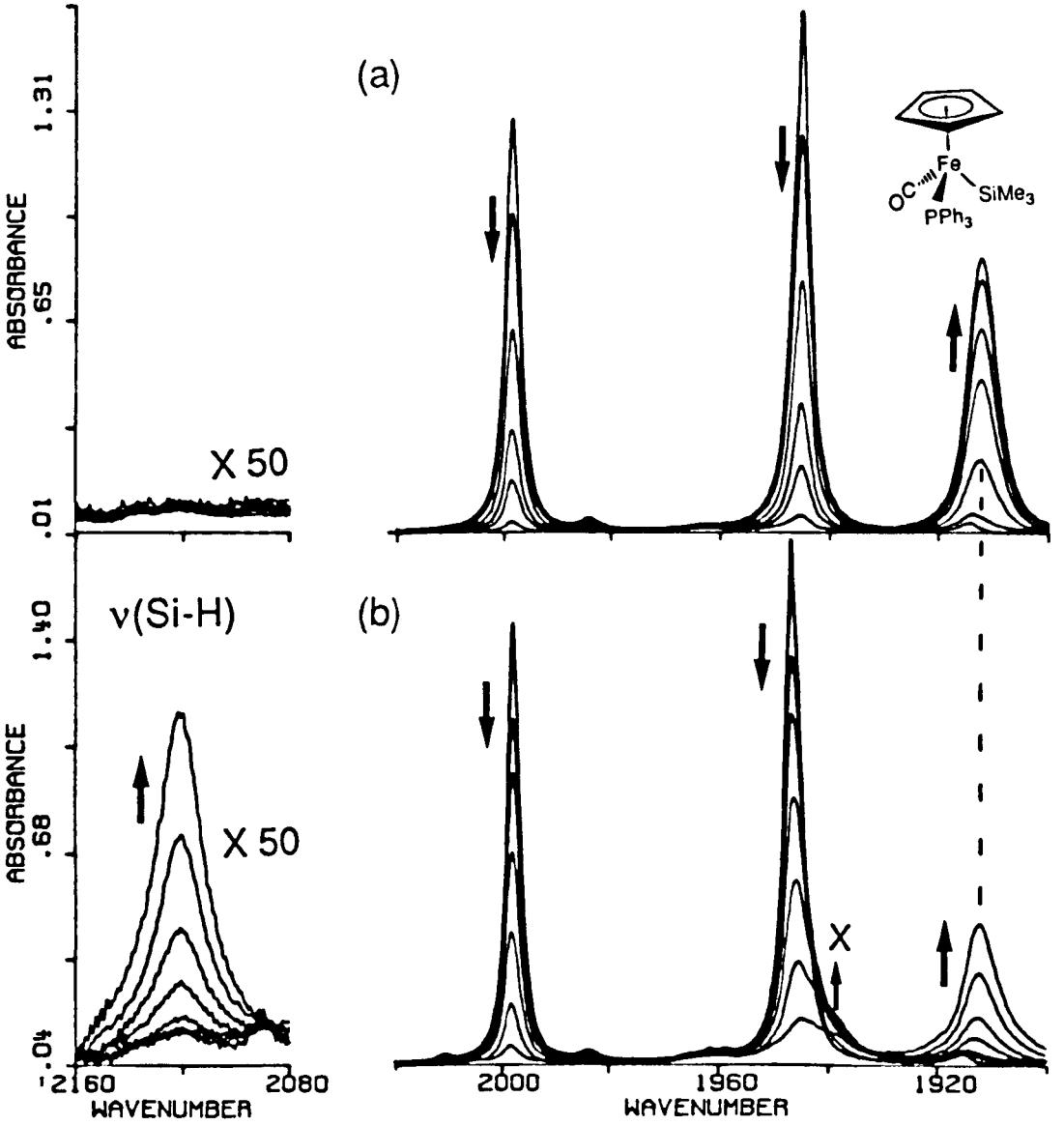
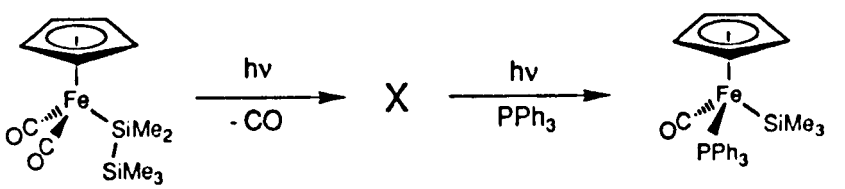


Figure 4.14: (a) IR spectra recorded after 0, 1, 8, 20, 40, 70 and 130 mins irradiation (>300 nm) of $FpSiMe_3$ (2.0×10^{-3} M) and PPh_3 (10^{-2} M) in n-heptane, showing production of the ν(CO) band of $CpFe(CO)(PPh_3)SiMe_3$. (b) IR spectra recorded after 0, 1, 3, 6, 13, 23, 55 and 120 mins irradiation (>300 nm) of $FpSiMe_2SiMe_3$ (2.0×10^{-3} M) and PPh_3 (X M) in n-heptane. Note the initial production of a shoulder due to X near 1940 cm^{-1}. The generation of $CpFe(CO)(PPh_3)SiMe_3$ on prolonged photolysis is matched by the growth of a ν(Si-H) band not produced in (a) (shown with an expanded absorbance scale). Arrows indicate the behaviour of particular absorptions during photolysis.

spectra, recorded during photolysis of $FpSiMe_2SiMe_3$ are displayed in Figure 4.14(b). The growth of a shoulder on the low frequency parent ν(CO) band indicates the generation of X, which is thermally stable in the presence of phosphine. On further photolysis the concentration of X reaches a maximum value, and then begins to decrease. At the same time, two new IR bands are observed to grow in at the same rate, at 1912 and 2121 cm^{-1}. The absorption at 1912 cm^{-1} corresponds exactly with that of the monosilyl phosphine complex, $CpFe(CO)(PPh_3)SiMe_3$ The 2121 cm^{-1} band corresponds to the ν(Si-H) mode, observed in all other experiments after prolonged photolysis of $FpSiMe_2SiMe_3$ in solution.

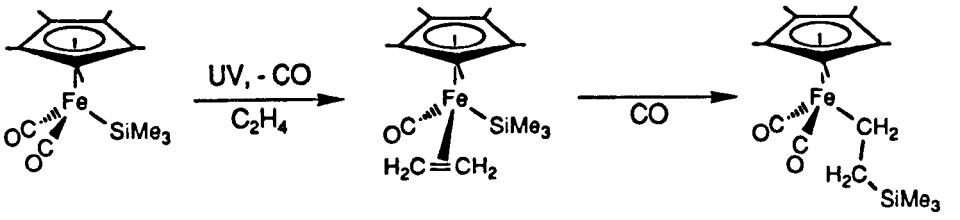
These results indicate that $FpSiMe_2SiMe_3$ does not undergo a simple carbonyl substitution reaction. Irradiation of $FpSiMe_2SiMe_3$ in solution, containing an excess of PPh_3, initially yields X as the only photoproduct. A secondary photochemical reaction leads to destruction of X and the production of the monosilyl phosphine substitution product, $CpFe(CO)(PPh_3)SiMe_3$ as shown in Equation 4.13.



4.13

Photolysis of $FpSiMe_3$ or $FpSiMe_2SiMe_3$ in the Presence of Ethylene

Randolph (1986) reported that irradiation of Fp^*SiMe_3 in the presence of ethylene results in formation of $Cp^*Fe(CO)(C_2H_4)SiMe_3$, in which the ethylene ligand is bound to the Fe centre in an η^2 fashion. Under an atmosphere of CO, the ethylene ligand is found to insert thermally into the Fe-Si bond to yield $Fp^*CH_2CH_2SiMe_3$. This insertion reaction occurs with a half life of approximately 5 minutes (Equation 4.14).



4.14

Randolph also noted preliminary results for the unsubstituted cyclopentadienyl analogue, $FpSiMe_3$, which undergoes similar reactions. The insertion reaction occurs much more slowly in this case, to the extent of approximately 25% completion in 8 hours.

Figure 4.15(a) shows the IR spectra recorded at intervals during the irradiation of a solution of $FpSiMe_3$ in n-heptane, with a pressure of 1 atm of ethylene. Depletion of the two ν(CO) bands of the starting material is apparent. However, the low frequency parent band decreases in intensity at a

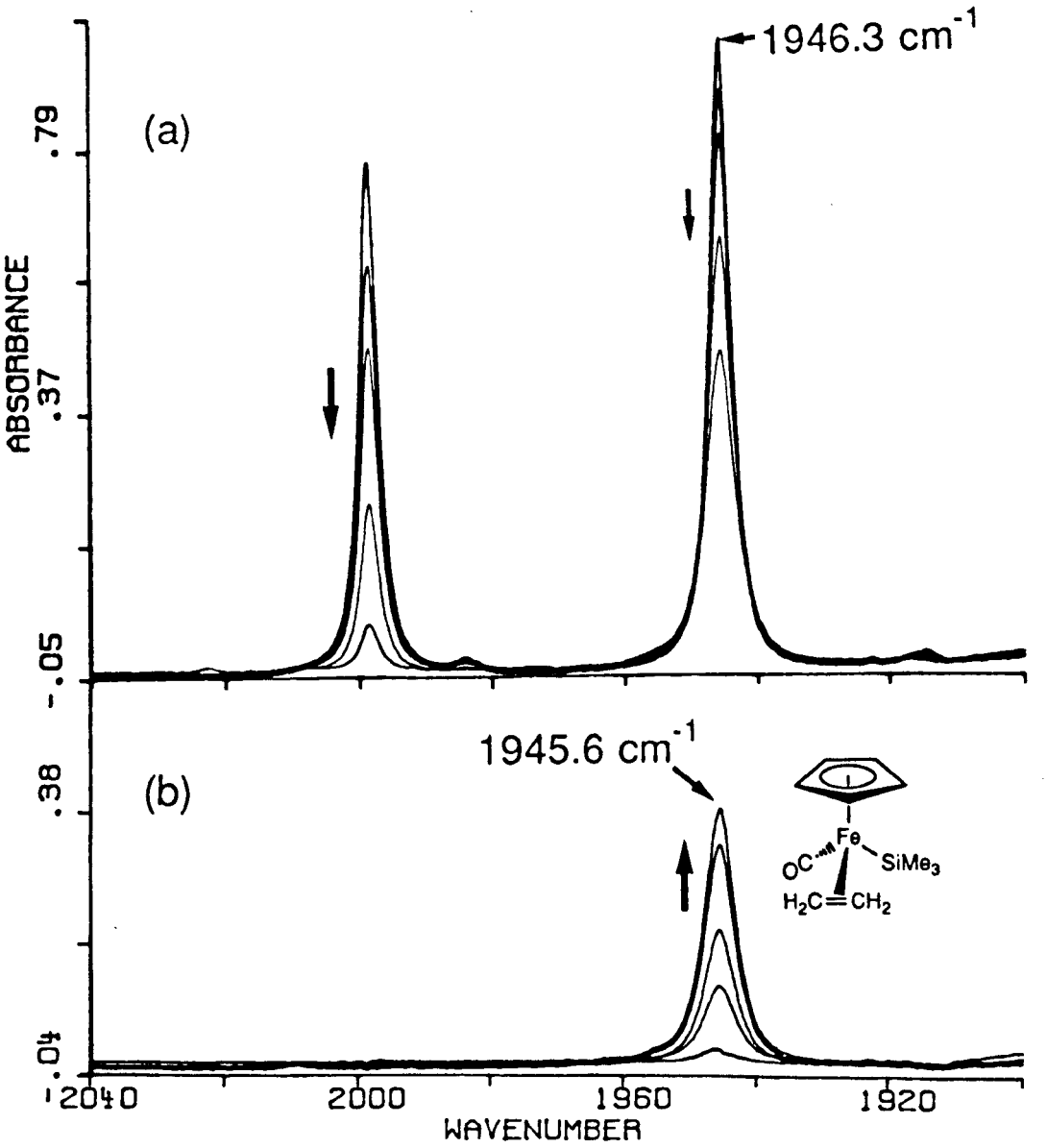


Figure 4.15: (a) IR spectra recorded after 0, 1, 3, 6, 15 and 30 mins irradiation (>300 nm) of $FpSiMe_3$ (1.2×10^{-3} M) in n-heptane under an atmosphere of ethylene. (b) The same spectra with the ν(CO) bands of $FpSiMe_3$ removed by computer subtraction. Note the growth of the ν(CO) band of $CpFe(CO)(\eta^2\text{-}C_2H_4)SiMe_3$. Arrows indicate the behaviour of particular absorptions during photolysis. (Peak position error +/- 0.2 cm^{-1}).

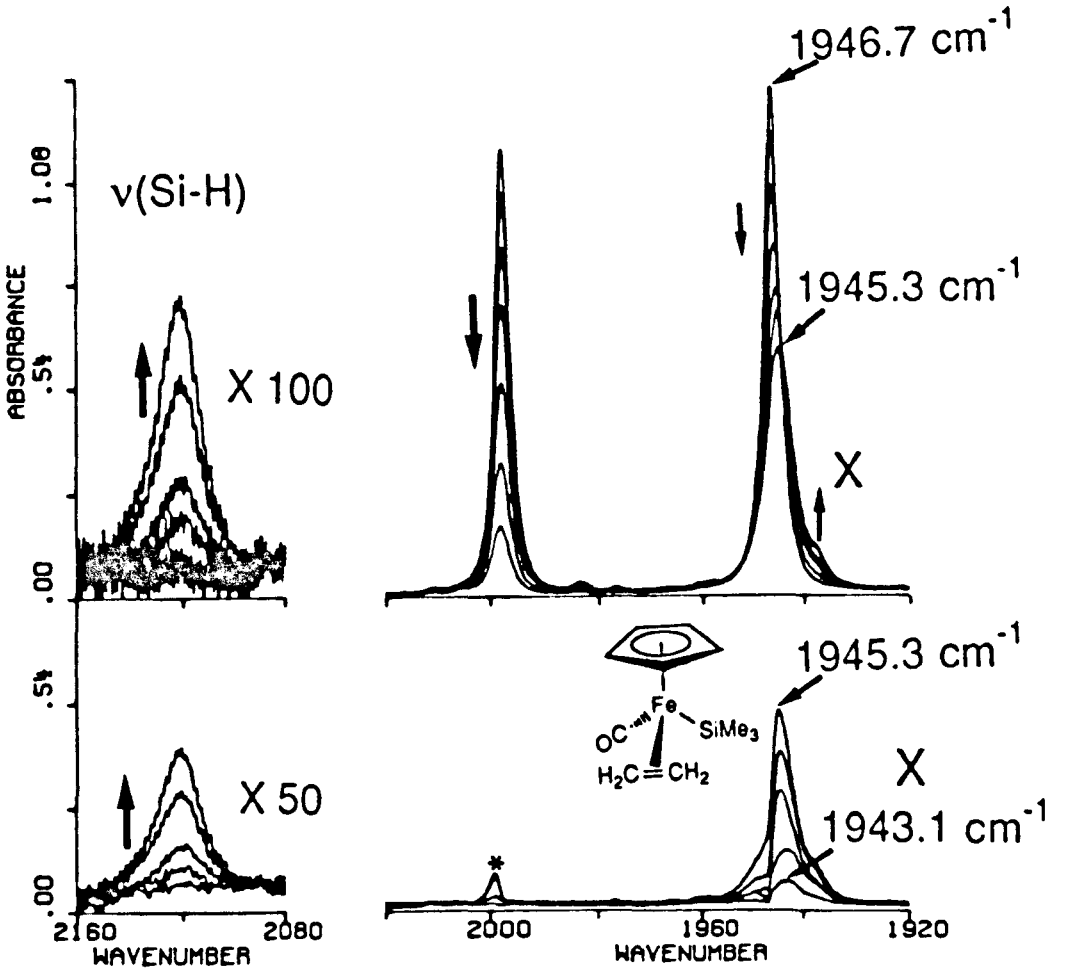
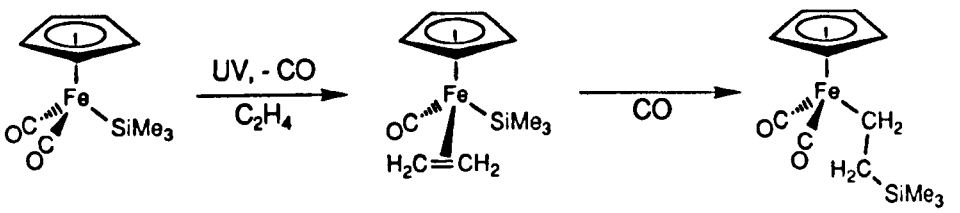


Figure 4.16: (a) IR spectra recorded after 0, 1, 3, 6, 12, 20 and 30 mins irradiation (>300 nm) of $FpSiMe_2SiMe_3$ (1.5×10^{-3} M) in n-heptane under an atmosphere of ethylene. (b) The same spectra with the ν(CO) bands of parent removed by computer subtraction. Note the shifts in peak absorption frequency due to initial production of X and generation of $CpFe(CO)(\eta^2\text{-}C_2H_4)SiMe_3$ on prolonged photolysis (Peak position error +/- 0.2 cm^{-1}). Arrows indicate the behaviour of particular absorptions during photolysis. The band marked with an asterisk is due to a small yield of $FpSiMe_3$. The ν(Si-H) region is shown with an expanded absorbance scale.

slower rate than the high frequency absorption, suggesting the presence of an IR band of another species underneath that of the low frequency parent band. Removal of the parent ν(CO) bands by computer subtraction results in the spectra displayed in 4.15(b) showing the growth of a single ν(CO) absorption at 1945.6 cm^{-1}. The ν(CO) absorption of the photoproduct corresponds with that of $CpFe(CO)(\eta^2\text{-}C_2H_4)SiMe_3$, which is reported to occur at 1944 cm^{-1} in hexane solution (Randolph 1986).

When most of the starting material had been consumed, the ethylene was replaced by a pressure of 1 atm of CO. After 65 hours, during which time the solution was kept in the dark, the band at 1945.6 cm^{-1} due to $CpFe(CO)(\eta^2\text{-}C_2H_4)SiMe_3$ had disappeared, and two new ν(CO) bands were present in the IR spectrum at 1952.7 and 2006.9 cm^{-1}. These correspond well with the frequencies previously assigned to the ethylene insertion product, $CpFe(CO)_2CH_2CH_2SiMe_3$, at 1951 and 2005 cm^{-1} in hexane (Randolph 1986). The reactions observed in this experiment are shown in Equation 4.15.



4.15

The IR difference spectrum illustrated in Figure 4.11(b) shows the effect of 60 seconds photolysis of a

solution of $FpSiMe_2SiMe_3$ in n-heptane under 1 atm of ethylene. This spectrum resembles those obtained after similar irradiation of $FpSiMe_2SiMe_3$ under Ar or in the presence of other dopants in solution (Figures 4.11(a),(c) and 4.13(b)). The positive band at 1943 cm^{-1} can again be assigned to X. There is no evidence for production of an ethylene complex in the early stages of this experiment.

Figure 4.16(a) shows a series of IR spectra recorded as photolysis continued. Removal of the ν(CO) bands of $FpSiMe_2SiMe_3$ by computer subtraction results in the spectra displayed in 4.16(b). This allows those bands due to photoproducts to be inspected. The growth of an absorption near 1940 cm^{-1} is apparent in these spectra. Initially, the peak position of this band is at 1943 cm^{-1}, due to production of X. An increase in intensity of the photoproduct absorption is accompanied by a shift to higher frequency. This is consistent with secondary formation of the ethylene complex, $CpFe(CO)(\eta^2\text{-}C_2H_4)SiMe_3$. The growth af an ν(Si-H) band at 2121 cm^{-1} is again apparent during this reaction.

Confirmation that the iron containing product is $CpFe(CO)(\eta^2\text{-}C_2H_4)SiMe_3$, was obtained by monitoring its thermal reaction with CO. Depletion of of the ν(CO) band of the ethylene complex was accompanied by the growth of the absorptions of the insertion product, $CpFe(CO)_2CH_2CH_2SiMe_3$ (Table 4.2).

Photolysis of $FpSiMe_3$ in the Presence of N_2.

Irradiation of $FpSiMe_3$ in an N_2 matrix results in the slow formation of the dinitrogen complex, $CpFe(CO)(N_2)SiMe_3$. Since this product is a coordinatively saturated species, it is of interest whether it can be observed in solution at room temperature.

Figure 4.17(a) shows the IR spectra obtained before and after 10 min > 300 nm irradiation of a solution of $FpSiMe_3$ in n-heptane, under a pressure of 1 atm of N_2. Since the bands observed due to photoproducts are relatively weak, these spectra are shown with an expanded ordinate scale, with the ν(CO) bands of the starting material off scale. Small amounts of the dimeric species, Fp_2, are produced by photolysis (as observed on irradiation of $FpSiMe_3$ under an argon atmosphere). However, two other new IR absorptions, shaded black in Figure 4.17(a), are observed after photolysis. These bands, which are not observed in the absence of N_2, occur at 1953 (a shoulder) and 2139.4 cm-1. These frequencies correspond well with the ν(CO) and ν(NN) absorptions of $CpFe(CO)(N_2)SiMe_3$ observed in a low temperature matrix (Table 4.1) and can reasonably be assigned to the same species.

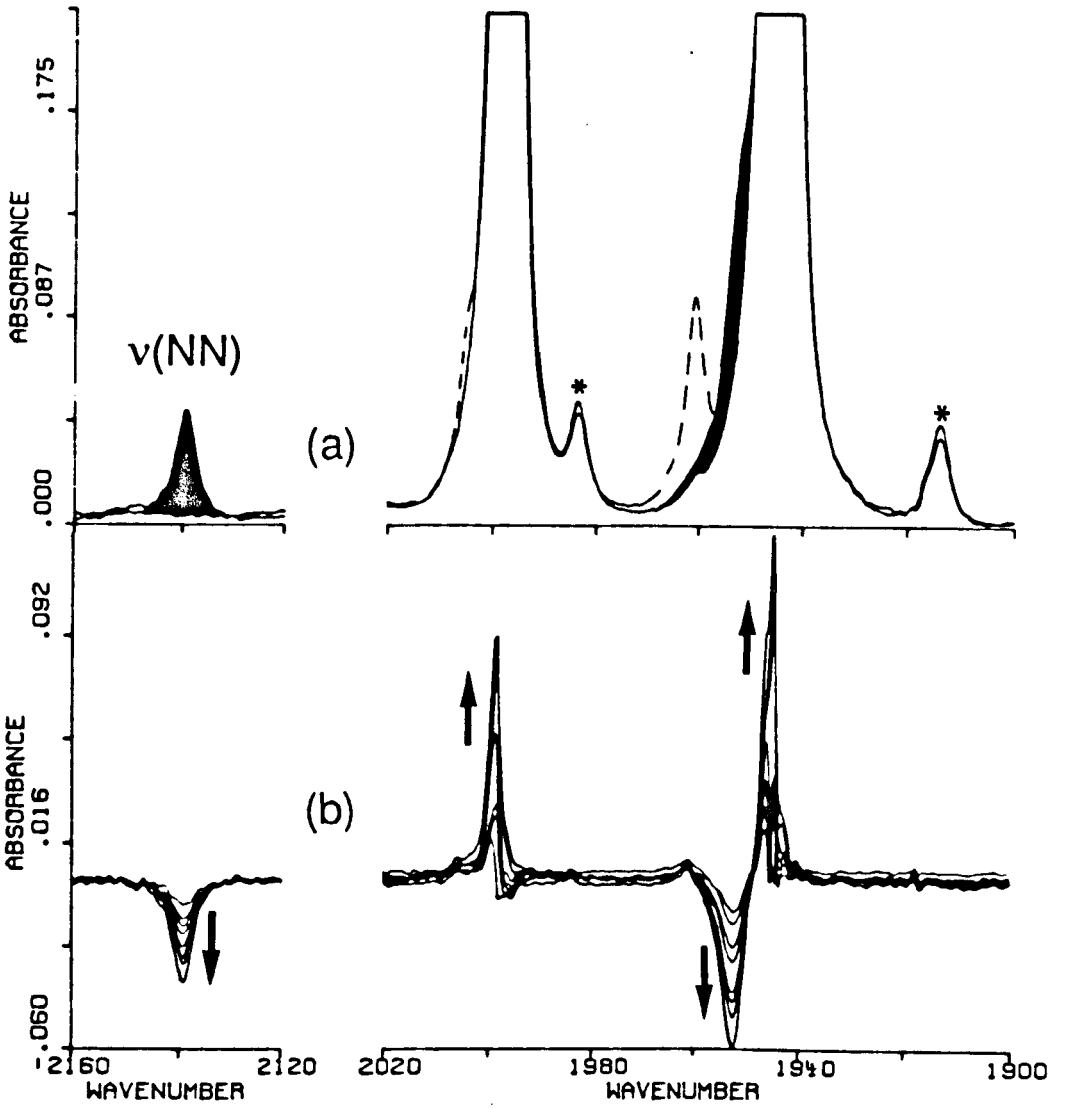
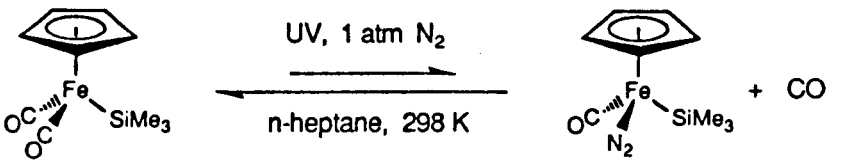


Figure 4.17: (a) Superimposed IR spectra obtained before and after 10 mins irradiation (>300 nm) of $FpSiMe_3$ (4.0×10^{-3} M) in n-heptane under an N_2 atmosphere. Bands due to Fp_2 are shown with broken lines. Absorptions coloured black are due to $CpFe(CO)(N_2)SiMe_3$. ^{13}CO satellites are marked with asterisks. (b) Difference spectra illustrating the thermal decay of $CpFe(CO)(N_2)SiMe_3$ and regeneration of $FpSiMe_3$, corresponding to times of 2, 5, 9, 15, 27, 38, 51 and 75 mins after switching off the UV lamp. Arrows indicate the behaviour of individual bands.

After photolysis, the solution was kept in the dark under 1 atm of N_2 , and periodically monitored using IR spectroscopy. Figure 4.17(b) shows a series of difference spectra recorded over a period of 75min under these conditions. The spectrum recorded immediately after completion of photolysis has been subtracted from each of the subsequent spectra, to reveal the progress of any thermal reactions. It can be seen that the ν(CO) and ν(NN) absorptions of $CpFe(CO)(N_2)SiMe_3$ decrease in intensity with time and that the two ν(CO) bands of the staring material are regenerated. After 75 mins, the absorptions of the dinitrogen complex had completely decayed. This chemistry is summarised in Equation 4.16.



4.16

These results show that, although $CpFe(CO)(N_2)SiMe_3$ can be generated photochemically in room temperature solution, this species is unstable with respect to the dicarbonyl, $FpSiMe_3$, even with an overpressure of N_2. The dinitrogen complex has a half life of ca. 20 mins under these conditions. The following section describes how liquid xenon solutions provide an ideal environment for a study of the photoreactivity of Fp-silyl complexes towards N_2.

4.6 THE PHOTOCHEMISTRY OF $FpSiMe_3$ AND $FpSiMe_2SiMe_3$ IN LOW TEMPERATURE LIQUID XENON SOLUTION

In order compare the photochemistry of $FpSiMe_3$ and $FpSiMe_2SiMe_3$ in the presence of N_2 more easily, it is necessary to carry out these reactions in an environment in which the N_2 complex is stabilised, thus enabling higher yields of this species to be produced. Liquid xenon provides an ideal medium in which to study this particular system for two reasons:

1) It is a low temperature solvent (ca. 160 - 230 K). Therefore, the lifetime of a coordinatively saturated species, which happens to be unstable at room temperature, can be greatly extended.

2) The cell used for these experiments enables a high overpressure of gas to be introduced above the solution. This means that large concentrations of dopants can be dissolved in solution. A pressure of N_2 helps to stabilise complexes containing coordinated dinitrogen ligand(s).

Other principal features of this technique are outlined in Chapter 1 and a brief description of the experimental set up is given in Chapter 6. Experiments on the Fp-silyl complexes in liquid xenon were carried out in collaboration with Mr. M. T. Haward.

Photolysis of $FpSiMe_3$ in Liquid Xenon

The Fp-silyl complexes under study dissolve readily in liquid xenon and it proved quite difficult to control the amount of iron complex in solution. Consequently, the ν(CO) absorptions of the starting material were often very intense, extending off scale at the start of an experiment. When this was the case, the amount of Fp-silyl complex in solution was monitored by observing the isotopic satellites due to natural abundance $CpFe(^{12}CO)(^{13}CO)$-silyl isotopomers.

Near UV irradiation (> 325 nm) of $FpSiMe_3$ in liquid xenon at -100°C results in no net photoreaction. This is in complete agreement with the observations made in room temperature solutions and low temperature matrices which imply rapid recombination of $CpFe(CO)SiMe_3$ with photoejected CO.

Figure 4.18(a) shows the IR spectra recorded before and after 30 mins irradiation of the same solution with a pressure of 150 psi of N_2 added to the cell. Photolysis leads to the growth of two new absorptions at 2139.5 and 1953.8 cm^{-1}, shaded black in Figure 4.18(a). These bands retain the same relative intensities and correspond well with the ν(CO) and ν(NN) modes of $CpFe(CO)(N_2)SiMe_3$, in an N_2 matrix or room temperature solution (Tables 4.1, 4.2). A much higher yield of the N_2 complex can be generated in

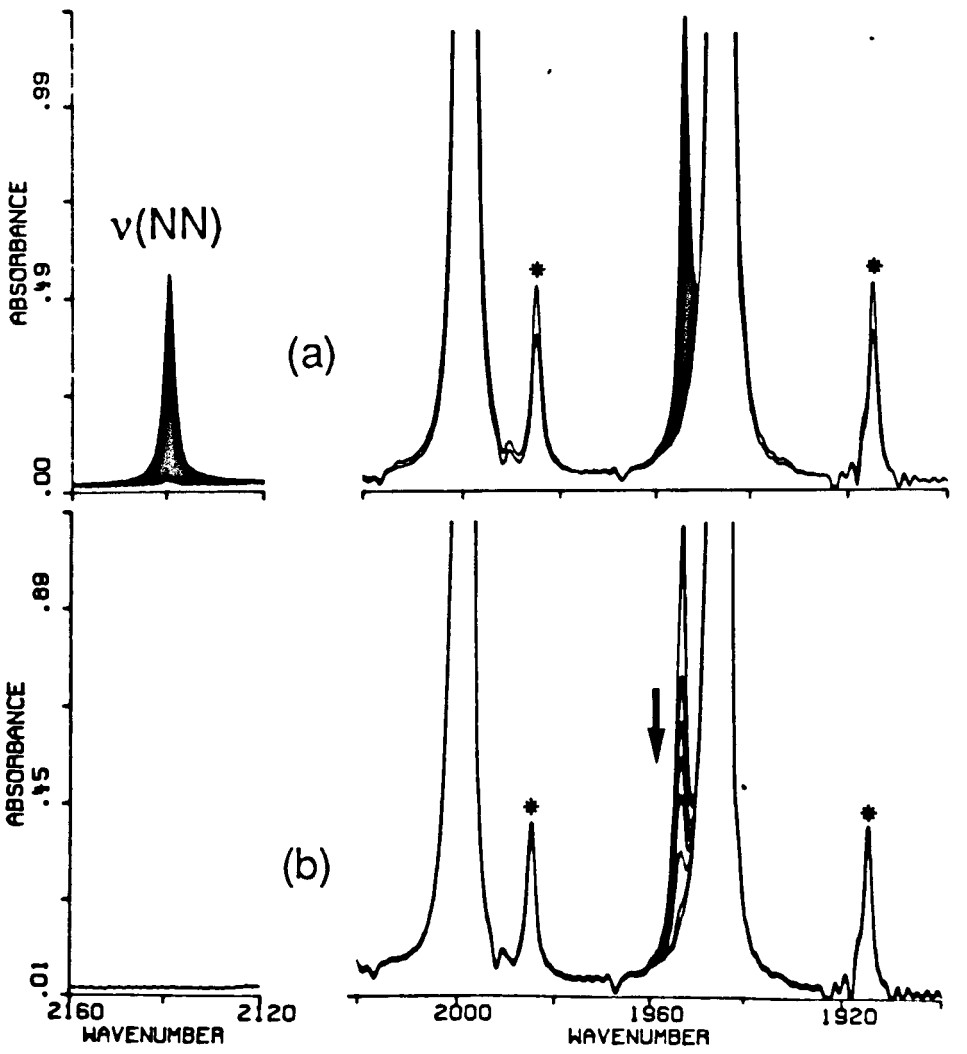
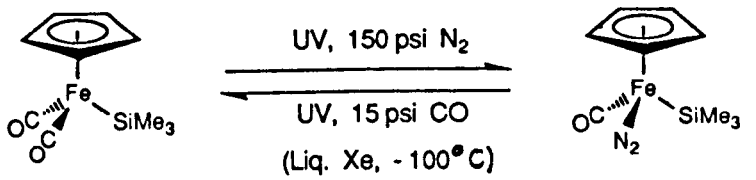


Figure 4.18: (a) Superimposed IR spectra obtained before and after 30 mins irradiation (>325 nm) of $FpSiMe_3$ in liquid Xe at -100°C with a pressure of 150 psi N_2 in the cell. New absorptions due to $CpFe(CO)(N_2)SiMe_3$ are coloured black. ^{13}CO satellites are marked with asterisks. (b) IR spectra after 0, 15, 45, 65, 85, 115, 175, 355 and 655 s subsequent >325 nm irradiation with a pressure of 15 psi CO in the cell, illustrating the decay of the ν(CO) band of $CpFe(CO)(N_2)SiMe_3$. The ν(NN) region is shown after removal of CO.

liquid xenon under these conditions than in matrices or room temperature solution. When the UV lamp is turned off, no decay of the IR absorptions of $CpFe(CO)(N_2)SiMe_3$ is observed, even when the cell is pressurised with CO.

Irradiation of the solution containing $CpFe(CO)(N_2)SiMe_3$ with an overpressure of 15 psi of CO results in depletion of the ν(CO) absorption of the N_2 complex (Figure 4.18(b)). The ν(NN) band could not be monitored during this reaction due to the strong absorption of dissolved carbon monoxide. However, the IR spectrum obtained after removal of CO reveals that the ν(NN) band of $CpFe(CO)(N_2)SiMe_3$ has also been destroyed by photolysis. The photochemistry observed in this experiment is shown in Equation 4.17.



4.17

Photolysis of $FpSiMe_2SiMe_3$ in Liquid Xenon

In contrast to the results obtained for $FpSiMe_3$, irradiation of $FpSiMe_2SiMe_3$ in undoped liquid xenon solution results in a net photochemical reaction. Figure 4.19(a) shows that photolysis (> 325 nm) leads to loss of starting material and the appearance of two photoproduct ν(CO) absorptions. The weak band at 1921.9 cm^{-1} is close to the absorption of the primary CO loss product, $CpFe(CO)SiMe_2SiMe_3$, observed in low temperature matrices and flash photolysis experiments.

The other new ν(CO) absorption appears initially as a shoulder on the low frequency parent band, but after prolonged photolysis, it is resolved as a separate peak at 1944.9 cm^{-1}. Allowing for a solvent frequency shift, this band is assigned to the same stable, secondary product, X, observed in hydrocarbon solvents at room temperature.

A slightly puzzling aspect of this experiment was that when the UV lamp was turned off, no decay of the weak band at 1921.9 cm^{-1} was observed. At room temperature $CpFe(CO)SiMe_2SiMe_3$ decays via an intramolecular process after flash photolysis of $FpSiMe_2SiMe_3$, to yield X. Although both of these species are produced in liquid xenon, the conversion of $CpFe(CO)SiMe_2SiMe_3$ to X is not directly observed.

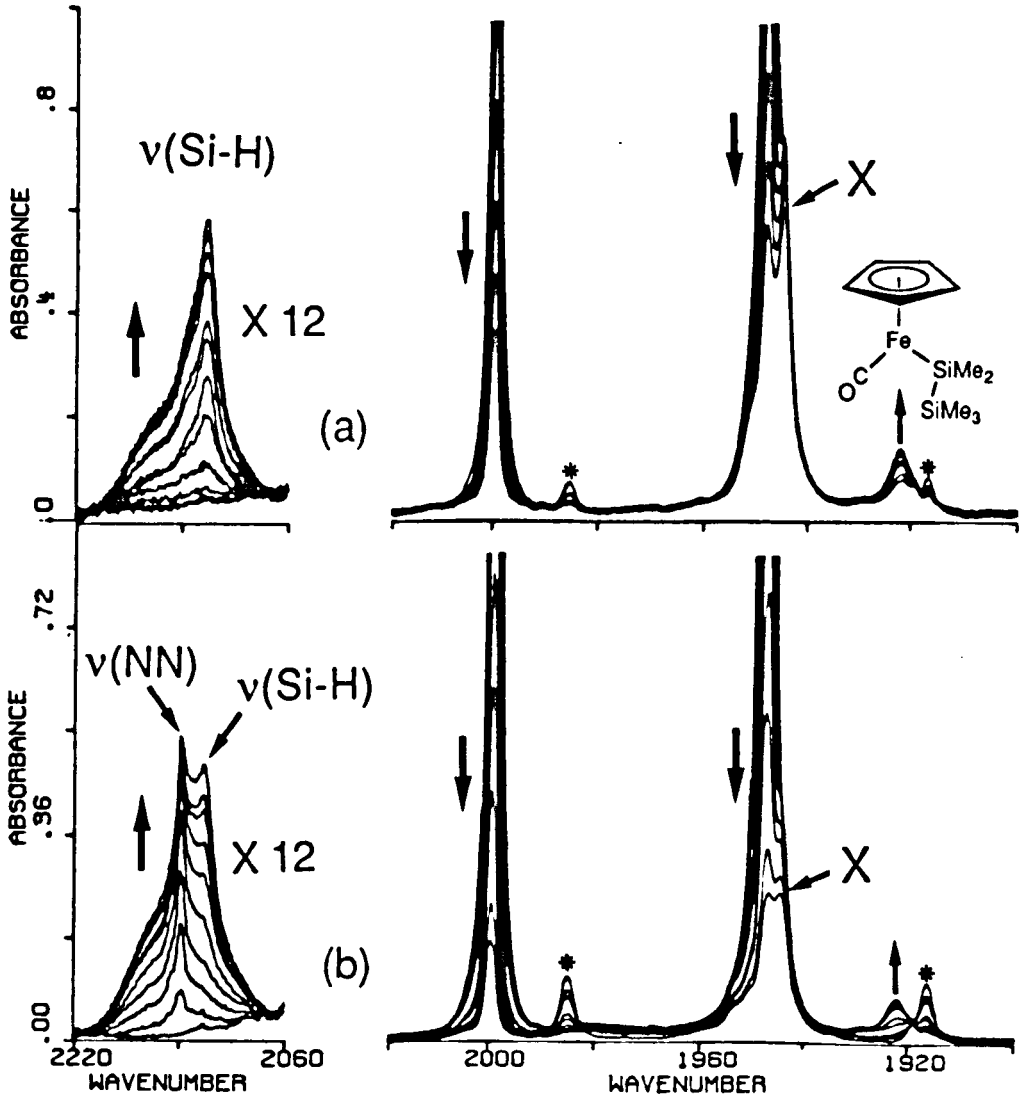


Figure 4.19: (a) IR spectra recorded during 7 mins photolysis (>325 nm) of $FpSiMe_2SiMe_3$ in liquid Xe at -100 °C. Note the production of bands due to $CpFe(CO)SiMe_2SiMe_3$, X and a ν(Si-H) absorption. (b) IR spectra recorded during 13 mins photolysis (>325 nm) of $FpSiMe_2SiMe_3$ in liquid Xe at -100 °C with a cell pressure of 150 psi N_2. Note the production of a weak ν(NN) band due to $CpFe(CO)(N_2)SiMe_3$ in addition to the photoproduct absorptions in (a). Arrows indicate the behaviour of individual absorptions during photolysis. The ν(Si-H) region is shown with an expanded absorbance scale.

The growth of a broad, weak absorption at 2121 cm^{-1} is also apparent in Figure 4.19(a). This resembles the band observed on irradiation of $FpSiMe_2SiMe_3$ in n-heptane solution at room temperature. This absorption is tentatively assigned as an Si-H stretching mode of an organosilicon species formed on deoligomerisation.

When the photolysis of $FpSiMe_2SiMe_3$ in liquid xenon had been completed, the xenon was boiled off, and the solution cell left in vacuo at room temperature for a prolonged period (ca. 14 days). When the cell was refilled with xenon, the IR spectrum of the resulting solution showed that a large amount of the photoproduct X was still present, and had redissolved in the xenon. This confirms the thermal stability of X.

In a separate experiment, a solution of $FpSiMe_2SiMe_3$ in liquid xenon was irradiated under a pressure of 150 psi N_2. The IR spectra obtained during photolysis are shown in Figure 4.19(b). Loss of starting material is accompanied by generation of the ν(CO) bands associated with $CpFe(CO)SiMe_2SiMe_3$ and X, as observed in the absence of N_2. The broad ν(Si-H) band at 2121 cm^{-1} is also produced, along with a narrower feature at 2139.5 cm^{-1}, not observed in the absence of N_2 (Figure 4.19(a)). This coincides with the ν(NN) band of $CpFe(CO)(N_2)SiMe_3$ in liquid xenon. The ν(CO) absorption of the N_2 complex is too weak to

be resolved from the low frequency parent ν(CO) band. Production of the dinitrogen complex occurs at a much slower rate than during the photolysis of $FpSiMe_3$ under identical conditions.

The photoreactivity of $FpSiMe_2SiMe_3$ and $FpSiMe_3$ towards N_2 in liquid xenon solution is very similar to that observed in n-heptane at room temperature with added ligands such as PPh_3 or C_2H_4. For the monosilyl complex, the substitution of a CO group by N_2, occurs in a clean photochemical reaction. For the disilyl complex, the major iron containing photoproducts are $CpFe(CO)SiMe_2SiMe_3$ and X. The production of small amounts of $CpFe(CO)(N_2)SiMe_3$ indicates that N_2 only co-ordinates to the metal complex after deoligomerisation of the silyl ligand has occurred.

TABLE 4.2: IR frequencies of species observed in solution in n-heptane and liquid xenon. (Error +/- 0.2 cm^{-1})

Complex	**n-heptane**	**Liq. Xe**
$FpSi_2Me_5$	1946.3	1947.7
	1997.6	1999.3
$FpSiMe_3$	1945.3	1946.1
	1998.5	1999.5
$CpFe(CO)SiMe_2SiMe_3$	1924[a]	1921.9
$CpFe(CO)SiMe_3$	1928[a]	-
X	1943	1944.9
$CpFe(CO)(PPh_3)SiMe_3$	1912.2	-
$CpFe(CO)(N_2)SiMe_3$	1952.6	1953.8
	2139.4	2139.5
$CpFe(CO)(n^2\text{-}C_2H_4)SiMe_3$	1945.6	-
$FpCH_2CH_2SiMe_3$	1952.7	-
	2006.9	-

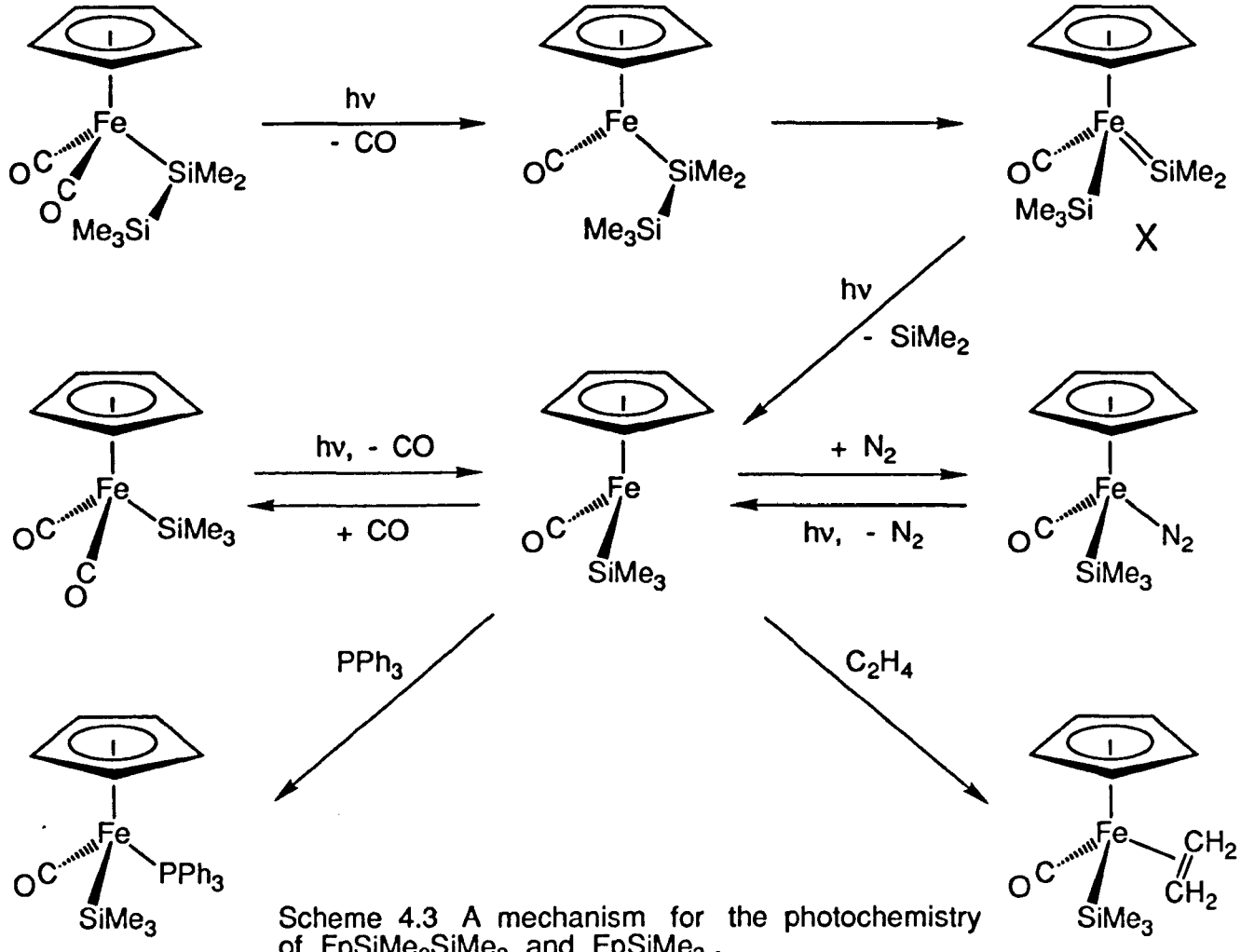
a Measured using fast TRIR spectroscopy.

4.7 DISCUSSION

A mechanism which explains the photochemistry observed for $FpSiMe_3$ and $FpSiMe_2SiMe_3$ is shown in Scheme 4.3. For each complex, absorption of a photon of UV light leads to ejection of a CO group. The monocarbonyl product formed from $FpSiMe_3$ reacts rapidly with CO to give back starting material, or with other ligands to give substituted products.

By contrast, $CpFe(CO)SiMe_2SiMe_3$ is unreactive towards potential ligands, and undergoes an intramolecular reaction to give X. It is proposed that X is a silyl(silylene) iron complex resulting from intramolecular oxidative addition of the Si-Si bond to the unsaturated iron atom. A secondary photochemical reaction leads to expulsion of an $SiMe_2$ fragment from X. The resulting 16 electron monosilyl complex can combine with a variety of ligands to give coordinatively saturated products.

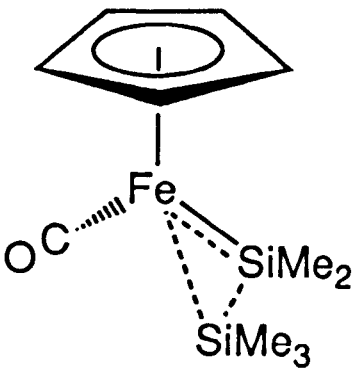
In this Discussion, the details of the reactions shown in Scheme 4.3 will be considered.



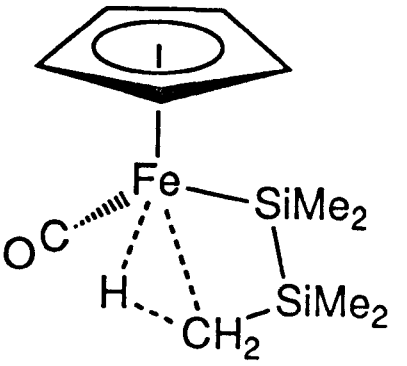
Scheme 4.3 A mechanism for the photochemistry of $FpSiMe_2SiMe_3$ and $FpSiMe_3$.

The Primary Photochemistry of $FpSiMe_2SiMe_3$

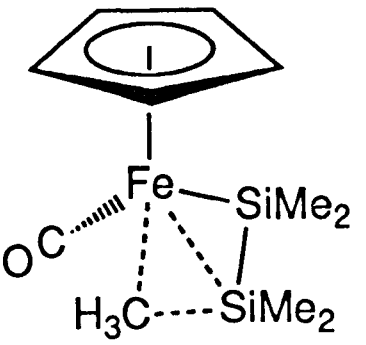
From the results described in this Chapter, it appears that the vacant coordination site caused by photodissociation of CO from $FpSiMe_2SiMe_3$ is blocked by an interaction with the disilyl ligand. Much recent research has been devoted to the study of three centre electronic interactions in organometallic complexes (Crabtree 1988). In these systems, H-H, C-H and related sigma-bonded groups are considered to act as ligands. Three possible interactions of this type for $CpFe(CO)SiMe_2SiMe_3$ are illustrated below:



1) Fe-Si-Si



2) Fe-C-H

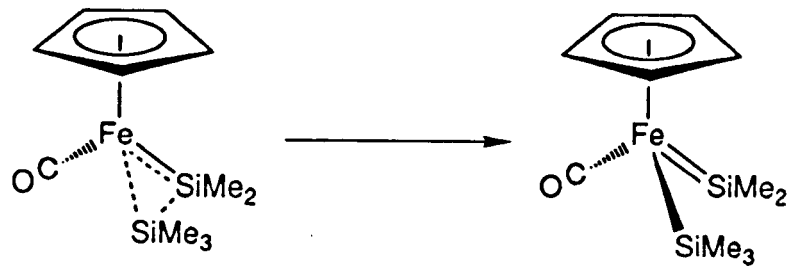


3) Fe-Si-C

No interactions involving an α-Si-CH_3 unit are considered, since the CO-loss photoproduct generated from $FpSiMe_3$ is not stabilised in a similar way.

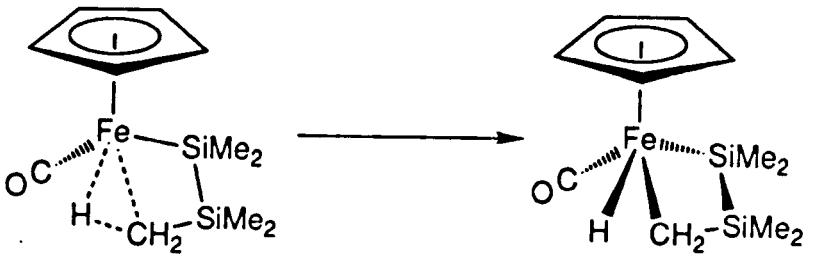
The primary photoproduct, $CpFe(CO)SiMe_2SiMe_3$ undergoes an intramolecular reaction in solution to give a thermally stable species, X. The shift of ν(CO) to higher frequency in X is consistent with an oxidative addition reaction. Each type of interaction depicted above can be regarded as an intermediate in an intramolecular oxidative addition reaction of the disilyl ligand. Three such reactions are illustrated below. Oxidative additions involving the Si-C or C-H bonds of methyl groups on the α-silicon atom are not considered, since the equivalent process is not observed for $FpSiMe_3$. (However, a recent report of H/D exchange in $(PMe_3)_4Os(H)SiMe_2R$ (R = Me, Et), suggests that intramolecular C-H oxidative addition is possible for a M-Si-C-H linkage (Berry 1989)).

a) Oxidative addition of the Si-Si bond.



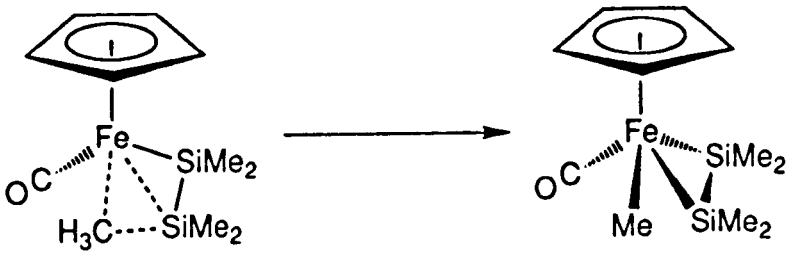
4.18

b) Oxidative addition of a C-H bond.



4.19

c) Oxidative addition of a Si-C bond.

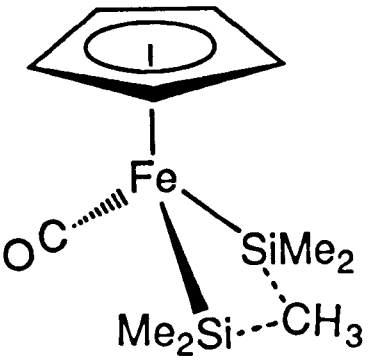


4.20

Reactions of the types shown in Equations 4.19 and 4.20 involving Si-C cleavage or γ-H transfer are not generally observed. By contrast, the reactivity of Si-Si bonds towards transition metal complexes is well known (Aylett 1982). The product of the reaction shown in Equation 4.18, has already been proposed as an intermediate in the photoinduced deoligomerisation of $FpSiMe_2SiMe_3$ (Pannell 1986, 1989, Tobita 1988). Further evidence for this process is provided by the nature of the photoproduct generated from $FpSiMe_2SiMe(OMe)_2$ (Ueno 1988). In this case, a product of Si-Si oxidative addition has been isolated and characterised by X-ray crystallography (see section 4.1).

The observed thermal stability of X can also explain the mixtures of monosilyl products observed on irradiation of $FpSiMe_2Ph_3$ and $FpSiMe_2SiMeEt_2$ (Equations 4.2, 4.3). There would clearly be sufficient time for intramolecular scrambling of alkyl and aryl groups in the proposed silyl(silylene) intermediates. Similar [1,3] sigmatropic shifts are known to be rapid on the NMR timescale in silaolefins (Equation 4.4) (Wiberg 1985).

An alternative structure resulting from oxidative addition of the Si-Si bond might possess a methyl group bridging the two Si atoms as shown below.



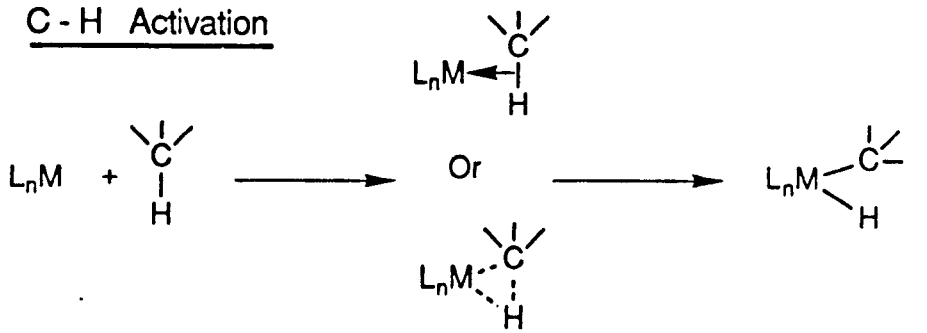
This molecule has a three centre, two electron bond between the two Si atoms and the bridging methyl group, reminiscent of the bonding in electron deficient molecules such as Al_2Me_6. Such a complex may be fluxional, with exchange of terminal and bridging alkyl groups. Further studies using ^{1}H, ^{13}C and ^{29}Si NMR spectroscopy may enable the detailed structure of X to be determined.

The Oxidative Addition of Covalent Bonds

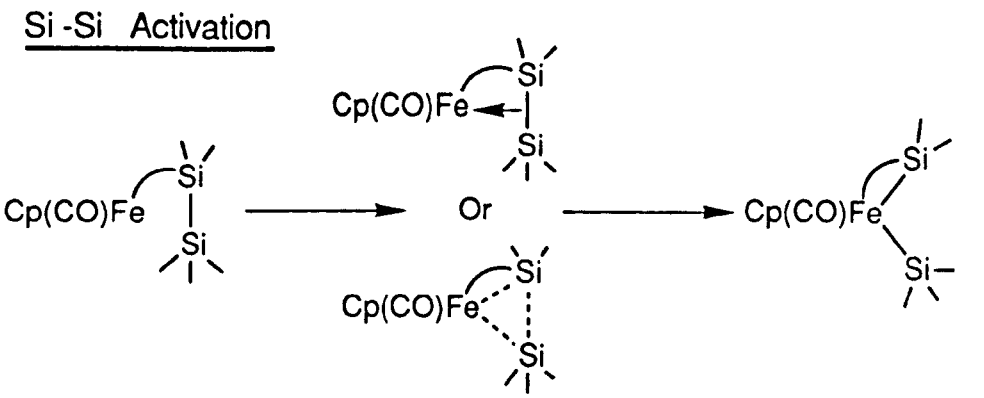
A close analogy can be drawn between Si-Si bond activation and C-H or H-H bond activation, both of which have recently attracted considerable interest amongst organometallic chemists (Crabtree 1988). One avenue of research has involved the identification of agostic three centre interactions between ligand C-H bonds and transition metal atoms (Brookhart 1983). Closely related are molecular dihydrogen complexes, containing η^2-H_2 ligands (Kubas 1988). Both of these examples can be considered as examples of arrested

oxidative addition, in which cleavage of the C-H or H-H σ-bond is incomplete. Molecular orbital calculations indicate that oxidative addition of an R-H bond (R = H or alkyl) to an unsaturated metal atom occurs in two steps as shown in Equation 4.21 (Rabaa 1987).

The intermediate species in this reaction contains a three centre interaction between the metal atom and the R-H bond in which oxidative addition is incomplete. A potential energy barrier is predicted to exist between this species and the final product, where complete oxidative addition of the R-H bond has occurred, as depicted in Figure 4.20. If this potential barrier is sufficiently large, the intermediate species may be stabilised.



4.21



4.22

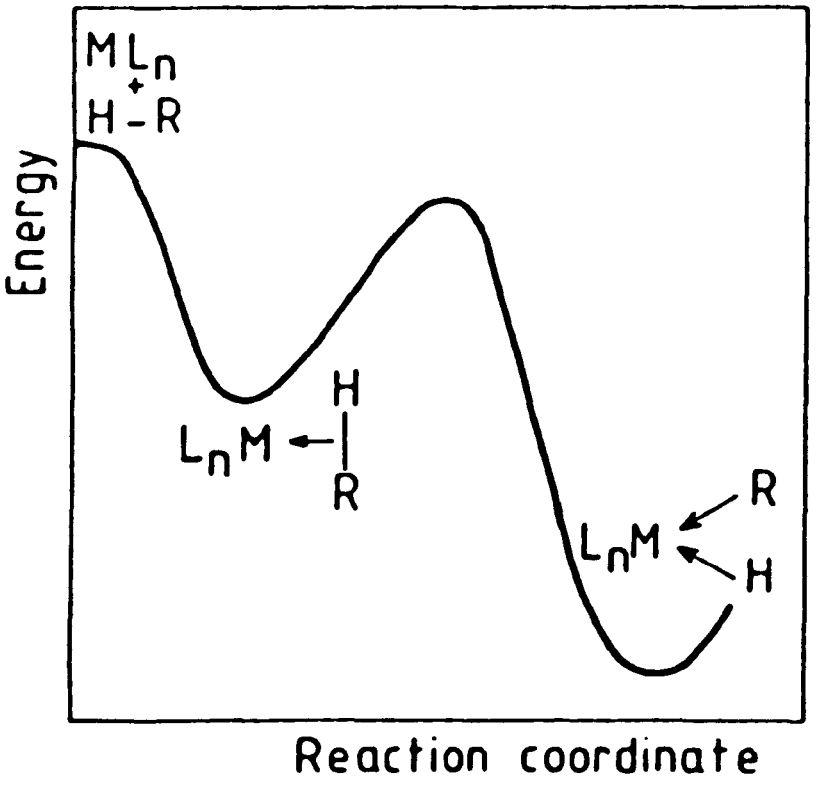
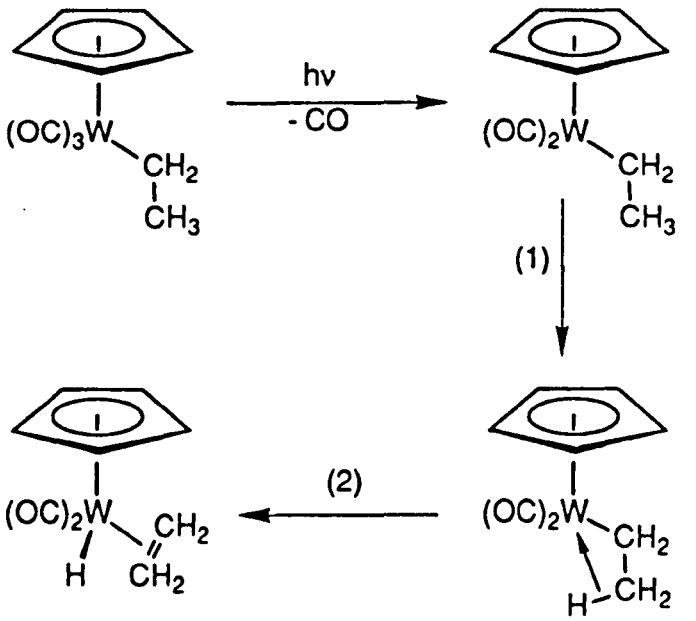


Figure 4.20: Schematic energy profile for the oxidative addition of R-H with a 16-e^- complex, ML_n. The height of the energy barrier and the depth of the minimum are arbitrary (they depend on the system considered). (Adapted from Rabaa (1987))

A similar two step process can be envisaged in the intramolecular oxidative addition of the Si-Si bond in unsaturated molecules such as $CpFe(CO)SiMe_2SiMe_3$ (Equation 4.22).

Matrix isolation and flash photolysis have previously given evidence for a two step mechanism in the oxidative addition of a C-H bond in an unsaturated tungsten species. In the reaction illustrated below, primary photodissociation of CO from $CpW(CO)_3CH_2CH_3$ leads to the 16 electron intermediate, $CpW(CO)_2CH_2CH_3$.



On the basis of UV/visible spectra of $CpW(CO)_2CH_2CH_3$ in alkane matrices at 77 K, it was suggested that the completely unsaturated molecule can isomerise (1) to give a complex with a β-agostic C-H interaction (Kazlauskas 1982b). There is no evidence for similar isomerism in $CpW(CO)_2CH_3$, which contains no β-hydrogens. On warming the alkane matrix to 195 K, $CpW(CO)_2CH_2CH_3$ undergoes thermal β-H transfer (2), yielding $CpW(CO)_2(\eta^2\text{-}C_2H_4)(H)$. Evidence for reactions (1) and (2), was also obtained in flash photolysis experiments in room temperature solution, monitored with UV/visible detection on picosecond and microsecond timescales (Yang 1986).

The photochemistry observed here for $FpSiMe_2SiMe_3$ provides evidence for the two step oxidative addition of an Si-Si bond to a 16 electron iron centre. The intermediate species, $CpFe(CO)SiMe_2SiMe_3$, containing a blocked coordination site has been observed in low temperature matrices and room temperature flash photolysis studies. In matrices the second step of the reaction does not occur. Presumably, at such low temperature, the potential energy barrier for this process is insurmountable. However, in room temperature solution, the reaction proceeds to give complete oxidative addition.

The Reactivity of Si-Si Bonds Towards Unsaturated Transition Metal Complexes

The electron donor properties of Si-Si bonds have been investigated by Traven (1973) and Sakurai (1973). It was found that the Si-Si bonds of permethyl-polysilanes can form charge transfer complexes with π-acceptors such as tetracyanoethylene (TCNE). In these complexes electron density is donated from an Si-Si σ-bond to the acceptor molecule. The donor character of Si-Si bonds may be related to the ability of a disilyl ligand to interact with an unsaturated metal centre.

Several reactions have been reported where Si-Si activation by transition metal complexes can be invoked to explain experimental observations. The photochemical deoligomerisation of the straight chain trisilyl iron complex, $FpSi_3Me_7$ (Pannell 1986) is clearly related to the current study (Equation 4.23).

$$FpSi_3Me_7 \xrightarrow{h\nu} FpSiMe_3 \qquad 4.23$$

In this case their are two Si-Si bonds in the silyl ligand of the starting material. It is not clear whether activation of the α or β Si-Si bond occurs initially.

When the straight chain silyl group attached to an Fp fragment is extended to four or more silicon atoms, photolysis does leads not to deoligomerisation, but rearrangement, giving a branched chain silyl ligand (Equations 4.24 and 4.25).

$$FpSi_4Me_9 \xrightarrow{h\nu} FpSi(SiMe_3)_3 \qquad 4.24$$

$$FpSi_6Me_{13} \xrightarrow{h\nu} FpSi(SiMe_3)_2Si_3Me_7 \qquad 4.25$$

The mechanisms of these reactions must involve both breaking and making of Si-Si bonds, probably mediated by an unsaturated Fe centre, formed by photodissociation of CO.

The photochemistry of the silylmethyl complexes, $FpCH_2SiMe_3$ and $FpCH_2SiMe_2SiMe_3$, is also particularly relevant to the current study, providing another example where the Si-Si bond in a ligand is cleaved (Pannell 1974). Irradiation of $FpCH_2SiMe_2SiMe_3$ results in a skeletal rearrangement of the disilylmethyl ligand (Equation 4.26).

$$FpCH_2SiMe_2SiMe_3 \xrightarrow{h\nu} FpSiMe_2CH_2SiMe_3 \qquad 4.26$$

Photolysis of the same complex in the presence of triphenylphosphine results in the production of a

phosphine substitution product in which the same skeletal rearrangement of the disilylmethyl ligand has already occurred (Equation 4.27).

$$FpCH_2SiMe_2SiMe_3 \xrightarrow[PPh_3]{h\nu} CpFe(CO)(PPh_3)SiMe_2CH_2SiMe_3 \qquad 4.27$$

It was found that substitution cannot occur without ligand rearrangement taking place.

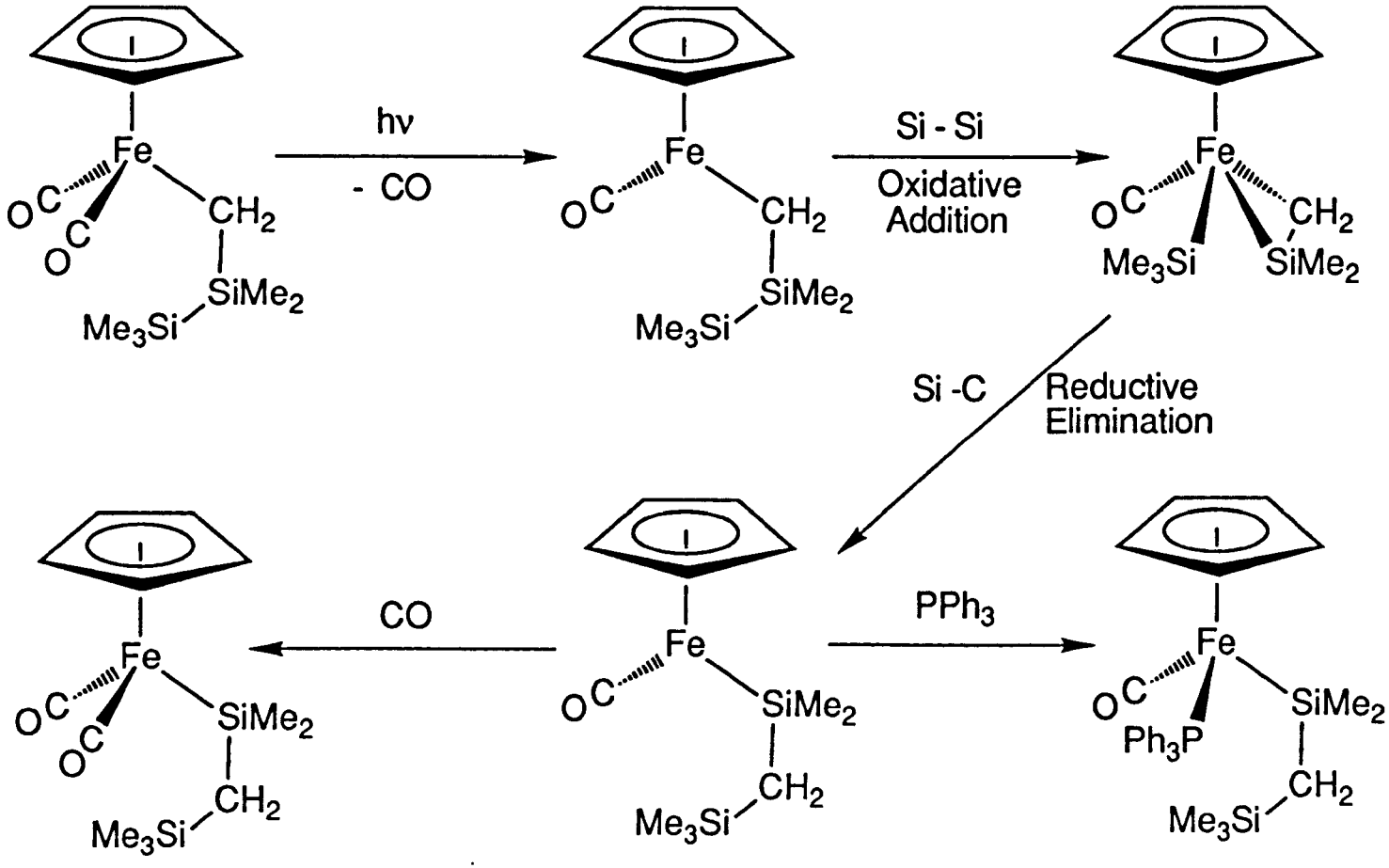
Photochemical treatment of the corresponding monosilylmethyl complex, $FpCH_2SiMe_3$, causes no ligand rearrangement, and in the presence of phosphines, straightforward substitution products are obtained (Equation 4.28).

$$FpCH_2SiMe_3 \xrightarrow[PR_3]{h\nu} CpFe(CO)(PR_3)CH_2SiMe_3 \qquad 4.28$$

(PR_3 = PPh_3, PPh_2Et or PPh_2Me)

A mechanism proposed by Pannell for the rearrangement of the disilylmethyl complex is not explicit as to the nature of the intermediates involved. In view of the results described in this Chapter, a likely mechanism is proposed in Scheme 4.4.

The primary photochemical step of this mechanism involves dissociative loss of CO to give the



Scheme 4.4: Possible mechanism for the photochemical rearrangement of the disilylmethyl ligand in $FpCH_2SiMe_2SiMe_3$, observed by Pannell (1974).

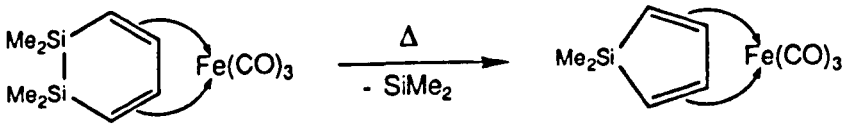
coordinatively unsaturated complex, $CpFe(CO)CH_2SiMe_2SiMe_3$. Subsequent migration of the β-$SiMe_3$ group from Si to Fe gives rise to a metallasilacyclopropane structure. The $SiMe_3$ group then undergoes a second migration, from Fe to C. The mechanism is completed by recombination with CO or coordination of PPh_3. The two successive migrations of the $SiMe_3$ group can be thought of as oxidative addition of an Si-Si bond, followed by reductive elimination of an Si-C bond. The importance of the presence of an Si-Si bond in the starting material is illustrated by the fact that no rearrangement is observed for $FpCH_2SiMe_3$, which contains only a single Si atom.

These observations resemble the differences in the photochemistry of $FpSiMe_2SiMe_3$ and $FpSiMe_3$, described in this Chapter. The only difference is that a methylene group is interposed between the silyl group and the iron atom. Thus, oxidative addition of the Si-Si bond involves β-, rather than α-migration of an $SiMe_3$ group, resulting in a metallasilacyclo- propane structure instead of a silylene complex.

The difference in structure of the proposed intermediates can explain why isomerisation occurs for $FpCH_2SiMe_2SiMe_3$, whereas net loss of an $SiMe_2$ unit occurs for $FpSiMe_2SiMe_3$. Intramolecular reductive elimination of a relatively strong Si-C bond can occur for $CpFe(CO)(CH_2SiMe_2)SiMe_3$, but no such route is

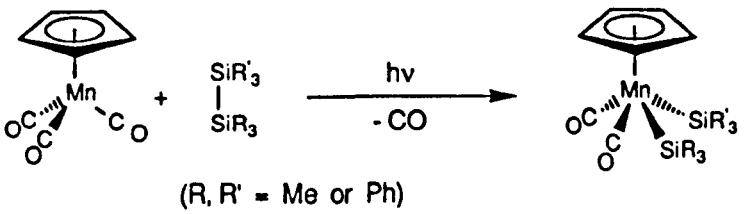
available for $CpFe(CO)(=SiMe_2)SiMe_3$ (X).

There are many other examples of Si-Si bond activation by transition metal compounds (Aylett 1982 and references therein). For example, thermolysis of a (η^2-1,2-disilacyclohexadiene)$Fe(CO)_3$ complex results in a novel ring contraction involving expulsion of an $SiMe_2$ unit (Equation 4.29) (Nakadaira 1979).



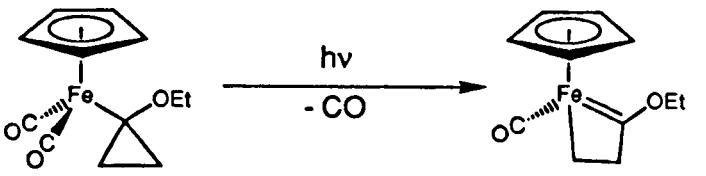
4.29

The 16 electron manganese fragment $CpMn(CO)_2$ is implicated in intermolecular activation of the Si-Si bonds of organodisilanes (Equation 4.30) (Schubert 1979)

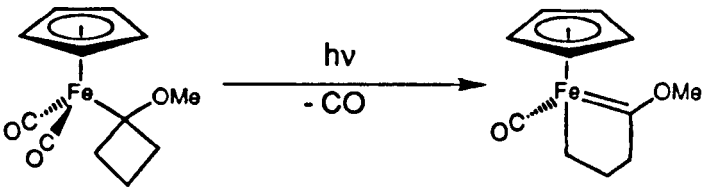


4.30

The photochemistry of FpR systems in which R contains a cycloalkyl unit is also relevant. Photodissociation of CO is followed by α-migration of an alkyl group, leading to ring expansion (Equations 4.31, 4.32).



4.31



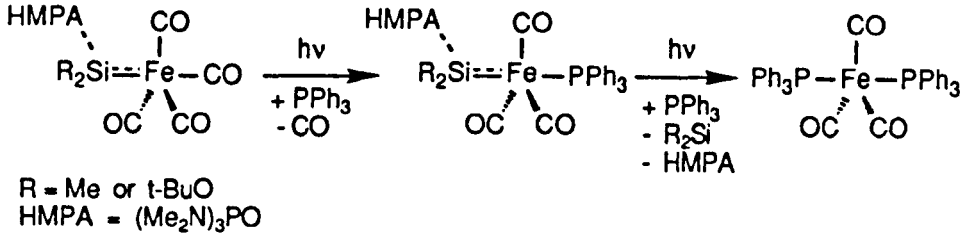
4.32

The products of these reactions contain Fe-C single and double bonds, resembling the silyl(silylene) iron structure proposed for X. Release of ring strain and product stabilisation by an alkoxy group are thought to promote C-C bond cleavage in these examples (Stenstrom 1986, Conti 1988).

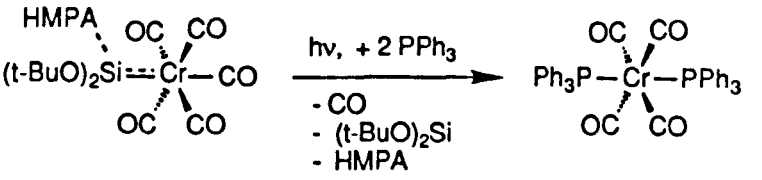
The Fate of the $SiMe_2$ Fragment

Irradiation of X in the presence of potential two electron donor ligands yields the substituted complexes, $CpFe(CO)(L)SiMe_3$ (L = CO, N_2, PPh_3 or C_2H_4). A likely intermediate in these reactions is the 16 electron species, $CpFe(CO)SiMe_3$, which is known to react rapidly with a range of ligands when generated photochemically from $FpSiMe_3$. Production of this species from X requires expulsion of an $SiMe_2$ fragment as the second photochemical step in the deoligomerisation of $FpSiMe_2SiMe_3$.

In a study of the photochemistry of several base-stabilised transition metal silylene complexes, Zybill et al (1989) showed that irradiation can cause substitution of the SiR_2(Base) unit by a phosphine ligand (Equations 4.33 and 4.34). This provides a precedent for the photochemical loss of an SiR_2 fragment from a transition metal complex. In these reactions, polymerisation of the SiR_2 units leads to polysilanes of approximate molecular weight 550.



4.33



4.34

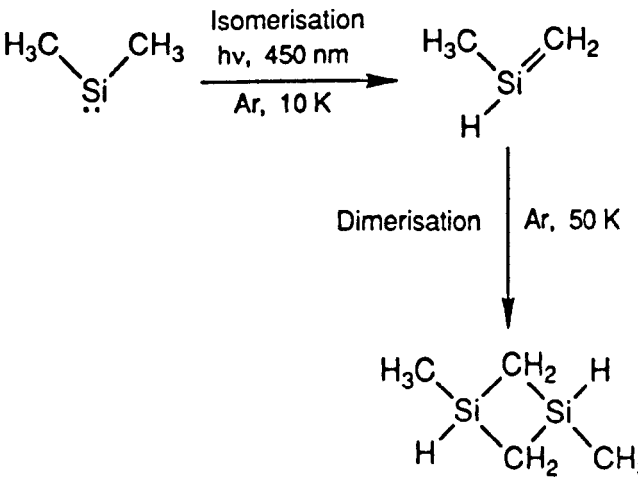
In previous studies on the $FpSiR_2SiR_3$ system, attempts to trap the $SiMe_2$ unit using silylene trapping reagents were unsuccessful (Pannell 1986, Tobita 1988). It was suggested that $SiMe_2$ might react with CO in solution. However, the net amount of CO liberated in this reaction is insufficient to react with all of the

expelled dimethylsilylene. Therefore it appears that an $SiMe_2$ moiety can be excluded from the iron complex without the production of free $SiMe_2$ in solution.

Dimethylsilylene can be generated photochemically in low temperature matrices from the cyclohexasilane, $(Me_2Si)_6$ (Equation 4.35) (Drahnak 1981).

$$(Me_2Si)_6 \xrightarrow[\text{Ar, 10 K}]{h\nu,\ 254\ nm} (Me_2Si)_5 + Me_2Si \qquad 4.35$$

On photolysis with visible light (450 nm), Me_2Si isomerises to give 1-methylsilene, $Me(H)Si{=}CH_2$. Subsequent warming of the matrix leads to dimerisation forming 1,3-dimethyl-1,3-disilacyclobutane (Equation 4.36).



4.36

The IR spectra reported included a matrix split

ν(SiH) mode at 2191 and 2198 cm^{-1} for 1-methylsilene, and bands at 2113, 2116 and 2134 cm^{-1} for 1,3-dimethyl-1,3-disilacyclobutane (which is probably formed as a mixture of cis and trans isomers. The ν(SiH) band of this cyclic dimer occurs at 2140 cm^{-1} at room temperature.

The secondary photochemical reaction of X is also accompanied by the production of an IR absorption in the Si-H stretching region. This provides strong circumstantial evidence that the $SiMe_2$ unit expelled from X can isomerise in solution under photochemical conditions. Isomerisation of $SiMe_2$ might even occur in the excited state, immediately after ejection from the iron complex. Isomerisation of dimethylsilylene under photochemical conditions provides a possible explanation for the inability to capture free Me_2Si with trapping reagents in previous studies on this system. The broad ν(SiH) band observed in these experiments absorbs at a frequency between the three bands assigned to 1,3-dimethyl-1,3-disilacyclobutane in an argon matrix (Drahnak 1981). It is possible that the same dimeric compound is generated in the reaction under study. However, no other evidence for the identity of this species was obtained.

4.8 CONCLUSIONS

The results presented in this Chapter confirm that the primary photochemical step in the deoligomerisation of $FpSiMe_2SiMe_3$ is dissociation of a CO ligand. Rapid recombination of the 16 electron fragment with CO is prevented by an interaction between the disilyl ligand and the vacant coordination site. At elevated temperatures the primary photoproduct undergoes an intramolecular reaction, rationalised as oxidative addition of the Si-Si bond to the unsaturated Fe atom. This results in formation of a silyl(silylene) iron complex, X, which is thermally stable in room temperature solution. A second photochemical step involves ejection of the dimethylsilylene fragment ($SiMe_2$) from X. It is thought that the $SiMe_2$ fragment gives rise to a product containing Si-H bond(s). Coordination of CO or another two electron donor ligand completes the reaction, giving a monosilyl iron complex, $CpFe(CO)(L)SiMe_3$ (L = CO, PPh_3, C_2H_4 or N_2).

CHAPTER 5

THE PHOTOCHEMISTRY OF DISILYL IRON COMPLEXES CONTAINING β-SILYL HYDROGENS

5.1 INTRODUCTION

The photochemistry of transition metal alkyl complexes containing β-hydrogens is well documented. For example, irradiation of $FpCH_2CH_3$ leads to elimination of ethylene, and production of FpH . The mechanism of this reaction has been unravelled using the low temperature matrix isolation technique (Kazlauskas 1982a, Mahmoud 1985). The primary photochemical step is CO-loss, giving a 16 electron metal centre. Subsequent β-H transfer from carbon to iron results in the rapid formation of the intermediate ethylene complex, $CpFe(CO)(\eta^2\text{-}C_2H_4)H$. Substitution of ethylene by CO gives the observed product (Equation 5.1).

$$FpCH_2CH_3 \xrightarrow[-CO]{h\nu} CpFe(CO)(\eta^2\text{-}C_2H_4)H \xrightarrow[-C_2H_4]{CO} FpH \qquad 5.1$$

Similar processes have been observed in other complexes containing β-C-H bonds ((Kazlauskas 1982b, Mahmoud 1984, Hooker 1984).

By contrast, there are relatively few examples of

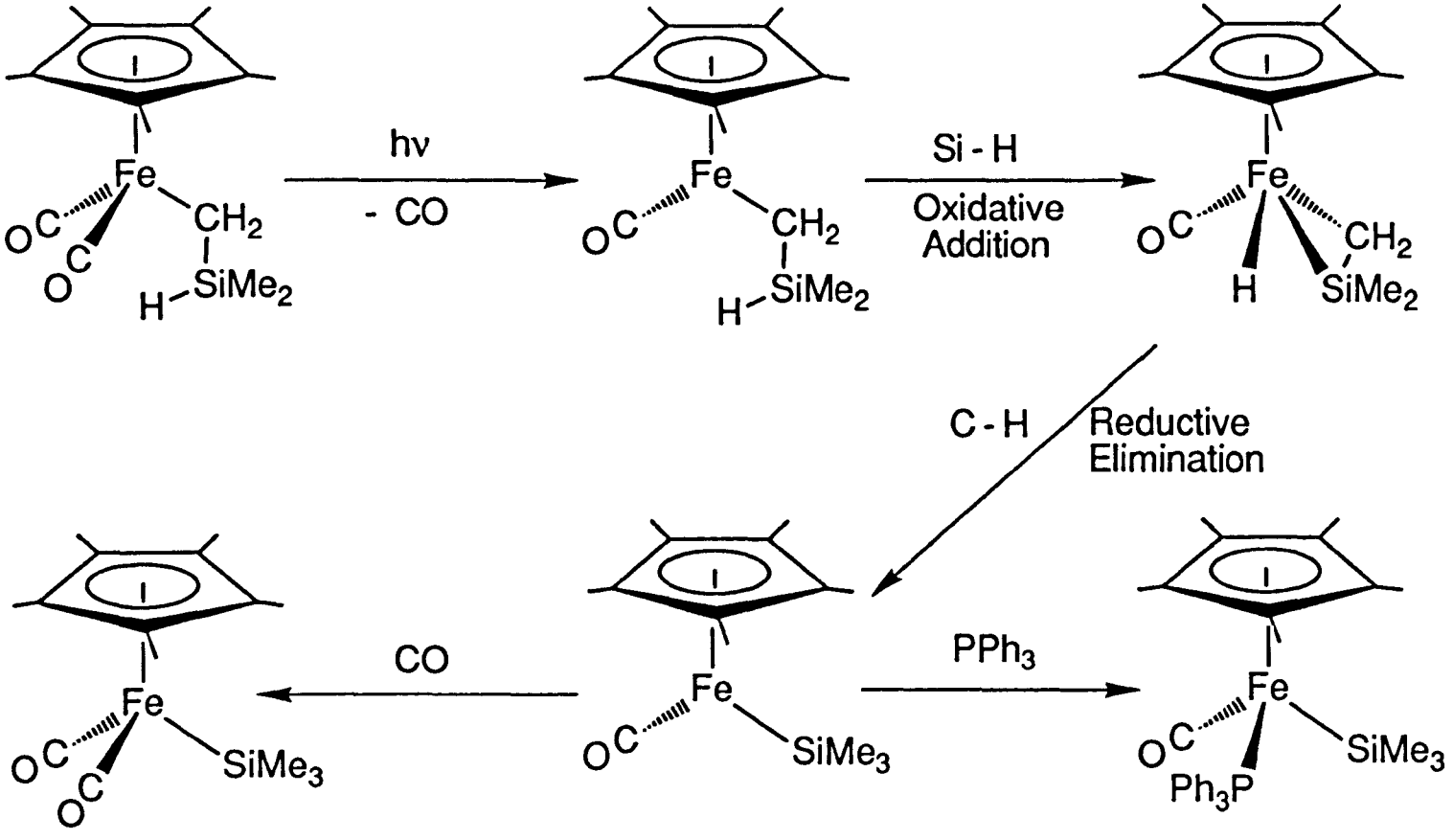
transition metal complexes containing Si-H bonds in a position β to the metal atom. In 1970 Pannell reported the preparation of the cyclopentadienyl iron dicarbonyl complex, $FpCH_2SiMe_2H$, which undergoes a rearrangement under photochemical conditions to give $FpSiMe_3$ (Equation 5.2)

$$FpCH_2SiMe_2H \xrightarrow{h\nu} FpSiMe_3 \qquad 5.2$$

A similar ligand rearrangement occurs when the complex is irradiated in the presence of triphenylphosphine (Equation 5.3)

$$FpCH_2SiMe_2H \xrightarrow[PPh_3]{h\nu} CpFe(CO)(PPh_3)SiMe_3 \qquad 5.3$$

The mechanism proposed for this rearrangement involves two successive hydrogen atom migrations, from silicon to iron and then from iron to carbon. This mechanism was confirmed by a study of the photochemistry of the analogous Cp^* complex, $Fp^*CH_2SiMe_2H$ in hydrocarbon glasses (Randolph 1987). The results of this investigation are summarised in Scheme 5.1. Photodissociation of CO is followed by rapid intramolecular oxidative addition of the Si-H bond to the 16 electron iron centre. The product of this β-hydrogen transfer has a metallasilacyclopropane structure, and is stable up to 225 K. (A similar



Scheme 5.1: Photochemistry of $Fp^*CH_2SiMe_2H$, observed by Randolph (1987).

structure has recently been identified by X-ray crystallography for $Cp^*Ru(PCy_3)(H)(CH_2SiPh_2)$ (Campion 1988)). Further warming leads to intramolecular reductive elimination of a C-H bond and coordination of CO or PPh_3. This mechanism is reminiscent of that proposed in Scheme 4.4 for the photochemical rearrangement of $FpCH_2SiMe_2SiMe_3$, with migrations of a β-hydrogen atom rather than a β-$SiMe_3$ group.

The closely related tungsten complexes, $(\eta^5\text{-}C_5R_5)W(CO)_3CH_2SiMe_2H$ (R = H, Me) undergo similar photoreactions in hydrocarbon glasses. Loss of CO is again followed by β-H transfer to give a metallasilacyclopropane (e.g. Equation 5.4).

$$CpW(CO)_3CH_2SiMe_2H \xrightarrow{h\nu} CpW(CO)_2(CH_2SiMe_2)H + CO \qquad 5.4$$

In both the iron and tungsten complexes described above, the β-Si-H bond is linked to the transition metal atom via a methylene ($-CH_2-$) fragment, giving an M-C-Si-H framework. It is of interest whether similar photochemistry is observed for molecules with an M-Si-Si-H skeleton. Several complexes with this structure have recently been synthesised, allowing such a study to be undertaken.

Preliminary research on the photolytic decomposition of these complexes has shown that the hydride, FpH and dimer, Fp_2, are the major iron containing products (Green 1989). Since it is known that FpH can be converted to Fp_2 under photochemical conditions (Blaha 1985b), it is likely that the hydride is the primary stable product in room temperature solution (Equation 5.5).

$$FpSiR_2SiR_2H \xrightarrow{h\nu} FpH + "Si_2R_4" \qquad 5.5\ (R = H, Me)$$

Similar treatment of $FpSiMe_2SiMe_3$, which contains no β-silyl hydrogens, does not result in formation of FpH. These observations suggest strongly that the hydride ligand in FpH produced from $FpSiR_2SiR_2H$ originates from the β Si atom of the silyl ligand. The silicon containing products of these reactions have so far eluded characterisation.

This Chapter describes how matrix isolation, flash photolysis and liquid xenon solution techniques have been applied in attempt to identify the intermediates involved in photochemistry of $FpSiMe_2SiMe_2H$ and $FpSiH_2SiH_3$.

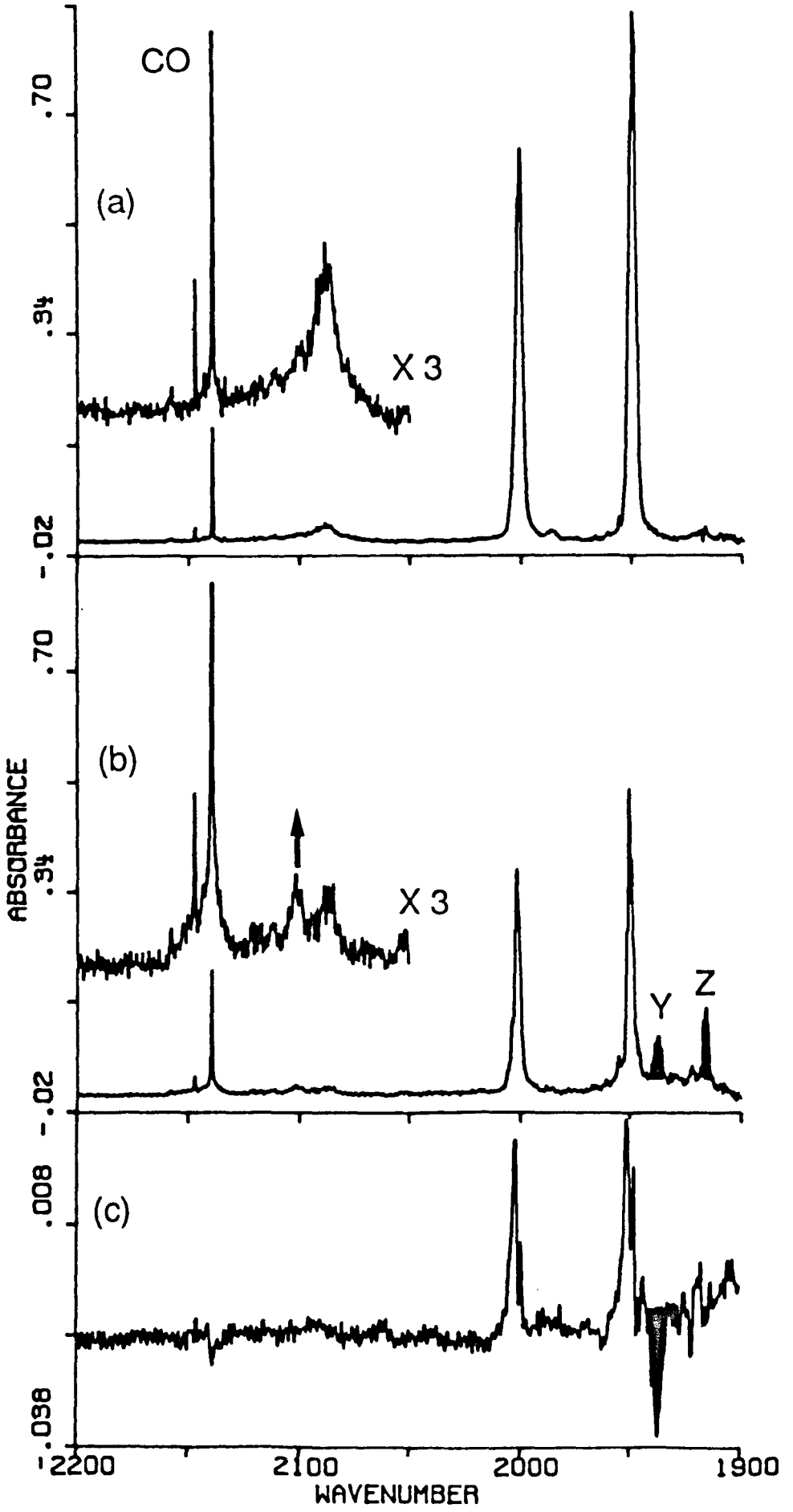
5.2 THE PHOTOCHEMISTRY OF $FpSiMe_2SiMe_2H$

Photolysis of $FpSiMe_2SiMe_2H$ in N_2 Matrices

Figure 5.1(a) shows the IR spectrum of $FpSiMe_2SiMe_2H$ isolated in an N_2 matrix at 12 K. The two intense absorptions near 2000 and 1950 cm^{-1} are due to the in-phase and out of phase ν(CO) modes of the dicarbonyl complex. At higher frequency, near 2090 cm^{-1} there is a much weaker band due to the ν(Si-H) mode of the disilyl ligand. The frequencies of these absorptions are close to those observed for $FpSiMe_2SiMe_2H$ in n-heptane solution at room temperature (see Table 5.1). The ν(CO) bands of $FpSiMe_2SiMe_2H$ are also very close to those of $FpSiMe_2SiMe_3$ (see Table 4.1). This suggests that replacement of a β-methyl group by a hydrogen atom has only minimal effect on the electron density of the iron atom. Likewise, the electronic absorption spectrum of $FpSiMe_2SiMe_2H$ in n-heptane, shown in Figure 5.2, is essentially identical to that of $FpSiMe_2SiMe_3$ (Figure 4.2(a)) with a maximum at 284 nm and a shoulder at ca. 330 nm.

Figure 5.1(b) shows the IR spectrum recorded after UV irradiation of the matrix containing $FpSiMe_2SiMe_2H$. The ν(CO) and ν(Si-H) bands of the starting material have been depleted, and several new absorptions are apparent. To low frequency of the parent ν(CO) bands there are two new bands labelled Y and Z, assigned as

Figure 5.1: (Overleaf) IR spectra illustrating the photochemistry of $FpSiMe_2SiMe_2H$ in an N_2 matrix at 12 K. (a) Before photolysis. (b) After 7 hrs 40 mins UV photolysis (230-345 nm); the bands coloured black are due to the photoproducts Y and Z as indicated; note the appearance of a new absorption in the ν(Si-H) region, shown with an expanded absorbance scale. (c) Difference spectrum illustrating the recombination of Y with CO after 6 hrs visible irradiation (>400 nm).


CO
(a)
X 3
.70
.34
-.02
(b)
X 3
Y
Z
.70
.34
-.02
ABSORBANCE
(c)
.008
-.038
2200
2100
2000
1900
WAVENUMBER

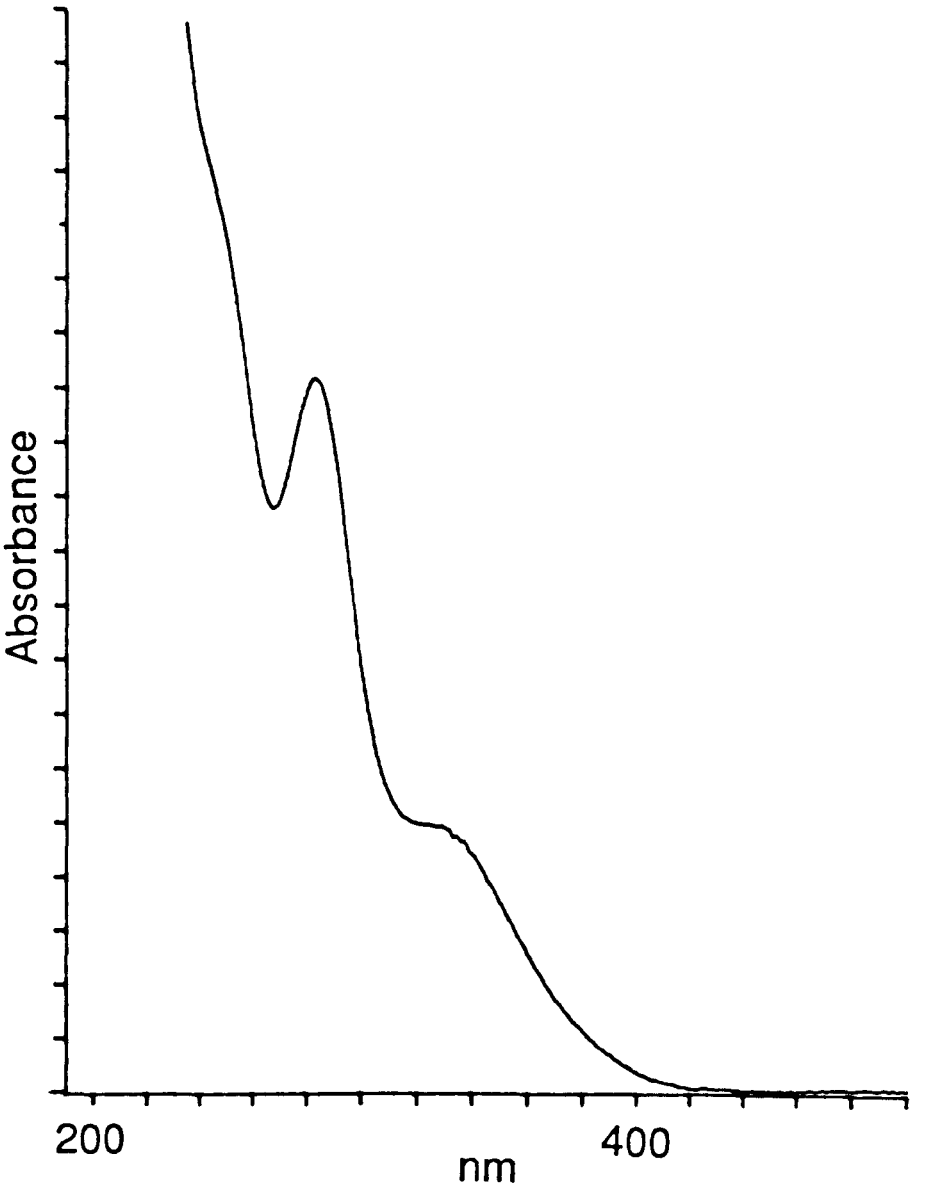


Figure5.2: Electronic absorption spectrum of $FpSiMe_2SiMe_2H$ in n-heptane solution at room temperature.

terminal ν(CO) stretching modes. Growth of the absorption at 2139 cm^{-1} shows that photolysis causes an increase in the amount of uncoordinated CO in the matrix. There is also a weak new absorption near 2100 cm^{-1} which is in the region normally associated with ν(Si-H) vibrational modes. The IR frequencies observed in this experiment are given in Table 5.1.

Subsequent visible photolysis (> 400 nm) leads to slow depletion of Y and the band due to free CO, along with the regrowth of the parent ν(CO) absorptions (Figure 5.1(c)). By contrast, no significant change is observed in the intensity of Z during visible photolysis. The different behaviour of the two photoproduct ν(CO) absorptions under these conditions indicates that they belong to different species, Y and Z. The absorptions in the ν(Si-H) region are too weak for any changes in intensity due to visible photolysis to be detected.

The IR spectral changes caused by UV photolysis are consistent with photodissociation of CO. Since two product ν(CO) bands are observed, which behave independently of each other, these absorptions can be assigned to two different monocarbonyl complexes. The appearance of a new ν(Si-H) absorption suggests that the Si-H bond remains intact in at least one of the photoproducts.

Throughout this experiment, no absorptions attributable to ν(NN) modes were observed, indicating that the N_2 matrix acts as an inert host for this system. The fact that no products containing N_2 ligands were generated suggests that the vacant coordination site caused by dissociation of CO can be blocked by an intramolecular interaction.

Similar photochemistry is observed for $FpSiMe_2SiMe_2H$ in argon matrices. The IR frequencies for this experiment are given in Table 5.1.

Flash Photolysis of $FpSiMe_2SiMe_2H$

Flash photolysis experiments on $FpSiMe_2SiMe_2H$ in room temperature solution were performed in collaboration with Mr. M. W. George. Figure 5.3 shows a series of time-resolved IR spectra obtained at 100 μs intervals after flash photolysis of $FpSiMe_2SiMe_2H$ in n-heptane under argon. Immediately after the photolysing UV laser pulse an intense negative absorption near 1950 cm^{-1} can be observed, corresponding to loss of starting material. The two positive bands are due to photoproducts generated by the UV pulse. These absorptions have maxima at 1937 and 1916 cm^{-1} respectively, which correspond extremely well with the photoproduct ν(CO) bands of Y and Z observed in low temperature matrices (see Table 5.1).

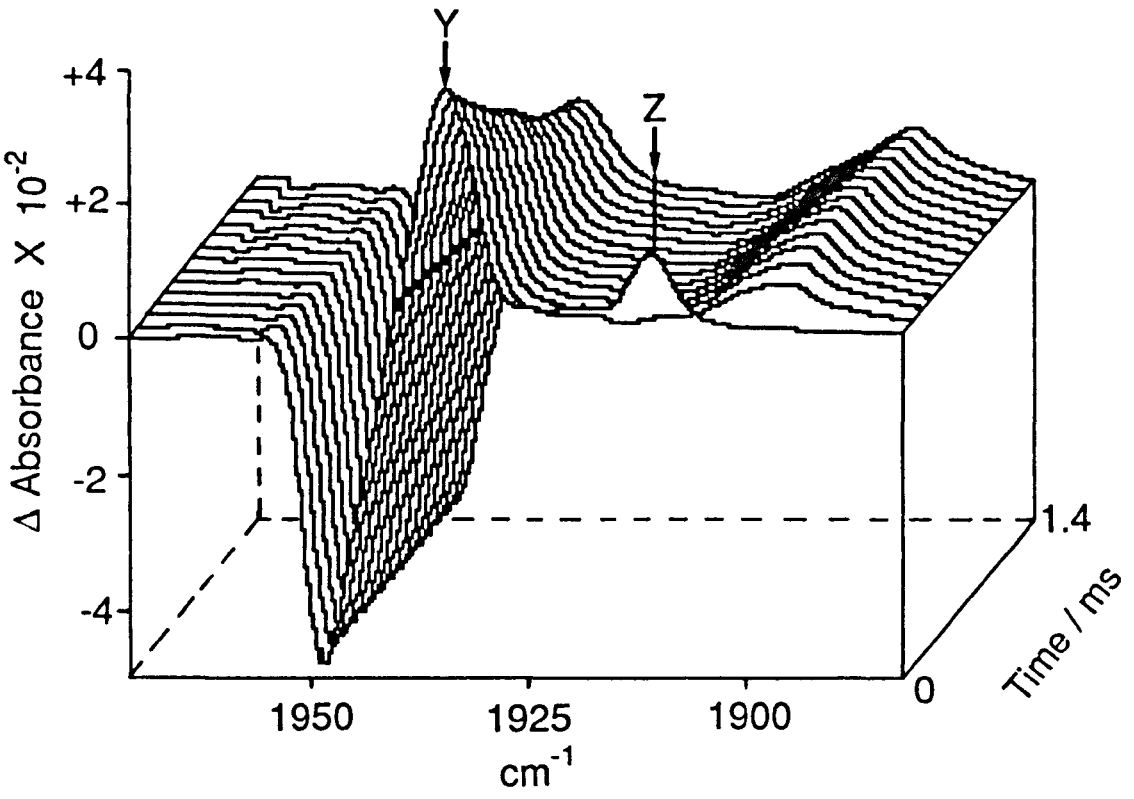


Figure 5.3: A series of time-resolved IR spectra obtained after flash photolysis of $FpSiMe_2SiMe_2H$ in n-heptane at room temperature under argon. The ν(CO) bands of the primary photoproducts, Y and Z are indicated. The time delay between each spectrum is 100 μs. Note the disappearance of the absorption of Z in the first 100 μs.

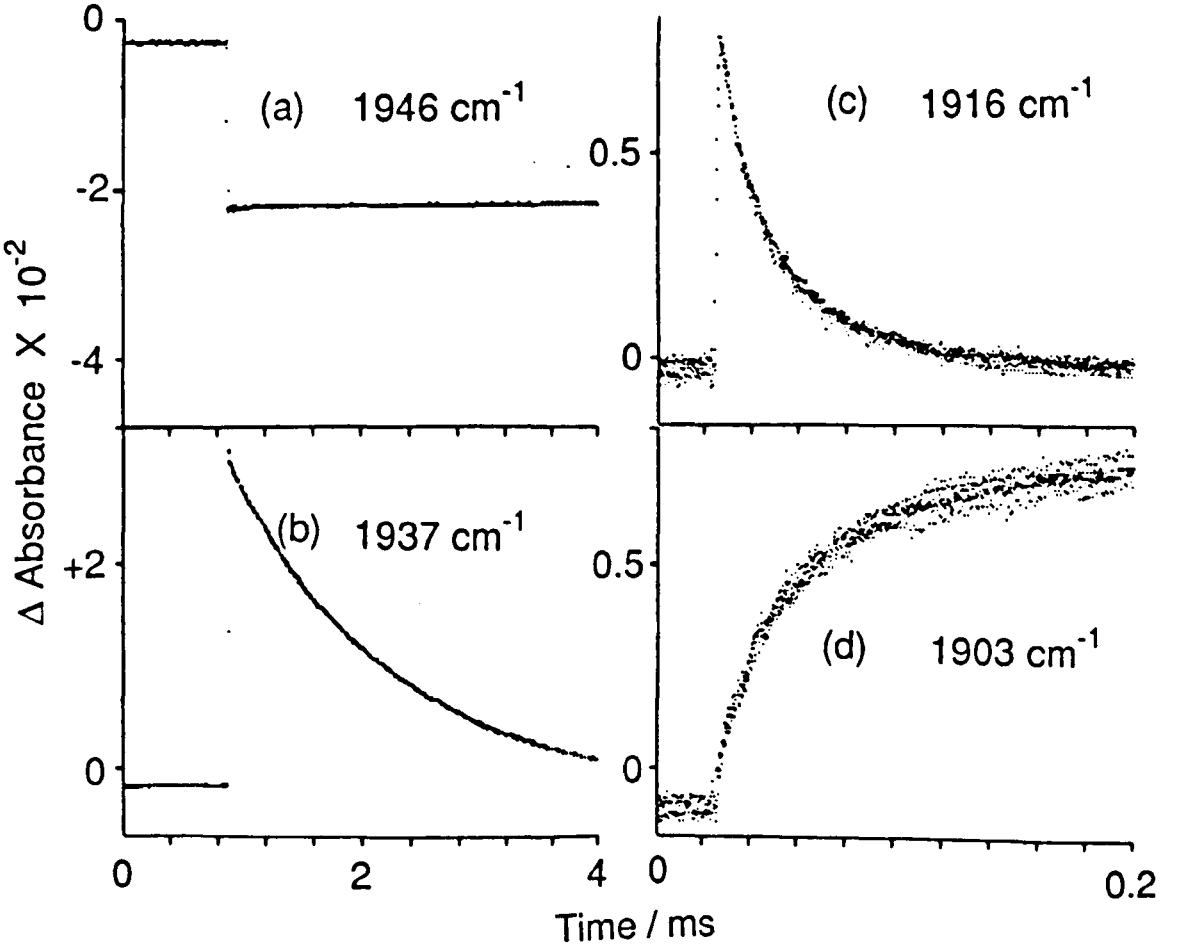


Figure 5.4: Transient IR absorption traces obtained on flash photolysis of $FpSiMe_2SiMe_2H$ in n-heptane at room temperature under argon. (a) 1946 cm^{-1}; depletion due to irreversible photochemical reaction of parent. (b) 1937 cm^{-1}; Formation and decay of primary photoproduct, Y. (c) 1916 cm^{-1}; formation and decay of primary photoproduct Z. (d) Growth of secondary product resulting from decay of Z. Note the different time and absorbance scales in these traces.

The intensity ratio of these two absorptions is ca 4:1, indicating that Y is the major product of flash photolysis in solution.

Some of the kinetic traces used to compile these spectra are shown in Figure 5.4. At 1946 cm^{-1}, there is a depletion of the low frequency parent ν(CO) band. No regeneration of this absorption occurs, indicating an irreversible photochemical reaction. The transient absorption at 1937 cm^{-1} is formed immediately after the flash and thereafter decays with first order kinetics and a half life of ca. 1.3 ms. The absorption at 1916 cm-1 is much shorter lived, decaying with first order kinetics and a half-life of 15 μs. The vastly different decay rates of these absorptions provide indisputable evidence that they are due to different species, Y and Z. A trace recorded at 1903 cm^{-1} shows the growth of an IR band which mirrors the decay of Y indicating the generation of a secondary product.

Figure 5.5 compares the kinetic traces obtained at 1937 cm^{-1} when the experiment is carried out under a pressure of 2 atm of argon or CO. The rate of decay of Y is increased by the presence of CO (half-life ca. 1.0 ms). This suggests that the decay of Y involves reaction with CO. By contrast, the rate of decay of Z is independent of CO concentration (half life 15 μs).

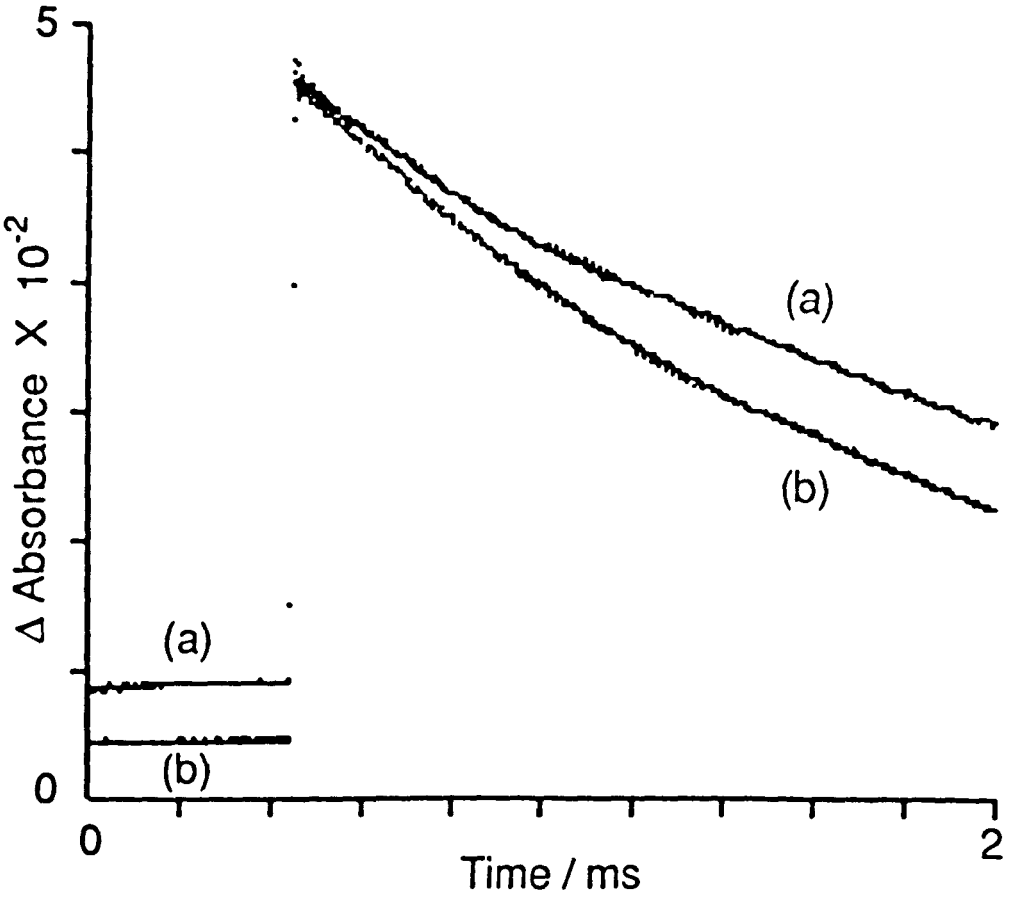


Figure 5.5: Transient IR absorption traces obtained at 1937 cm^{-1}, on flash photolysis of $FpSiMe_2SiMe_2H$ in n-heptane under (a) 2 atm argon and (b) 2 atm CO. Note the increased rate of decay of the absorption due to Y in the presence of CO.

Photolysis of $FpSiMe_2SiMe_2H$ in Liquid Xenon

The photochemistry of $FpSiMe_2SiMe_2H$ in liquid xenon was investigated in collaboration with Dr. S. M. Howdle. The IR spectra shown in Figure 5.6 were obtained during an experiment in which $FpSiMe_2SiMe_2H$ was irradiated in liquid xenon at -100°C. Photolysis leads to depletion of the parent IR absorptions and generation of a ν(CO) band at 1936.3 cm^{-1} (shaded black in Figure 5.6(b)). This corresponds to the absorption of Y observed in low temperature matrices and room temperature hydrocarbon solution. As observed in flash photolysis experiments, Y is the major primary photoproduct. The ν(CO) band of Z at 1916 cm^{-1} is not detected under these conditions. However, a weak product band is apparent at 1896 cm^{-1}, which is close to the frequency of the IR absorption observed to grow in from the decay of Z at room temperature (see above).

Figure 5.6(c) shows the IR spectrum obtained after switching off the UV lamp. The photoproduct absorptions have decayed, and several new IR bands are apparent. The strongest and most significant of these occur at 2023.4 and 1967.5 cm^{-1}, and can be assigned to the iron hydride, FpH. This is the same product observed in room temperature photolysis experiments (Green 1989). These absorptions are already present with low intensity in Figure 5.6(b).

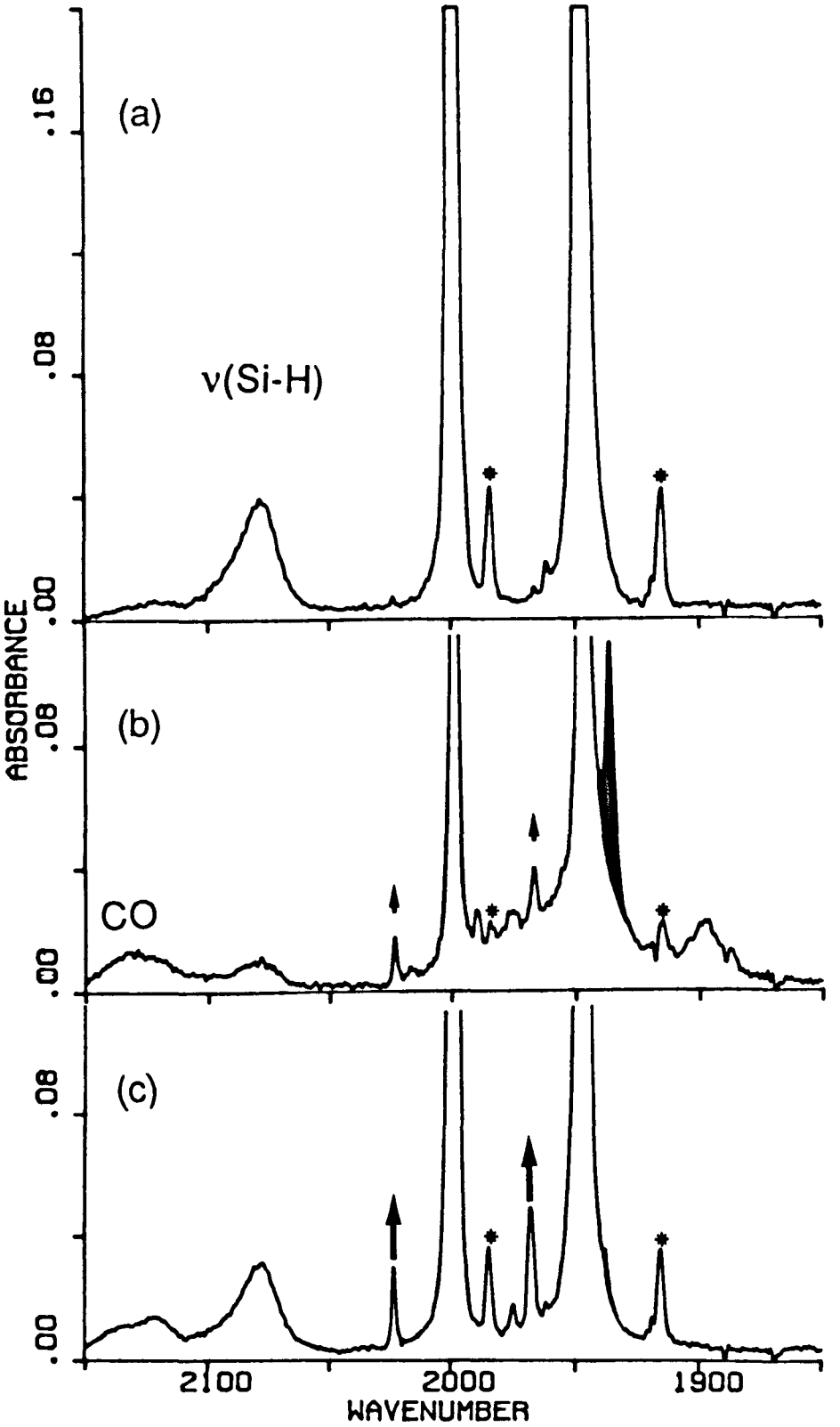
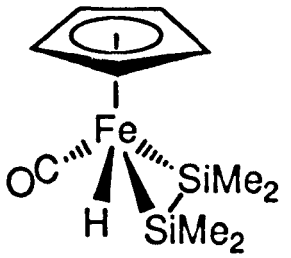


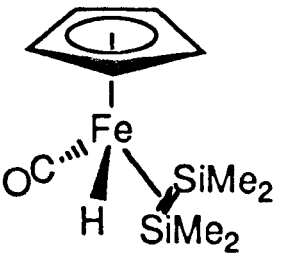
Figure 5.6: IR spectra illustrating the photochemistry of $FpSiMe_2SiMe_2H$ in liquid xenon at -100°C. (a) Before photolysis; the bands narked with asterisks are due to ^{13}CO satellites. (b) After 2mins near UV photolysis (>300 nm); the band coloured black is due to Y. (c) 5 mins after switching off the UV lamp; the arrowed bands are due to FpH.

Discussion

The results of these experiments suggest that UV photolysis of $FpSiMe_2SiMe_2H$ results in CO-loss, with the production of two monocarbonyl species, Y and Z, with quite different properties.

One possible fate for the 16 electron complex resulting from CO-loss is β -H migration from silicon to iron (i.e. oxidative addition of the Si-H bond). Such a reaction would result in the formation of the product illustrated below. The structure of this complex can be drawn either with a metalladisila-cyclopropane three membered ring, or with an $Me_2Si{=}SiMe_2$ fragment bound sideways on to the iron atom as an η^2-disilene ligand (c.f. η^2-olefin coordination)





The reaction of $(dppe)PtCl_2$ or $(dppe)Pt(C_2H_4)$ (dppe = $Ph_2CH_2CH_2PPh_2$) with $HMe_2SiSiMe_2H$ has recently been shown to produce $(dppe)Pt(Si_2Me_4)$, with a similar structure to those shown above. The reaction was proposed to proceed via two Si-H oxidative addition reactions, followed by extrusion of H_2 (Pham 1989). A

similar structure has also been proposed for the complex $(Si_2Me_4)Fe(CO)_4$ (Pakkanen 1981).

In the studies on $Fp^*CH_2SiMe_2H$ described in the Introduction to this Chapter, the ν(CO) band of $Cp^*Fe(CO)(CH_2SiMe_2)H$ shifts by 39 cm^{-1} to low frequency relative to the mean position of the two parent ν(CO) bands (Randolph 1987). A similar shift would be expected for a Si-H oxidative addition product after CO loss from $FpSiMe_2SiMe_2H$. Thus a ν(CO) frequency of 1936 cm^{-1} can be predicted for the structure shown above. The ν(CO) band of Y occurs at a 1937.4 cm^{-1} in an N_2 matrix, which concurs excellently with this prediction. Several other pieces of evidence agree with this assignment:

1) By analogy with studies on $Fp^*CH_2SiMe_2H$ and $(\eta^5\text{-}C_5R_5)W(CO)_2CH_2SiMe_2H$ (R = H, Me), the intramolecular oxidative addition of a β-Si-H bond is expected to be a facile process. In flash photolysis experiments, Y is observed immediately after the UV pulse. Y is also the major primary photoproduct observed in both flash photolysis and liquid xenon solution experiments.

2) The decay of Y in liquid xenon is accompanied by production of the hydride FpH. This can be explained by loss of the Si_2Me_4 fragment and recoordination of CO. In room temperature solution, Y decays more

rapidly under an atmosphere of CO. However, the generation of FpH is not observed on the timescale of the flash photolysis experiments.

3) The lifetime of Y in room temperature solution is much longer than those observed for unsaturated CO-loss products in other systems. In addition, substantial quantities of Y can be generated in liquid xenon at -100°C. These observations are indicative of a relatively stable species, reminiscent of the metallasilacyclopropane complex formed upon CO loss from $Fp^*CH_2SiMe_2H$ (Scheme 5.1), which is stable up to a temperature of 225 K.

No IR band attributable to a ν(Fe-H) mode of Y was observed in any of the experiments described here. This is not surprising in view of the low intensity expected for such an absorption.

Since Y is assigned as an Si-H oxidative addition product, it is possible that the minor product, Z, contains an intact Si-H bond. The ν(SiH) band observed near 2100 cm^{-1} in low temperature matrices might be assigned to Z. However, assignment of a structure for this species presents difficulties. If Z were the 16 electron CO-loss species, prior to β-H transfer, one would expect to observe conversion from Z to Y. No such conversion was observed under any conditions.

By analogy with the photochemistry of $FpSiMe_2SiMe_3$ described in Chapter 4, Si-Si activation can be envisaged as a process occurring in competition with Si-H activation. However, the properties of Z are very different from the primary photoproduct observed from $FpSiMe_2SiMe_3$, so this is unlikely. It is noteworthy that the disilyl ligand in $FpSiMe_2SiMe_2H$ contains C-H bonds which may also be susceptible to oxidative addition to an unsaturated iron centre. However, no evidence for such a process was obtained in experiments on $FpSiMe_3$ and $FpSiMe_2SiMe_3$, which also contain C-H bonds, so this possibility is also considered unlikely.

It is possible that Z is not a monocarbonyl species, and has other ν(CO) absorptions which are weak or masked by stronger spectral features. Alternative photochemical processes might involve Fe-Si cleavage or η^5-η^3 Cp ring hapticity change. Fe-Si homolysis can be ruled out since no ν(CO) bands attributable to the Fp radical were observed. (The ν(CO) frequencies for this species are known from TRIR experiments on the dimer, Fp_2 (Dixon, 1986, 1987, 1989)). Cyclopentadienyl ring slippage has been reported for FpMe in CO matrices, yielding $(\eta^3\text{-}C_5H_5)Fe(CO)_3Me$ (Mahmoud 1985). An η^5-η^3 hapticity change would result in a 16 electron iron centre which could be trapped by an intramolecular Si-H oxidative addition reaction, giving $(\eta^3\text{-}C_5H_5)Fe(CO)_2(Si_2Me_4)H$.

5.3 THE PHOTOCHEMISTRY OF $FpSiH_2SiH_3$

Flash Photolysis of $FpSiH_2SiH_3$ in Room Temperature Solution

Attempted matrix isolation experiments on $FpSiH_2SiH_3$ were hindered by contamination of the sample with the decomposition product, FpH. Even very small amounts of the hydride in the sample resulted in large contamination of the matrix, due to its high volatility relative to $FpSiH_2SiH_3$. Thus it was found to be impossible to prepare a matrix without isolation of significant amounts of FpH, as well as the desired compound. Greater success might be achieved by using a hydrocarbon glass or polymer film as the matrix medium for this complex. Neither of these techniques require sample vapourisation in order to prepare the matrix, so the presence of trace amounts of FpH would lead to fewer problems.

However, room temperature solution experiments could be performed on $FpSiH_2SiH_3$. An FTIR spectrum of a solution of the complex in n-heptane showed that contamination with FpH was minimal under these conditions. Figure 5.7 shows a "stack-plot" of time-resolved IR spectra recorded after flash photolysis of $FpSiH_2SiH_3$ in n-heptane solution under an argon atmosphere. It is similar to the stack-plot recorded under the same conditions for $FpSiMe_2SiMe_2H$,

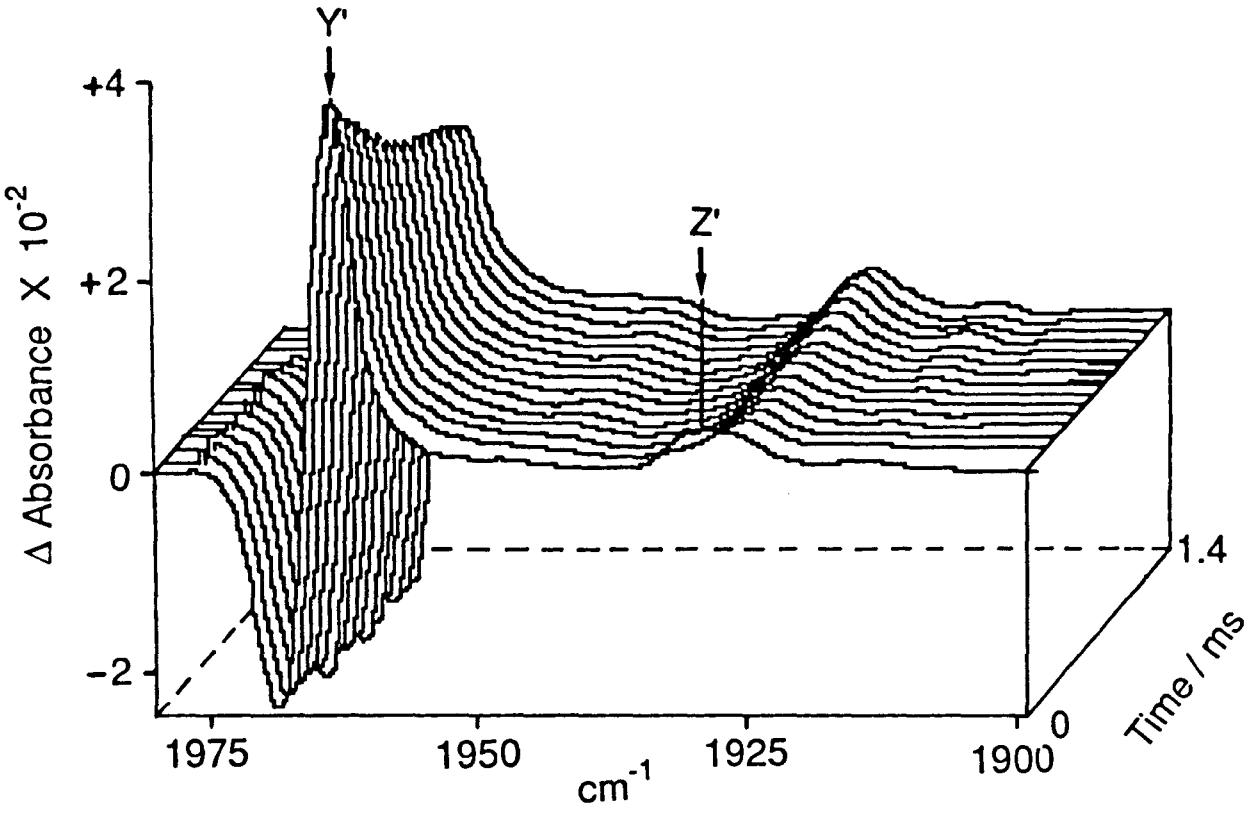


Figure 5.7: A series of time-resolved IR spectra obtained after flash photolysis of $FpSiH_2SiH_3$ in n-heptane at room temperature under argon. The ν(CO) bands of the primary photoproducts, Y' and Z' are indicated. The time delay between each spectrum is 100 μs. Note the disappearance of the absorption of Z' in the first 100 μs.

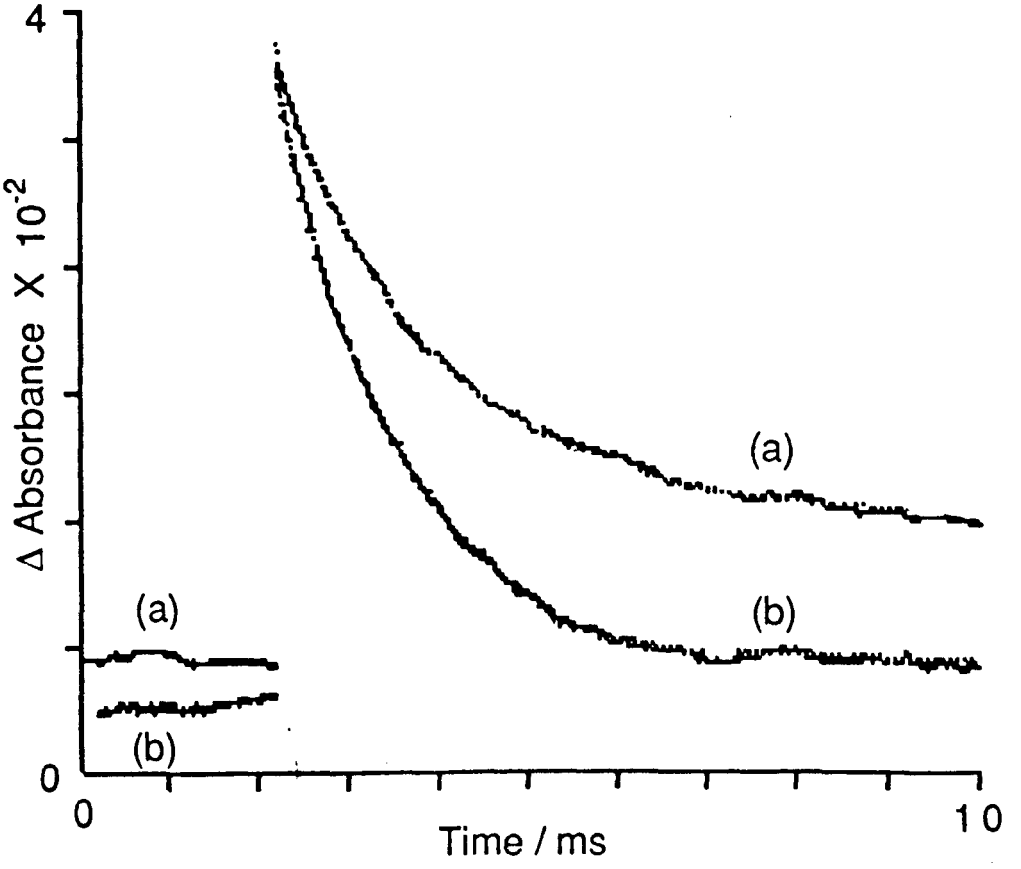
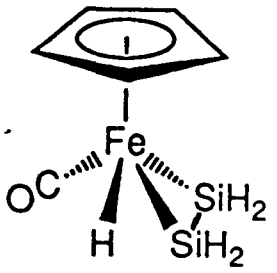


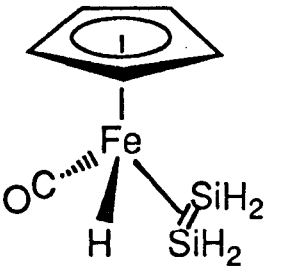
Figure 5.8: Transient IR absorption traces obtained at 1963 cm^{-1}, on flash photolysis of $FpSiH_2SiH_3$ in n-heptane under (a) 2 atm argon and (b) 2 atm CO. Note the increased rate of decay of the absorption due to Y' in the presence of CO.

shown in (Figure 5.3).

Flash photolysis causes irreversible depletion of the low frequency parent ν(CO) band at 1968 cm^{-1} and generation of an intense transient absorption at 1963 cm^{-1}, labelled Y'. The frequency of this band is 26 cm^{-1} below the mean of the two parent ν(CO) absorptions, which is consistent with its assignment as a product of Si-H oxidative addition, by analogy with $Fp^{*}CH_2SiMe_2H$ (Randolph 1987). Y' decays with a half-life of ca. 1.9 ms, which is of the same order of magnitude as the decay of Y.

Figure 5.8 compares the kinetic traces obtained at 1963 cm^{-1} when the experiment is carried out under a pressure of 2 atm of argon or CO. The rate of decay of Y' is increased by the presence of CO (half-life ca. 1.1 ms). This suggests that the decay of Y' involves reaction with CO. The photoproduct Y' exhibits similar characteristics as Y (see above) and can similarly be assigned as a product of intramolecular Si-H oxidative addition after photodissociation of CO. The structure of Y' can be drawn with either a metalladisilacyclopropane structure or an η^2-$H_2Si{=}SiH_2$ ligand as illustrated below.





The proposed structure of Y' is the first example of a complex involving Si_2H_4, the silicon analogue of coordinated ethylene.

It should be noted that unlike $FpSiMe_2SiMe_2H$, the silyl ligand in $FpSiH_2SiH_3$ contains both α and β hydrogens. Thus, α-H migration from silicon to iron is an alternative process. However β-H transfer is generally the preferred process when there is a choice of pathways (Kazlauskas 1982a, Mahmoud 1985).

In addition to Y', there is a second, much weaker primary shorter-lived photoproduct band at 1929 cm^{-1}, labelled Z'. Its decay is matched by the growth of a secondary product with an IR absorption at 1925 cm^{-1}. This behaviour resembles that of Z in experiments on $FpSiMe_2SiMe_2H$. Similar arguments apply to the identity of Z' as those outlined above for Z. Further experiments on $FpSiH_2SiH_3$, such as photolysis in liquid xenon, were prevented by decomposition of the sample.

Table 5.1: IR frequencies (cm^{-1}) of $FpSiMe_2SiMe_2H$ $FpSiH_2SiH_3$ and their photoproducts in matrices at 12 K, and room temperature hydrocarbon and low temperature liquid xenon solutions[a].

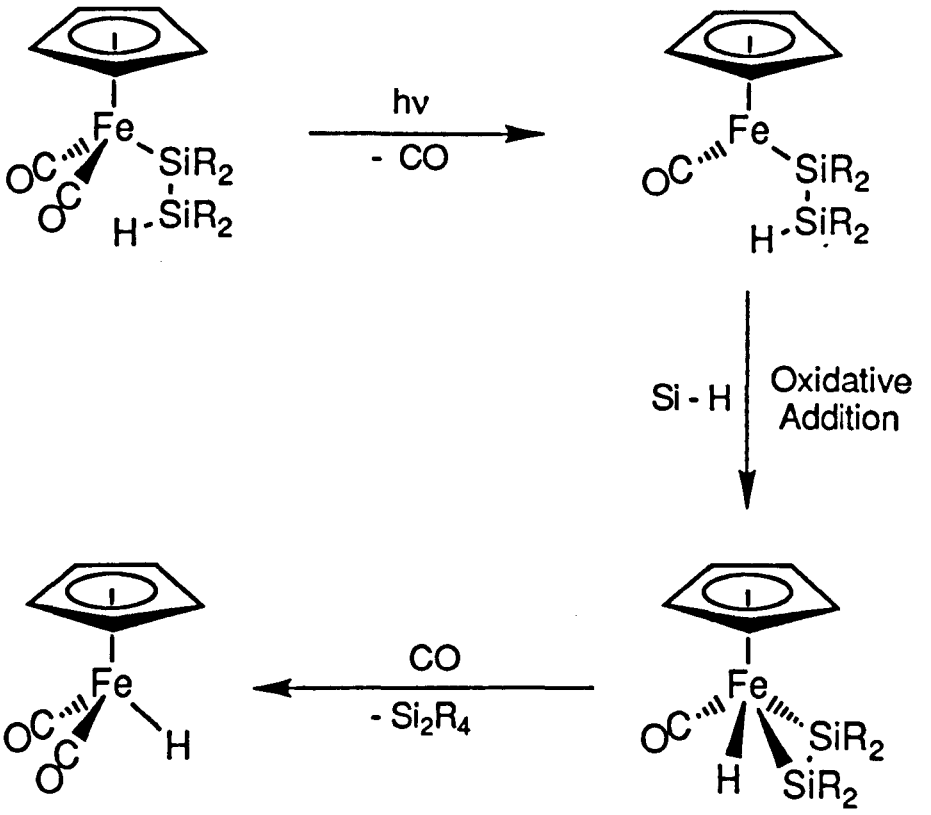
	Matrix/Solvent			
Complex	**Ar**	**N_2**	**Liq. Xenon**	**n-heptane**
$FpSiMe_2SiMe_2H$	1950.9	1949.0	1946.9	1946.8
	2002.7	2000.2	1998.5	1998.0
ν(SiH)	2075	2089	2079	2077
Y	1939.4	1937.4	1936.3	1937[b]
Z	1918.0	1916.2	-	1916[b]
ν(SiH)	-	2102	-	-
$FpSiH_2SiH_3$	1967.5	1967.5	-	1966
	2014.4	2015.3	-	2011
ν(SiH)	2095	2088	-	2091
ν(SiH)	-	-	-	2135
Y'	-	-	-	1963[b]
Z'	-	-	-	1929[b]

a Error +/- 0.2 cm^{-1} for solution spectra.

b Measured using fast TRIR spectroscopy.

5.4 CONCLUSIONS

The photochemistry of Fp-disilyl complexes is greatly modified by the presence of β-silyl hydrogens in the starting material. The results presented in this Chapter suggest that the major pathway following photodissociation of CO is rapid intramolecular β-H transfer from silicon to iron. This process occurs even in low temperature matrices. The products of β-H migration can be formulated with a metalladisilacyclopropane structure or with an η^2-disilene ligand coordinated to the iron centre. Subsequent loss of the Si_2R_4 fragment and coordination of CO leads to the iron hydride product FpH as illustrated in Scheme 5.2. It appears that β-H transfer occurs in preference to Si-Si oxidative addition in these complexes. In addition, less well defined minor processes are observed. The current evidence does not indicate the role of these side reactions in the photochemistry of this system.



Scheme 5.2: A mechanism for the photochemical conversion of $FpSiR_2SiR_2H$ to FpH (R = H, Me).

THE PHOTOCHEMISTRY OF CYCLOPENTADIENYL IRON DICARBONYL SILYL COMPLEXES

SUMMARY

The results described in Chapters 4 and 5 of this Thesis have demonstrated how the application of a variety of techniques can be extremely useful in solving mechanistic problems of this nature. Each method provides a partial description of the system under study, which must be combined to reveal an overall pattern.

These findings complement previous studies of the photochemistry of FpR complexes. Primary dissociation of CO leads to a photoproduct of the general formula CpFe(CO)R. This fragment can then recombine with CO or with an added ligand L. Alternatively, for certain ligands, R, intramolecular trapping of the unsaturated complex may occur.

In Section Two of this Thesis, such intramolecular trapping has been a common theme. In the case of $CpFe(CO)SiMe_2SiMe_3$, the trapping is rationalised as an Fe-Si-Si three centre electronic interaction which blocks the vacant coordination site after CO-loss. In solution, this interaction leads to intramolecular oxidative addition of the Si-Si bond of the disilyl

ligand to the iron atom. The product is an iron silylene complex which is thermally stable but which undergoes photochemical loss of an $SiMe_2$ fragment.

For the complexes containing β-silyl hydrogens, rapid β-H transfer from silicon to iron is thought to occur, giving products with a metalladisilacyclopropane or η^2-disilene structure. Such complexes are implicated in the photochemical conversion of $FpSiR_2SiR_2H$ to FpH.

No such trapping is observed for $CpFe(CO)SiMe_3$, which undergoes rapid reactions with a variety of ligands.

CHAPTER 6

EXPERIMENTAL TECHNIQUES

Most of the experimental techniques used to produce the results presented in this Thesis are well known and have been described elsewhere in detail. This Chapter outlines the principal methods used to study intermediates in organometallic photochemistry, namely matrix isolation, liquid xenon solutions, and fast TRIR spectroscopy. The theory and advantages of FTIR spectroscopy are also discussed.

6.1 THE MATRIX ISOLATION APPARATUS

The heart of the matrix isolation apparatus is a cold, polished spectroscopic window, on the surface of which a film of matrix material can be deposited. The apparatus necessary for a matrix to be prepared on such a window, has been described extensively by previous workers (Church 1982, Fletcher 1985, Firth 1987). The main features of the system are outlined below.

The spectroscopic window (CsBr) is clamped in a silver-plated copper holder between indium gaskets to ensure a good thermal contact. The threaded window holder is screwed into a copper block at the bottom of

the cryogenic cooler, again using an indium gasket. A thermocouple is also mounted on the copper block, together with an electrical heater. Each of these is connected to an Air Products Model APD-E digital temperature controller/indicator. This allows the temperature of the spectroscopic window to be accurately monitored and adjusted.

Cooling is achieved using the modified Stirling cycle of an Air Products helium-filled Displex system, consisting of a compressor module and a two stage displacer/expander unit. Helium is compressed and transferred to the displacer/expander unit via flexible metal hoses with self sealing Aeroquip couplings. The gas then enters a two stage expansion chamber, and as it expands, does work against a piston, thus losing thermal energy and cooling the system. The expanded gas is then returned to the compressor to begin the cycle once more. The closed cycle of the Displex system means that it can, in theory, be run indefinitely. However, in practice, small leaks require that the system be periodically refilled with helium. The minimum temperature attainable by the Displex is ca. 10 K.

The matrix window is surrounded by a copper radiation shield, which is cooled to 77 K by the first stage of the Displex. Thermal leaks, which are proportional to the fourth power of the temperature

difference, are greatly reduced by the radiation shield.

The cryostat is enclosed by a thick glass vacuum shroud, fitted with the appropriate spectroscopic windows to allow UV/visible photolysis and IR or UV/visible spectroscopy. The shroud is evacuated to a pressure of ca. 10^{-6} torr using an Edwards 63mm (2") oil diffusion pump backed with a rotary pump. The shroud also includes inlet ports fitted with B14 sockets allowing for the introduction of sample and matrix gases during matrix deposition.

Matrix Deposition

There are two principal methods by which frozen gas matrices can be deposited on a cooled spectroscopic window. Both involve introduction of a small pressure of gas into the vacuum shroud, which subsequently condenses as a thin film on the surface of the matrix window. When the sample which is to be matrix isolated has sufficient vapour pressure at room-temperature, the technique known as "Pulsed Deposition" can be utilised. This involves preparation of a gas bulb containing a mixture of both the sample and matrix gases in the required ratio (commonly sample:matrix gas = 1:2500). The gas bulb is placed on a vacuum frame, which is connected to the glass shroud surrounding the matrix window. Portions of the gas mixture are allowed into

the vacuum shroud in discrete pulses, which freeze in successive layers on the window to build up the matrix. Matrices can be prepared quite quickly in this manner, and are often crystal clear, aiding spectroscopic measurement.

However, if the sample to be isolated has insufficient room temperature vapour pressure for a gas mixture to be prepared, another method, known as "Slow Spray-On" is required. In this technique the sample is slowly sublimed onto the matrix window from a container connected to the vacuum shroud. The sample can be heated or cooled to give the correct rate of vapourisation. Simultaneously, a flow of matrix gas is allowed to enter the shroud through a needle valve, such that it is co-condensed with the sample onto the matrix window. Under these controlled conditions, the sample can be isolated in a large excess of frozen matrix gas over a period of several hours.

In principal, any compound which sublimes without decomposition can be matrix isolated in this manner. This technique suffers by comparison with Pulsed Deposition due to the longer time required for spraying on a matrix. A small leak in the system can lead to significant contamination of the matrix (with CO_2 and H_2O for example) over a few hours. Matrices deposited by Slow Spray-On are often more cloudy than those prepared by the Pulse On method. A light scattering

matrix can cause difficulties in recording UV/visible spectra, or when when making spectroscopic measurements using plane polarised light (see below).

The Slow Spray-On technique was used for all of the matrix isolation experiments described in this thesis, due to the low volatility of the compounds under study. Two different arrangements for sample temperature control were utilised. For experiments on the platinum dimers, $(CpPt(CO))_2$ and $(Cp^*Pt(CO))_2$, a solid state thermoelectric cooler (Peltier cooler) was employed, as previously described by Fletcher (1985) and Firth (1987). The Peltier cooler is mounted between a water cooled jacket and a copper block, into which is screwed a threaded copper tube containing the sample. The sample can be cooled or warmed by ca. +/- 40°C relative to the water temperature, by application of the appropriate EMF to the device. Before and after deposition of the matrix, the sample is cooled to prevent vapourisation. During spray-on, the sample temperature is controlled by varying the EMF applied. A thorough description of the procedure to be followed when using the Peltier cooler to spray on a sample is given by Firth (1987).

The alternative arrangement for Slow Spray-On matrix deposition is depicted in Figure 6.1. The sample is held in an ampoule fitted with a Young's tap (A) and B14 socket. This assembly is connected to an

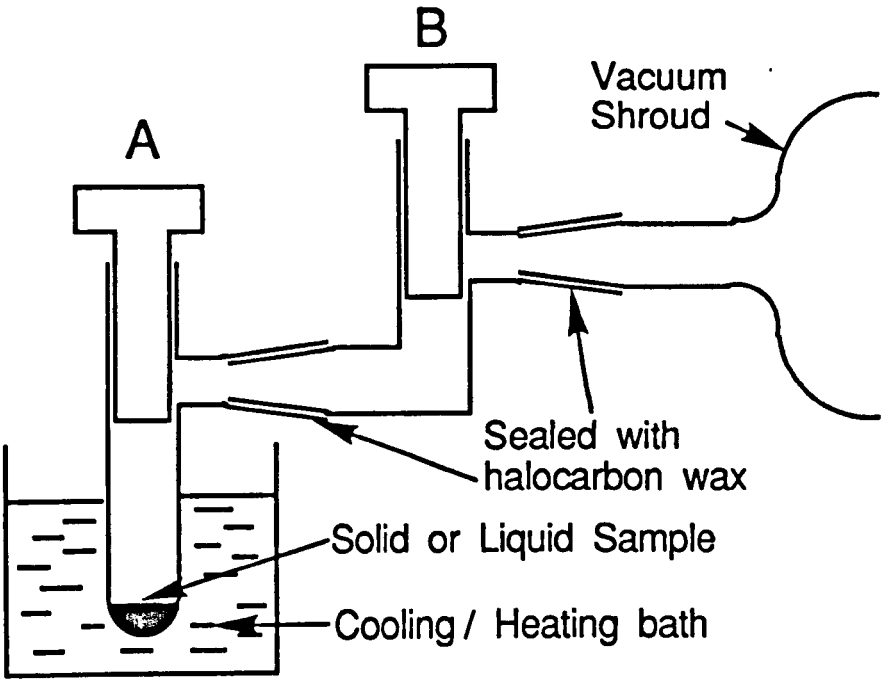


Figure 6.1: Apparatus used for slow spray-on of metal carbonyls

inlet port of the glass shroud via an intervening Young's tap (B). Each of the ground glass joints is sealed with halocarbon wax. The procedure to be followed when using this set-up is outlined below:

1) The following conditions should be met before beginning an experiment:
   Clean spectroscopic matrix and shroud windows
   Compressor Helium Pressure = 215 +/- 10 psi
   Shroud Pressure = 10^{-6} Torr
   Gas handling line Pressure = 10^{-3} Torr

2) Seal sample tube onto B14 cone of Tap B.

3) Open Tap B, followed by Tap A in order to evacuate sample tube. After ca. 5 minutes the shroud vacuum should have returned to 10^{-6} Torr. The sample can be cooled if necessary during this procedure.

4) Close Taps A and B prior to Displex cool-down

5) Prepare a bulb of matrix gas and cool down the Displex to 12 K as previously described by Firth (1987). Set the temperature controller to 20 K and the Displex heater to 5 W, in order to warm the matrix window to 20 K. (This window temperature is found to give matrices of better optical quality).

6) Allow a pulse of matrix gas to enter the shroud and condense on the matrix window. This provides a better foundation for the matrix than a bare CsBr window (Firth 1987)

7) Open the needle valve to allow a flow of matrix gas to enter the shroud, such that the Penning gauge reads ca. 5 X 10^{-5} Torr. This shroud pressure should be maintained throughout deposition of the matrix, by adjusting the needle valve. This corresponds to an approximate matrix gas deposition rate of 2 mmol hr^{-1} (Fletcher 1985).

8) Immerse the sample tube in a heating bath or cooling slush bath of the appropriate temperature, if required, and allow time to equilibrate.

9) Open taps A and B slightly to allow the vapour pressure of the sample to enter the shroud, and co-condense with matrix gas on the spectroscopic window.

10) After ca. 10 minutes spray-on, turn the matrix window into the IR beam, and record a spectrum. The intensity of the sample ν(CO) absorptions in the IR spectrum indicate whether any adjustment of the sample temperature is necessary to give the correct spray-on rate. (The strongest absorption of the sample should reach an absorbance of 1 after

about three hours matrix deposition). The progress of the spray-on should be checked periodically in this manner.

11) When the IR spectrum shows that sufficient sample has been isolated, close the needle valve and Taps A and B to end the spray-on. Turn off the Displex heater to cool the matrix to ca. 12 K. The sample tube can now be removed from the system. This enables unstable samples to be placed under an argon atmosphere and refrigerated.

With a new compound, it is usually necessary to carry out several trial experiments to determine the optimum spray-on conditions for matrix preparation.

The table below shows the typical spray-on temperatures used for each of the compounds studied in this work.

Compound	Peltier Current(Amps)	Temperature(^{o}C)
$(CpPt(CO))_2$	5	50
$(Cp^*Pt(CO))_2$	10	65
$(CpNi(CO))_2$	-	70
$Os_2(CO)_9$	-	25
$Os_2(CO)_8(\mu\text{-}C_2H_4)$	-	25
$FpSiMe_3$	-	-10
$FpSiMe_2SiMe_3$	-	25
$FpSiMe_2SiMe_2H$	-	20
$FpSiH_2SiH_3$	-	-25

The Matrix Cryostat for MCD Spectroscopy

MCD measurements on $Cp^*_2Pt_2(\mu\text{-}CO)$ were attempted using the matrix isolation cryostat at the University of East Anglia, in collaboration with Dr. R. Grinter and Dr. R. G. Graham. The cryostat has previously been described in detail by Graham (1986). Its principal features are a sapphire matrix window, held in strain free mountings, with one surface of the window in contact with a reservoir of liquid helium, giving a cooling range of 4.2 - 60 K. By reducing the pressure above the liquid helium using a rotary vacuum pump, the window temperature can be further depressed as low as 1.5 K. A superconducting magnet provides a maximum magnetic field of 8 T at 4.2 K and 10 T at 2.2 K. MCD spectra were recorded using a Cary 61 spectropolarimeter.

6.2 LIQUID NOBLE GAS TECHNIQUES

Experiments on the Fp-silyl complexes using liquid xenon as a solvent were performed in collaboration with Mr. Steve M. Howdle and Mr M. A. Haward. The high pressure, low temperature cell used for these experiments has been described in detail by Simpson (1982) and Upmacis (1986). Essentially it consists of a liquid nitrogen cooled solution chamber, surrounded by a vacuum jacket, to prevent condensation of atmospheric water vapour. The cell has two pairs of windows, such that IR spectra can be taken simultaneously with photolysis of the solution. The optical path length of the cell is ca. 2 cm. The solution is stirred magnetically.

6.3 FLASH PHOTOLYSIS/FAST TIME-RESOLVED IR SPECTROSCOPY

Flash photolysis experiments on $(Cp^{*}Pt(CO))_2$ and $(CpPt(CO))_2$ were carried out in collaboration with Dr. A. J. Dixon. Those on the $(CpNi(CO))_2$, and the Fp-silyl complexes were performed in collaboration with Mr. M. W. George. The apparatus used for fast TRIR spectroscopy has been described in detail elsewhere (Poliakoff 1986, Dixon 1986). The photolysing source is a Lumonics Hyperex-440 excimer laser operating on XeCl, giving a UV pulse of wavelength 308 nm and

duration 10 ns. Transient changes in IR absorption are detected by monitoring the transmitted intensity of IR light from a continuous-wave, line-tunable CO laser. Kinetic traces are recorded for each of the CO laser lines (ca. 4 cm^{-1} separation between lines), such that a time-resolved IR spectrum can be built up "point by point." The solution cell (pathlength 1 mm) is connected to a flow system, so that for each flash of the UV laser, the cell is filled with a fresh batch of solution. All solutions were thoroughly degassed on a vacuum line fitted with a rotary pump (10^{-1} Torr or better) and then kept under a pressure (2 atm) of argon or the appropriate reactive gas.

6.4 ROOM TEMPERATURE SOLUTION PHOTOCHEMISTRY

Solutions were photolysed in a pyrex Schlenk tube, fitted with a rubber septum. This enabled portions of the solution to be removed by syringe, for spectroscopic analysis at intervals during the experiment. Solutions were degassed as for TRIR experiments and then kept under 1 atm of the appropriate gas (Ar, N_2, CO or C_2H_4). All solution FTIR spectra were recorded on the Nicolet MX-3600 or 730 interferometers, with a resolution of 2 cm^{-1}.

6.5 INFRARED SPECTROSCOPY

The main features of the IR spectrometers used in this work are outlined below:

Dispersive Spectrometer - Perkin-Elmer 580B

This instrument is a fairly sophisticated double beam, ratio recording, grating spectrometer, with a maximum resolution capability of 0.4 cm^{-1}. It can operate in transmittance, absorbance or single beam modes. Selection of one of several integrated scan modes, combining functions such as slit width, scan speed and time constant, enables optimum scanning conditions to be set.

The main application of this spectrometer was in monitoring the progress of matrix deposition during slow spray on. A wire grid polariser is also fitted to the PE 580B instrument. This was used to calibrate the IR polariser used to record dichroic FTIR spectra (see below). The PE 580B can also be interfaced with the PE 3600 data station for spectral manipulation and storage. However, the routine use of FTIR spectroscopy has largely superceded this function.

Fourier Transform Infrared Spectrometers

The use of Fourier Transform infrared spectroscopy is now widespread, and has been discussed extensively (Griffiths 1975).

Three interferometers have been used during the course of this work, all manufactured by Nicolet Instruments Limited. The Nicolet 7199 and Nicolet MX-3600 are both used in conjunction with a Model 1280 computer data station. The features of both systems have been described extensively (Church 1982, Fletcher, 1985, Firth 1987, Horton-Mastin 1988) and only brief details are given here.

Nicolet 7199 (used for matrix isolation work on $(CpNi(CO))_2$, $Os_2(CO)_9$, $Os_2(CO)_8(\mu\text{-}C_2H_4)$ and Fp-silyl complexes).

Detectors: Mercury Cadmium Telluride (MCT) or Indium Antimonide (both liquid nitrogen cooled)

Maximum Resolution: 0.06 cm^{-1}

Working Resolution: 0.5 cm^{-1} (32K data points collected, 256K data points in Fourier transformation) for matrix spectra.

Nicolet MX-3600 (used for matrix isolation work on $(CpPt(CO))_2$ and $(Cp^*Pt(CO))_2$ and solution spectroscopy)

Detector: Triglycine Sulphate (TGS) (room temperature operation).

Maximum Resolution: 0.7 cm^{-1}

Working Resolution: 0.7 cm^{-1} (32K data collect, 256K Fourier transform) for matrix spectra.

2 cm^{-1} (16K data collect, 32K Fourier transform) for solution spectra.

Nicolet 730 This is the latest interferometer to be added to the laboratory in Nottingham, complete with its own data station. This instrument was used solely for recording solution spectra during this research.

Detectors: MCT (liquid nitrogen cooled)
TGS (room temperature operation)

Maximum Resolution: 0.3 cm^{-1}

Working resolution: 2 cm^{-1} (16K data collect, 32K Fourier transform)

Theory of FTIR Spectroscopy

Figure 6.2 shows the principal features of the Michelson-Morley interferometer used for FTIR spectroscopy. Infrared light from the broadband source impinges on the germanium beamsplitter, which splits the incident beam into two components of approximately equal energy. Approximately 50% of the light is transmitted by the beam splitter, and is directed onto the fixed mirror. The remainder of light is reflected by the beamsplitter onto the moving mirror. After reflection of the two beams of light by the two mirrors, they recombine at the beamsplitter. Here, constructive or destructive interference occurs, depending on the wavelength of light, and the difference in path lengths travelled by the two beams. Approximately 50% of the light is now directed in a beam towards the sample. (The remainder returns to the source, due to the geometry of the interferometer). Certain frequencies of IR light are selectively absorbed by the sample, and the intensity of the resulting beam is recorded by the IR detector. IR intensity is measured as a function of time during the displacement of the moving mirror, which travels at constant velocity.

The situation when the two mirrors are equidistant from the beamsplitter is referred to as "Zero Path Difference" or ZPD. Since the pathlengths of light

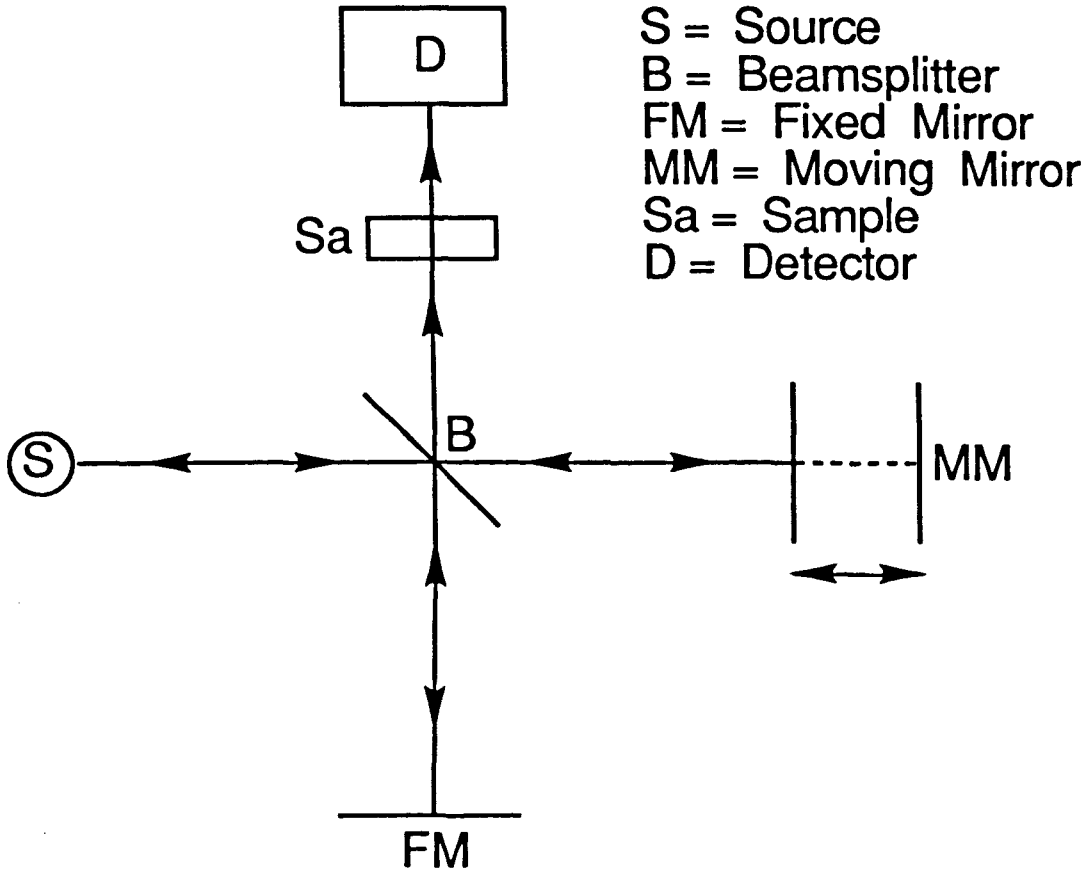


Figure 6.2: Schematic drawing of the Michelson-Morley Interferometer

returning from each mirror are identical in this instance, the two beams are exactly in phase. Thus, constructive interference occurs for all wavelengths of light. For light of wavelength λ, constructive interference also occurs when the position of the moving mirror is such that the path difference is equal to $n\lambda$ ($n = 1,2,3,...$). Conversely, destructive interference occurs when the path difference is equal to $n\lambda/2$ ($n = 1,3,5,...$). In this situation, the beams of light returning from the two mirrors are out of phase.

Therefore, for each wavelength of light, a graph of intensity against distance travelled by the moving mirror takes the form of a cosine wave with a maxima where the path difference is $n\lambda$ ($n = 0,1,2,...$). In this manner, each wavelength of light is modulated as a cosine wave of a different frequency, which depends upon the velocity of the moving mirror. The only position where constructive interference occurs for all wavelengths is at the ZPD leading to a large intensity of IR light known as the centre burst.

The signal recorded by the detector is called an interferogram which consists of a summation of all the modulated cosine waves, produced by the different frequencies of the broad band IR source (4000-400 cm^{-1}). The signal is stored digitally in the computer memory. An interferogram is a so-called "time-domain"

measurement, since the total IR intensity is recorded as a function of time. This needs to be converted to a conventional "frequency-domain" spectrum which exhibits IR intensity as a function of frequency. The mathematical function which converts a single frequency into a cosine wave is called a Fourier transformation. Hence, an interferogram is the Fourier transform of the spectrum of incident IR light. Therefore, an inverse Fourier transformation is necessary to convert the interferogram to the frequency-domain. Due to the large number of frequencies involved, a powerful computer is required to perform this calculation.

The result of this calculation is a so-called single beam spectrum. It gives the IR detector response as a function of frequency. To convert this into a spectrum of transmittance vs. frequency, the single beam spectrum must be ratioed against a background measurement, recorded with no sample in the beam. (Transmittance = I_s/I_o , where I_s and I_o are, respectively. the detector responses with or without sample. This is normally expressed as a percentage).

For matrix isolation experiments, backgrounds were recorded through the shroud and matrix window during cooldown, before deposition of the matrix. For solution spectra, backgrounds were recorded through the cell containing pure solvent, so that solvent absorptions were not present in the final spectrum.

Finally, transmittance spectra are generally converted into absorbance units according to the relationship,

$$\text{Absorbance} = -\log_{10}(T/100)$$

where the transmittance, T, is a percentage. The linear relationship between absorbance and sample concentration stated by Beer's law means that this scale is useful in quantitative analysis.

Advantages of FTIR Spectroscopy

There are several intrinsic advantages resulting from the use of a Fourier transform IR spectrometer as opposed to a dispersive type instrument:

Mechanical Simplicity: The only continuously moving component of an FTIR spectrometer is the moving mirror. This results in little instrument wear and high reliability.

Felgett Advantage: Whereas a dispersive instrument observes each IR frequency consecutively, all frequencies are observed simultaneously by an FTIR spectrometer as a "multiplexed" signal. As a result, a spectrum of equivalent signal to noise ratio can be recorded by FTIR in a fraction of the time required by a dispersive spectrometer. This means that the time taken to average over a large number of scans is not

excessive, leading to enhanced sensitivity. Rapid scanning is also helpful when monitoring reaction kinetics.

Jaquinot Advantage: The slit of a dispersive spectrometer is necessarily narrow to give acceptable resolution. By contrast, an FTIR instrument has a much larger optical aperture, since the resolution is only limited by the distance the mirror travels. The result is a much higher energy throughput, which again increases sensitivity. This is particularly helpful when thick, scattering matrices are necessary for observation of inherently weak vibrational modes.

Connes Advantage: Spectra recorded using dispersive instruments must be calibrated with standard spectra, with accurately known band positions (e.g HCl, H_2O, CO_2, polystyrene). In the case of FTIR spectroscopy, there is an internal calibration system, which makes use of the monochromatic light output of a HeNe reference laser. The laser light is directed into the interferometer, which converts it into a cosine wave (see above). Each zero crossing of this wave is used as a signal to initiate collection of data points by the computer. Thus the exact position of the moving mirror is monitored with great accuracy. Each data point in the resulting spectrum is automatically calibrated to 0.01 cm^{-1}, by this internal reference system.

Stray Light: In dispersive instruments, stray light within the spectrometer can lead to inaccurate absorbance readings. In an FTIR spectrometer there is no equivalent of stray light since, each frequency of IR light is uniquely modulated by the interferometer.

Sample Heat-up: Thermal problems can be encountered due to the proximity of the source to the sample in dispersive spectrometers. In FTIR instruments the sample is further removed from the source. Also the IR intensity at the sample is low for most of the mirror scan, increasing substantially at the ZPD centre-burst.

Sample Emission: Emission of IR light by the sample is not modulated and so is not observed by the detector.

Plotting Errors: Tracking errors sometimes occur in the analogue plotter of a dispersive instrument, leading to inaccurate frequencies and intensities. The digital data of an FTIR spectrum is plotted with a highly accurate digital plotter.

Data Manipulation: Rapid Fourier transformation of interferograms requires a a powerful computer as an integral part of an FTIR spectrometer. This computer can also be applied to other aspects of data manipulation such as spectral subtraction, baseline correction, integration, library searching, peak picking, and smoothing.

One disadvantage of FTIR spectroscopy is that the atmospheric concentrations of H_2O and CO_2 can change significantly between measurement of single beam spectra of the background and sample. The resultant spectrum is thus contaminated with the IR bands of these gaseous species. In particular, the H_2O bending mode gives rise to rotational-vibrational peaks in the region 1900 - 1400 cm^{-1}, which can interfere considerably with the ν(CO) absorptions of metal carbonyls. However, the spectrum can be simplified by spectral subtraction. (A spectrum of atmospheric water vapour can be obtained by ratioing two single beam spectra taken before and after purging the interferometer with dry N_2).

6.6 UV/VIS SPECTROSCOPY

All UV/visible spectra were recorded using Perkin-Elmer Lambda 5 spectrometer. This is a high performance double beam ratio recording instrument, with an integrated microcomputer. The spectrometer can be interfaced with the PE 3600 data station, which enables spectral storage and manipulation. The data system also allows averaging of many scans, which improves spectral signal/noise ratio. The application of this system to the measurement of UV/visible spectra of matrices has been described in detail by Horton-Mastin (1988).

6.7 PHOTOLYSIS SOURCES

The main photolysis source was a Philips HPK 125 W medium pressure Hg arc lamp, which emits a series of intense bands of radiation between 250-600 nm. The lamp was equipped with a 4 cm quartz water filter to remove IR radiation for photolysis of matrices of the dinuclear platinum complexes. For the dinuclear osmium and nickel complexes, and Fp-silyl compounds, the lamp was focused on the matrix with quartz optics. The same system was employed for irradiation of room temperature hydrocarbon solutions.

Generally, UV photolysis was undertaken using a broad band aqueous solution filter. The filter comprised of a 4 cm path length cell containing an aqueous solution of $NiSO_4$ (400 gdm^{-3}) and $CoSO_4$ (200 gdm^{-3}). It transmits light in the range 230-345 nm. Where a particular wavelength is stated (e.g. 290 nm) a Balzer's interference filter was used to give a narrow band pass for selective photolysis (+/- 10 nm). Near UV or Visible photolysis was achieved by using a glass filter with the appropriate cut off wavelength (e.g. > 400 nm).

An alternative source of intense long wavelength light was a Kodak slide projector with a 180 W tungsten halogen bulb. Glass filters could be conveniently placed in the slide compartment, and the

beam focused onto the matrix with an appropriate lens. This lamp was particularly useful for long wavelength photolysis in the experiments on the di-osmium complexes (Chapter 3).

For thick or cloudy matrices, the window was rotated through 180° to photolyse through the back, as well as the front of the window, for maximum efficiency. This procedure is also of use when the intensity of photolysing light is reduced by absorption filters.

6.8 POLARISED PHOTOCHEMISTRY

The theory of polarised photochemistry has been discussed in the introductory section on dinuclear metal carbonyls. Here, the practice of the technique is described:

The matrix isolated sample is photolysed with plane polarised light, using a Polacoat 105 UV WMR polariser on a quartz substrate. Spectra are then recorded through a polariser oriented either parallel or perpendicular to the plane of photolysis. Comparison of the two spectra recorded at each stage of the experiment reveals whether linear dichroism is present in the absorption bands of matrix isolated species. Polarised UV/Visible spectra were obtained

using the same polariser as for photolysis (above). IR polarisation was achieved using an aluminised grid mounted on KRS-5, held in a rotatable calibrated disk.

In experiments where the MX-3600 interferometer was used for IR spectroscopy, the plane of photolysis was at 45° to the vertical. Spectra were recorded with the IR polariser in the spectrometer sample compartment, oriented at +/- 45° to the vertical (i.e. 0° or 90° relative to the photolysis plane). The polarisation characteristics of the MX-1 bench have been investigated by Fletcher (1985), who found that this arrangement gives equal IR energy throughput at each orientation.

In experiments where the 7199 interferometer was used for IR spectroscopy, the polariser was mounted directly in front of the IR detector. A new mount, designed specifically for this purpose is illustrated in Figure 6.3.

In this arrangement, the IR beam is reflected by several mirrors between the sample and the polariser. The IR beam travels parallel to the spectrometer bench (i.e. horizontally). For light polarised at 45° to the vertical, reflections in the horizontal plane can result in elliptical polarisation in the reflected beam. To avoid this problem, a vertical plane of photolysis was used, with IR spectra recorded through

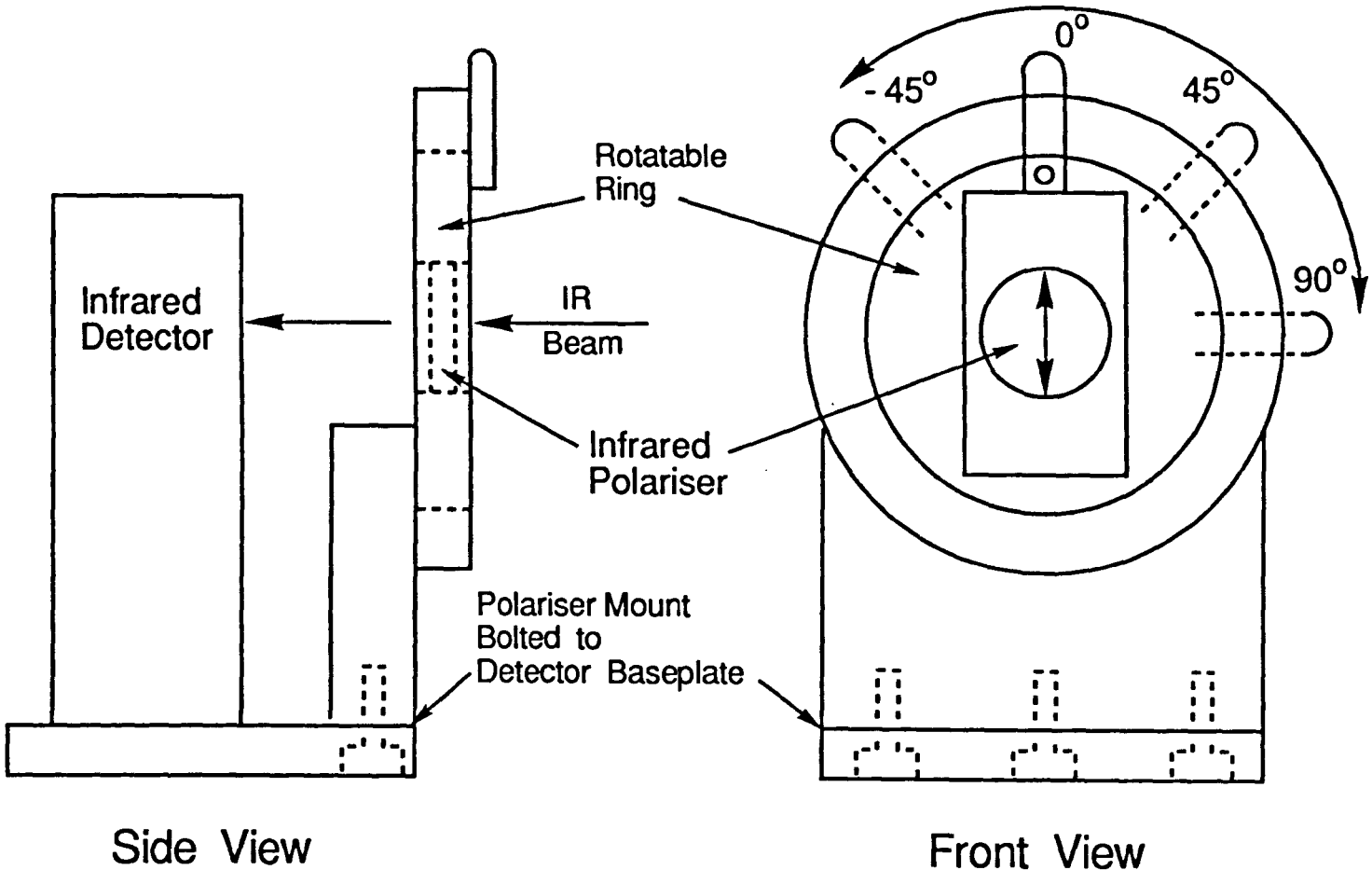


Figure 6.3: Design of Polariser Mount used to record dichroic infrared spectra on the Nicolet 7199 interferometer.

either a vertical or horizontal polariser.

The polarisation characteristics of the 7199 bench mean that the energy throughput differs between these two orientations. This did not cause any difficulties, since single beam background spectra could be recorded through the IR polariser in each position. Subsequent spectra were ratioed against the background of the same polarisation.

Polarised photochemistry requires a clear matrix, since a cloudy sample causes light scatter, with consequent depolarisation of incident irradiation (either in the photolysing light or the spectrometer beam). The resulting dichroism can be greatly reduced by a cloudy matrix. In practice, it was found that N_2 matrices provided the clearest samples for polarised photochemistry.

6.9 CHEMICALS

The platinum dimers $(CpPt(CO))_2$ and $(Cp^*Pt(CO))_2$ (including a 50% ^{13}CO enriched sample), and iron silyl complexes $FpSiMe_3$, $FpSiMe_2SiMe_3$, $FpSiMe_2SiMe_2H$, and $FpSiH_2SiH_3$ were gifts from Dr. N. M. Boag of the University of Salford. The dinuclear osmium complexes, $Os_2(CO)_9$ and $Os_2(CO)_8(\mu\text{-}C_2H_4)$ were gifts from Professor J. R. Norton of Colorado State University. $Os_2(CO)_9$ was stored under CO and refrigerated to prevent decomposition. The nickel dimer, $(CpNi(\mu\text{-}CO))_2$ was purchased from Aldrich Chemicals. It was found that after storage for several months, the sample was contaminated by a small amount of nickelocene, Cp_2Ni, identifiable by its green colour. This decomposition product was removed by sublimation on a vacuum line.

The matrix gases, Ar, N_2 and CH_4 (99.99%) were obtained from Messer Griesheim and Research grade CO from BOC. Research grade Xe, for use in liquid Xe experiments, was also obtained from BOC. Aldrich HPLC grade n-heptane was freshly distilled over CaH_2 under a nitrogen atmosphere.

REFERENCES

H. B. **Abrahamson**, M. C. Palazzotto, C. L. Reichel and M. S. Wrighton, J. Am. Chem. Soc., 101, 4123 (1979).

M. J. **Almond** and A. J. Downs in "Spectroscopy of Matrix Isolated Species" (ed. R. J. H. Clark and R. E. Hester), Advances in Spectroscopy, Vol. 17, Wiley, Chichester (1989).

F. R. **Anderson** and M.S. Wrighton, Inorg. Chem., 25, 112 (1986).

B. J. **Aylett**, Adv. Inorg. Chem. Radiochem., 25, 1, (1982).

T. J. **Barton**, R. Grinter, A. J. Thomson, B. Davies, and M. Poliakoff, J. C. S. Chem. Commun., 841 (1977).

G. A. **Battiston**, G. Bor, U. K. Dietler, S. F. A. Kettle, R. Rossetti, G. Sbrignadello, and P. L. Stanghellini, Inorg. Chem., 19, 1961 (1980).

S. E. J. **Bell**, K. C. Gordon and J. J. McGarvey, J. Am. Chem. Soc., 110, 3107 (1988).

J. A. **Belmont** and M.S. Wrighton, Organometallics, 5 1421 (1986).

B. R. **Bender**, R. Bertoncello, M. R. Burke, M. Casarin, G. Granozzi, J. R. Norton, and J. Takats, Organometallics, 8, 1777 (1989).

D. H. **Berry** and L. J. Procopio, J. Am. Chem. Soc., 111, 4099 (1989).

J. P. **Blaha** and M. S. Wrighton, J. Am. Chem. Soc., 107, 2694 (1985a).

J. P. **Blaha**, B. E. Bursten, J. C. Dewan, R. B. Frankel, C. L. Randolf, B. A. Wilson, and M. S. Wrighton, J. Am. Chem. Soc., 107, 4561 **(1985b)**.

N. M. **Boag**, R. J. Goodfellow, M. Green, B. Hessner, J. A. K. Howard, and F. G. A. Stone, J. C. S. Dalton Trans., 2585 **(1983)**.

N. M. **Boag**, D. Boucher, J. A. Davies, R. W. Miller, A. A. Pinkerton and R. Syed, Organometallics, 7, 791 **(1988a)**.

N. M. **Boag**, Organometallics, 7, 1446 **(1988b)**.

P. L. **Bogdan** and E. Weitz, J. Am. Chem. Soc., in press **(1989)**.

G. **Bor** and K. Noack, J. Organomet. Chem., 64, 367 **(1974)**.

P. S. **Braterman**, "Metal Carbonyl Spectra", Academic Press **(1975)**.

M. **Brookhart** and M. L. H. Green, J. Organomet. Chem., 250, 395 **(1983)**.

J. K. **Burdett**, R. N. Perutz, M. Poliakoff and J. J. Turner, J. C. S., Chem. Commun., 157, **(1975)**.

J. K. **Burdett**, M. Poliakoff, J. J. Turner and H. Dubost "Advances in Infrared and Raman Spectroscopy", Vol. 2, Ch. 1, Wiley, Cichester **(1976)**.

J. K. **Burdett**, J. M. Grzybowski, R. N. Perutz, M. Poliakoff, J. J. Turner and R. F. Turner, Inorg. Chem., 17, 147 **(1978)**.

M. R. **Burke**, J. Takats, F.-W. Grevels, and J. G. A. Reuvers, J. Am. Chem. Soc., 105, 4092 **(1983)**.

B. E. **Bursten**, S. D. McKee and M. S. Platz, J. Am. Chem. Soc., 111, 3429, **(1989)**.

L. R. **Byers** and L. F. Dahl, Inorg. Chem., 19, 680 **(1980)**.

B. K. **Campion**, R. H. Heyn and T. D. Tilley, J. Am. Chem. Soc., 110, 7558 **(1988)**.

W. J. **Carter**, J. W. Kelland, S. J. Okrasinski, K. E. Warner and J. R. Norton, Inorg. Chem., 21, 3955 **(1982)**.

G. **Cerveau**, G. Chauviere, E. Colomer and R. Corriu, J. Organomet. Chem., 210, 343 **(1981)**.

T.-M. **Chan**, J. W. Connolly, C. D. Hoff and F. Millich, J. Organomet. Chem., 152, 287 **(1978)**.

S. P. **Church**, Ph.D. Thesis, University of Nottingham, **(1982)**.

S. P. **Church**, M. Poliakoff, J. A. Timney, and J. J. Turner Inorg. Chem. 22, 3259 **(1983)**.

S. P. **Church**, H. Hermann, F.-W. Grevels, and K. Schaffner, J. C. S., Chem. Commun., 785 **(1984)**.

R. **Colton**, G. J. Commons and B. F. Hoskins, J. C. S. Chem. Commun., 363 **(1975)**.

N. J. **Conti** and W. M. Jones, Organometallics, 7, 1669 **(1988)**.

F. A. **Cotton**, Prog. Inorg. Chem., 21, 1 **(1976)**.

F. A. **Cotton** and J. M. Troup, J. C. S., Dalton Trans., 800 **(1974)**.

R. H. **Crabtree** and M. Lavin, Inorg. Chem., 25, 805 **(1986)**.

R. H. **Crabtree** and D. G. Hamilton, Adv. Organomet. Chem., 28, 299 **(1988)**.

O. **Crichton** and A. J. Rest, J. C. S., Dalton Trans., 986 **(1977)**.

O. **Crichton**, A. J. Rest and D. J. Taylor, J. C. S., Dalton Trans., 167 **(1980)**.

B. **Davies**, A. McNeish, M. Poliakoff, M. Tranquille and J. J. Turner, Chem. Phys. Letts., 52, 477 **(1977)**.

J. H. **Darling** and J. S. Ogden, J. C. S. Dalton Trans., 2496, **(1972)**.

J. **Dewar** and H. O. Jones, Proc. Roy. Soc., A76, 558 **(1905)**.

A. J. **Dixon**, M. A. Healy, P. M. Hodges, B. D. Moore, M. Poliakoff, M. B. Simpson, J. J. Turner, and M. A. West, J. C. S. Faraday Trans. 2, 82, 2083 **(1986a)**.

A. J. **Dixon**, M. A. Healy, M. Poliakoff and J. J. Turner, J. C. S. Chem. Commun. 994 **(1986b)**.

A. J. **Dixon**, S. J. Gravelle, L. J. van de Burgt, M. Poliakoff, J. J. Turner and E. Weitz, J. C. S. Chem. Commun. 1023 **(1987)**.

A. J. **Dixon**, Ph.D. Thesis, University of Nottingham **(1989)**.

T. J. **Drahnak**, J. Michl and R. West, J. Am. Chem. Soc., 103, 1846, **(1981)**.

I. R. **Dunkin**, P. Haerter, and C. J. Shields, J. Am. Chem. Soc., 106, 7248 **(1984)**.

C. **Eaborn**, D. A. R. Harper, P. B. Hitchcock, S. P. Hopper, K. D. Safa, S. S. Washburne, D. R. M. Walton, J. Organomet. Chem., 186, 309 **(1980)**.

D. J. **Fettes**, R. Narayanaswamy and A. J. Rest, J. C. S. Dalton Trans., 2311 **(1981)**.

E. O. **Fischer** and C. Palm, Chem. Ber., 91, 1725, **(1958)**.

E. O. **Fischer**, H. Schuster-Woldan and K. Bittler, Z. Naturforsch., Teil B, 18, 429 **(1963)**.

S. **Firth**, W. E. Klotzbuecher, M. Poliakoff, and J. J. Turner, Inorg. Chem., 26, 3370 **(1987a)**.

S. **Firth**, Ph.D. Thesis, University of Nottingham **(1987b)**.

S. C. **Fletcher**, Ph.D. Thesis, University of Nottingham, **(1985)**.

S. C. **Fletcher**, M. Poliakoff and J. J. Turner, Inorg. Chem., 25, 3597 **(1986)**.

C. R. **Folkes** and A. J. Rest, J. Organomet. Chem., 136, 355 **(1977)**.

E. J. **Forbes** and N. Iranpoor, J. Organomet. Chem., 236, 403 **(1982)**.

T. A. **Ford**, H. Huber, W. Klotzbuecher, M. Moskovits and G. A. Ozin, Inorg. Chem., 15, 1666 **(1976)**.

C. **Giannotti** and G. J. Merle, J. Organomet. Chem., 105, 97 **(1976)**.

D. S. **Ginley**, C. R. Bock and M. S. Wrighton, Inorg. Chem. Acta., 23, 85 **(1977)**.

B. P. **Gracey**, S. A. R. Knox, K. A. MacPherson, A. G. Orpen and S. R. Stobart, J. C. S. Dalton Trans., 1935 **(1985)**.

R. G. **Graham**, R. Grinter, D. R. Stern and K. Timms, J. Phys. E: Sci. Instrum., 19, 776 **(1986)**.

M. **Green**, Ph.D. Thesis, University of Salford (1989).

P. R. **Griffiths**, "Chemical Infrared Fourier Transform Spectroscopy", Wiley-Interscience, New York (1975).

L. A. **Hanlan** and G. A. Ozin, J. Am. Chem. Soc., 96, 6324 (1974).

R. T. **Hembre**, C. P. Scott and J. R. Norton, J. Am. Chem. Soc., 109, 3468 (1987).

A. F. **Hepp** and M. S. Wrighton, J. Am. Chem. Soc., 105, 5934 (1983).

A. F. **Hepp**, J. P. Blaha, C. Lewis, and M. S. Wrighton, Organometallics, 3, 174 (1984).

R. S. **Herrick**, A. B. Frederick and R. R. Duff Jr., Organometallics, 8, 1120 (1989).

R. B. **Hitam**, K. A. Mahmoud and A. J. Rest, Coord. Chem. Rev., 55, 1 (1984).

R. **Hoffmann**, Angew. Chem., Int. Ed. Engl., 21, 711 (1982).

R. H. **Hooker**, K. A. Mahmoud, and A. J. Rest, J. C. S., Chem. Commun., 1022 (1983).

R. H. **Hooker**, A. J. Rest and I. Whitwell, J. Organomet. Chem., 266, C27 (1984).

R. H. **Hooker**, Ph.D. Thesis, University of Southampton (1986).

A. S. L. **Horton-Mastin**, Ph.D. Thesis, University of Nottingham (1988).

H. **Huber**, E. P. Kundig, M. Moskovits and G. A. Ozin, J. Am. Chem. Soc., 97, 2097 (1975).

D. K. **Huggins**, N. Flitcroft and H. D. Kaesz, Inorg. Chem., 4, 166 **(1965)**.

J. L. **Hughey**, C. R. Bock and T. J. Meyer, J. Am. Chem. Soc., 97, 4440 **(1975)**.

S. A. Jackson, Ph.D. Thesis, University of Nottingham **(1988)**.

V. J. **Johnston**, F. W. B. Einstein and R. K. Pomeroy, J. Am. Chem. Soc., 109, 8111 **(1987)**.

R. J. **Kazlauskas** and M. S. Wrighton, Organometallics, 1, 602 **(1982a)**.

R. J. **Kazlauskas** and M. S. Wrighton, J. Am. Chem. Soc., 104, 6005 **(1982b)**.

G.-Y. **Kiel**, J. Takats and F.-W. Grevels, J. Am. Chem. Soc., 109, 2227 **(1987)**.

R. B. **King** and K. H. Pannell, Inorg. Chem., 7, 1510 **(1968)**.

R. B. **King**, K. H. Pannell, C. R. Bennett and M. Ishaq, J. Organomet. Chem., 19, 327 **(1969)**.

G. J. **Kubas**, Acc. Chem. Res., 21, 120 **(1988)**.

E. P. **Kundig**, D. McIntosh, M. Moskovits, and G. A Ozin, J. Am. Chem. Soc., 95, 7234 **(1973)**.

E. P. **Kundig**, M. Moskovits, and G. A. Ozin, Ang. Chem. Int. Ed. Engl., 14, 292 **(1975)**.

C. **Lewis** and M. S. Wrighton, J. Am. Chem. Soc., 105, 7768 **(1983)**.

K. A. **Mahmoud**, A. J. Rest, H. G. Alt, M. E. Eichner and B. M. Jansen, J. C. S. Dalton Trans., 175 **(1984)**.

K. A. **Mahmoud**, A. J. Rest and H. G. Alt, J. C. S. Dalton Trans., 1365 **(1985)**.

A. **McCamley** and R. N. Perutz, private communication **(1988)**.

P. **McArdle** and A. R. Manning, J. Chem. Soc. (A), 717 **(1971)**.

D. **McIntosh**, M. Moskovits and G. A. Ozin, Inorg. Chem., 15, 1669 **(1976)**.

T. J. **Meyer** and J. V. Caspar, Chem. Rev., 85, 187 **(1985)**.

L. **Mond**, C. Langer and F. Quincke, J. Chem. Soc., 57, 749 **(1890)**.

L. **Mond** and C. Langer, J. Chem. Soc., 59, 1090 **(1891)**.

B. D. **Moore**, M. B. Simpson, M. Poliakoff, J. J. Turner, J. C. S. Chem. Commun., 972 **(1984)**.

J. R. **Moss** and W. A. Graham, J. C. S., Chem. Commun., 835 **(1970)**.

J. R. **Moss** and W. A. Graham, J. C. S., Dalton Trans., 95 **(1977)**.

K. M. **Motyl**, J. R. Norton, C. K. Schauer and O. P. Anderson, J. Am. Chem. Soc., 104, 7325 **(1982)**.

Y. **Nakadaira**, T. Kobayashi and H. Sakurai, J. Organomet. Chem., 165, 399 **(1979)**.

J. R. **Norton** and B. R. Bender, unpublished results **(1989)**.

T. **Pakkanen** and R. C. Kerber, Inorg. Chim. Acta., 49, 47 **(1981)**.

K. H. **Pannell**, J. Organomet. Chem., 21, P17 **(1970)**.

K. H. **Pannell** and J. B. Rice, J. Organomet. Chem.,78, C35 **(1974)**.

K. H. **Pannell**, C. C. Wu and G. J. Long, J. Organomet. Chem., 186, 85 **(1980)**.

K. H. **Pannell**, J. Cervantes, C. Hernandez, J. Cassias and S. Vincenti, Organometallics, 5, 1056 **(1986)**.

K. H. **Pannell**, L.-J. Wang and J. M. Rozell, Organometallics, 8, 550 **(1989a)**.

K. H. **Pannell**, J. M. Rozell and C. Hernandez, J. Am. Chem. Soc., 111, 4482 **(1989b)**.

E. K. **Pham** and R. West, J. Am. Chem. Soc., 111, 7667 **(1989)**.

T. S. **Piper**, D. Lemal and G. Wilkinson, Naturwissen--schaften, 43, 129 **(1956)**.

R. N. **Perutz** and J. J. Turner, J. C. S. Faraday II, 452 **(1973)**.

R. N. **Perutz**, Ph.D. Thesis, University of Cambridge **(1974)**.

M. **Poliakoff** and J. J. Turner, J. Chem. Soc.(A), 2403 **(1971)**.

M. **Poliakoff** and J. J. Turner, J. C. S., Dalton Trans., 2276 **(1974)**.

M. **Poliakoff**, unpublished results **(1972)**.

M. **Poliakoff** and E. Weitz, Adv. Organomet. Chem., 25, 277 **(1986)**.

A. J. **Poe** and C. V. Sekar, J. Am. Chem. Soc., 108, 3673 **(1986)**.

K. R. **Pope** and M. S. Wrighton, Inorg. Chem., 24, 2792 **(1985)**.

H. M. **Powell** and R. V. G. Ewens, J. Chem. Soc., 286 **(1939)**.

H. **Rabaa**, J.-Y. Saillard and U. Schubert, J. Organomet. Chem., 330, 397 **(1987)**.

C. L. **Randolph** and M. S. Wrighton, J. Am. Chem. Soc., 108, 3366 **(1986)**.

C. L. **Randolph** and M. S. Wrighton, Organometallics, 6, 365 **(1987)**.

H. **Sakurai**, M. Kira and T. Uchida, J. Am. Chem. Soc., 95, 6826 **(1973)**.

G. **Schmid** and E. Welz, Ang. Chem., Int. Ed. Engl., 16, 785 **(1977)**.

U. **Schubert** and A . Rengstl, J. Organomet. Chem., 170, C37 **(1979)**.

Y. **Stenstrom** and W. M. Jones, Organometallics, 5, 178 **(1986)**.

A. E. **Stiegman** and D. R. Tyler, Acc. Chem. Res., 17, 61 **(1984)**.

D. A. **Straus**, T. D. Tilley, A. R. Rheingold and S. J. Geib, J. Am. Chem. Soc., 109, 5872 **(1987)**.

R. L. **Sweany** and T. L. Brown, Inorg. Chem., 16, 415 **(1977a)**.

R. L. **Sweany** and T. L. Brown, Inorg. Chem., 16, 421 **(1977b)**.

J. **Takats**, Polyhedron, 7, 931 **(1988)**.

H. **Tobita**, K. Ueno and H. Ogino, Chem. Letters, 1777 **(1986)**.

H. **Tobita**, K. Ueno and H. Ogino, Bull. Chem. Soc. Jpn., 61, 2797 **(1988)**.

V. F. **Traven** and R. West, J. Am. Chem. Soc., 95, 6824 **(1973)**.

P. M. **Treichel** and D. A. Komar, J. Organomet. Chem., 206, 77 **(1981)**.

G. **Trinquier** and R. Hoffmann, Organometallics, 3, 370 **(1984)**.

J. J. **Turner**, M. Poliakoff and M. A. Healy, Proc. XXVI Int. Conf. on Coord. Chem., Porto **(1988)**.

K. **Ueno**, H. Tobita and H. Ogino, J. Am. Chem. Soc., 110, 4092 **(1988)**.

R. K. **Upmacis**, Ph.D. Thesis, University of Nottingham **(1986)**.

N. **Wiberg**, J. Organomet. Chem., 273, 141 **(1984)**.

N. **Wiberg**, G. Wagner and G. Muller, Ang. Chem. Int. Ed. Engl., 24, 229 **(1985)**.

M. J. **Winter**, Adv. Organomet. Chem., 29, 101 **(1989)**.

M. S. **Wrighton** and G. L. Geoffroy, "Organometallic Photochemistry", Academic Press, New York **(1979)**.

M. S. **Wrighton** and D. S. Ginley, J. Am. Chem. Soc., 97, 4246 **(1975)**.

G. K. **Yang**, K. S. Peters and V. Vaida, J. Am. Chem. Soc., 108, 2511 **(1986)**.

R. J. **Ziegler**, J. M. Burtlitch, S. E. Hayes and W. M. Risen, Jr., Inorg. Chem., 11, 702 **(1972)**.

C. **Zybill** and G. Muller, Organometallics, 7, 1368 **(1988)**.

C. **Zybill**, D. L. Wilkinson, C. Leis and G. Muller, Ang. Chem. Int. Ed. Engl., 28, 203 **(1989)**.